

A Multi-Scale Approach in Mapping the Sedimentological and Hydrostratigraphical Features of Complex Aquifers

by

Matthew N. Schumacher

A thesis
presented to the University of Waterloo
in fulfillment of the
thesis requirement for the degree of
Master of Science
in
Earth Sciences

Waterloo, Ontario, Canada, 2009

©Matthew N. Schumacher 2009

Author's Declaration

I hereby declare that I am the sole author of this thesis. This is a true copy of the thesis, including any required final revisions, as accepted by my examiners.

I understand that my thesis may be made electronically available to the public.

Matthew Schumacher

Abstract

Accessibility to consistent subsurface hydrostratigraphic information is crucial for the development of robust groundwater flow and contaminant transport models. However, full three-dimensional understanding of the subsurface geology is often the missing link. Construction of watershed-scale hydrostratigraphic models continues to be limited by the quality and density of borehole data which often lack detailed geologic information. This can become a serious problem where rapid sediment facies changes and intricate sediment architecture occur. This research is motivated by the idea that if we can understand more about the distribution of sediments and structures of complex deposits, we learn more about depositional processes and how they affect the internal geometry of a deposit and the distribution of hydraulic properties. One approach is to study surficial excavations (e.g. sand and gravel pits) that often punctuate shallow aquifers.

The purpose of this study is to develop and test a method of integrating high-resolution georeferenced stratigraphic and sedimentologic information from sand and gravel pits as a means to better document sedimentologic data and improve understanding of the depositional environments. The study area is located within the Waterloo Moraine, in southwestern Ontario, and is an unconsolidated shallow aquifer system with a complex internal architecture and sediment heterogeneity. The method involves the integration of high-resolution field data with borehole and geophysical information in a computer-based 3D environment. A total of fourteen virtual sedimentary sections were constructed by georegistering digital photographs within a framework of georeferenced positions collected using a reflectorless total station and GPS. Fourteen sediment facies have been described in the field. These include crudely stratified gravel beds, planar and cross-laminated sandy strata (ripple and dune scales), along with laminated and massive silty and clayey beds. Calculated hydraulic conductivities span over seven orders of magnitude. The analysis of a single excavation has shown contrasting sediment assemblages from one end of the pit to the other, highlighting the complexity of the Waterloo Moraine. The heterogeneous and deformed layers of gravel, sand, and mud may be the product of an ice-contact to ice-proximal environment, whereas the extensive sandy assemblages may reflect an intermediate subaqueous fan region. The results also suggest that the borehole database overestimates the amount of fine-grained material in the study area. Finally, this research demonstrates that it is possible to build in a timely manner a 3D virtual sedimentologic database. New emerging technologies will lead to increased resolution and accuracy, and will help streamline the process even further. The possibility of expanding the 3D geodatabase to other excavations across the region in a timely manner is likely to lead to improved hydrostratigraphic models and, by extension, to more efficient strategies in water resources planning, management and protection.

Acknowledgements

This project would not have existed without the assistance of several individuals and I wish to recognize them for all of their support in this thesis.

First I want to thank Dr. Martin Ross for his support, guidance and even tolerance during this project. My education and knowledge is vastly superior now due to his supervision and I must say that I have developed a deeper appreciation for 3D modeling because of him. Merci beaucoup!

Next, I must acknowledge my wife Elizabeth Brown. She put up with a lot of my geological geekiness and provided much love and support, which encouraged me in my pursuit of a graduate degree. Without her constant reinforcement, I would never have finished and I hope I end up being, at the least, a good return-on-investment for her.

I want to thank David Sharpe and Hazen Russell from the Geological Survey of Canada for helping to bring this project into existence. Their invaluable assistance ensures that I will achieve my goal of becoming a “sedimentary hydrogeologist”.

I want to express my gratitude to Dr. Anthony Endres, Dr. David Rudolph, Dr. Christopher Stohr, Brewster Conant, Colby Steelman, Scott Piggott, Marcelo Sousa, Asha Philar, Roberta Adams, Lisa Atkinson and Matthew Vanderkooy for assisting me in this thesis. They each provided their own expertise and facilitated in gathering the results needed. Their contributions are extremely appreciated and I cannot thank them enough for their assistance and patience.

Last, I cannot forget to show my appreciation to Jim Kieswetter and the crew at Kieswetter Holdings for allowing me access into their operation so I could conduct this work and attain my degree. Their patience and attentiveness will not be forgotten.

Table of Contents

List of Figures.....	viii
List of Tables	xi
List of Equations	xii
1 - Introduction	1
1.1 Background	1
1.2 The Multi-Scale Aquifer Analogue Approach.....	4
1.3 Purpose of Study	7
1.4 Study Area.....	8
2 - General Setting of Study Area	10
2.1 The Waterloo Moraine	10
2.1.1 Physiography and Geology.....	10
2.1.2 Hydrogeology	16
3 - Methodology.....	18
3.1 Archival Data Collection.....	18
3.1.1 Stratigraphic Model and Borehole Record	18
3.1.2 GIS	18
3.1.3 Groundwater Model Grid.....	19
3.2 Field Data Collection	19
3.2.1 Coordinate Positioning Survey Procedure	20
3.2.2 GPS Surveying System.....	20
3.2.3 Total Station Reflectorless Surveying System.....	24
3.2.4 Combining the GPS and Total Station Methods.....	25
3.2.5 Digital Image Acquisition.....	26
3.2.6 Facies Documentation.....	26
3.2.7 Sedimentary structures	27
3.2.8 Ground Penetrating Radar.....	27

3.3	Geomodelling Work.....	28
3.4	Lab Data	33
3.4.1	Sample Gathering and Analysis.....	33
3.4.2	Hydraulic Conductivity Calculations.....	34
4 -	Results and Interpretation.....	36
4.1	Sedimentary Study	36
4.1.1	Sediment sections and their virtual 3D reconstruction	36
4.1.2	Lithofacies.....	37
4.1.3	Paleoflow	42
4.2	Sedimentary Interpretation.....	42
4.2.1	Eastern Side of Study Area.....	43
4.2.2	Western Side of Study Area.....	53
4.3	Hydrostratigraphic Study	55
4.3.1	Hydrofacies	55
4.4	Subsurface Analysis	60
4.4.1	Regional Stratigraphic Model.....	60
4.4.2	Hydrogeology	60
4.4.3	Ground Penetrating Radar.....	61
4.5	Depositional Interpretation.....	64
4.6	Testing the Borehole Database	71
5 -	Discussion	77
5.1	The Multi-Scale Approach.....	77
5.1.1	Application of Equipment and Tools.....	77
5.1.2	Field Data Acquisition	78
5.1.3	Hydraulic Parameter Calculations	79
5.1.4	Summary of the Approach.....	79
5.2	Other Techniques	80
5.2.1	Terrestrial Laser Scanning	80
5.2.2	Photogrammetry.....	81
5.3	Initiation of a Waterloo Moraine Database.....	84
5.4	Groundwater Modelling Applications	85

6 - Conclusion	88
Bibliography	90
Appendices	99
Appendix A – Facies Classification.....	100
Appendix B – Section Data and Information.....	102
Appendix C – Images for the Sections	106
Appendix D – Hydraulic Conductivity Calculations.....	134
Appendix E – Grain Size Distribution Curves.....	137
Appendix F – Paleoflow Measurements	158
Appendix G – Data Disc	161

List of Figures

Figure 1-1: Location of the study area within southern Ontario;	2
Figure 1-2: A simplified flow diagram used in the basin analysis approach.....	3
Figure 1-3: An illustration depicting the Aquifer Analogue Concept	5
Figure 1-4: The concept of using a multi-scale approach in sedimentary deposits.....	6
Figure 1-5: Location of the Alder Creek watershed and the study site Kieswetter Holdings .	9
Figure 2-1: The location of moraines in southern Ontario	10
Figure 2-2: Conceptual geological model of Waterloo Region.....	11
Figure 2-3: A 3D representation of the full subsurface stratigraphy at the study area	12
Figure 2-4: Drift thickness in the Waterloo Region	13
Figure 2-5: Surficial geology of the Waterloo Region and Waterloo Moraine	14
Figure 2-6: Location of the spurs associated with the Waterloo Moraine.....	15
Figure 2-7: Recharge and developed areas of the Waterloo Moraine	17
Figure 2-8: The simplified hydrostratigraphy for the Waterloo Region.....	17
Figure 3-1: Comparison of groundwater modeling cells used for study on Alder Creek.....	19
Figure 3-2: Setup of the RTK GPS station	21
Figure 3-3: The rover unit for the GPS survey system with an attached computer.....	22

Figure 3-4: A total station setup and ready to take measurements of a section.....	24
Figure 3-5: Conducting the GPR profile using a PulseEKKO 100A unit	27
Figure 3-6: Workflow diagram illustrating the procedure to create virtual sections.....	28
Figure 3-7: Georeferenced survey points in a 3D virtual environment coded by elevation ..	29
Figure 3-8: An interpolated surface based on the data points for a section.....	30
Figure 3-9: A series of positioned voxets representing a section	31
Figure 3-10: An example of a completed section with the images draped onto the surface .	31
Figure 3-11: An example of a stratigraphic grid (SGrid) for a section.....	32
Figure 4-1: The location of all sections studied at Kieswetter Holdings.....	36
Figure 4-2: Rapid massive loading of gravel producing dewatering structures	38
Figure 4-3: A rose diagram of the paleoflow data in 10 degree increments.....	42
Figure 4-4: Heterolithic bedding at section J.....	43
Figure 4-5: A gravel bedform found at Section B	44
Figure 4-6: A selection of features for the 2007 sections in the eastern side of pit.....	45
Figure 4-7: Select features from 2008 sections in the eastern part of pit	47
Figure 4-8: The formation and types of sheath folds.....	49
Figure 4-9: Piggyback thrusting with distal, intermediate and proximal zones.	51
Figure 4-10: A ball and pillow structure resulting in deformed mud beds.....	52

Figure 4-11: A series of architectural elements at Section H	53
Figure 4-12: A portion of section K (top) and its facies interpretation (bottom)	54
Figure 4-13: The GPR profile path, with position markings	62
Figure 4-14: The resulting GPR profile conducted at Kieswetter Holdings.....	63
Figure 4-15: The facies associations connected with various jet-efflux models	65
Figure 4-16: Conceptual model of a subaqueous fan system	66
Figure 4-17: Principal characteristics of an ice-contact underwater fan	67
Figure 4-18: Portion of Section C displaying beds of resedimented material	68
Figure 4-19: Isolated clasts, or possible dropstones, in laminated sandy material	69
Figure 4-20: Direction of decreasing heterogeneity and deformation for the research area .	70
Figure 4-21: Location of the tested boreholes around the study area.....	71
Figure 5-1: Creation of a virtual surface using data from Sirovision	83
Figure 5-2: Location of groundwater modeling locations and points.....	86

List of Tables

Table 1: Summary of observed facies and their respective facies class	39
Table 2: Facies Proportions for each Section at Kieswetter Holdings.....	40
Table 3: Hydraulic conductivity summary, based on facies, for each sample collected	41
Table 4: A summary of the mud facies	56
Table 5: A summary of the sand facies.....	57
Table 6: A summary of the gravel facies	59
Table 7: Calculated Facies Proportions from Boreholes within the Waterloo Moraine.....	73
Table 8: Facies Proportion of the Near-Surface Boreholes	74
Table 9: Comparison between all proportion methods	75

List of Equations

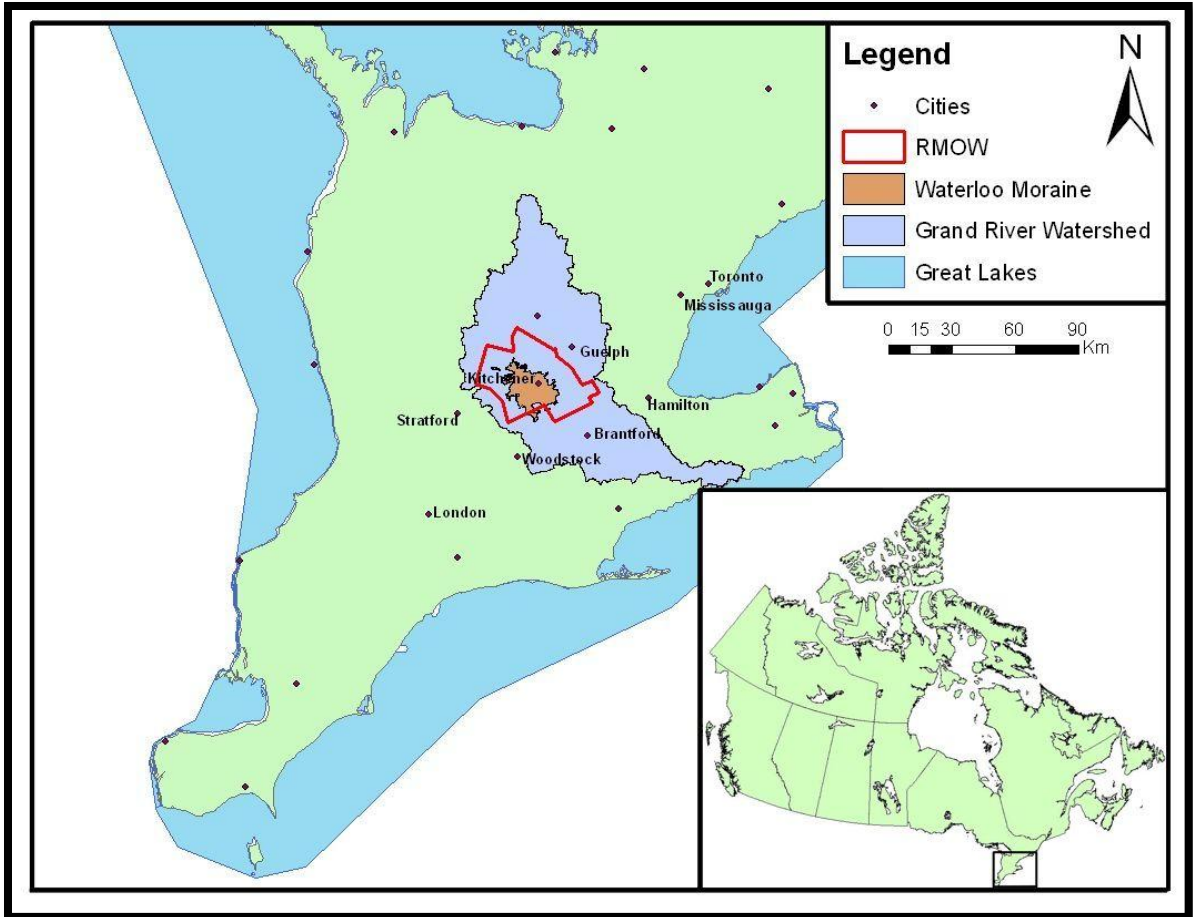
Equation 1: Hazen Equation.....	34
Equation 2: Porosity Equation.....	34
Equation 3: Kozeny-Carmen Equation.....	34
Equation 4: Breyer Equation	34
Equation 5: Terzaghi Equation.....	35

1 - Introduction

1.1 Background

Understanding areas of source water has become a priority in Canada as concern for potable groundwater supplies has grown in the past decade ([TEC, 2004](#); [Rivera et al., 2005](#)). In southern Ontario, moraines are prominent topographical features of the landscape and some of these glacial deposits have proven to be excellent areas for aquifers. A three-dimensional (3D) understanding of the subsurface geology and accessibility to a consistent hydrostratigraphic model is necessary in order to adequately model groundwater flow within these aquifers. However, these aquifers frequently comprise intricate sediment bodies consisting of highly heterogenous materials that are difficult to reconstruct and model in three dimensions. This is especially true for the Waterloo Moraine, one of the most complex glacial deposits in southern Ontario, and the source for groundwater in the Regional Municipality of Waterloo (RMOW) ([Figure 1-1](#)).

Rapid facies changes, heterolithic bedding and a potential for an excessive amount of deformation prevent simple lateral stratigraphic correlation of borehole data. To effectively map complex glacial deposits, a knowledge-driven approach is required to understand the internal distribution of sediment facies and structures within complex deposits, such as in the Waterloo Moraine envelope. The internal sedimentology of stratified moraines have more recently become the focus of scientific investigations to develop depositional models (e.g. [Russell & Arnott, 2003](#); [Russell et al., 2007](#)) which are needed to understand the subsurface geology from limited information (i.e. [Sharpe et al., 2002](#); [Bajc & Shiota, 2007](#)).



**Figure 1-1: Location of the study area within southern Ontario;
inset shows location within Canada**
Produced using GRCA data

The method used to study sedimentary basins and the internal assemblages of sedimentary deposits is generally referred to as *basin analysis*, and was originally developed by petroleum geologists to increase the success rate of exploration programs and to better characterize hydrocarbon reservoirs ([Sharpe et al., 2002](#)). The basin analysis approach can also be applied to hydrogeology. It consists of integrating various sources of stratigraphical and sedimentological information (e.g. stratigraphic sections, borehole databases, field data) in order to determine the most appropriate conceptual depositional models and to reconstruct the evolution of a basin and its internal characteristics. This information is then used to help build geologically consistent hydrostratigraphic models that are the framework of

groundwater flow models. This procedure is an iterative process that eventually leads to the quantitative understanding of groundwater flow systems ([Figure 1-2](#)).

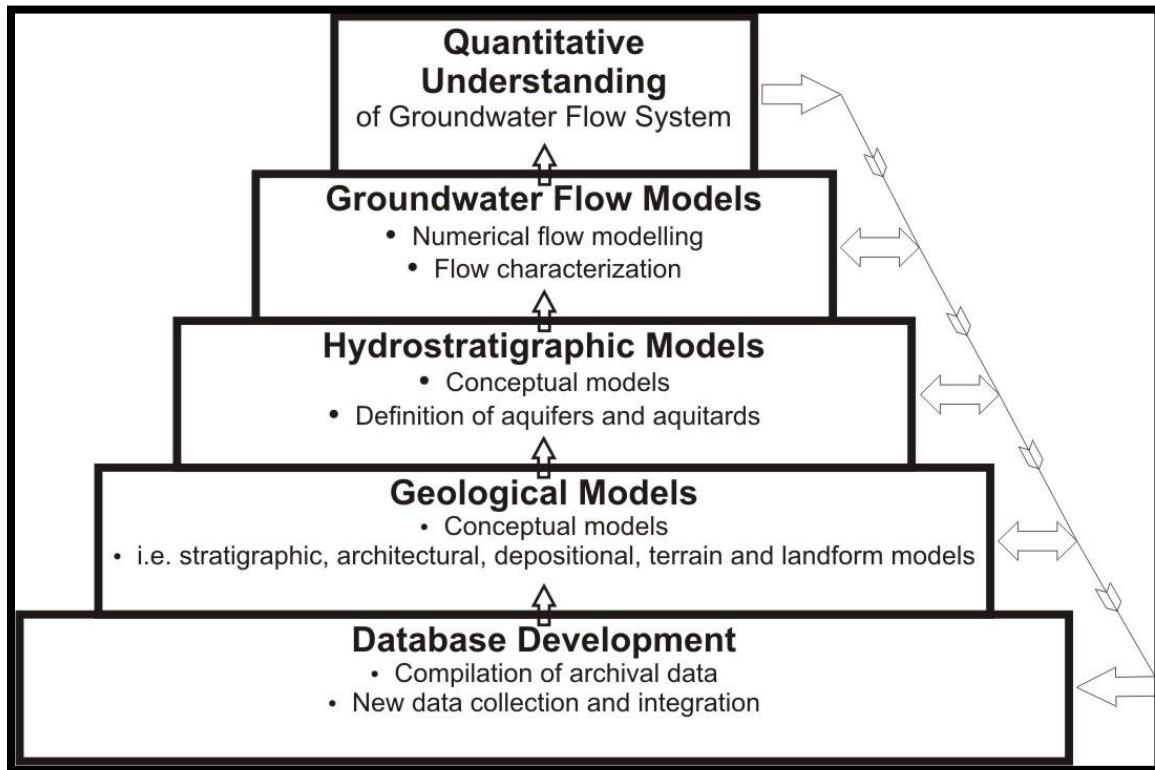


Figure 1-2: A simplified flow diagram used in the basin analysis approach
Redrawn and modified from Sharpe et al., 2002

Depositional models are a schematic representation of what is expected in terms of sediment assemblages in a particular environment and are generally based on a large number of investigations from around the world ([Walker and James 1992](#)). The models continue to evolve as new investigations may provide insights that lead to changes and refinement. These models may be used as a guide or predictive tool to produce more consistent or robust geological and groundwater flow models ([Miall, 2000](#); [Sharpe et al., 2002](#)). As pointed out by [Ross et al., 2005](#), this knowledge-driven approach is a much more powerful alternative to the direct interpolation of subsurface data (e.g. [Klingbeil et al., 1999](#); [Bellian et al., 2005](#)). However, the paucity of detailed sedimentologic data, especially subsurface data, adds to the

complexity of the problem. How to determine which depositional model is suitable for an area when the sedimentology of the deposit is poorly documented? One approach in overcoming this limitation is to extract as much information as possible from surface exposures and use that knowledge to improve analysis of near-surface data (e.g. GPR, seismic data) and to develop detailed reconstructions of the near-surface environment. The assumption is made that this effort can provide an accurate representation of the vadose zone environment that are potential analogs to comparable sedimentary features identified at greater depth into the saturated zone. The detailed reconstructions are thus used to better constrain the deeper and less accessible parts of the aquifer system. This approach has proved to be useful in other glacial settings ([Kostic et al. 2005](#)) and is here referred to as the *multi-scale aquifer analogue approach*.

1.2 The Multi-Scale Aquifer Analogue Approach

Traditionally, hydrogeologists have gathered hydraulic data from different well measurements and tests to estimate key values like hydraulic conductivity (i.e. [Hvorslev, 1951](#); [Bouwer & Rice, 1976](#); [Rehfeldt et al., 1992](#)). Different mathematical approaches are then used to interpolate these values between the control points (i.e. [Binley et al., 2001](#); [Odong, 2008](#)). Although this can work in simple settings, it is difficult to obtain geologically consistent representations in more complex sedimentary sequences. One type of sedimentological information which is rarely used in hydrogeologic investigations is obtained from the study of surface outcrops. The use of this information for characterizing aquifers is based on the premise that multiple excavations in an area are likely to expose the stratigraphic units and internal sediment characteristics that are representative (or analogous) to those forming the aquifer at depth. [Figure 1-3](#) illustrates this concept. This approach is generally referred to as the aquifer analogue approach (i.e. [Whittaker & Teutsch, 1999](#); [Heinz & Aigner, 2003](#); [Kostic et al., 2005](#)). By combining information from boreholes and excavations, as well as geophysical surveys, it is possible to develop an understanding of the stratigraphy and sedimentology of an aquifer at multiple scales and describe the aquifer in a way that is relevant to hydrogeology.

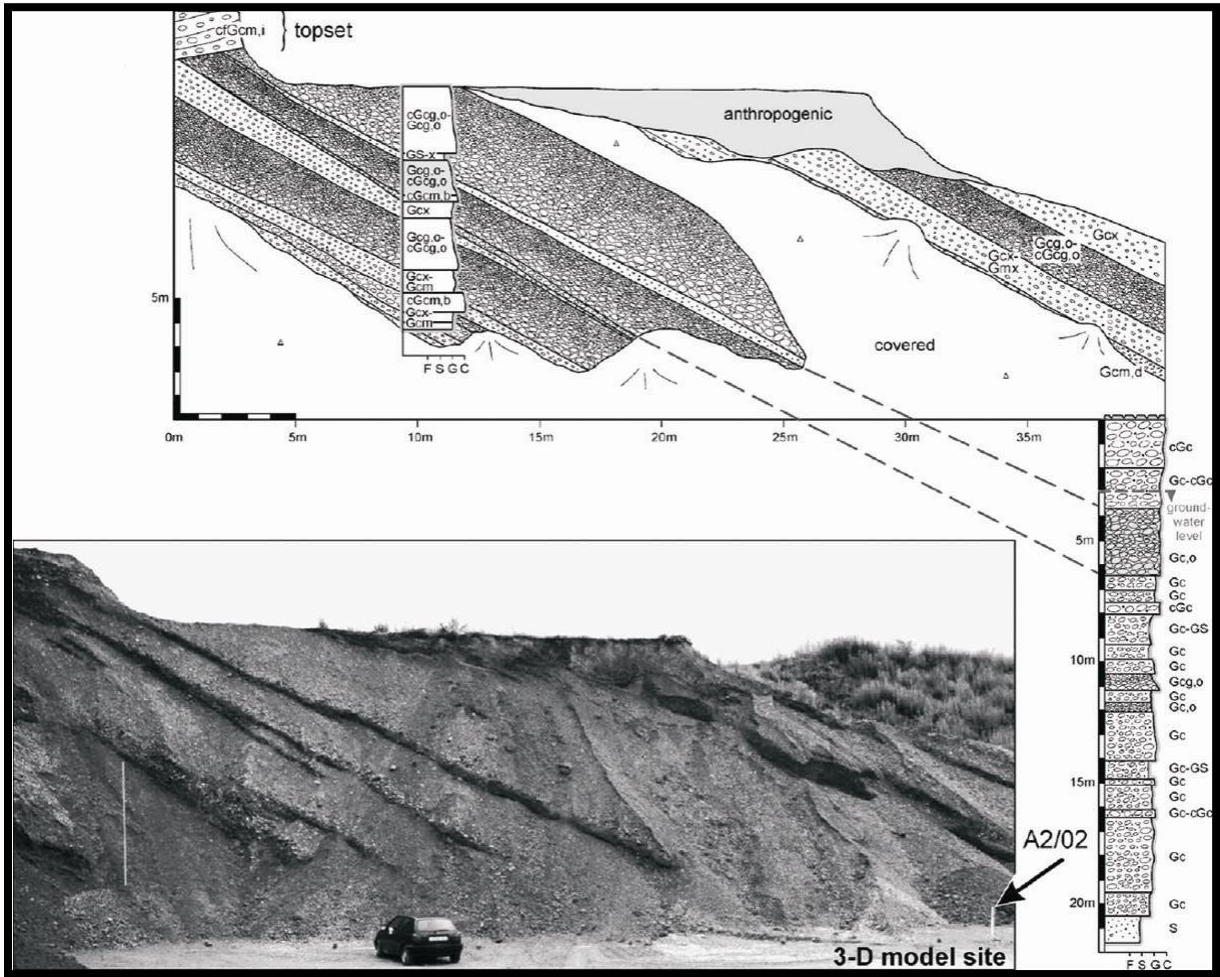


Figure 1-3: An illustration depicting the Aquifer Analogue Concept

Interpreted facies (top) from a documented outcrop (bottom) linking to the subsurface units defined by a borehole log (right). From Kostic et al., 2005

This process of linking sedimentologic data at various scales with hydrogeologic applications has been used in a number of studies and is sometimes referred to as aquifer-sedimentology (i.e. [Huggenberger & Aigner, 1999](#)), or dynamic stratigraphy (i.e. [Heinz & Aigner, 2003](#)). The main motivation for using these techniques is that if we understand more about the sedimentology of an aquifer, we learn more about the geologic controls on heterogeneity and the processes that may have created them. This approach leads to a predictive model that can be used to constrain interpolation techniques, and to better hydrostratigraphic representations.

The six scales proposed by [Heinz & Aigner \(2003\)](#) and illustrated in [Figure 1-4](#) are: 1) particles and pores (micro scale), important in the geochemistry of groundwater; 2) strata (meso scale), also known as hydrofacies, forming the smallest mappable hydrostratigraphic units; 3) depositional elements (macro scale), also known as architectural elements dominating the hydraulic conductivity of an aquifer; 4) facies bodies (mega scale), representing the compartments of an aquifer; 5) genetic sequences (mega scale), creating the separation of aquifer units; and finally 6) basin fill (giga scale), the complete assemblage of all the results and interpretation into their broader regional context.

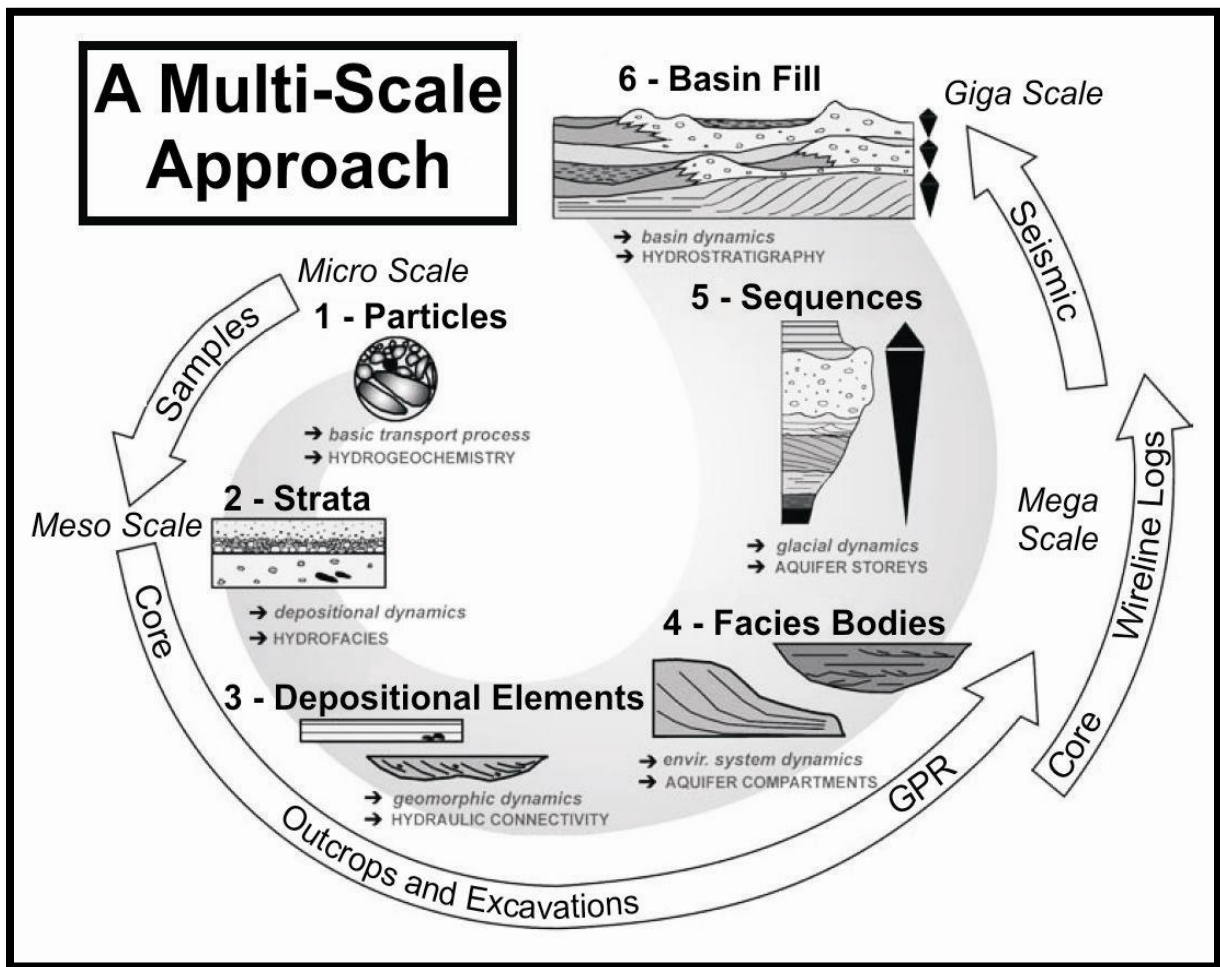


Figure 1-4: The concept of using a multi-scale approach in sedimentary deposits and its relation to hydrogeologic applications
 Modified from Heinz & Aigner, 2003

However, this multi-scale approach is rarely used in a way that allows the detailed descriptions of sedimentary sections to be stored in a georeferenced database. Here we argue that there is a real advantage in georeferencing all such information. For example, boreholes provide one venue of looking into the geology of the subsurface, but the data is generally stored in digital databases that do not offer the possibility visualizing the samples. It is thus difficult to apply Quality Assurance and Quality Control (QA/QC) checks on these records. In addition, one cannot go beyond the level of details provided by the database. There is therefore a need to develop a new generation of databases whereby the material being described can also be visualized by experts using the data. With technological advances providing relatively affordable technology in data collection, geological modeling and visualization ([Ross et al., 2005](#); [Paton et al., 2007](#); [Kessler et al., 2009](#)), it has become feasible to develop such databases. These databases can then be used to build complex models in a reasonable amount of time. Traditional techniques such as stratigraphic logging, strike and dip measurements and photomosaic mapping, can be combined with data from methods in surveying and GPS systems to acquire the three-dimensional data needed to create a model ([Thurmond, 2004](#)). In fact, 3D modeling techniques are essential for the mapping of glacial sediments for hydrogeologic studies due to their inherent complexity ([Venteris, 2007](#)).

1.3 Purpose of Study

The main goal of this study is to develop and test an approach to collect georeferenced sedimentologic information from surficial excavations, store this information in a 3D system, and use it for sedimentologic and hydrostratigraphic analyses. More specifically, the objectives are to:

- a) Describe and analyze the lithofacies along a series of sections in an excavation in part of the Waterloo Moraine and relate them to hydrofacies characteristics;

- b) Generate virtual sections and curvilinear grid models of the facies architecture, and integrate geophysical data (GPR), field measurements (e.g. paleoflow), and laboratory analyses (e.g. grain size data). This data will form the building blocks of a 3D geodatabase;
- c) Investigate the facies proportions from the curvilinear grids;
- d) Compare borehole data in the vicinity of the pit against the sedimentologic observations made in the pit (objective A) in order to determine whether the facies proportions in the borehole database are similar to observations;
- e) Evaluate the feasibility of the approach for sub-watershed investigations in terms of technological and time constraints, costs, and scaling issues.

1.4 Study Area

The study area is located in the Alder Creek Watershed, specifically a section of the Waterloo Moraine, to coincide with on-going hydrogeological study by J.P. Jones and M. Sousa at the University of Waterloo. The Alder Creek is a tributary of the Nith River, and is part of the Grand River watershed that drains into Lake Erie ([Figure 1-1](#)). Aggregate pits are abundant in the ice-marginal moraines of southern Ontario because many contain large volumes of sand and gravel, which are accessible close to the ground surface. These deposits, which also generally make up the aquifer systems, are counted on for groundwater resources. These pits provide an excellent place for study as they give a glimpse into the structure of the glacial deposits. All of the work done for this study was conducted at Kieswetter Holdings, a sand and gravel extraction company that has been in operation on Bleams Road in Kitchener for several generations. This pit is located within the Waterloo Moraine and along the boundary of the Alder Creek basin ([Figure 1-5](#)). The pit is modestly-sized, providing great potential for study while being subject to little interference from

everyday operations. Kieswetter Holdings is located just south of the hamlet of Mannheim, which is home to Waterloo Region’s artificial aquifer recharge facility ([RMOW, 2009](#)). This water treatment plant pumps raw water from the Grand River and releases treated water into the Waterloo Moraine, which houses the local aquifer system.

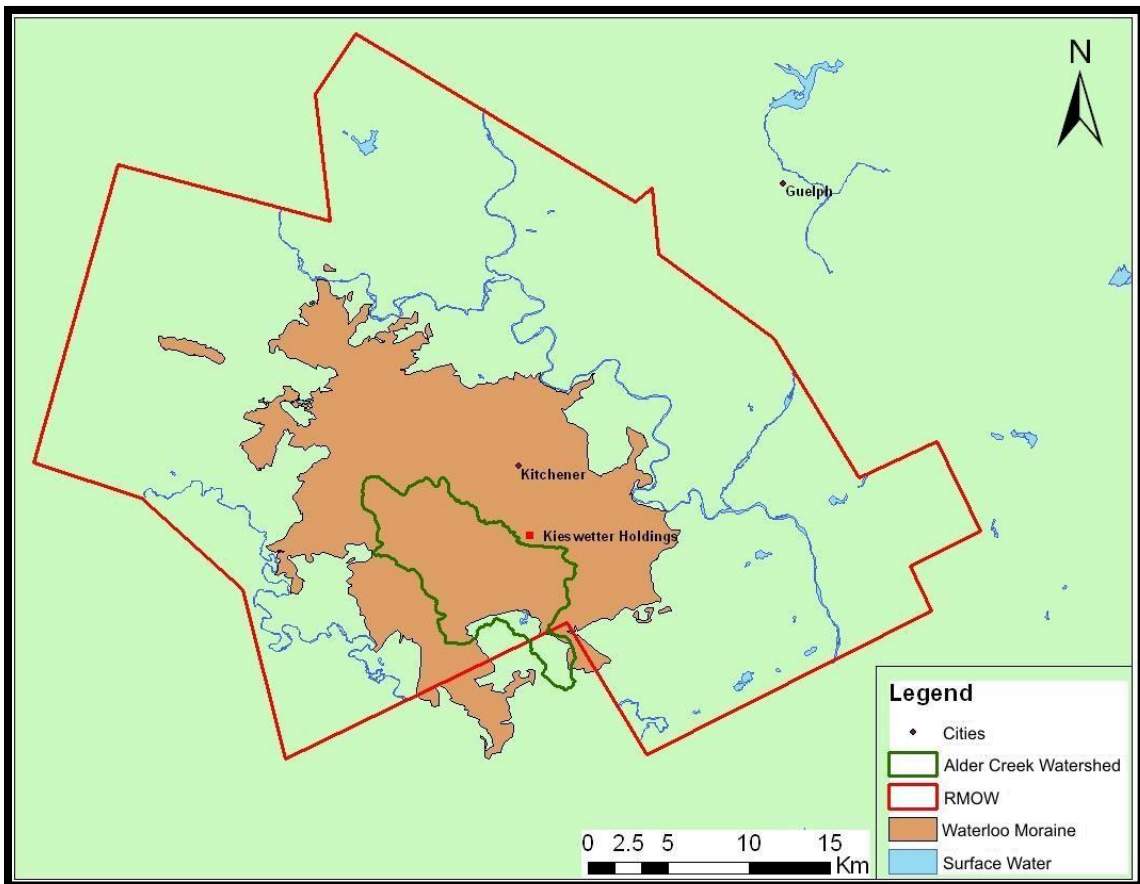


Figure 1-5: Location of the Alder Creek watershed and the study site Kieswetter Holdings in relation to the Waterloo Moraine and Waterloo Region
Produced from GRCA GIS data.

2 - General Setting of Study Area

2.1 The Waterloo Moraine

2.1.1 Physiography and Geology

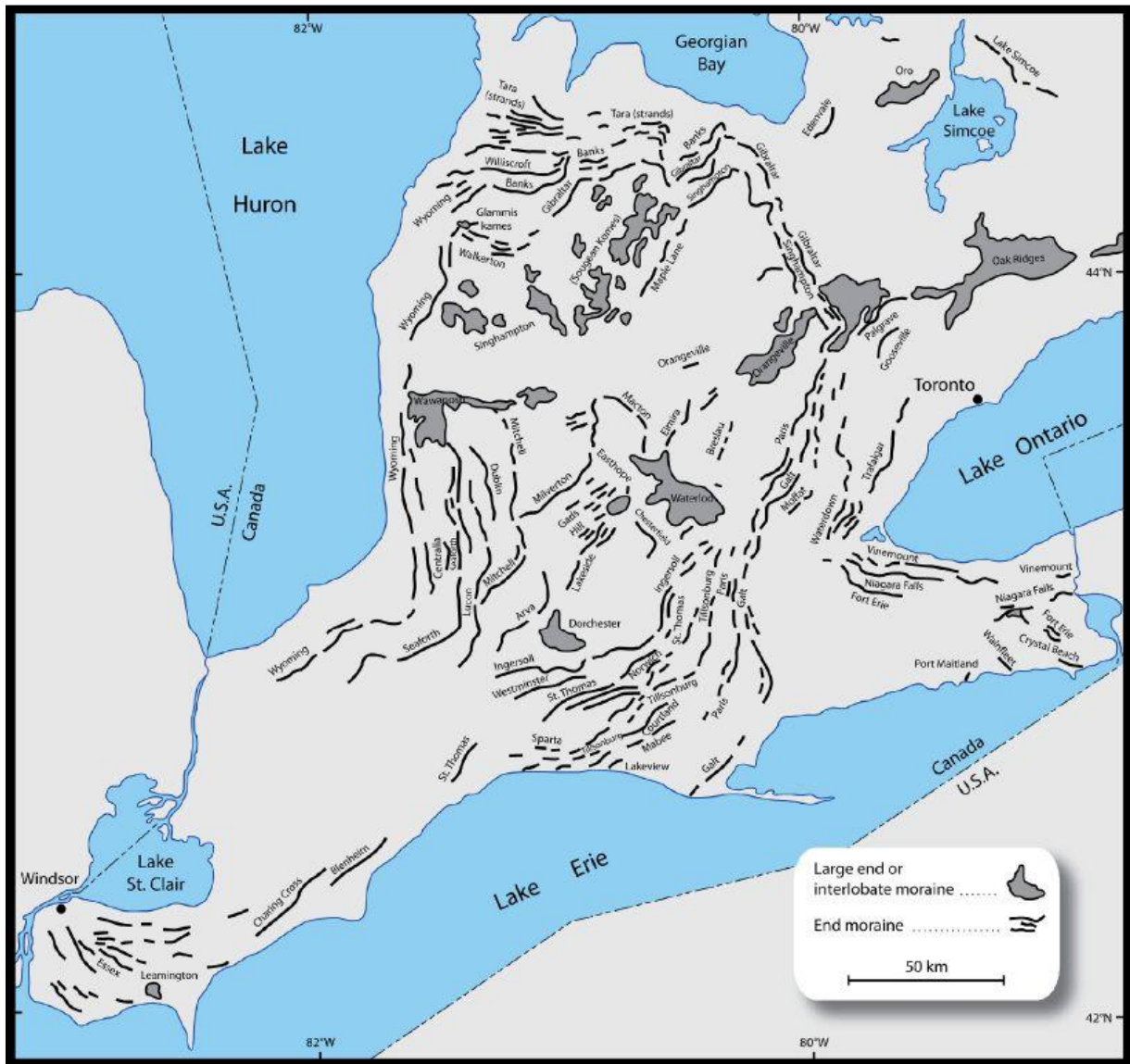


Figure 2-1: The location of moraines in southern Ontario
From Russell et al., 2009; redrawn from Barnett et al., 1991.

Southern Ontario is an area of Canada that is characterized by an extensive and generally thick cover of Quaternary sediments that for the most part were deposited during the last glaciation ([Barnett et al., 1991](#)) with the final retreat of the ice sheet leaving the area about 13,000 years BP ([Karrow, 1993](#)). As seen in [Figure 2-1](#), some of these glacial deposits are described as moraines, first mapped by [Taylor \(1913\)](#) and further classified on the basis of their composition by [Chapman & Putnam \(1943, 1984\)](#). The surficial geology of the Waterloo Moraine area has been mapped by Karrow ([1987, 1993](#)) while [Martin & Frind \(1998\)](#) presented the first reconstruction of its subsurface geometry at regional scale for hydrogeologic applications. With increasing awareness and the need to understand and protect source water areas ([TEC, 2004](#)), the Ontario Geological Survey (OGS) embarked on a regional three-dimensional mapping project that resulted in the release of a new regional reconstruction of the stratigraphic architecture of the area ([Bajc & Shirota, 2007](#)).

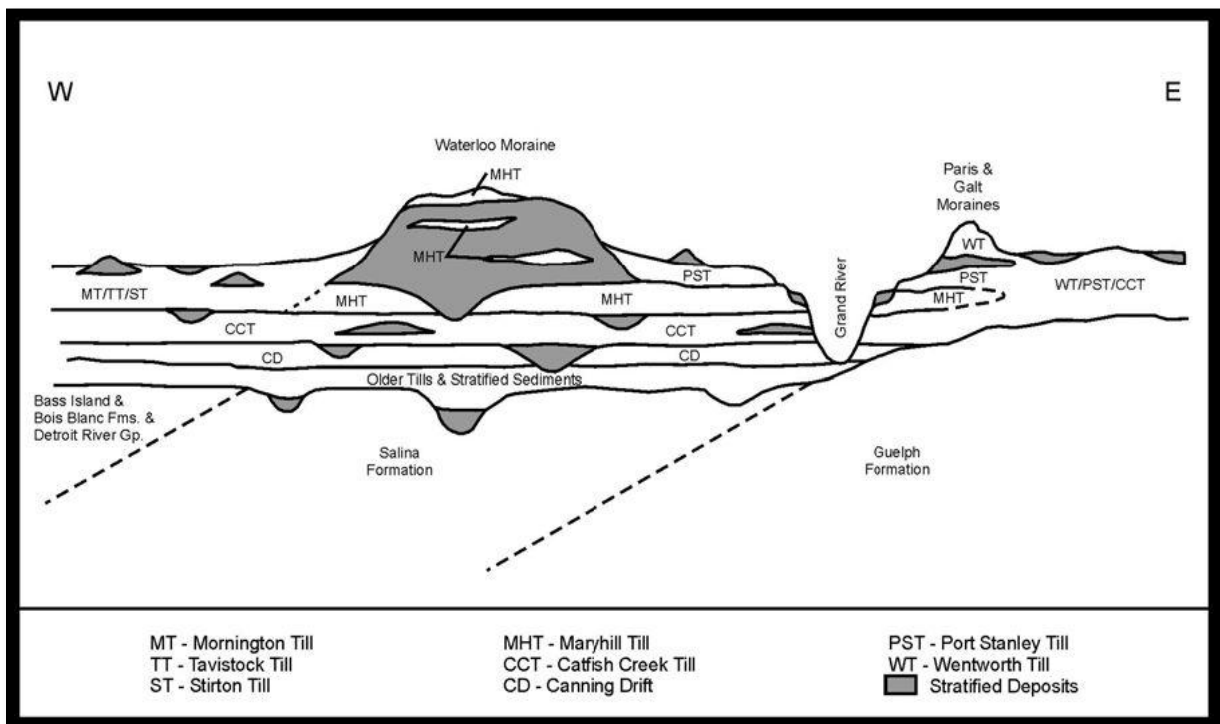


Figure 2-2: Conceptual geological model of Waterloo Region
From Bajc et al., 2004

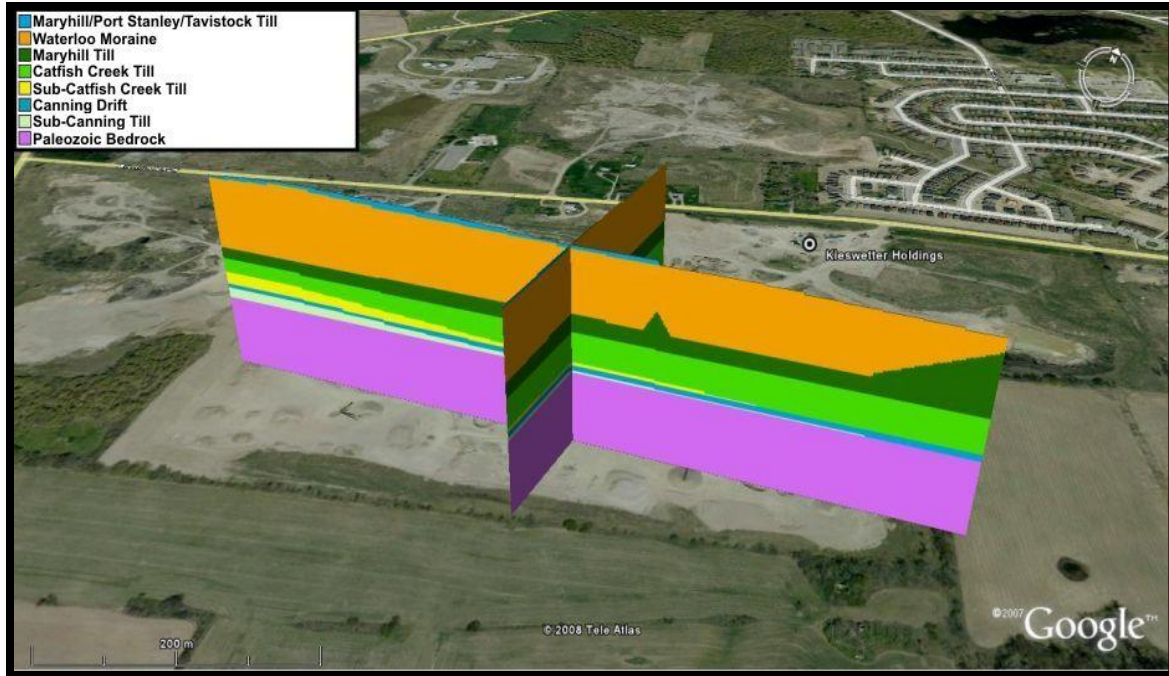


Figure 2-3: A 3D representation of the full subsurface stratigraphy at Kieswetter Holdings from a Google Earth application (Modified from Bajc & Shirota, 2007)

This reconstruction provides more constraints on the regional stratigraphic architecture of the Quaternary basin fill, which consists of several units that include the Waterloo Moraine, Catfish Creek Till and several other units ([Figure 2-2](#)). Although these models are of great value, they do not provide information on the internal structures and sediment properties of any individual unit. The internal stratigraphy of the Waterloo Moraine is more complex, differing from the regional stratigraphy of the area and taking up approximately 50% of the drift thickness ([Figure 2-3](#)). It also contains the most important aquifer units in the region. Drift thicknesses in the Waterloo Moraine area range from 40 to 140 metres (m); Kieswetter Holdings rests on an estimated 100 meters of drift ([Figure 2-4](#)). Much remains to be done to understand and reconstruct the internal architecture and sediment properties of the Waterloo Moraine. The challenge is significant, which partly explains why the Waterloo Moraine has only recently become a focus of more detailed sedimentological and hydrogeological studies at the watershed scale (e.g. [Frind et al., 2006](#); [Russell et al., 2007](#)).

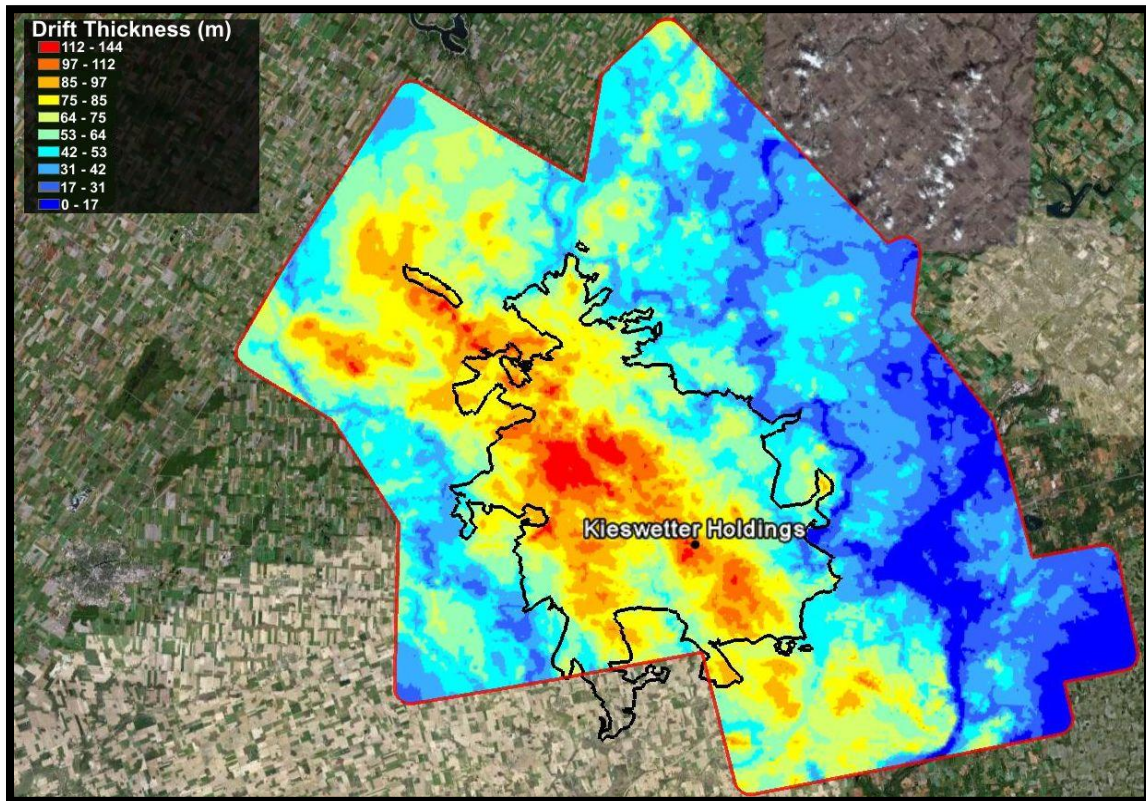


Figure 2-4: Drift thickness in the Waterloo Region
 Modified from Bajc & Shirota, 2007

The Waterloo Moraine is a large ice-contact sediment complex that is located in central southwestern Ontario and is generally contained within the boundaries of the Regional Municipality of Waterloo ([Figure 1-1](#)). The Moraine covers 400 square kilometers (km²) in area with topographic highs up to 420 metres above sea level (m.a.s.l.), and is very hummocky in nature with relief up to 50 metres in some areas. The origin of the moraine is thought to result from the interactions of three converging ice lobes: the Georgian Bay, Ontario/Erie and Huron lobes of the Laurentide Ice Sheet (LIS) and their associated meltwater inputs. [Karrow \(1993\)](#) classifies the Waterloo Moraine as being a kame moraine. The moraine overlies the regional Catfish Creek Till. It has a core of sand and gravel and is partly capped by deglacial tills such as Port Stanley Till. The Waterloo Moraine does outcrop at the surface but also underlays pockets of till ([Figure 2-5](#)) while overlying the

Maryhill Till ([Figure 2-2](#)). According to this reconstruction, the moraine was overridden on its sides by the fluctuating ice lobes prior to their final retreat from the area.

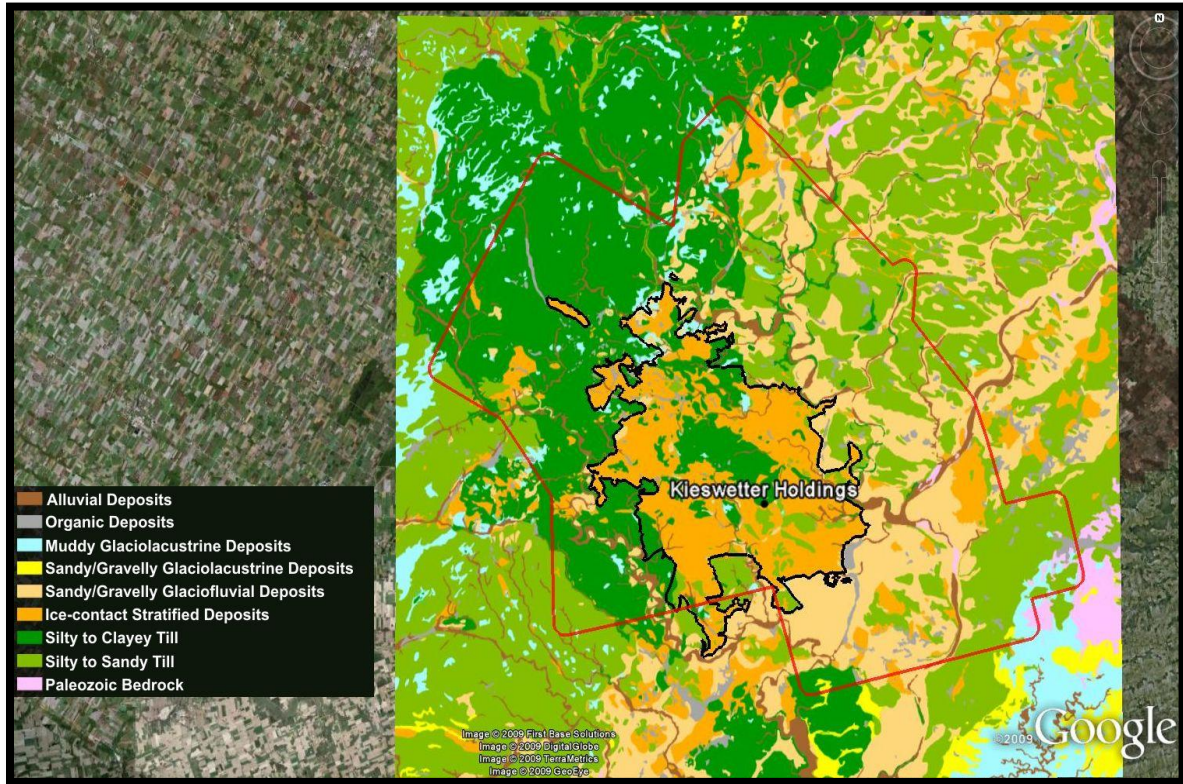


Figure 2-5: Surficial geology of the Waterloo Region and Waterloo Moraine
Modified from Bajc & Shirota, 2007

[Karrow \(1993\)](#) also includes several projections to be a part of the Waterloo Moraine, such as the Washington Spur to the southwest, the Philipsburg Spur to the west, the Crosshill Spur to the northwest and the gravel-rich Hawkesville Spur to the north ([Figure 2-6](#)). [Karrow & Paloschi \(1996\)](#) produced the first stratigraphic cross section of the Moraine and suggested that the moraine was formed during the Port Bruce Phase due to the incorporation of Maryhill Till throughout the Waterloo Moraine. Recent sedimentary studies of the Waterloo Moraine present it as a stratified moraine displaying high-energy deposits which are a result of high-energy, voluminous events associated with a sub-aqueous fan system ([Russell et al., 2007](#)). The moraine appears to be very similar in composition to the Oak Ridges Moraine, a

physiographic feature that extends for 160 kilometres (km) from the Niagara Escarpment eastward to the vicinity of Trenton and is up to 20 km wide and up to 160 m thick ([Figure 2-1](#)). The Oak Ridges Moraine is believed to have been formed by a series of episodic meltwater discharges best illustrated by a jet-efflux subaqueous fan model ([Russell & Arnott, 2003](#)).

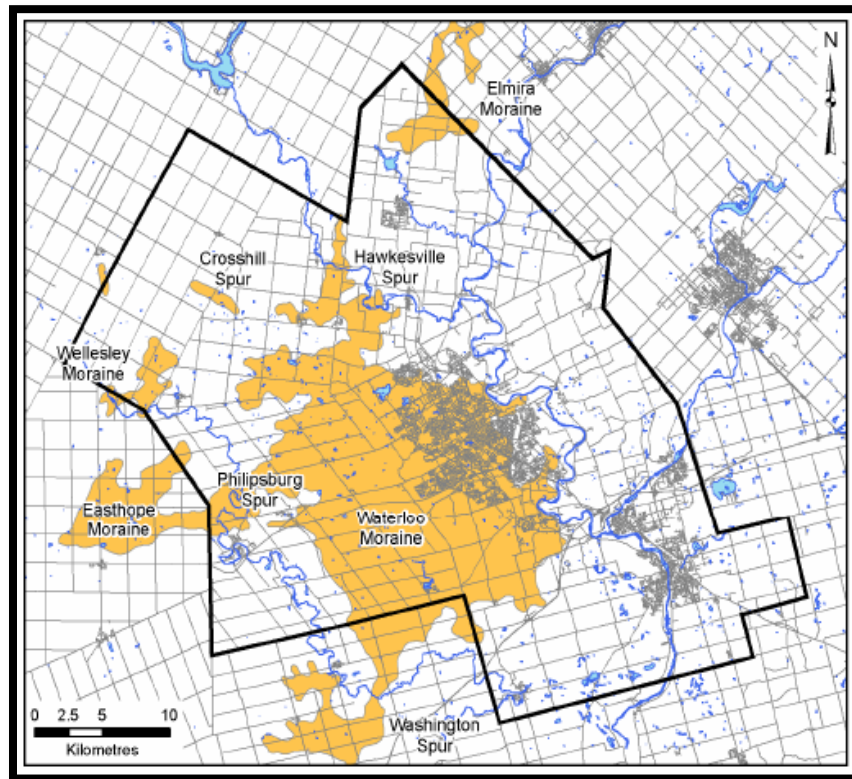


Figure 2-6: Location of the spurs associated with the Waterloo Moraine
From Bajc & Shirota, 2007

However, the Waterloo Moraine is generally described as a highly intricate, stratified deposit which origins have yet to be fully understood ([Karrow, 1993](#)). According to [Karrow & Paloschi \(1996\)](#), the Waterloo Moraine consists of a core of sand and gravel with interbedded fine-grained diamictic units, generating an extensive and complex aquifer/aquitard system ([Martin & Frind, 1998](#)). More than one depositional environment may have been involved in the formation, and there are thus many unanswered questions about the origin of the

Waterloo Moraine. Additional sedimentological studies are needed to improve knowledge on the aquifer architecture, heterogeneity and future groundwater modeling ([Russell et al., 2007](#)).

2.1.2 Hydrogeology

The aquifers within the Waterloo Moraine provide approximately 75% of the water used in the Regional Municipality of Waterloo, which equates to a pumping rate of about 110,000 m³/ day ([Frind et al., 2006](#)), making it a very important source of groundwater recharge for the Waterloo Region ([Figure 2-7](#)). The Region then pumps water from these aquifers deep within the Waterloo Moraine for use, such as well K26, located near the village of Mannheim (<http://region.waterloo.on.ca>). This region is forecasted to grow at 1.55% per annum for the next 30 years ([RMOW, 2006](#)); therefore, the collection of hydrogeological data is needed to ensure the proper source water protection and planning for this Region ([TEC, 2004](#)). The Waterloo Moraine is undoubtedly one of Ontario's most significant regional aquifers, but the stratigraphy is very complex and hydraulic conductivity is exceptionally variable throughout the deposit ([Bajc & Shirota, 2007](#); [Martin & Frind, 1998](#)).

The hydrostratigraphy is generally simplified for modeling and conceptual purposes ([Figure 2-8](#)). [Martin and Frind \(1998\)](#) were the first to discuss the hydrostratigraphy of the Waterloo Moraine as a complete system all the way down to bedrock with four general aquitard and four general aquifer units. The Waterloo Moraine was not depicted as a distinct, separate feature. [Martin and Frind \(1998\)](#) further remark that the uppermost aquifer, Aquifer 1 (the Waterloo Moraine), is thought to include reworked Maryhill Till and is the most extensive and regionally continuous unit as well as the most productive source of water while lower aquifers are discontinuous pockets of reworked glaciofluvial deposits. Recent hydrogeological study of the Waterloo Moraine by [Bajc & Shirota \(2007\)](#) has attempted to define aquifer vulnerability and recharge areas of the Waterloo Moraine. This work was to help preserve the quality and sustainability of the groundwater resources through understanding the stratigraphic architecture of the geologic units that hold water. Creation

of a three-dimensional model improved on the hydrostratigraphic model with the goal of improving understanding of the geologic controls on the distribution of recharge and discharge areas at the regional scale.

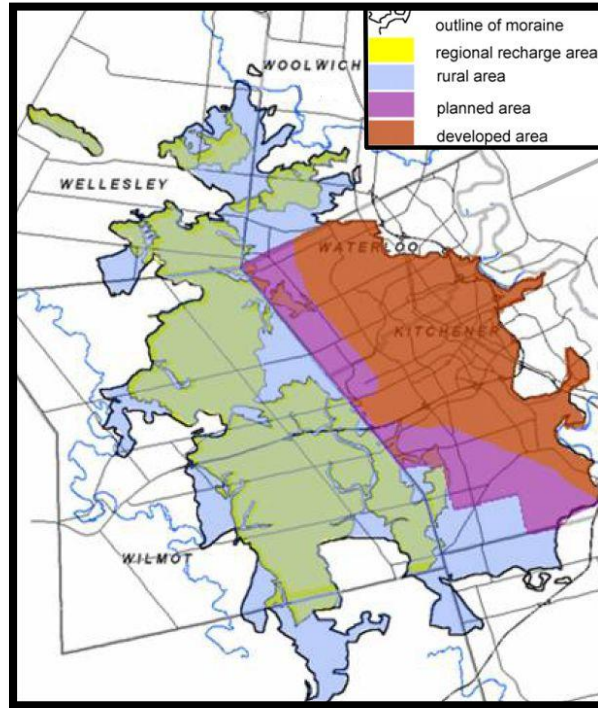


Figure 2-7: Recharge and developed areas of the Waterloo Moraine
Modified from RMOW, 2007.

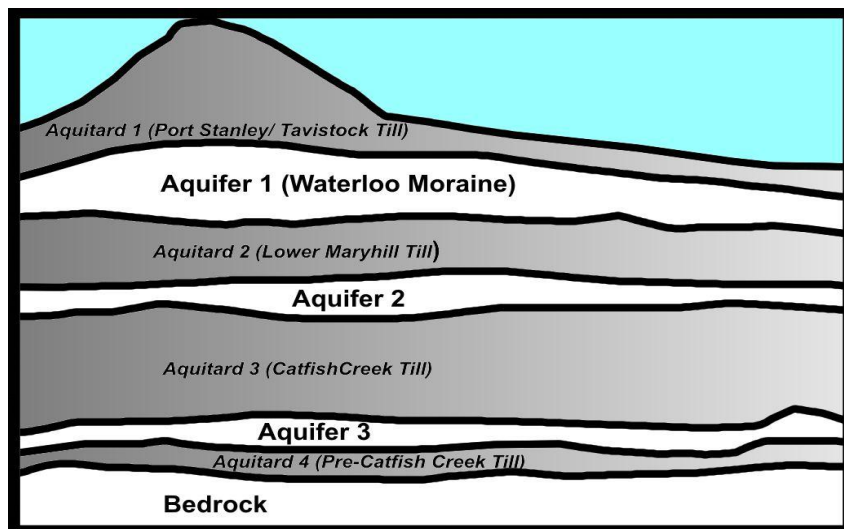


Figure 2-8: The simplified hydrostratigraphy for the Waterloo Region
Redrawn and modified from Martin & Frind, 1998

3 - Methodology

3.1 Archival Data Collection

3.1.1 Stratigraphic Model and Borehole Record

To set the foundation needed to develop any model, the collection of archival data is imperative. The data collected for this study was saved and put into the 3D modeling program gOcad Suite 2.5.2 (<http://www.pdgm.com/products/gocad.aspx>). For archival data, the work done by [Bajc & Shiota \(2007\)](#) provided a great deal of the information due to its extensive borehole database and the 3D stratigraphic interpretation of the Waterloo Region. This model is a simplified representation of the stratigraphy in the RMOW, from surface to bedrock; however, the model designates the Waterloo Moraine as a single unit. The borehole database was narrowed down to 50 logs in the area around Kieswetter Holdings by defining the limits of an area between the Universal Transverse Mercator (UTM) coordinates of northings 4804000-4805500m and eastings of 538000-540000m in UTM Zone 17.

3.1.2 GIS

The use of geographic information systems (GIS) is ideal for displaying the location of any data. Google Earth and Environmental Systems Research Institute's (ESRI) ArcGIS suite were the two programs employed to present geographical information. Google Earth is a simple, user-friendly program, and the GIS work presented by [Bajc & Shiota \(2007\)](#) utilized this tool. Generating complex maps is best done using the ArcGIS software but the operation of this software requires some significant training. Direct GIS data was acquired from the Grand River Conservation Authority (GRCA), including information regarding watersheds and political boundaries for the Region, and from GeoBase, the Canadian national GIS archive (<http://www.geobase.ca>).

3.1.3 Groundwater Model Grid

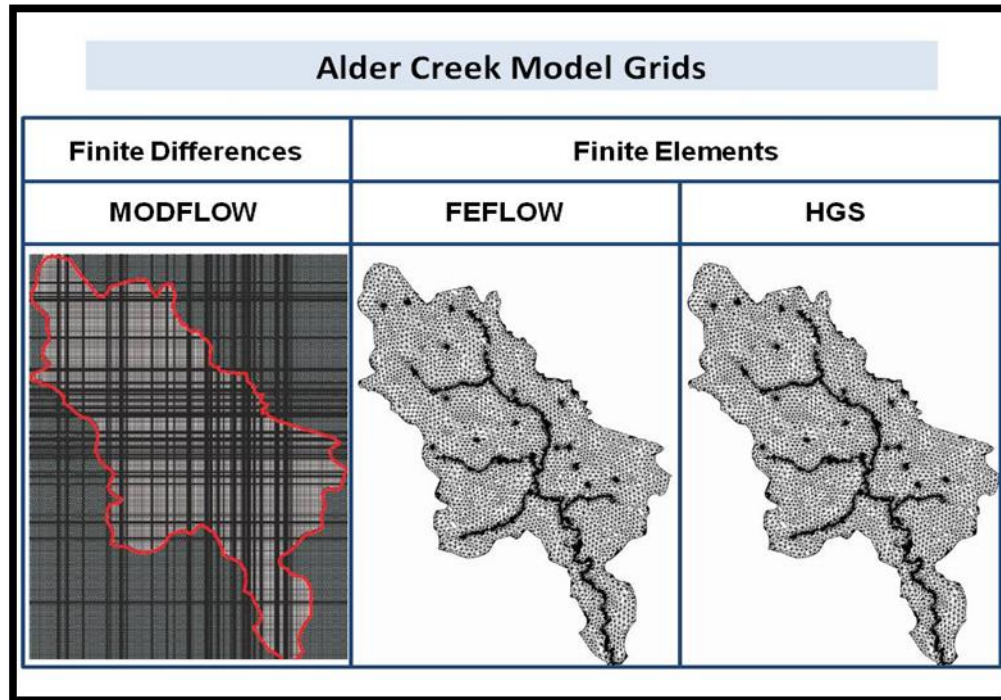


Figure 3-1: Comparison of groundwater modeling cells used for study on Alder Creek
From M.Sousa, personal communication

Current groundwater modeling uses computer programs to estimate groundwater flow. For work done on Alder Creek, there are three programs being used: MODFLOW (U.S.G.S. MODular three-dimensional finite-difference groundwater FLOW model) ([Harbaugh et al., 2000](#)), FEFLOW (Finite Element subsurface FLOW system) ([Diersch, 2006](#)), and HGS (HydroGeoSphere; [Therrien et al., 2006](#)) ([Figure 3-1](#)). Each cell in a groundwater model has its own properties with values attached. In this research, the results from the sedimentologic investigation would be evaluated to assess if the density of cells and elements covering the study area, along with their associated properties, were sufficient in groundwater modeling applications.

3.2 Field Data Collection

Recent developments in geospatial technologies are changing the way we acquire, visualize, and analyze geological data at all scales ([Wawrzyniec et al., 2007](#)). Modern surveying

techniques that collect geospatial information at the scale of observation include differential global positioning systems (GPS), total station surveying, and digital photogrammetry (e.g. [Hodgetts et al., 2004](#)), all of which utilized in this study. Georeferenced data points were acquired at the Kieswetter Holdings sandpit using these methods. Although the points will be positioned with high precision, the density of points obtained is expected to be insufficient to reproduce the exact detail of the exposed outcrop. However, sections can be broken into several different regions to honour their true orientation and to minimize the radial distortion in the images. This is believed to provide sufficient accuracy to reconstruct the stratigraphic architecture at the scale of the sandpit at a much more affordable cost than with more expensive tools such as terrestrial LiDAR systems ([Stohr et al., 2009](#)).

3.2.1 Coordinate Positioning Survey Procedure

Each section studied at Kieswetter Holdings was positioned in three-dimensional space. The survey procedure involves the strategic use of both a GPS surveying system and a reflectorless total station surveying system. The procedure is outlined below and was first summarized in [Ross et al. \(2008\)](#). The methodology allows very accurate location control to the site and overcomes the problem of making survey measurements on cliff faces that are relatively fragile and not amenable to classical surveying techniques such as those involving placing survey rods on individual target survey locations.

3.2.2 GPS Surveying System

The main purpose of using a GPS is to provide very accurate UTM survey control by establishing at the site an accurate permanent benchmark that could then be used to establish temporary benchmarks near the sections of interest. A Z-Max RTK (Real-Time Kinetic) GPS Surveying System (Thales Navigation Inc.) is used in this study to provide centimeter level accuracy of surveyed locations ([Figure 3-2](#)). As with the process in other GPS systems, locations are determined by receiving and interpreting data sent by satellites that orbit around the Earth. Each satellite systematically transmits information about its identity, location and time to the GPS receivers on the ground, and then the ground location is calculated from this data in real time. The accuracy of the calculated location is dependent on the number of

satellites in view and their locations (i.e. the “constellation” of satellites) and therefore, accuracy of computed locations can change over time. “Mission planning” is performed to examine the constellation of satellites and identify, for each day, the best times to acquire GPS data.



Figure 3-2: Setup of the RTK GPS station, a Thales Navigation Z-Max GPS survey system

A permanent benchmark (KTBM1) was set up at a location just south of and above the pit in order to be safe from excavation disturbance and within reasonable distance of the study areas. The benchmark consists of a 4-foot long 1-inch diameter solid steel rod driven into the ground. To determine the UTM coordinates of this benchmark, the GPS system was used in a static mode. On September 14 2007, the GPS base station receiver was set up over the benchmark and allowed to remain stationary (i.e., be static), to record raw satellite data over approximately 2.5 hours. This data was then combined with raw satellite data acquired at

provincially and federally maintained receivers located at Port Weller, Kingston and Parry Sound, Ontario to calculate the actual location and elevation of the KTBM1 benchmark. The post-processing of these data sets was performed using the software GNSS Solutions version 2.00.03 (Thales Navigation, Inc.), and the calculated benchmark coordinates were determined to have an accuracy of 0.026 m horizontally and 0.04 m vertically at 95% confidence.



Figure 3-3: The rover unit for the GPS survey system with an attached Allegro computer controller

With the new known coordinates of the permanent benchmark, the GPS system was then used in RTK mode to establish a series of temporary benchmarks near the cliff faces that were being mapped. The temporary benchmarks were necessary for setting up the reflectorless total station system that obtained the actual cliff face coordinates. The first step in using the GPS system was to set up the GPS base station receiver on the KTBM1 location and use the known coordinates. A radio transmitter with a range of 5 to 10 km ([Figure 3-2](#)) was then used to transmit the appropriate correction factors to a second receiver on the “rover” unit ([Figure 3-3](#)), which used the correction factor along with its own satellite data that it was receiving to calculate its position in real time as the rover was moved from location to location (i.e., RTK). In essence, the coordinates of any location that was physically accessible to the rover could be measured by positioning the rover at the desired location and taking a reading. The GPS rover was used to obtain UTM coordinates for a temporary benchmark to within 0.015 m horizontally and 0.024 m vertically (relative to the permanent benchmark KTBM1).

The GPS survey system is superior to using the total station for establishing the coordinates for the temporary benchmarks because: (a) the GPS system can instantaneously provide coordinates (each reading took less than a minute) for any location within radio range (5 - 10 km) of the base; (b) temporary benchmark locations can be chosen without having to be within the line-of-sight of the permanent benchmark and, (c) there is no need to enter potentially dangerous areas of active mining within the sand pit to complete the survey (i.e., no need for traversing the sand pit with foresights and back sights typically necessary for total station work). The GPS system was not used to survey the actual cliff faces because cliff faces are relatively fragile (e.g., subject to collapse) and not amenable to techniques involving climbing on the cliff face or placing the rover (or even conventional survey rods) on individual survey locations. In some cases, the cliff face itself was not physically accessible or it was physically impossible to place the rover on survey locations (e.g. a spot under an overhang or halfway up a high cliff). A reflectorless total station surveying system was used to successfully survey those points.

3.2.3 Total Station Reflectorless Surveying System



Figure 3-4: A total station setup and ready to take measurements of a section

A Sokkia SET630R reflectorless total station survey system (Sokkia Co., Ltd.) was used to obtain the actual locations on an outcrop face ([Figure 3-4](#)). A total station survey instrument functions both as a theodolite and as an electronic distance meter (EDM). The theodolite capability of the total station enables measurement of both the horizontal and vertical angles of the scope as its orientation is changed to sight specific targets. The EDM provides measurements of distance from itself to a reflective target by sending a sophisticated series of electromagnetic waves in the direction of the visually sighted target and analyzing the reflected returning waves. If the total station is set up at a known location and with a known orientation (oriented by sighting on another known location), it can electronically combine the angle and distance data of a sighted point (target) to calculate the coordinates (northing, easting and elevation) of the point. The target may be a specially designed piece of reflector equipment like a prism on a rod, but for this project points were marked out in spray chalk on

the face or measured at the base of a metre-long scale stick. These targets, called a reflectorless measurement, were obtained without the use of a prism. Distance measurements using the reflectorless method of the SET630R are accurate to within ± 6 mm and this was the procedure used to obtain the coordinates on section walls. This method had the advantage that no rod (or rover) had to be held at the target location to obtain accurate coordinates at the point.

3.2.4 Combining the GPS and Total Station Methods

Both the GPS and total station systems were combined to obtain accurate location measurements of positions on the cliff faces from within the sand pit. First the GPS system was used to establish the UTM coordinates of the permanent benchmark, and then the GPS base station was placed over that known point. The GPS rover was then used to determine the UTM coordinates of several benchmarks (i.e. wooden stakes, painted stones) located throughout the pit, in sight of the cliff faces to be studied. The locations of these benchmarks were noted and programmed into a handheld GPS device to be located at a time when needed.

When a section was selected to be studied, the total station was set up in a position where it was in sight of both the section to be studied and at least four different benchmarks. Using the resection feature of the total station, the station calculated electronically where it was in UTM coordinates after sighting three different benchmarks and aligning them with their coordinates. The fourth benchmark was used as a check and to establish error. With the total station location established in this way, the operator could take reflectorless position measurements (UTM northing, easting and elevation coordinates) at any point on the nearby section face. Surveyed locations were marked by marker sticks representing stations ([Figure 3-4](#)), spray chalk, or natural targets (rocks, ridges etc.) present. Stations were labeled using two numbers representing the year of study, KI for the location of Kieswetter Holdings and followed by the station number (i.e. 07KI12 for 2007, Kieswetter Holdings and Station 12). Points surveyed with the total station had an approximately relative accuracy of 0.01 m

(horizontally and vertically) from a particular set-up location and had an approximate absolute accuracy in UTM coordinates of about 0.05 m horizontally and 0.075 vertically.

3.2.5 Digital Image Acquisition

High-resolution photographs of ten megapixels of the sediment sections were taken to capture detailed images of sediment layering and facies, and to be used later for photo draping on georeferenced surfaces (cf. [Geomodelling](#) work section). Under ideal conditions, the photograph is acquired by shooting in a direction that is perpendicular to the sediment section to minimize distortion. The part of a section to be included in a single photograph should be near vertical and without significant indentation. These conditions are generally not too difficult to find in active sandpits but may require multiple shots from different angles to acquire perpendicular images along the most extended and irregular sections. Precautions were taken to ensure that the target points used in the total station survey were visible on each of the photographs to facilitate the draping process. Better results would be achieved by making the corners of the photograph correspond exactly to target points, facilitating in the georeferencing of the image. When this is not possible, good results could be achieved by acquiring a sufficient number of location points to form a rectangle defining the outer limit of the photograph to be georeferenced.

3.2.6 Facies Documentation

[Boyce & Eyles \(2000\)](#) describe architectural element analysis as a methodology that emphasizes the description of lithofacies assemblages, their geometry as defined by their bounding discontinuities. A macroform, such as architectural elements, consist of genetically related lithofacies with sedimentary structures showing similar orientations and bounding surfaces that extend from the top to the bottom of the element and these series of facies constitute a facies assemblage ([Miall, 2000](#)). Architectural element analysis is an effective technique for describing heterogeneity in glacial deposits that involves documenting the facies observed in an outcrop at a scale large enough to determine the depositional history ([Miall, 1985](#)). Field notes were taken to record essential information about the elements, such as nature of bounding surfaces and internal geometry, seen at the research site.

Describing the sedimentary facies was based on the lithofacies classification created by [Miall \(1978\)](#) and found in [Appendix A](#). The documented details complemented the pictures taken at the sections for study and future interpretation.

3.2.7 Sedimentary structures

It is important in architectural analysis to measure the orientation of sedimentary structures such as ripples, dunes, and synsedimentary folds. This data adds an essential third dimension to two-dimensional outcrops ([Miall, 1996](#)), and provides information on the sedimentary conditions at time of deposition. Paleoflow measurements were taken using a traditional Brunton compass to record strike and dip of planar surfaces such as bedding planes, along with trend and plunge of linear features.

3.2.8 Ground Penetrating Radar



Figure 3-5: Conducting the GPR profile using a PulseEKKO 100A unit with 100MHz antennae

Ground-penetrating radar (GPR) is a non-invasive geophysical tool that transmits short pulses of electromagnetic waves (10 MHz – 1 GHz) into the earth. These propagating waves respond to changes in subsurface electrical properties, so that part of the signal is reflected back to the surface ([Davis & Annan, 1989](#)). In a sandy environment, reflected signals

recorded at the surface are generally interpreted as a reflecting interface (i.e., sedimentary boundary). A reflection profile is constructed by collecting data at regularly defined intervals along the transect and results in a two-dimensional image of the subsurface environment. Common-midpoint (CMP) soundings, on the other hand, systematically separate a transmitting and receiving antenna about a central point, which provides an estimate of subsurface wave velocity. Here, GPR surveys were performed using a separate transmitting and receiving antenna which allowed operation in both fixed-offset reflection profiling and multi-offset (CMP) modes. An extensive GPR profile was created using a PulseEKKO 100A unit with a 100MHz antenna ([Figure 3-5](#)) with the profile designed to help link the eastern and western part of the pit, connecting most sections together when viewing the subsurface stratigraphy. Processing of the data used the software package EKKOView Deluxe and was conducted by Dr. Anthony Endres at the University of Waterloo. Further detail on the GPR method can be found in [Davis & Annan \(1989\)](#) and [Neal \(2004\)](#).

3.3 Geomodelling Work

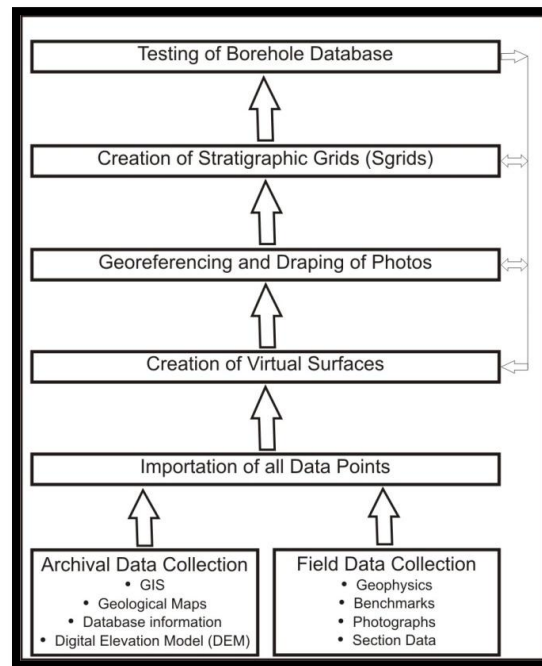


Figure 3-6: Workflow diagram illustrating the procedure exercised in creating the virtual sections used to test the borehole database

The virtual sediment sections were created using gOcad Suite 2.5.2 (Paradigm; <http://www.paradigmgeo.com>). The procedure, which can be seen in [Figure 3-6](#), starts with the collection of all available “old” data that is archived (i.e. geological maps, GIS, etc.) as well as the “new” data that was collected in the field (i.e. sections, benchmarks, etc.). All this information is digitized as a column-based ASCII file, or text file, and imported into the software. After the importation of these data points, they can be separated into different categories, or regions, depending on what the type of data it is ([Figure 3-7](#)).

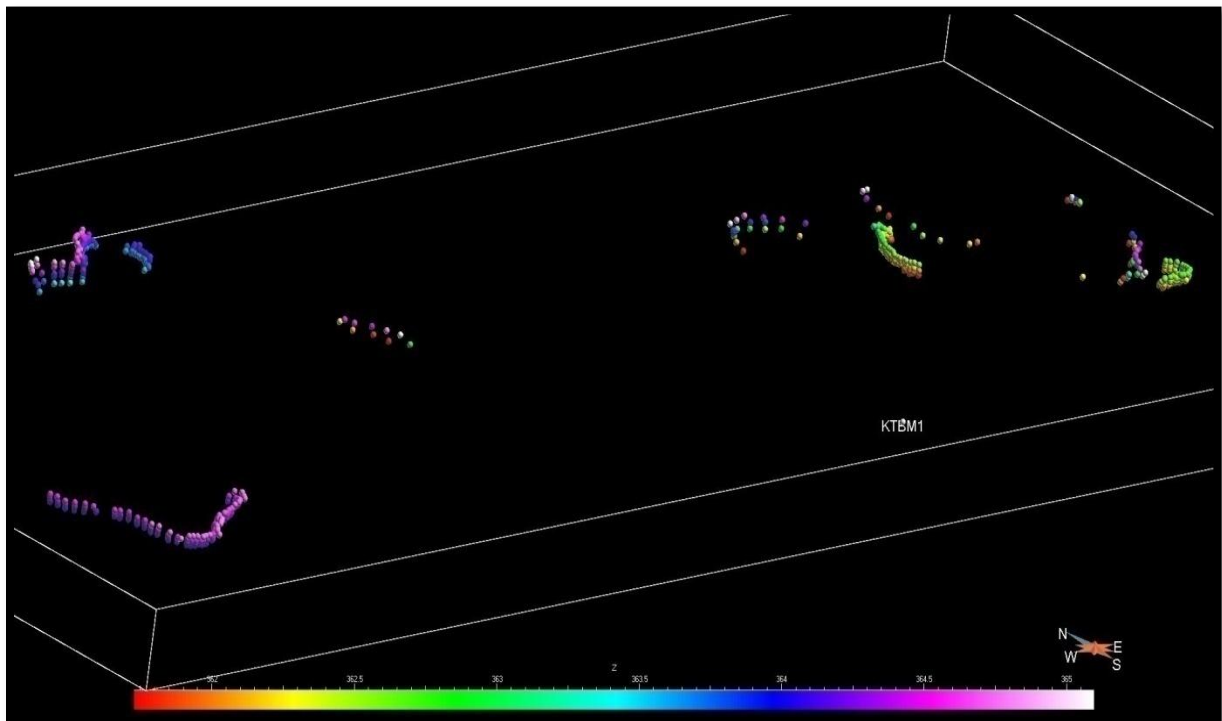


Figure 3-7: Georeferenced survey points in a 3D virtual environment coded by elevation

Each section had a collection of surveyed points that would aid in the creation of its 3D virtual representation. To begin, all the points for one section were used to create a surface ([Figure 3-8](#)) while triangles are used represent the space between each connected point. More triangles can be added by “splitting” them which is helped in interpolating the surface using the built-in *Discrete Smooth Interpolation* algorithm (DSI) (cf. [Mallet, 1989](#) for

details). Any bad triangles can be removed, especially along the borders and switch triangle orientations where necessary to improve the 3D representation of the section.

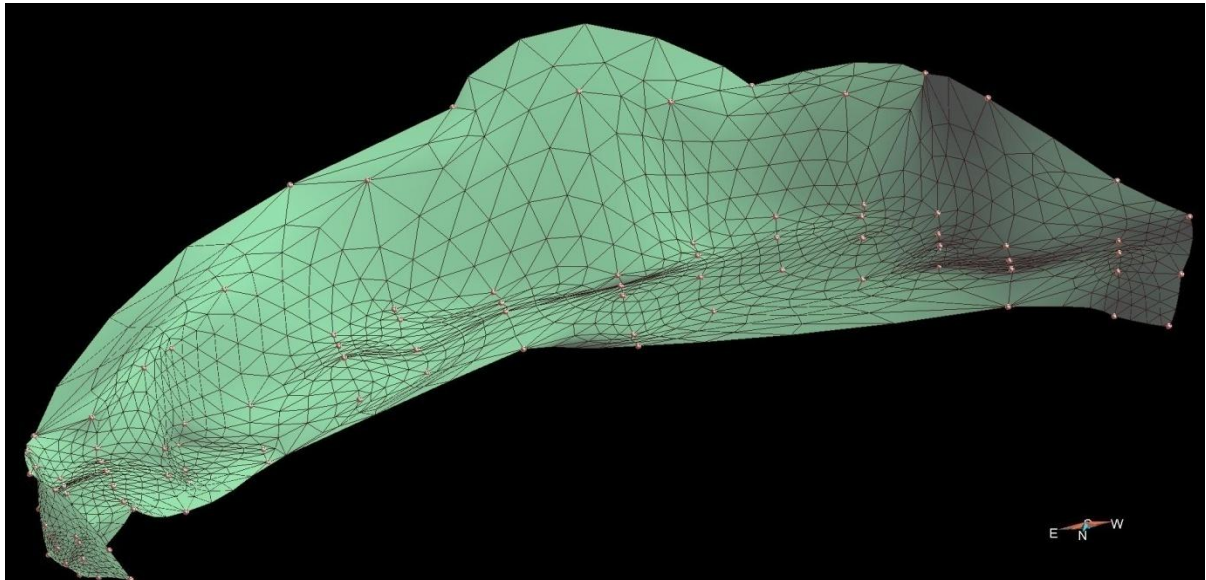


Figure 3-8: An interpolated surface based on the data points for a section

After the surfaces have been created, all the digital photos of the sections can be imported into gOcad as an individual voxel. Knowing the positions of the origin (assigned to the top left corner) of the image, the point u (the top right corner) and the point v (the bottom left corner), these pictures can be georeferenced and repositioned in the virtual space. Once all the pictures of a section are located, they produce a representative fence diagram for that section ([Figure 3-9](#)). These images can then be draped onto the generated surface of the section to produce a constructed virtual section such as the example seen in [Figure 3-10](#). Except for four points at the top of the section, there is a very good fit between the control nodes representing the survey points on the section and the targets (white dots/bottom of scale sticks) on the draped image. The small offset between some of the points (generally <50 cm of offset) is due to slight radial distortion in the images. In case of a small misfit between the GPS points and their corresponding targets on the images, the latter can be adjusted (fine-tuning step) by resizing the problematic 2D-voxel until the targets on the image match the control points on the surface. The pictures used in the creation of virtual

sections in this study were cropped and set in a sequence to further reduce the amount of distortion with the corner positions (i.e. origin, u and v) corresponding to their target positions ([Figure 3-9](#)).

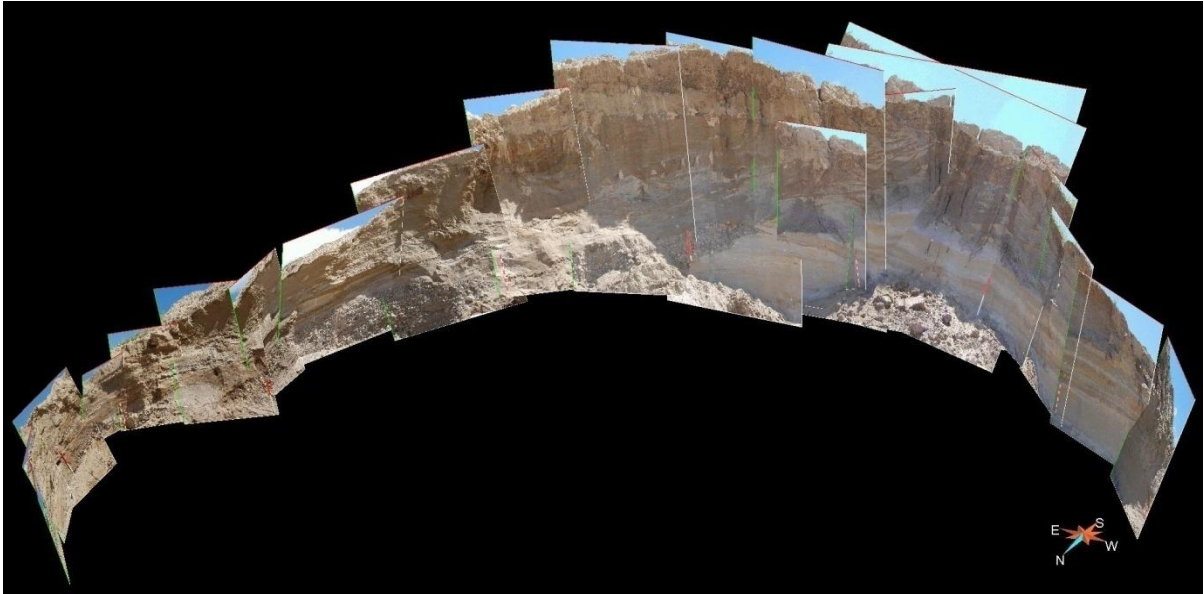


Figure 3-9: A series of positioned voxets representing a section



Figure 3-10: An example of a completed section with the images draped onto the surface

The creation of a stratigraphic grid (SGrid) is derived from the virtual section. Major bedding boundaries, including the top and bottom of each section, are traced using the curve tool. Surfaces are generated for each of these curves in the XY plane and will honour these curves as a constraint in the interpolation process. Once all the surfaces are created, a 3D SGrid workflow can begin with a property value and colour assigned for each facies and applied to its specific region in the SGrid (Figure 3-11). In cases where multiple facies exist within one defined facies region, manual selection of cells is needed in order to assign different property values that will reflect the different facies existing in that region. This procedure is conducted throughout the 3D representation. The SGrid was kept to an approximate thickness of one metre thick due to keep account for the 3D nature into these sections.

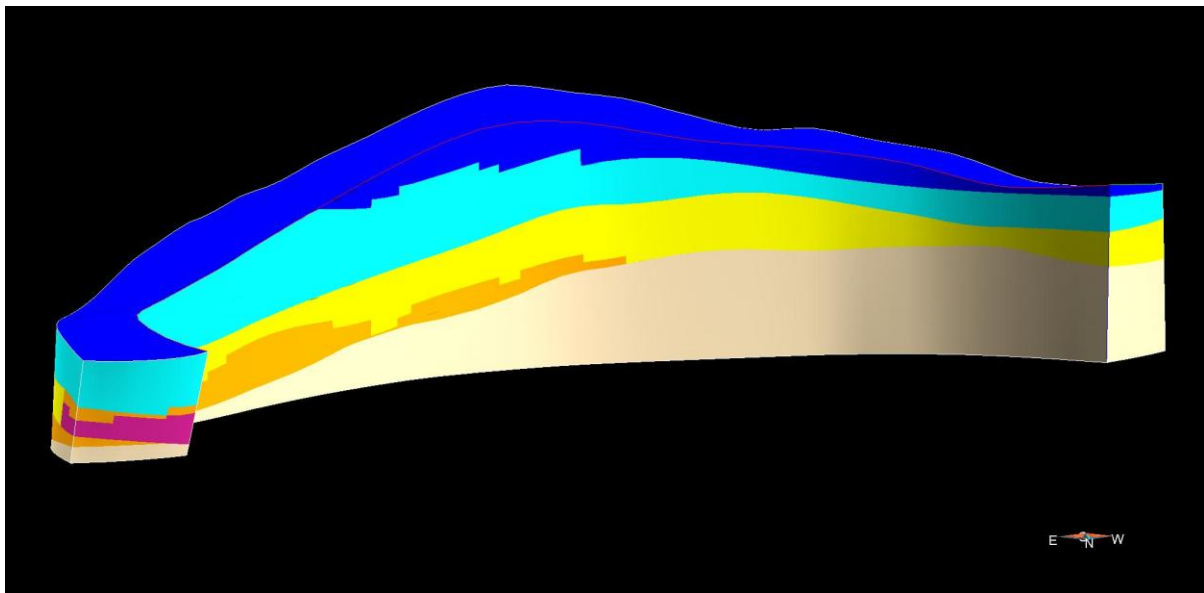


Figure 3-11: An example of a stratigraphic grid (SGrid) for a section

The dark blue represents the Fm facies followed by Fl (light blue), Sp (yellow), Gms (orange), Scr (beige) and Sd (violet) (cf. Appendix A for facies code).

The borehole database for the defined research area was imported into the geomodelling software by converting all database information into a text files, one for the location of boreholes and another denoting the markers used in the stratigraphy for the boreholes. These

markers were then simplified into mud, sand and gravel units, based on their records. Two tests would be conducted, one for the total extent of the Waterloo Moraine and one for the extent of the excavation (15 metres) of the Waterloo Moraine that the sections exposed. The total length for each of the three sediment types was summed up for every borehole (i.e. 5 metres total of mud, 20 metres total of sand and 10 metres total of gravel) throughout the entire Waterloo Moraine and for the first 15 metres below the surface. The length of each sediment type was then divided by the length for its respective test. These calculations are the representative fractions for each sediment class in each borehole. To calculate the representative fractions from the documented sections, the SGrids were used. In gOcad the property feature “Calculate Volume” was utilized for each facies region. The facies were simplified down to the three sediment classes (i.e. muds, sands and gravels) and were divided by the total volume the respective section. The results of the sections were then compared against the outcome from the boreholes.

3.4 Lab Data

3.4.1 Sample Gathering and Analysis

Each documented facies witnessed at each studied section was carefully sampled for various laboratory analyses, most notably grain size. Samples were labeled based on proximity to the nearest station followed by the sample number gathered at that station (i.e. 08KI04-02 being the second sample gathered at station 08KI04). Analysis of the samples were conducted by the Geological Survey of Canada and used a combination of sieving (grains >2mm), Camsizer (grains 2mm-0.063mm) and a Lecotrac LT100 Particle Size Analyzer (grains <0.063mm). The Camsizer is an optically-based instrument that images a falling curtain of sediment and then establishes the grain size of each particle in the impression ([Moore et al., 2006](#)), while the Lecotrac LT100 uses lasers and arrays to measure particle size. The results from these analyses were used to empirically calculate hydraulic conductivity (K) values and find a representative value for their respective facies.

3.4.2 Hydraulic Conductivity Calculations

In this study, the Hazen ([Hazen, 1892](#)), Kozeny-Carmen ([Carmen, 1956](#)), Breyer ([Odong, 2008](#)) and Terzaghi ([Terzaghi, 1964](#)) methods were used. Based on the conclusions of [Odong \(2008\)](#), the former three are most likely to produce realistic K values while Terzaghi is thought to be ideal for gravels. The first equation, the Hazen method ([Equation 1](#)), is the most commonly used empirical formula to estimate hydraulic conductivity values from grain size data:

$$\text{Equation 1: Hazen Equation}$$
$$K = g/v \cdot 6 \times 10^{-4} \cdot [1 + 10(n - 0.26)] \cdot d_{10}^2$$

The variable 'g' is the gravitational constant and is equal to 9.81 m/s² while the variable 'v' is the kinematic viscosity of water, being equal to dynamic viscosity divided by the fluid density. Viscosity is based on groundwater temperature and is generally assumed to be the annual average air temperature of the area. This temperature for the study area was found to be 10°C ([Robertson et al., 2007](#)) and yields a value 1.267x10⁻⁶ m²/s for kinematic viscosity. The 'd₁₀' is the diameter of the grain where 10% of the sample is smaller than the rest.

Porosity (n) of the samples was estimated using the following equation ([Equation 2](#)) from [Vukovic & Soro, 1992](#) and noted by [Odong, 2008](#):

$$\text{Equation 2: Porosity Equation}$$
$$n = 0.255 (1 + 0.83U)$$

The variable 'U' is known as the uniformity coefficient and is equal to the d₆₀/d₁₀ ratio.

The Kozeny-Carmen equation ([Equation 3](#)) is expressed by the following:

$$\text{Equation 3: Kozeny-Carmen Equation}$$
$$K = g/v \cdot 8.3 \times 10^{-3} \cdot [n^3 / (1 - n)^2] \cdot d_{10}^2$$

Calculations using the Breyer method ([Equation 4](#)) were done by using the equation:

$$\text{Equation 4: Breyer Equation}$$
$$K = g/v \cdot 6 \times 10^{-4} \cdot \log (500/U) \cdot d_{10}^2$$

The Terzaghi equation ([Equation 5](#)) used for calculating hydraulic conductivity is as follows:

Equation 5: Terzaghi Equation
$$K = g/v \cdot C \cdot [(n-0.13)^2 / (1-n)^{1.5}] \cdot d_{10}^2$$

The variable 'C' represents the sorting coefficient and is equal to the ratio of the d_{75} grain size divided by the d_{25} grain size.

4 - Results and Interpretation

4.1 Sedimentary Study

4.1.1 Sediment sections and their virtual 3D reconstruction

The research conducted at Kieswetter Holding has produced a total of fourteen sections, five in 2007 (A to E), and nine that were studied in 2008 (F to N). These sections are divided into the eastern and western areas ([Figure 4-1](#)). In 2007, the focus was in the western part of the pit while sections in 2008 were distributed throughout the pit to study areas of interest and link data from the previous year. A total of 107 stations were created to delineate the sections ([Appendix B](#)) with extra point data gathered for the three-dimensional work. Images of the sections can be found in [Appendix C](#) displaying features used in their 3D construction and the documented facies assemblies for each location.

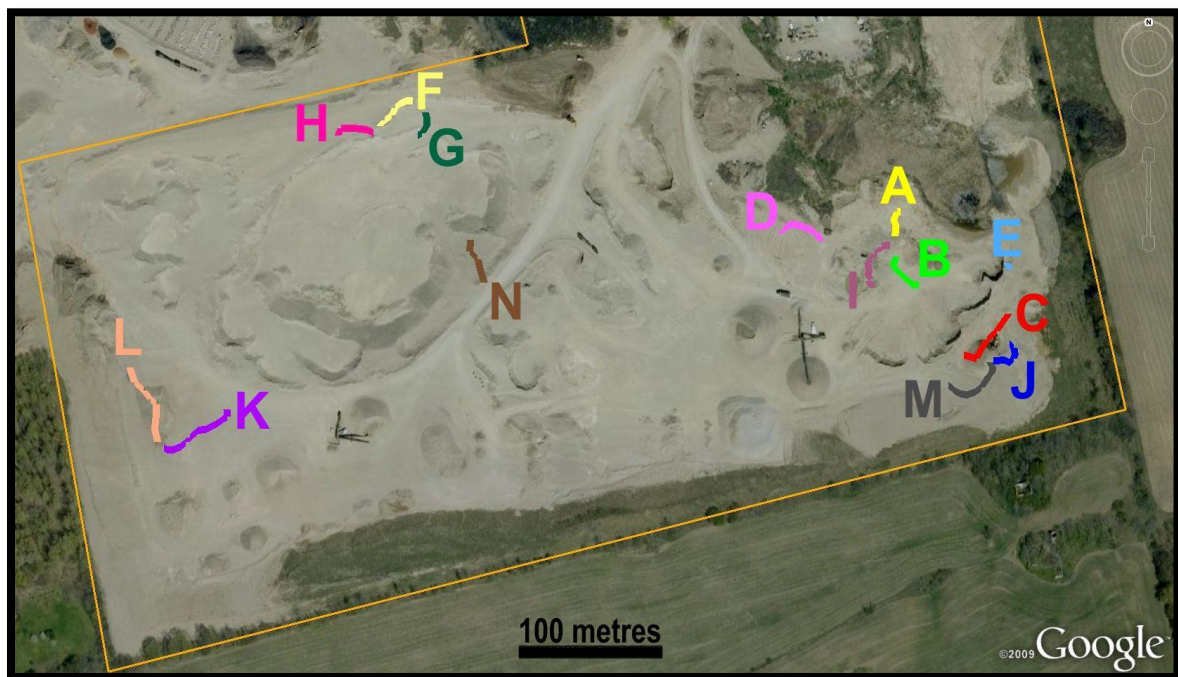


Figure 4-1: The location of all sections studied at Kieswetter Holdings
Note the western (F, G, H, L, K & N) and eastern (A, B, C, D, E, I, J & M) areas

The creation of the virtual sections produced sound reconstructions. Error was on the order of decimeters between surveyed points and respective location on the image except for section F where it reached two meters in error. This inaccuracy was due to radial displacement and is greatest on the periphery of images. The error was reduced by cropping several images and stacking them beside each other ([Figure 3-8](#)).

4.1.2 Lithofacies

Fourteen different facies were observed and recorded at Kieswetter Holdings over the course of the research period from August 2007 to October 2008 but were reduced down to nine hydrofacies ([Table 1](#)). This simplification was based on sediment type, deposition and grain size distribution. An example would be the hydrofacies cross-bedded sands (Sp) where the lithofacies Sp, St and Sh are generally medium sand units, deposited at the boundary between upper and low flow regimes and exhibit similar grain size curves. The mud units, which include all diamicton units, were the predominant sediment in the eastern part of the pit while sand was clearly abundant in the western part of the pit but existed throughout the pit, along with gravel. Massive muds existed at the ground surface, or the top of the pit, and diamicton units would be included in this classification. Surficial diamicton units did not appear to be of glacial origin and could have been created from the reworking of sediment by employees of the pit, but this assumption could not be confirmed as these units were inaccessible for study. Muds displayed structures such as laminae and interbedded massive units, as well as one section showing a massive mud unit to be the result of dewatering from rapid massive loading ([Figure 4-2](#)).

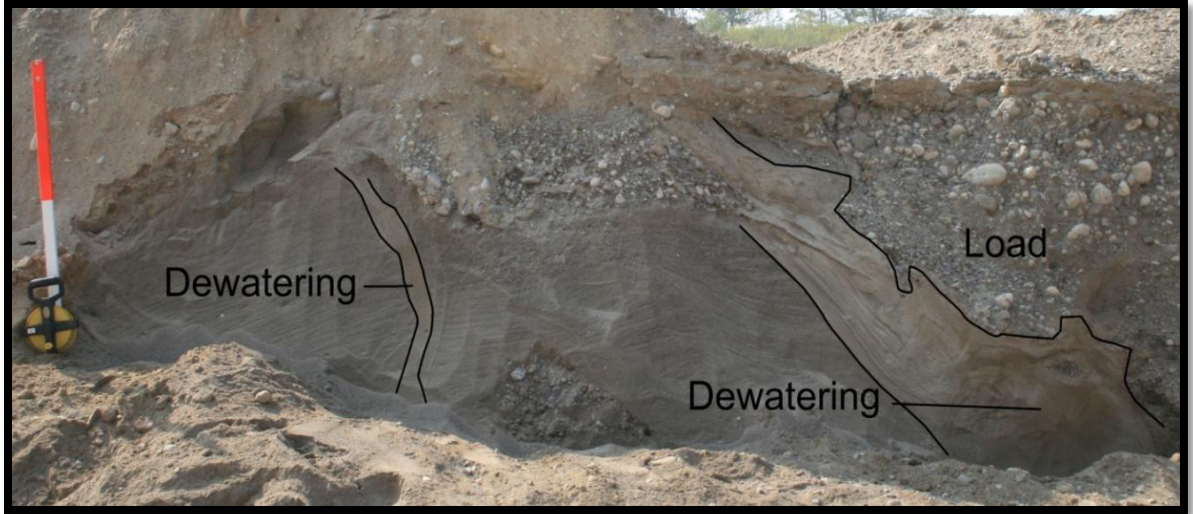


Figure 4-2: Rapid massive loading of gravel producing dewatering structures at section B

Planar and trough bedded sands were the most common sand facies throughout the pit, along with climbing ripples. Horizontal, deformed and laminated sandbeds were held to only the eastern side, with isolated pebbles appearing in a laminated sand bed at section D. Gravel beds were typically found in the eastern part of the pit, with planar gravel beds being the dominant gravel facies. In these planar beds, openwork gravels could be found as well as massive units, both clast and matrix supported, nearby. All the facies were further classified into massive and laminated muds; cross-bedded, laminated, climbing ripple and deformed sands; massive, cross-bedded and openwork gravels ([Table 1](#)). This classification was arranged to simplify the modeling process and was based on common depositional environments and features. The proportion of each of these facies classes was calculated using volume measurements from the stratigraphic grids of each section ([Appendix C](#)), and these results can be found in [Table 2](#). All the samples gathered were divided into their respective facies and lead to assigning a hydraulic conductivity (K) for the unit ([Table 3](#); [Appendix D](#)) from each of their respective grain size distribution curves ([Appendix E](#)). The K values were empirically derived but would aid in defining the hydrofacies characteristics for the lithofacies at the sand pit.

Table 1: Summary of observed facies and their respective facies class (cf. Appendix A for facies codes)

Sediment Type	Facies Code	Hydrofacies	Description	Interpretation
Mud	Fl	Fl	Fine laminations in mud material	Rhythmic deposition of silts and clays settling out from suspension
	Fm	Fm	Structureless, massive mud	Fine material settling out from suspension
	Fm(w)		Massive mud unit being the result of dewatering	Overlying load forcing mud unit up into coarser material
Sand	Sh	Sp	Horizontal bedding of medium to coarse sand	Parallel to bedding surface beds created under upper flow regime conditions (i.e. Cheel et al., 1990)
	Sp		Planar cross-bedding	Downflow migration of 2D dunes in the upper part of a low-flow regime (i.e. Allen, 1984)
	St		Trough cross-bedding	Downflow migration of 3D dunes in the upper part of a low-flow regime (i.e. Allen, 1984)
	Sl	Sl	Fine sand in laminated beds	Rhythmic deposition of fine sand, silt and clay settling out of suspension, due to waning sediment input
	Sl(d)		Fine sand in laminated beds with isolated clasts	Clasts shed from an iceberg or glacial terminus into a deposit of laminated sand (e.g. Lonne, 1995)
	Scr	Scr	Climbing ripples	Decreased flow capacity in low-flow regime (i.e. Hiscott, 1994)
	Sd	Sd	Deformed sand bedding	Sand beds altered due to deformation processes such as glaciotectionics and loading
Gravel	Gm	Gms	Massive gravel, clast supported	Debris flow deposit (i.e. Miall, 1996)
	Gms		Massive gravel, matrix supported	Debris flow deposit (i.e. Miall, 1996)
	Go	Go	Openwork Gravel	Uncertain; groundwater (Browne, 2002; Kleinhaus, 2005); primary sorting (Shaw & Gorrell, 1991)
	Gp	Gp	Planar cross-bedding of gravel beds	Longitudinal barform migration (i.e. Brennand & Shaw, 1996)

Table 2: Facies Proportions for each Section at Kieswetter Holdings

Section	Facies	Representative Volume (m ³)	Proportion	Section	Facies	Representative Volume (m ³)	Proportion
A	Fl	11.70	10.10%	H	Fm	90.00	17.42%
	Gms	73.03	63.03%		Gms	36.92	7.15%
	Gp	5.28	4.56%		Scr	107.38	20.78%
	Sd	25.86	22.32%		Sp	282.36	54.65%
B	Fm	0.19	2.32%	I	Fm	135.31	38.84%
	Gms	0.27	3.22%		Gms	8.03	2.30%
	Go	0.08	0.93%		Go	1.87	0.54%
	Gp	7.14	85.24%		Gp	6.57	1.89%
	Sp	0.69	8.28%		Sd	196.64	56.44%
C	Fm	9.53	13.65%	J	Fl	26.98	23.74%
	Gms	5.49	7.86%		Fm	18.71	16.46%
	Sp	54.81	78.49%		Gms	18.46	16.24%
D	Fm	74.61	22.07%		Go	0.28	0.25%
	Sd	178.88	52.91%	Sp	49.24	43.32%	
	Sl	84.59	25.02%	K	Gms	23.73	5.68%
E	Fm	0.37	22.54%		Scr	5.19	1.24%
	Gms	1.20	72.95%		Sl	8.06	1.93%
	Sp	0.07	4.50%		Sp	380.81	91.15%
F	Fm	122.81	38.42%	L	Scr	543.13	34.38%
	Gms	0.55	0.17%		Sp	1036.51	65.62%
	Scr	70.85	22.17%	M	Fl	426.85	22.11%
	Sp	125.42	39.24%		Fm	298.60	15.46%
G	Fm	8.85	15.80%		Gms	366.78	19.00%
	Gp	4.19	7.48%		Scr	431.01	22.32%
	Scr	9.11	16.28%	Sd	25.03	1.30%	
	Sd	8.84	15.78%	Sp	382.64	19.82%	
	Sp	25.00	44.66%	N	Gms	30.56	7.00%
			Sp		406.28	93.00%	
Average	Facies	Overall Proportion					
	Fl	4.00%					
	Fm	14.50%					
	Scr	8.37%					
	Sd	10.62%					
	Sl	1.93%					
	Sp	38.77%					
	Gms	14.61%					
	Go	0.12%					
	Gp	7.08%					

Table 3: Hydraulic conductivity summary, based on facies, for each sample collected (cf. Appendix D for K calculations and Appendix E for grain size data)

Facies	Sample Number	K average (m/s)	Facies	Sample Number	K average (m/s)
Sp	07KI04-01	1.02E-04	Scr	08KI04-01	9.03E-05
	07KI03-02	2.13E-06		08KI04-03	9.24E-06
	07KI07-01	7.17E-04		08KI50-02	4.12E-05
	07KI18-01	5.21E-06		08KI58-03	1.24E-05
	07KI18-02	1.64E-04		08KI60-02	1.38E-05
	07KI19-01	8.68E-06		08KI63-02	1.06E-05
	08KI04-02	1.42E-04		08KI67-03	4.66E-06
	08KI12-01	1.43E-05		08KI67-04	1.67E-05
	08KI12-02	2.21E-04		08KI69-02	4.07E-06
	08KI44-01	3.77E-04		08KI70-01	5.23E-06
	08KI44-02	1.56E-04	Sh	07KI04-02	1.06E-06
	08KI44-03	3.46E-04		07KI12-03	1.79E-05
	08KI45-01	2.97E-04		07KI13-01	1.02E-07
	08KI50-01	6.73E-04		07KI15-02	6.27E-04
	08KI58-01	3.38E-04	Fl	07KI05-02	1.15E-07
	08KI58-02	2.92E-04		08KIM1-01	2.11E-08
	08KI60-01	4.56E-04		08KIM1-02	2.20E-08
	08KI60-03	2.16E-04	Fm	07KI05-01	1.15E-08
	08KI63-01	3.90E-04		07KI12-02	6.54E-08
	08KI63-03	2.21E-04		07KI16-01	4.42E-09
08KI64-01	1.77E-04	07KI17-03		4.10E-09	
08KI66-01	1.22E-05	07KI23-01		1.99E-08	
08KI67-01	4.96E-06	08KII1-02		4.81E-08	
St	07KI20-03	2.42E-06	Fm(w)	07KI15-01	5.12E-09
	08KI46-01	5.27E-04		08KIM1-05	1.91E-08
	08KI46-02	3.42E-04	Gm	07KI07-02	5.35E-03
	08KI46-03	2.76E-04	Go	07KI09-01	3.71E-02
	08KI46-04	5.53E-04		08KI71-01	2.51E-03
	08KI48-01	1.99E-04	Gp	07KI09-02	2.32E-03
	08KI48-02	5.64E-04		08KI71-02	2.47E-03
	08KI48-03	5.54E-04		08KII1-01	3.03E-03
	08KI64-02	2.95E-04		08KIM1-04	1.72E-03
	08KI64-03	2.82E-04	Gms	07KI03-01	4.78E-04
	08KI67-02	8.81E-05		07KI03-03	2.46E-07
	08KI69-01	3.09E-05		07KI12-01	2.24E-04
Sl	07KI20-01	3.27E-06		07KI16-02	2.93E-04
Sl(d)	07KI20-02	8.93E-05		07KI17-01	2.20E-06
Sd	07KI17-02	2.01E-06		08KI70-02	4.15E-03
	08KI70-03	1.04E-05	08KIM1-03	1.47E-03	

4.1.3 Paleoflow

During sample collection, additional paleocurrent data was gathered. A total of fifty-three measurements were performed over the course of the study period, focusing on the foreset orientation of sandy bedforms ([Appendix F](#)). The paleocurrent data illustrates a primarily northwestern flow direction with some divergence ([Figure 4-3](#)). The deviations from the principal direction could reflect swings in the sediment source's flow direction or suggest a turbulent depositional environment. The paleoflow data was integrated into the geomodelling process.

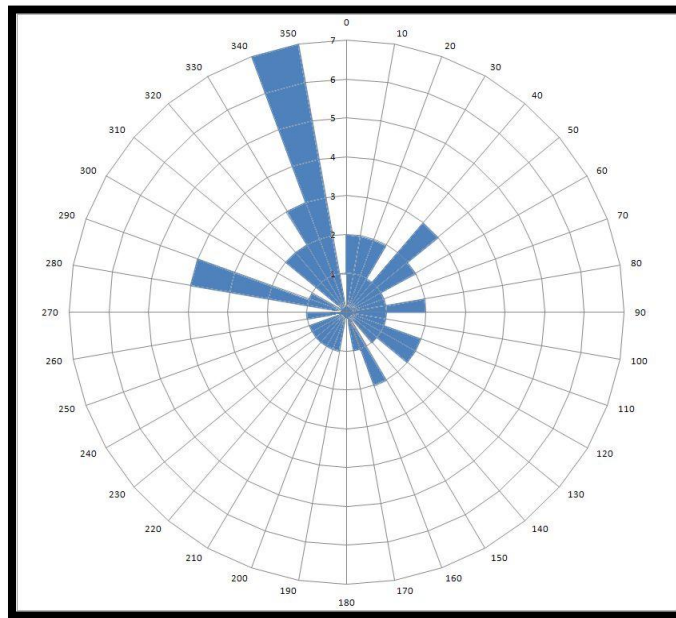


Figure 4-3: A rose diagram of the paleoflow data in 10 degree increments (cf. Appendix F for paleoflow measurements)

4.2 Sedimentary Interpretation

The sedimentology of Kieswetter Holdings can be separated into two areas, the eastern and western parts of the pit ([Figure 4-1](#)). The eastern area is characterized by the existence of muds, sands and gravels, such as in the heterolithic bedding observed ([Figure 4-4](#)). Also in this side of the pit, there is cross-stratification of gravels and deformation features whereas in the western part of the pit, it is predominantly sandy material that displays dune-scale cross

stratification, ripple-scale climbing cross stratification, and cut-and-fill channels. Diamicton appears to be present over the entire pit area as a cap to these sediments. Only a few of the outcrops of diamicton were sampled (i.e. 08KII1-02), with the interpretation of them not being of glacial origin. This diamicton could be the result of pit workers bulldozing fine material away from production areas; however, it is not fully ruled out that all near-surface diamicton units were of a glacial source.



Figure 4-4: Heterolithic bedding at section J

Note the heterolithic beds (sand and muds) at the top, and sand and gravel mixture at the bottom

4.2.1 Eastern Side of Study Area

The eastern portion of the study area contained the Sections A, B, C, D, E, I, J and M, with each section being unique from the others, as seen by the images in [Appendix C](#). This area of Kieswetter Holdings generally displays an overall fining-upward sequence with gravel located at the bed floor, followed by sandy units and topped off by muds. Section A is an example of this overall grading, as it consists of planar and massive gravel at the base overlaid by deformed sands and topped by laminated and massive mud units. The gravel units consist of slightly imbricated rounded and sub-rounded cobbles which display iron staining. The deformed sands consist of sheath folds ([Figure 4-6A](#)), centimeter scale normal faults, cementation of some sand as well as an elongated recumbent fold that represents a side profile of a sheath fold ([Figure 4-6C](#)). Laminated fines units are interbedded with

massive mud units 2-5cm thick and appear to be rhythmic (Figure 4-6B). Section B predominantly contains planar, openwork and matrix-supported massive gravel with some medium to coarse planar sand and massive fine material. This massive fine material appears to be a result of loading (Figure 4-2). A laterally accreted barform that produces alternating integration of openwork gravels with polymodal and bimodal massive gravels containing a sandy matrix is visible at Section B with paleoflow to the northwest (Figure 4-5). Section C contains much heterolithic bedding as mud, sand and gravel units are often interbedded with each other. Deformation occurs as some sand beds had a measured dip up to 81° (Figure 4-6D), probably due to loading from a slump, and there is also a small, bent diapir (Figure 4-6E). Section D is composed of fine to medium-grained deformed sand beds showing detached folds that are overlaid by laminated fine sands and capped by laminated muds. Section E is the smallest section studied and is composed of matrix-supported massive gravel with some planar sand units interbedded with the gravel. This section is capped off by massive mud.

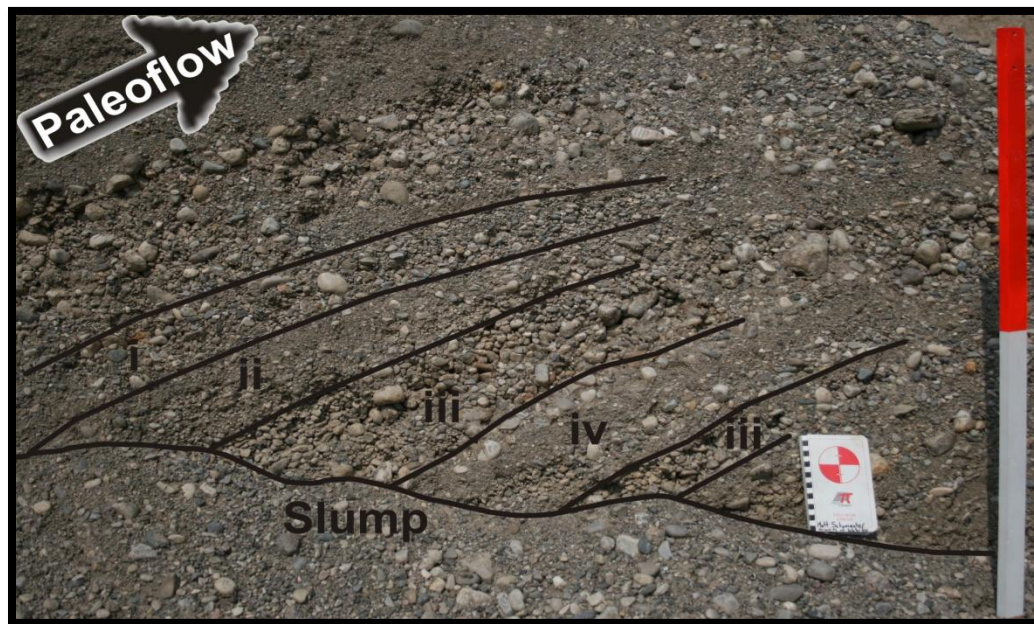


Figure 4-5: A gravel bedform found at Section B

Composed of bimodal gravel (i), matrix supported gravel (ii), openwork gravel (iii) and polymodal gravel (iv); metre-long stick as well as centimeters on notebook for scale and with paleoflow towards the northwest (note the arrow, going into the picture).

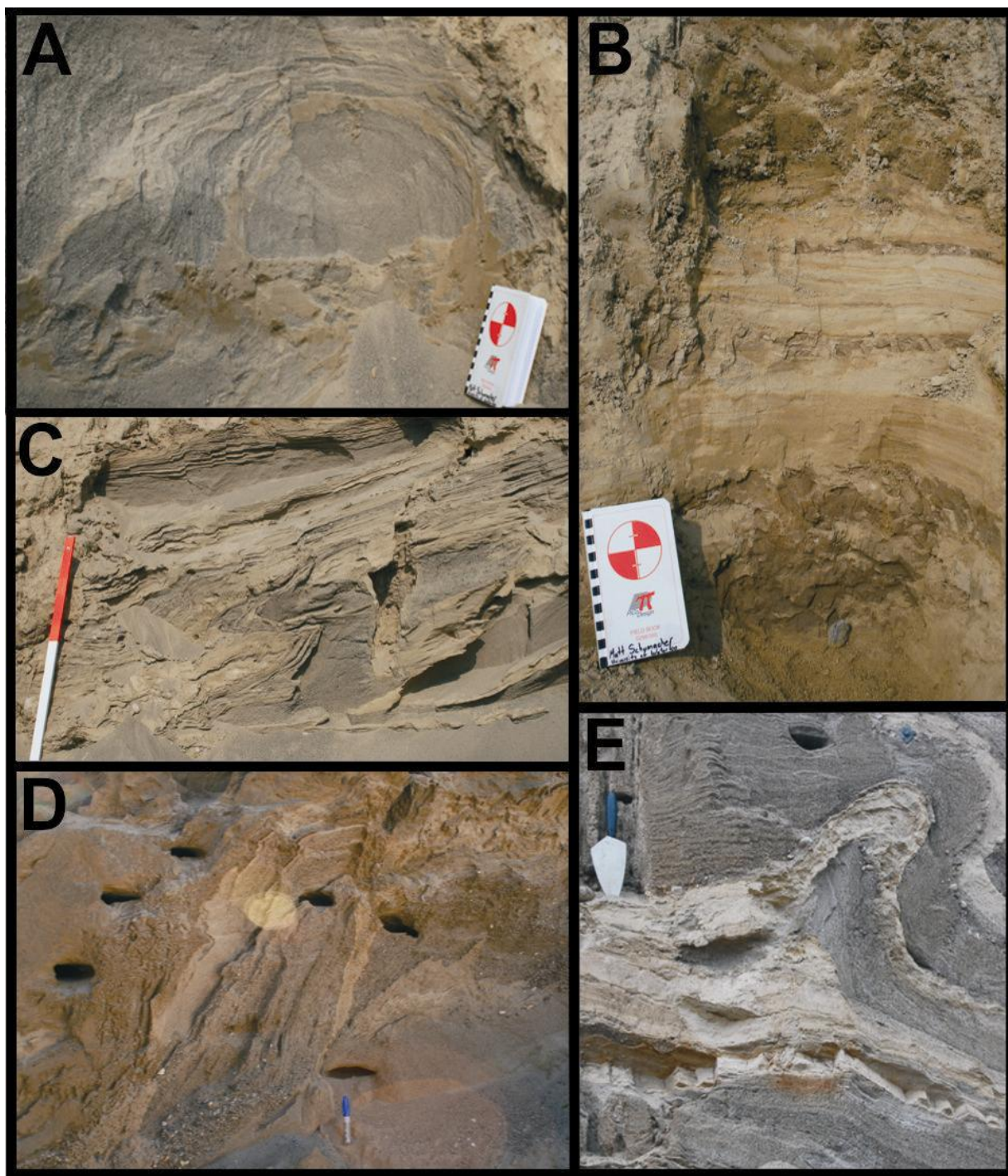


Figure 4-6: A selection of features noted at the 2007 sections in the eastern side of pit
A: Sheath fold at Section A with a fold axis of 236° ; centimeter scale noted on book; **B:** Alternating laminated and massive mud units at Section A; **C:** Recumbent fold in deformed sands at Section A; note metre stick for scale; **D:** Highly inclined beds ($\sim 80^{\circ}$) at Section C; the pen is 10cm in length; **E:** A small, bent diapir seen at Section C; the trowel is 30 cm in length.

Section I is considered to be an extension of sections A and B through further excavation at the pit. Section I illustrated more significant deformed bedding of sands, small units of laminated fine material between some sand beds, with beds generally dipping to the west ([Figure 4-7A](#)). Folding and faulting were prevalent here, as seen by a significant reverse fault at Section I ([Figure 4-7B](#)). Gravel units such as matrix-supported massive material and cross-bedded planar cobbles were exposed at the base of the section and made up a small percentage of the facies proportion of this section ([Table 2](#)), while a significant amount of diamicton capped the deformed sands. Sections J and M are considered extensions of Section C. Section J simply had heterolithic bedding ([Figure 4-4](#)) overlaying gravelly sand. Section M was composed of many different facies where matrix-supported gravel was overlaid by medium-grained planar sand and an erosional surface eroded into an extensive climbing ripple unit. These sands were extensively deformed locally as seen by the sheath fold ([Figure 4-7C](#)). These units were below both laminated and massive mud units. Prior to documenting Section M, a sheath fold with an axis of 168° was recorded in the laminated mud area; however, this area was excavated before study could be initiated ([Figure 4-7D](#)).

The mud portion of the eastern area is quite extensive. The massive and laminated mud caps the sandy units and appears to be laterally continuous. Diamicton elements were classified as massive muds as there is the potential that this facies could be a result of anthropogenic activity. It was observed that pit employees continually rework and relocate mud material in order to access any aggregate material below. Regardless, these units were still notated as it is assumed that in the registry of borehole records, reworked surficial materials would be logged as muds in the documentation of a borehole record. This simplification was implemented for consistency, but defining any surficial till would be ignored in this study as surficial diamictons could not be assured to be of glacial origin. Genuine geologically sourced massive muds that occurred in areas unaffected by pit operations were determined to be the consequence of a water column being situated over the area. Laminated muds were also observed and these resulted from seasonal influences and changing sediment inputs.

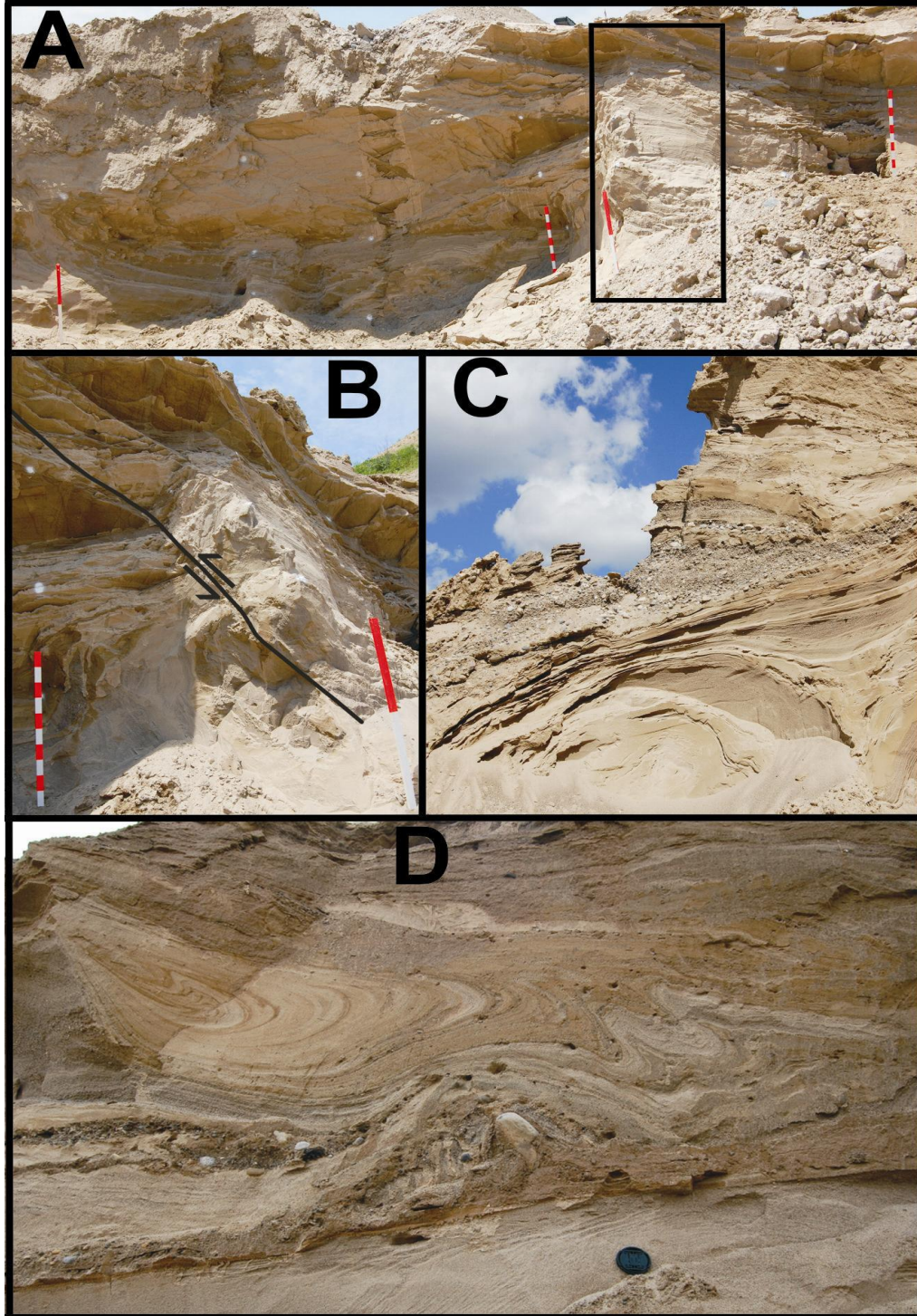
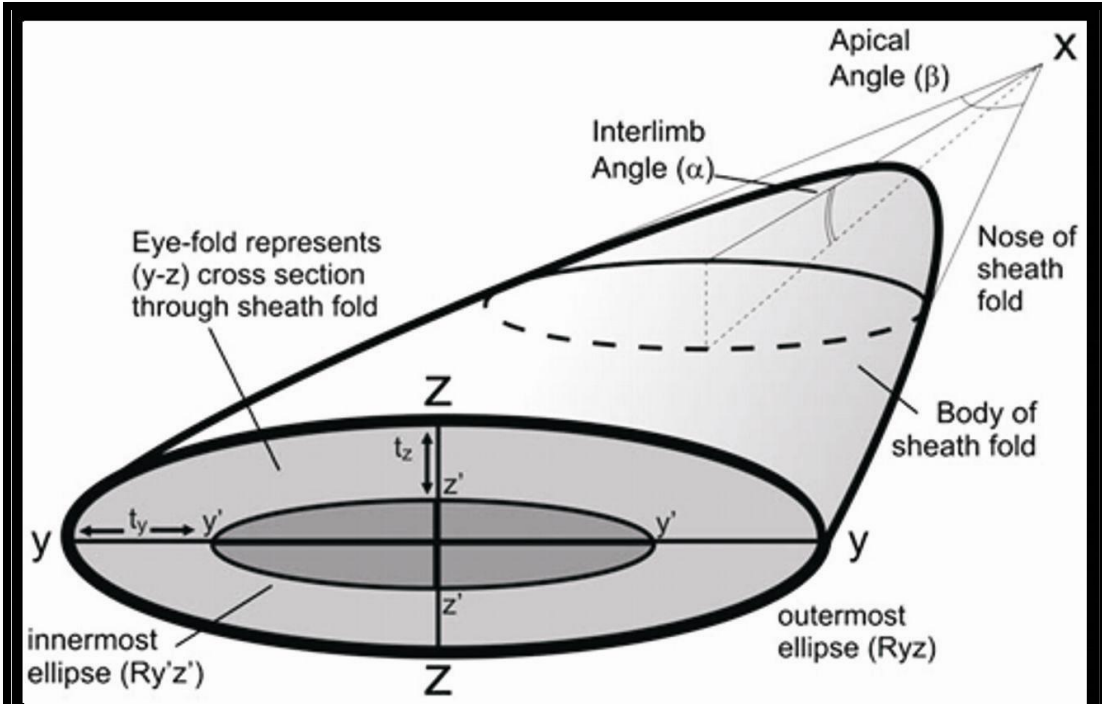


Figure 4-7: Select features from 2008 sections in the eastern part of pit

A: Beds at Section I all dipping towards the west; inset notates location of significant reverse fault; scale sticks are one meter; **B:** Close-up of reverse fault at Section I; **C:** Sheath fold at Section M half buried by talus material with an unmeasured fold axis; **D:** An observed sheath fold with a fold axis of 168° located between Sections C and M, lens cap diameter is 6.2cm.

Gravel facies were prominent near the pit floor, making unit thickness to be minimum estimates. Observed clasts were generally no bigger than cobble scale, but were well-rounded. The gravel showing imbrication in massive units were near gravel cross-beds and could have resulted from lateral accretion deposits similar to that in [Figure 4-5](#). The cross-stratified planar gravels observed at Sections B and I indicate a paleoflow towards the northwest. The noticeable iron staining is probably an indication of past or recent vadose processes leading to precipitation of an iron-coating. The sand element in the eastern side of the pit is notably the most deformed and was found as a bedform or mixed among gravels and muds. Sand becomes more extensive to the west, such as at Section D, where the sand was most likely deposited as cross-stratified trough bedding but was later deformed.

The significant amount of deformation on the eastern side of pit appears to be localized in this area and generally shows that westward principal stress component. As the Waterloo Moraine has been determined to be of glacial origin (i.e. [Karrow, 1993](#); [Bajc & Shiota, 2007](#)), glaciotectonism is a probable cause of these features. Glaciotectonics can be defined as the displacement of glacial materials through ductile and brittle deformation as a result of the stresses from glacial ice ([Benn & Evans, 1998](#)). There are two major types of stress associated with glaciotectonics: proglacial (compressional) and subglacial (extensional or tensile) ([Croot, 1987](#); [Hambrey & Huddart, 1995](#)). [Hambrey & Huddart \(1995\)](#) give examples of proglacial deformation features including open folds, chevron folds, listric thrusts dipping up-glacier and nappes, as well as subglacial features which include highly attenuated folds, sheath folds, and diamictons with streamlined pods of sand or rock. According to this classification, the sheath folds witnessed at Kieswetter Holdings would indicate a subglacial deformation zone.



A: A drawing displaying the x (direction of shear), y and z (cross section) axes of a sheath fold with the inter-limb angle (α) and apical angle (β) of the folded hinge-line. Elliptical ratios for the outer-most ring (R_{yz}) and inner-most ring ($R_{y'z'}$) are illustrated along with the determination of thickness of a layer is measured along its respective axis (i.e. t_y or t_z).

Sheath-Fold Type	Name	Cross-sectional Illustration	Ratio
Type A	Eye-Fold		$R_{yz} = R_{y'z'}$
Type B	Bulls-Eye Fold		$R_{yz} > R_{y'z'}$
Type C	Cats-Eye Fold		$R_{yz} < R_{y'z'}$

B: A chart explaining the difference between the different types of sheath folds

Figure 4-8: The formation and types of sheath folds
Modified from Alsop et al., 2007.

Sheath folds are ductile deformations that are thought to form from the rotation and stretching of irregular folds from high shear strains ($\gamma > 10$) ([Cobbold & Quinquis, 1980](#)). [Figure 4-8A](#) depicts the geometry of a sheath folds while [Figure 4-8B](#) illustrates how the ratio between the outermost and innermost ellipses determines the type of sheath fold. The distinctive eye pattern of a sheath fold is only visible when looking at a cross-section that runs perpendicular to the direction of shear ([Figure 4-8A](#)). The sheath fold observed at Section A ([Figure 4-6A](#)) had a fold axis of 236° indicating a shear direction to the southwest. The sheath located between Sections C and M ([Figure 4-7D](#)) had an apparent fold axis of 168° as it was viewed at an oblique angle and did not display the typical eye-fold cross-section. The sheath at Section M ([Figure 4-7C](#)) did not have its fold axis measured thus, shear direction was not truly determined; however, the geomodelled section suggests a west southwest fold axis for this feature.

Another deformation feature seen was the small diapir structure at Section C. A diapir is formed in a subglacial environment when saturated mud material becomes quickly overlaid by coarser material and a load is applied. This loading creates downward pressures around the coarse material, forcing the mud material up inside the coarse deposit ([Banerjee & McDonald, 1973](#)). This diapir would have formed near an ice-contact environment as sediment slumped into a mud bed and bent towards the west, possibly away from the ice face. This deformation, along with the sheath folds, are types of sedimentary ductile deformations that can occur at the front of an ice advance ([Benn & Evans, 1998](#)), which in this area came from the east.

The deformation seen in the eastern part of the pit is similar to that of the piggyback thrusting and found in proglacial settings ([van der Wateren, 1985](#)). As a glacier advances forward over an area of deposited sediment, multiple thrust faults are created that become superimposed on each other, or piggybacked, due to compressional forces. [Mulugeta and Koyi, 1987](#) characterized piggyback thrusting into three domains ([Figure 4-9](#)). The distal domain is characterized by low angle thrusts, overturned and sheath folds and slumping. The

next domain, the intermediate domain, has steeper, rotated blocks with concave-up listric thrusts while the proximal domain, the last domain, consists of vertical blocks that are laterally compacted. Section I ([Figure 4-7A](#)) shows slightly rotated beds along with a steep reverse fault making it possible that there is an underlying intermediate domain, but not enough evidence to back this claim. If a glacier advances over piggyback thrust blocks, subglacial deformation can occur on top of proglacial tectonic features if there is not enough energy for more thrusting ([van der Wateren, 1985](#); [Benn & Evans, 1998](#)).

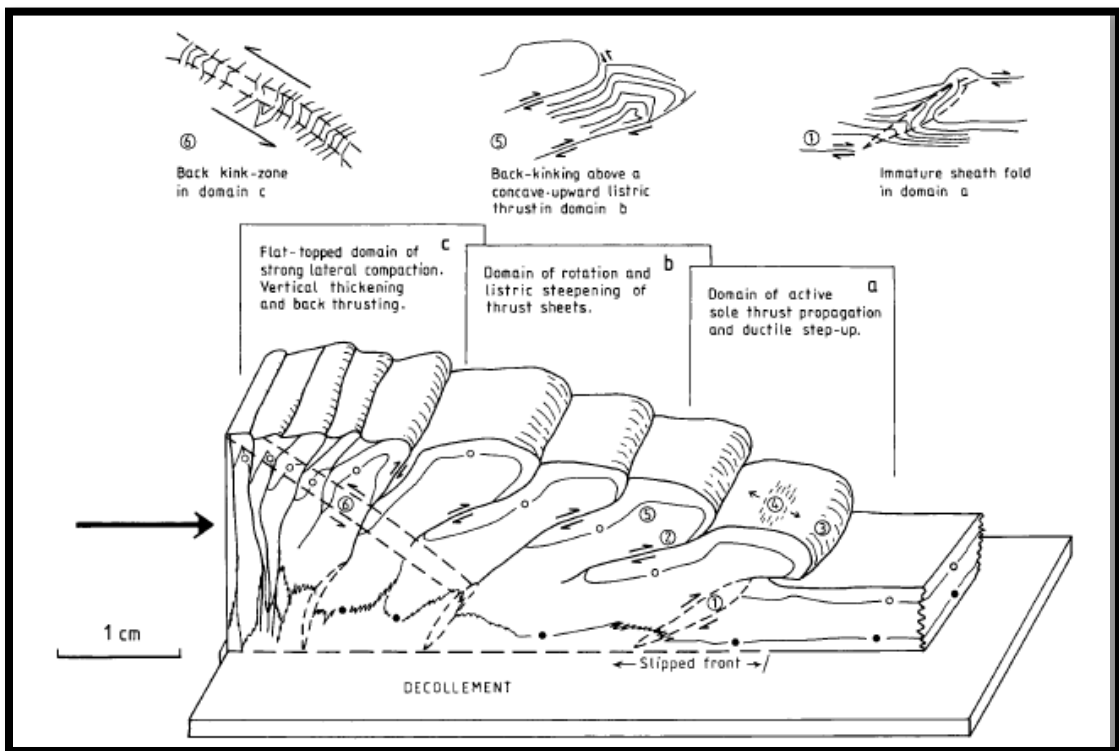


Figure 4-9: Piggyback thrusting with distal (A), intermediate (B) and proximal (C) zones.
From Mulugeta and Koyi, 1987

The superimposing of thrust faults is a common glaciotectonic deformation caused by compression created when a glacier progresses. The glacier came from the east with the direction of this ice movement established by the sheath fold at Section A, the bend in the diapir, as well as the reverse fault at Section I ([Figure 4-7B](#)). The occurrence of an extended recumbent fold, possibly a side profile of another sheath fold, at Section A ([Figure 4-6C](#)) and

the multiple sheath folds support the claim of a distal area of piggyback thrust faults and would help to explain the deformed bedding at Section D. These features could have occurred when glacial ice advanced sediment forward, producing high shear strains and extending these pliable beds forward. [Figure 4-7D](#) illustrates a sheath fold that is just above a shear plane created when the glacier ice advanced.

The highly dipping beds at Section C could be a result of a significant slump of material falling into mud, creating a large ball and pillow structure ([Figure 4-10](#)). A slump is a likely reason for the diapir located at Section C and in the proximity of the near-vertical beds. A significant load of sediment falling into mud could force the fine material into an overlying coarse deposit creating the diapir. These ductile formations may overlie a preexisting proglacial tectonic structure as Section I could illustrate an intermediate domain of thrust faulting. The steep reverse fault and possible rotated blocks make this theory plausible, but there is no other evidence to support this argument. The evidence recorded from the deformations in the eastern side of the pit suggests that these features were ductile deformations created in a distal domain of piggyback thrusting of sediment.



Figure 4-10: A ball and pillow structure resulting in deformed mud beds at the end of Section C possibly creating the nearby vertical beds

4.2.2 Western Side of Study Area

The western area of the Kieswetter pit was essentially all sand, combining cross-stratified deposits with cut-and-fill channels. The non-climbing cross-stratified sands were deposited from ripple to dune scale in both planar and trough forms and are represented by the Sp facies. Climbing cross-stratification of ripples were present at all western sections and deposition of these ripples varied from subcritical to supercritical. These climbing deposits represent a flow regime that had an abundant sediment supply that quickly lost transport competence (e.g. [Hiscott, 1994](#)). The cut-and-fill channels that existed contained significant planar bedding units and provide sources of gravel in this area of the pit. These channels tend to overlay and scour into sandy bedforms, such as at Sections F and G, but clearly demonstrated at Section H ([Figure 4-11](#)) and are possibly capped off by a diamicton. Cross-laminated climbing ripple beds of 0.5 - 1 meter thickness were noticeable at these three sections. No deformation features were observed at any of these three sections.

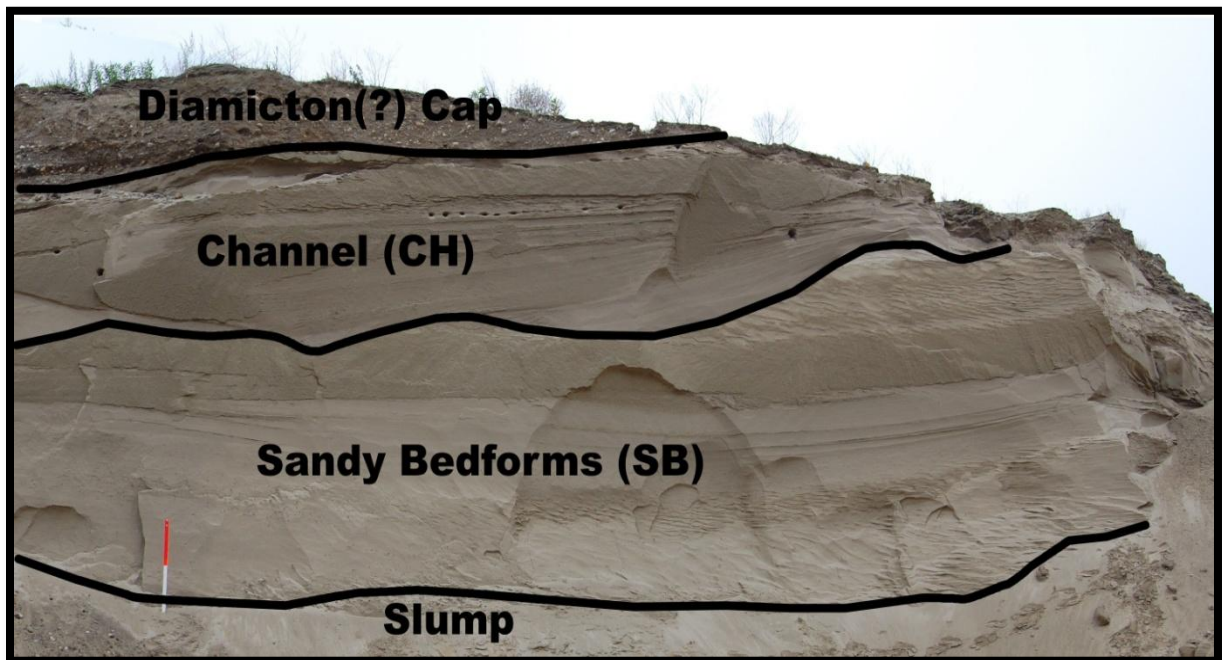


Figure 4-11: A series of architectural elements at Section H (Metre-long stick used for scale)

Section K was the longest section studied at Kieswetter Holdings and took 1.5 days to document. This section was predominately constructed of dune scale planar and trough cross-bedding with some cross-laminated climbing ripples and a large cut-and-fill channel revealing gravel beds in its base topped off by horizontal sand bedding (Figure 4-12). The dune scale cross-beds had thicknesses of about 1-2 meters whereas the climbing ripples were up to 0.3 meters thick. Section L was essentially an extension of Section K and was composed in the same fashion except there was no gravel. Section N was the last section studied, and it was composed of another large-scale channel at the base with horizontally-bedded sand overlaid by dune scale sandy trough cross-beds. There was a small pocket of matrix-supported gravel near the top of the section.

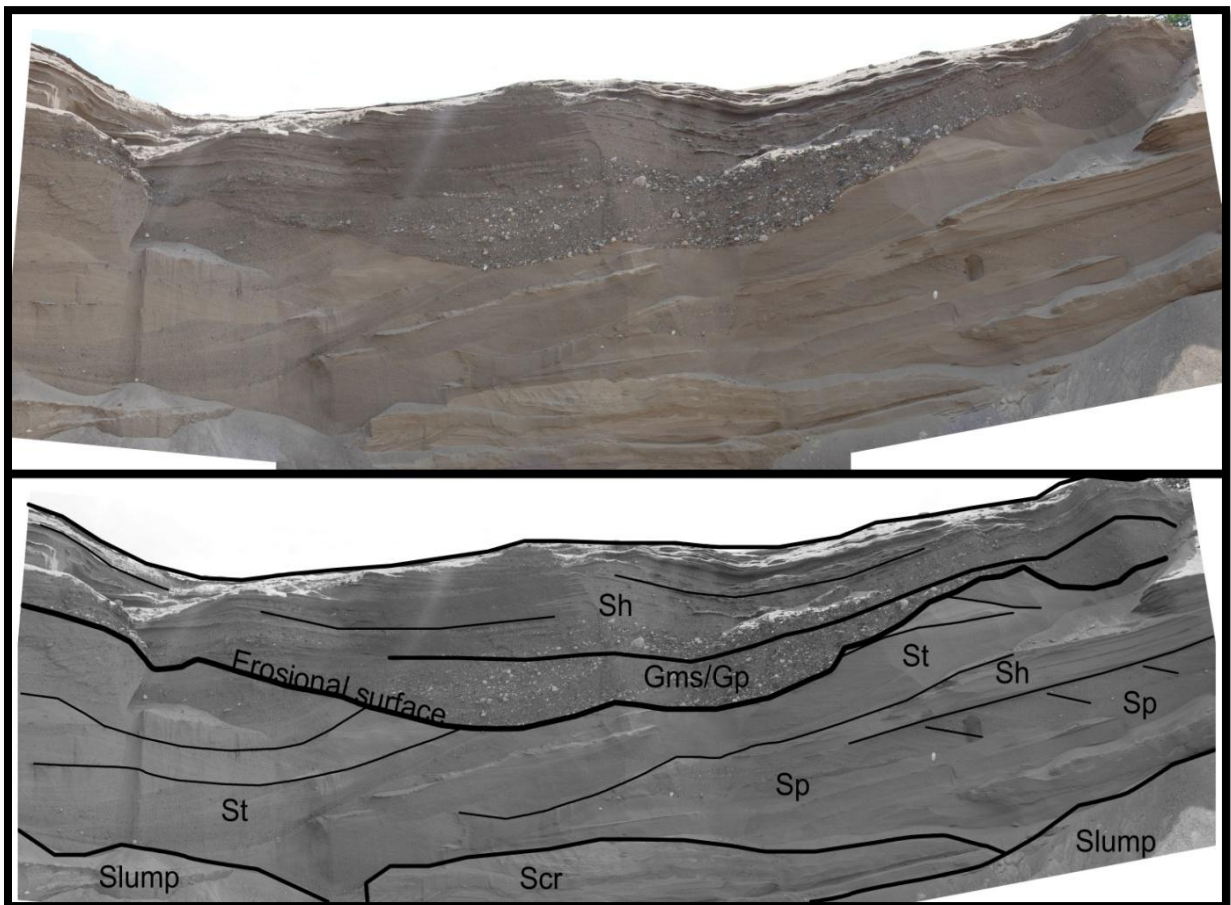


Figure 4-12: A portion of section K (top) and its facies interpretation (bottom)

4.3 Hydrostratigraphic Study

4.3.1 Hydrofacies

Hydrofacies is a term referring to relatively homogenous, but anisotropic, units that are hydrogeologically meaningful ([Poeter & Gaylord, 1990](#)) and can be determined from the lithofacies analysis and hydraulic property measurements. The fourteen different lithofacies observed had samples collected and hydraulic conductivity (K) values calculated ([Appendix D](#)) based on their grain size distribution curves ([Appendix E](#)) using different empirical methods (refer to [Section 3.3.2](#) in this thesis). The results from each approach were within one order of magnitude except for the Terzaghi method, which produced hydraulic conductivity values up to three orders higher than the other methods. The three methods were then combined to form an overall average for hydraulic conductivity from each sample ([Table 3](#)) as this was determined to be the best method to estimate the hydraulic parameter based on facies characteristics. In-situ field testing of the facies for hydraulic parameters, such as an air permeameter, was unavailable, but is recommended in future studies to supplement the hydraulic conductivity data ([Poulsen et al., 2001](#)).

As a result of this work, nine hydrofacies classes were created. For each class, all respective hydraulic conductivity values determined from the grain size analyses were averaged together to form an overall hydraulic conductivity for that hydrofacies unit. These results are summarized in [Tables 4, 5](#) and [6](#), divided into muds, sands and gravels respectively. The mud units would represent aquitards as they present low hydraulic conductivity values, are very cohesive and without any macropores. However, these units did not appear to be laterally continuous throughout the entire pit, which would create windows into the sand-based aquifer units below.

TABLE 4: A SUMMARY OF THE MUD FACIES


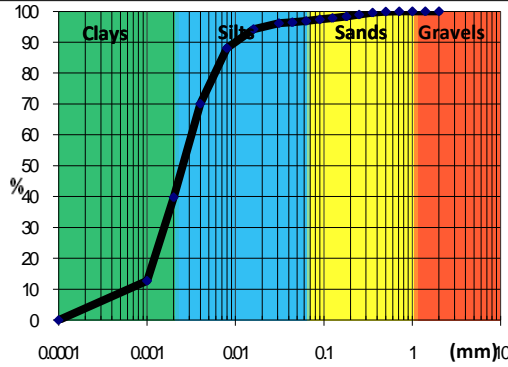

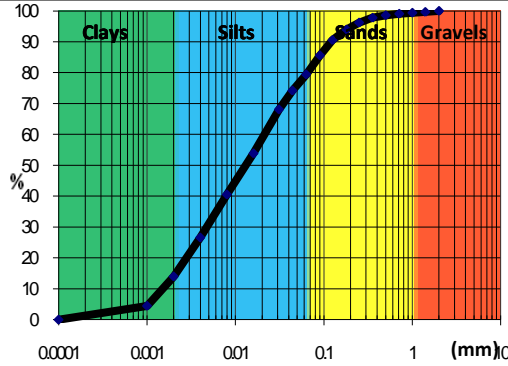

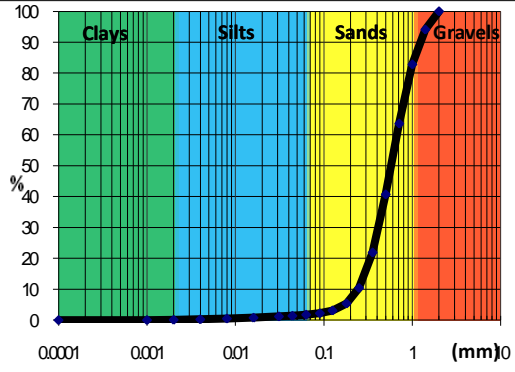

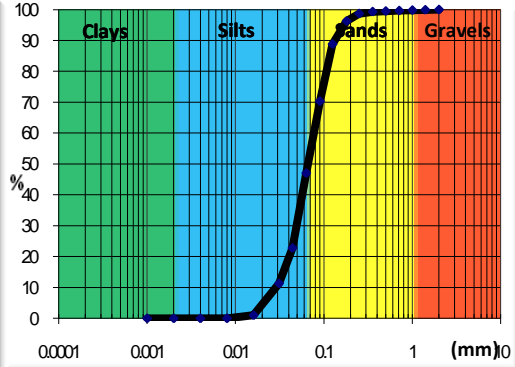
Hydrofacies	Image	Description	Grain Size Distribution	Averaged Hydraulic Conductivity
<p style="text-align: center;">Massive Muds (Fm)</p>		<p>Fine material that exhibits no bedding structure; units range from 0.2-1 meter thick; usually found to be a dark brown to reddish colour; beds have been found interbedded with sand and silt deposits</p>		<p style="text-align: center;">$K = 2.2 \times 10^{-8}$ $\pm 2.3 \times 10^{-8}$ m/s</p>
	<p style="text-align: center;">Facies Included Fm; Fm(w)</p>	<p style="text-align: center;">Number of Samples 8</p>		<p style="text-align: center;">Located at Sections B,C,D,E,F,G,H,I,J,K,M</p>
<p style="text-align: center;">Laminated Muds (FI)</p>		<p>Silt-rich material that displays laterally continuous laminae; tends to overlie sandy deposits and be interbedded with massive mud units; units reach up to 1 meter in thickness</p>		<p style="text-align: center;">$K = 5.3 \times 10^{-8}$ $\pm 5.4 \times 10^{-8}$ m/s</p>
	<p style="text-align: center;">Facies Included FI</p>	<p style="text-align: center;">Number of Samples 3</p>		<p style="text-align: center;">Located at Sections A, J, M</p>

TABLE 5: A SUMMARY OF THE SAND FACIES

Hydrofacies	Image	Description	Grain Size Distribution	Averaged Hydraulic Conductivity
<p style="text-align: center;">Cross-bedded Sands (Sp)</p>		<p>Well-sorted, medium sand deposits that can display uniform dipping unless in areas of deformation; beds have a thickness of millimeter scale but units can be up to 3 meters thick; laterally continuous</p>		<p style="text-align: center;">$K = 2.6 \times 10^{-4}$ $\pm 2.1 \times 10^{-4}$ m/s</p>
	<p style="text-align: center;">Facies Included St; Sp; Sh</p>	<p style="text-align: center;">Number of Samples 35</p>		<p style="text-align: center;">Located at Sections B, C, E, F, G, H, J, K, L, M, N</p>
<p style="text-align: center;">Climbing Ripples (Scr)</p>		<p>Subcritical to supercritical ripples composed of fine sands; beds are on the scale of millimeters while units are generally half-meter thick; appears to be laterally continuous</p>		<p style="text-align: center;">$K = 2.1 \times 10^{-5}$ $\pm 2.7 \times 10^{-5}$ m/s</p>
	<p style="text-align: center;">Facies Included Scr</p>	<p style="text-align: center;">Number of Samples 10</p>		<p style="text-align: center;">Located at Sections F, G, H, K, L, M</p>


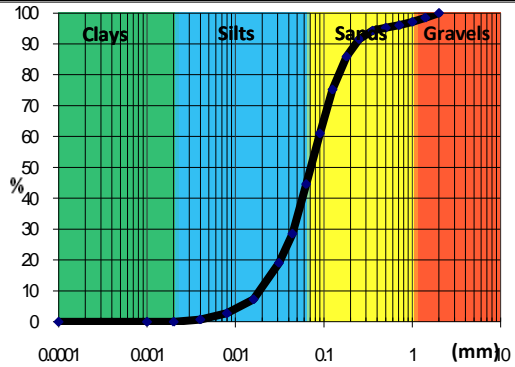

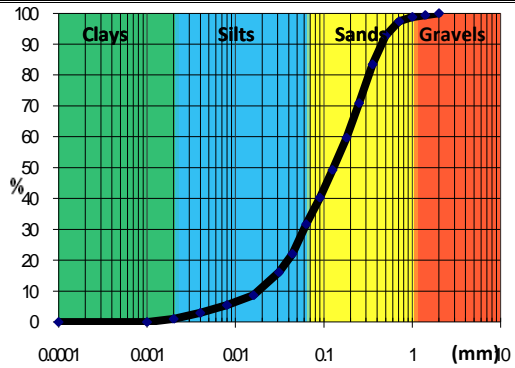

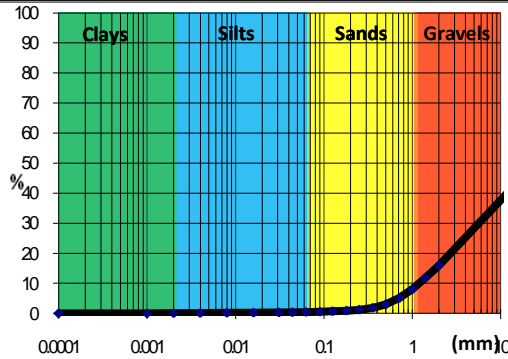

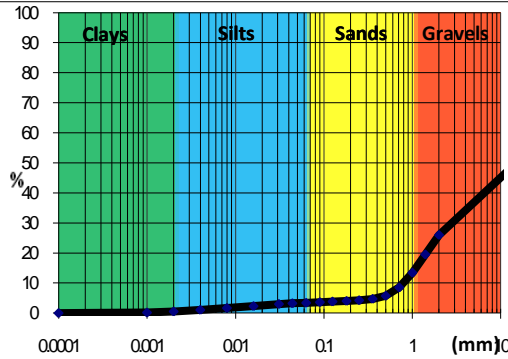

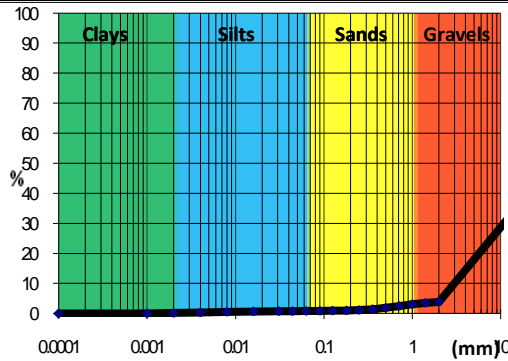
Laminated Sands (SI)		<p>A silty-sand feature that has millimeter-thick laminae with the existence of dropstones; localized deposit that overlies cross-bedded sands</p>		$K = 4.6 \times 10^{-5}$ $\pm 6.1 \times 10^{-5} \text{ m/s}$
	<p>Facies Included SI; SI(d)</p>	<p>Number of Samples 2</p>	<p>Located at Sections D, K</p>	
Deformed Sand Beds (Sd)		<p>Chaotic deposits that are result of folding, faulting and dewatering; mixture of fine to coarse sands that can be interbedded; units are found up to 1m thick; unsure of lateral extent</p>		$K = 6.2 \times 10^{-6}$ $\pm 5.9 \times 10^{-6} \text{ m/s}$
	<p>Facies Included Sd</p>	<p>Number of Samples 2</p>	<p>Located at Sections A, D, G, I, M</p>	

TABLE 6: A SUMMARY OF THE GRAVEL FACIES

Hydrofacies	Image	Description	Grain Size Distribution	Averaged Hydraulic Conductivity
Massive Gravel (Gms)		Poorly sorted sediment mixture of rounded cobble to pebble clasts and sand matrix that display no sedimentary features; total thickness is unknown but is greater than 1 m thick; appears to be laterally extensive		$K = 1.5 \times 10^{-3}$ $\pm 2.1 \times 10^{-3} \text{ m/s}$
	Facies Included	Number of Samples		Located at Sections
	Gm; Gms	8		A, B, C, E, F, H, I, J, K, M, N
Cross-Bedded Gravel (Gp)		Foreset-type bedding of rounded gravel in sandy matrix that range from being poorly to moderately sorted, rounded material; bed thickness ranges from 0.1- 1 meter		$K = 2.4 \times 10^{-3}$ $\pm 5.4 \times 10^{-4} \text{ m/s}$
	Facies Included	Number of Samples		Located at Sections
	Gp	4		A, B, G, I
Openwork Gravel (Go)		Contained within planar cross bedded gravels, this is a matrix-free, moderately sorted unit; contains rounded pebbles that provide a conduit for groundwater; beds are up to 0.1 m thick		$K = 2.0 \times 10^{-2}$ $\pm 2.5 \times 10^{-2} \text{ m/s}$
	Facies Included	Number of Samples		Located at Sections
	Go	2		B, I, J

These windows into the aquifer units below have both a very important effect in redirecting the flow field and significant implications in source water protection ([Martin & Frind, 1998](#)). The cross-bedded sands would be considered aquifers as they contain medium sands and a suitable K value. The deformed sands and climbing ripples would be poor aquifers as they have an inadequate hydraulic conductivity for an aquifer due to their incorporation of fine sands and silts. The gravel units would make superior aquifers as illustrated by their calculated hydraulic conductivities. The porous nature of these facies, especially the openwork gravels, would provide excellent conduits for water flow but also an easy route for contaminants if they entered into the aquifer system.

4.4 Subsurface Analysis

4.4.1 Regional Stratigraphic Model

In [2007 Bajc & Shirota](#) produced the first 3D stratigraphical model of the Waterloo Region, improving upon the work done by [Martin & Frind \(1998\)](#). This new model gives a simplified representation of the subsurface stratigraphy as seen in [Figure 2-3](#) and contains data that can be imported into 3D modeling software which was an invaluable resource for information about the Waterloo Moraine as well as aquifer information. The creators of this model are planning on updating it with a new version that takes borehole quality into account, allowing for much better control of unit geometry and including more data that can be used in geodatabases ([Bajc, personal communication](#)).

4.4.2 Hydrogeology

Groundwater monitoring at the gravel pit indicates that groundwater flow in the area travels in a northeastern direction with a water table elevation of about 331.5 m.a.s.l. ([Pinchin, 2008](#)). Depth to the water table occurs at about 25-30 meters below the surface providing an extensive vadose zone to be studied. The Waterloo Moraine is estimated to be fifty meters thick in the area of Kieswetter Holdings (Figures [2-3](#) & [2-4](#)) producing a vadose zone that represents 50%-60%, by volume, of the Waterloo Moraine system. The sections studied

range in height from 0.5 meters (section E) to about 9 meters in height (Section H). Collectively, these sections expose the first 15 metres of the vadose zone for direct study.

4.4.3 Ground Penetrating Radar

In this study, a 450 meter profile was conducted from the east to the west end of the study pit in an attempt to link as many of the studied sections as possible using 100MHz antennae with a station spacing of 0.25 meters ([Figure 4-13](#)). In addition, four common mid-point (CMP) soundings were collected at the 10m, 150m, 305m and 440m positions along the profile to convert reflector travel time to a corresponding depth. The reflection profile collected across the study area is shown in [Figure 4-14](#). Analysis of the CMP soundings showed that subsurface velocities were approximately 0.095 m/ns from 0 m to 350 m position and 0.065 m/ns from 350 m to 450 m on the profile.

The purpose of this profile was to supplement the borehole data and the sections observed in the pit. While the reflection profile cannot be used to differentiate between various reflection events (i.e. unique characterization of different facies), these GPR data permit lateral correlation between facies characterized from knowledge of facies associations, borehole logs and architectural units. GPR data also display the erosional surfaces separating different architectural elements as it represents a change in physical properties ([Asprion, 1998](#)). GPR could reach the resolution required to detect changes at the lithofacies scale as long as the right GPR profile is designed and planned for ([Neal, 2004](#))



Figure 4-13: The GPR profile path, with position markings, (black) and CMP locations (yellow) linking the subsurface stratigraphy of the studied sections (colours)

The GPR profile appears to show sandy bedforms throughout the section with at least one channel, an onlapping sequence of sand and areas of high and low reflection amplitudes (Figure 4-14). The zone characterized by high reflectivity is thought to be associated with well-sorted sand sequences. A few reflectors are truncated at the top indicating erosion surfaces through the sequence. The lower amplitude and more attenuated zone is associated with windblown silt from stockpiled aggregate piles compacting on the pit floor. Here, signal attenuation is thought to be the result of increased percentage of fine-grained material (i.e. silt and clay) underlying the sand material. The underlying finer-grained material noted in the central portion of the profile could be the integration of Maryhill Till into the Waterloo Moraine (i.e. [Bajc & Shirota, 2007](#)), which may have produced a small perched aquifer. The onlapping sequence represents the infill of a channel by well-sorted sand layers. A small channel is observed in the poor reflection area orientated normal to the profile. These channels very well could have formed in a subaqueous fan environment, leading away from the ice front.

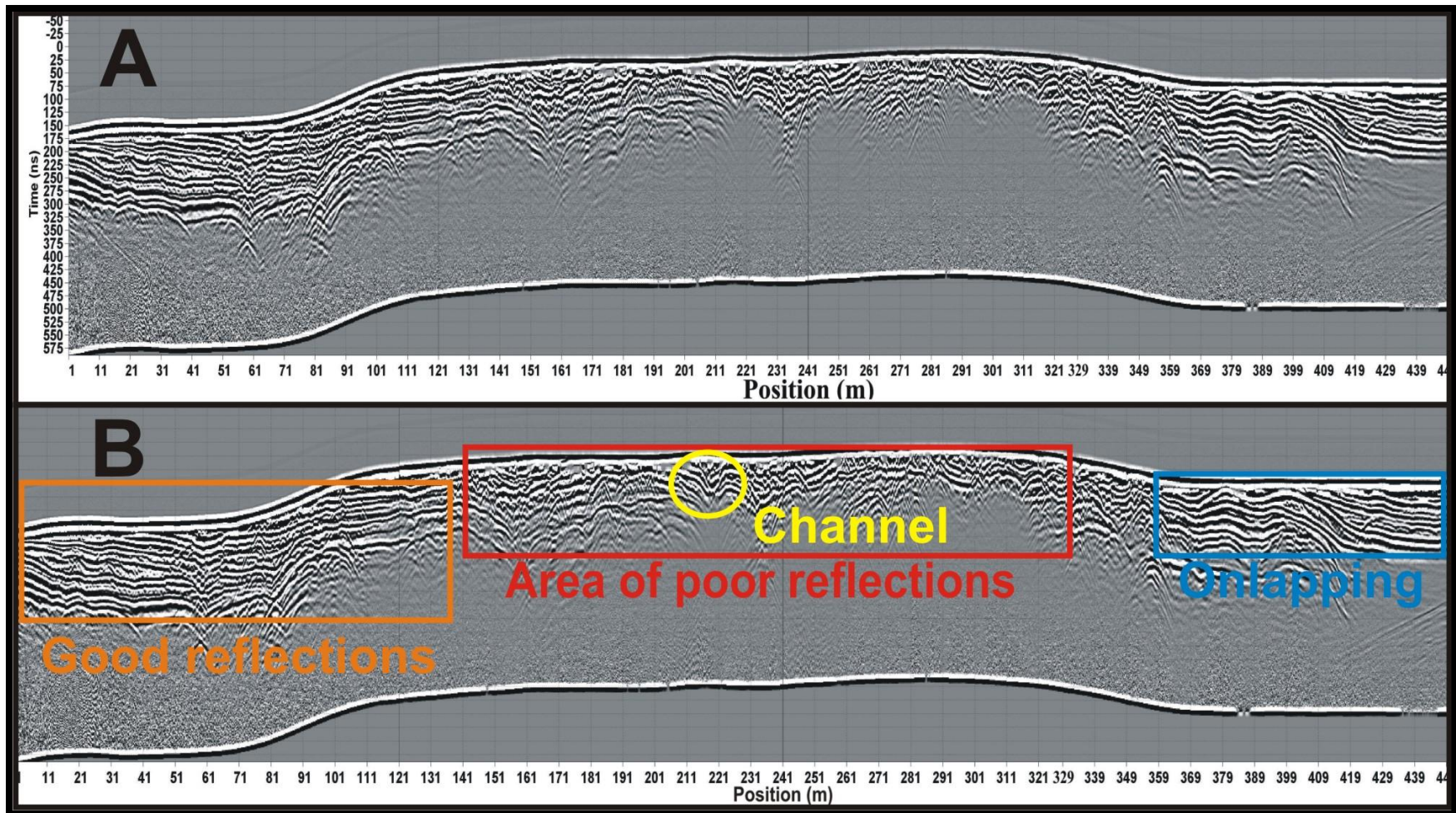


Figure 4-14: The resulting GPR profile conducted at Kieswetter Holdings with reflection times (A) and the interpretation of subsurface features (B) with paleoflow generally from left to right

4.5 Depositional Interpretation

The sequence of facies successions is characteristic of a given depositional setting ([Walker, 1992](#)). A close examination of the facies and their associations in the study area may thus help understand the origin of the Waterloo Moraine. This study found fourteen facies, which were subdivided into facies classes. Their interpretation of deposition can be found in [Table 1](#). The eastern part of the pit has a general facies association of massive and cross-bedded gravel underlying cross-bedded sands and climbing cross-stratified ripples. These sandy bedforms are capped by laminated and massive mud units. Sections A and M best illustrate this overall association while Sections C, I and J support the facies succession, but are highly deformed. The western area is typically formed of sandy bedforms with cut-and-fill channels. It is generally agreed upon (i.e. [Karrow, 1993](#); [Bajc & Shiota, 2007](#)) that the Waterloo Moraine is an ice-marginal deposit. Based on the facies associations at Kieswetter Holdings, the deposition of the Waterloo Moraine can be locally related to glaciofluvial and subaqueous channel environments ([Eyles & Eyles, 1992](#)).

Recent sedimentary studies of the Waterloo Moraine assert that the moraine was the consequence of an esker-fed jet-efflux subaqueous fan deposit ([Russell et al., 2007](#)), a combination of the depositional environments described by [Eyles & Eyles, 1992](#). [Russell & Arnott \(2003\)](#) best describe the formation of a glaciogenic subaqueous system based on evidence from the Oak Ridges Moraines, and the Waterloo Moraine is thought to be analogous that moraine ([Russell et al., 2007](#)). The model proposed by [Russell & Arnott \(2003\)](#) suggests that an esker was the transport mechanism for the sediment, with a jet-efflux outlet and the deposition occurring due to rapid flow expansion. The loss of transport competence at the ice margin as the flow changed from a confined conduit flow to either an open or ice-covered water column resulting in a fan environment. The type of jet-efflux is dependent on the position of the outlet as it enters the water body ([Figure 4-13](#)) with a modifier of a hydraulic jump, which is a transition from supercritical to subcritical flow (i.e. [Rajaratnam & Subramanyan, 1986](#)).

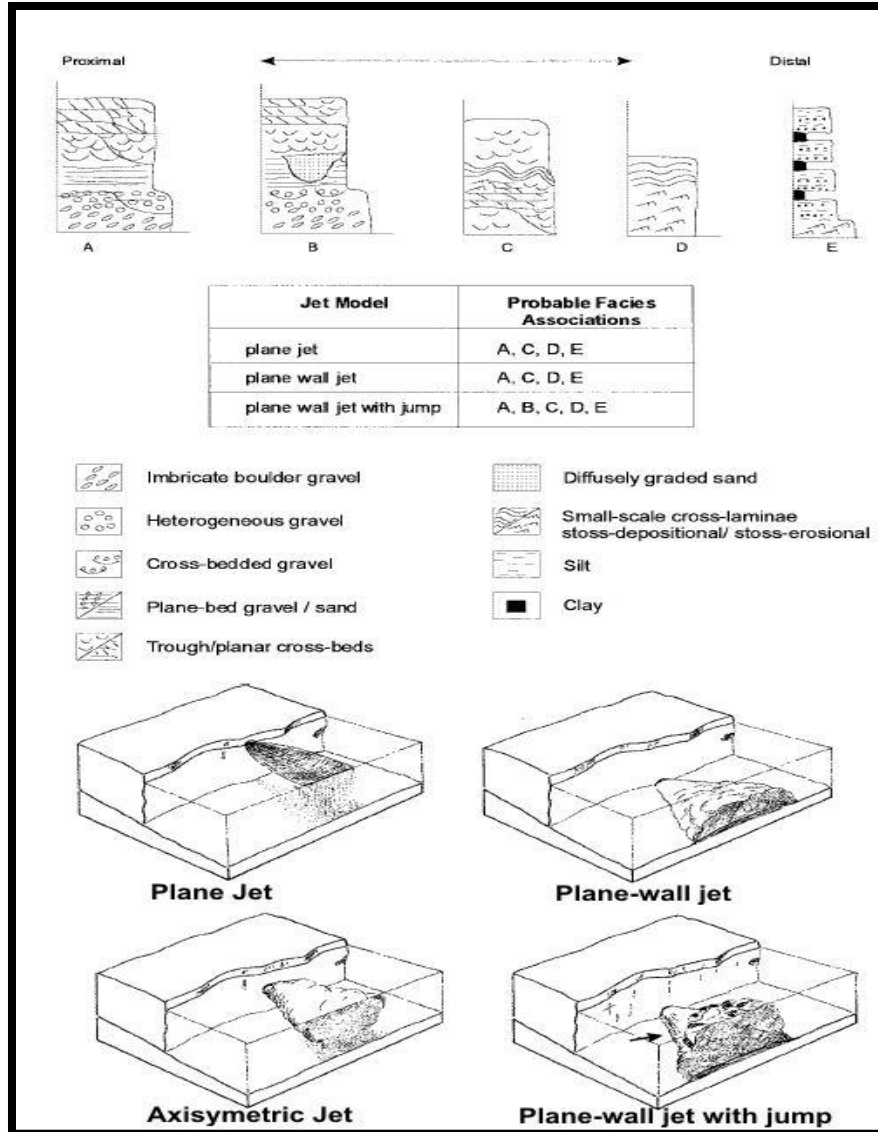


Figure 4-15: The facies associations connected with various jet-efflux models
 Modified from Russell & Arnott, 2003

The assemblages of the eastern area would be similar to the facies associations A to C in [Figure 4-15](#) indicating a depositional environment between proximal and intermediate regions of the fan. [Figure 4-16](#) is a conceptual model for the creation of a subaqueous fan, and this area would be representative of the zone of flow establishment and the transition zone. Diffusely graded sand is proposed to be the product from a hydraulic jump ([Russell & Arnott, 2003](#)) and illustrated in association B of [Figure 4-15](#) and transition zone of [Figure 4-](#)

16. In the absence of this facies, it can be assumed that no hydraulic jump took place. However, as [Kostic & Parker \(2007\)](#) demonstrated, and given the right conditions, hydraulic jumps do not always occur when the sediment is very coarse. The western part is defined by mostly sandy planar and trough cross-bedding with interbedded cross-stratified climbing ripples. This association matches facies associations C and D from [Figure 4-15](#) denoting this area as an intermediate to distal area and are of established flow ([Figure 4-16](#)) of a subaqueous fan deposit.

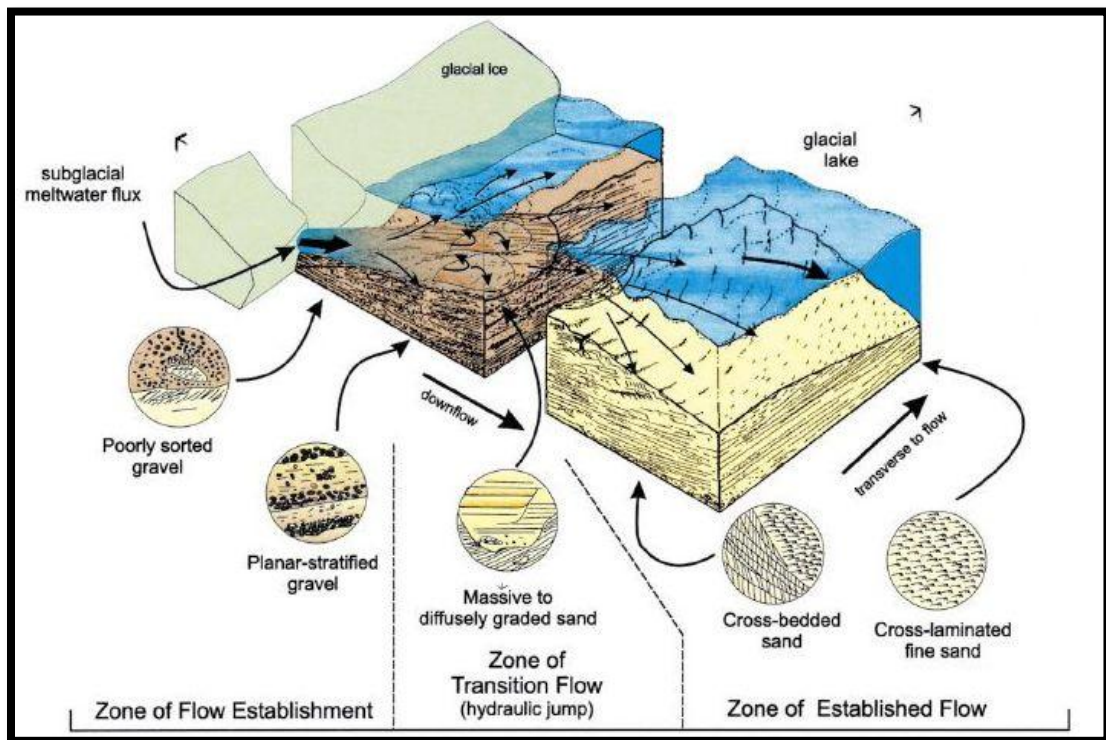


Figure 4-16: Conceptual model of a subaqueous fan system

Modified from Russell & Arnott, 2003

Additional support for the subaqueous fan interpretation is found in [Lønne, 1995](#) and defines a subaqueous fan as a block of coarse sediment deposited within a water column displaying well-bedded foreset and bottomset deposits, but lacking any subaerial, stream-laid or delta-plain facies ([Figure 4-17](#)). Although there are differences in the sedimentation processes of glaciolacustrine versus glaciomarine environments due to density contrasts, there are also

similarities. [Lønne, 1995](#) provides four criteria to recognize a submarine fan deposit and to distinguish it from other glaciomarine environments: 1) resedimented subglacial material; 2) submarine outwash deposits; 3) ice-rafted material and 4) glaciotectonic deformation. Resedimented subglacial material is generally a result of sediment gravity flows near a glacier's terminus ([Reading, 1996](#)). Resedimented material is believed to have occurred at Sections C, J and M ([Figure 4-18](#)). In the units classified as F1 at these sections, fine laminated material does exist, but is incorporated with cobble clasts and gravel units. The heterolithic bedding created ([Figure 4-4](#)) would have been a result of glacier advancement as the ice front would have created debris flows. The laminated fines units must have existed before the advancement and it is proposed that they settled out in a distal proglacial lake setting before the readvancement of the glacier.

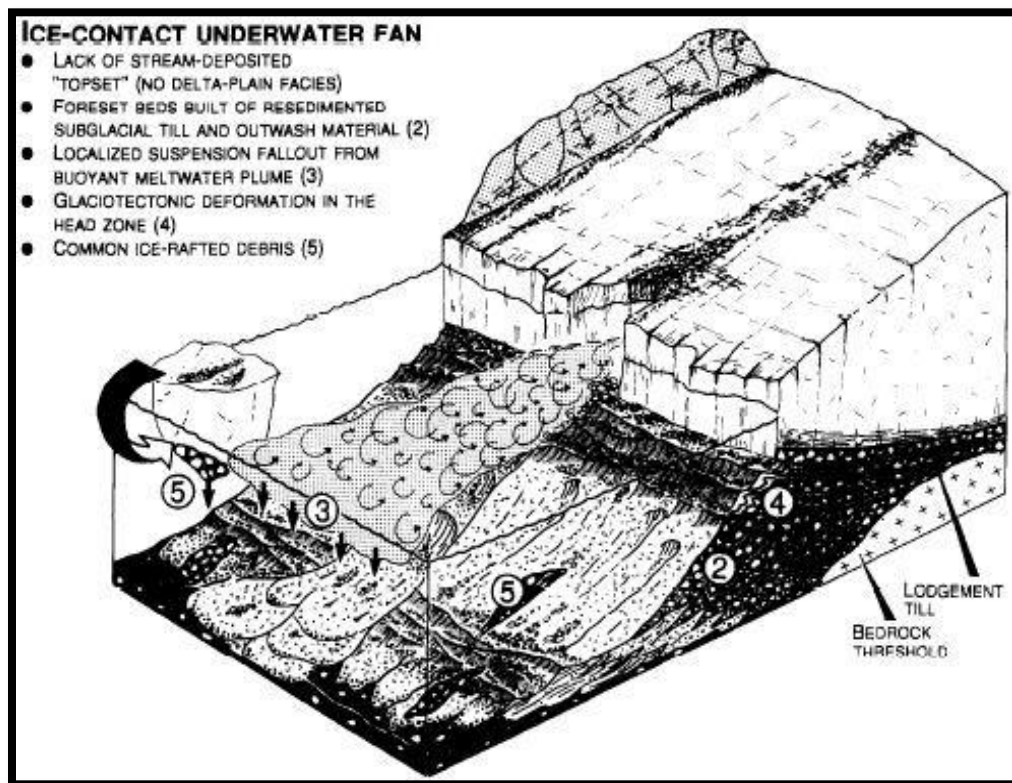


Figure 4-17: Principal characteristics of an ice-contact underwater fan
Modified from Lønne, 1995



Figure 4-18: Portion of Section C displaying beds of resedimented material with a general strike and dip of N043/27

The facies assemblages in the western part of the pit are believed to be representative of subaqueous outwash deposits. These deposits are readily recognizable by a relatively high textural maturity with good sorting along with the presence of channels containing traction-based coarse material ([Lønne, 1995](#)). Outwash deposits are believed to be illustrated best at Sections H ([Figure 4-11](#)) and K ([Figure 4-12](#)) where the movement of textural mature sand dunes gets truncated by the formation of channels. Ice-rafted material is known to be shed from icebergs and from partly floating glacier termini, signifying a very ice-proximal location (i.e. [Benn & Evans, 1998](#)). Occurrences of isolated clasts were found at Section D in laminated sandy material near the top of the section ([Figure 4-19](#)). The possible dropstones are thought to have fallen from an iceberg's melted upper surface ([Ovenshine, 1970](#)). The last criterion for recognition of a subaqueous fan is the presence of glaciotectonic

features. The discovery of sheath folds provides a strong case for glaciotectonism and is supported by the thrust block evidence at Section I, as mentioned earlier in this chapter.

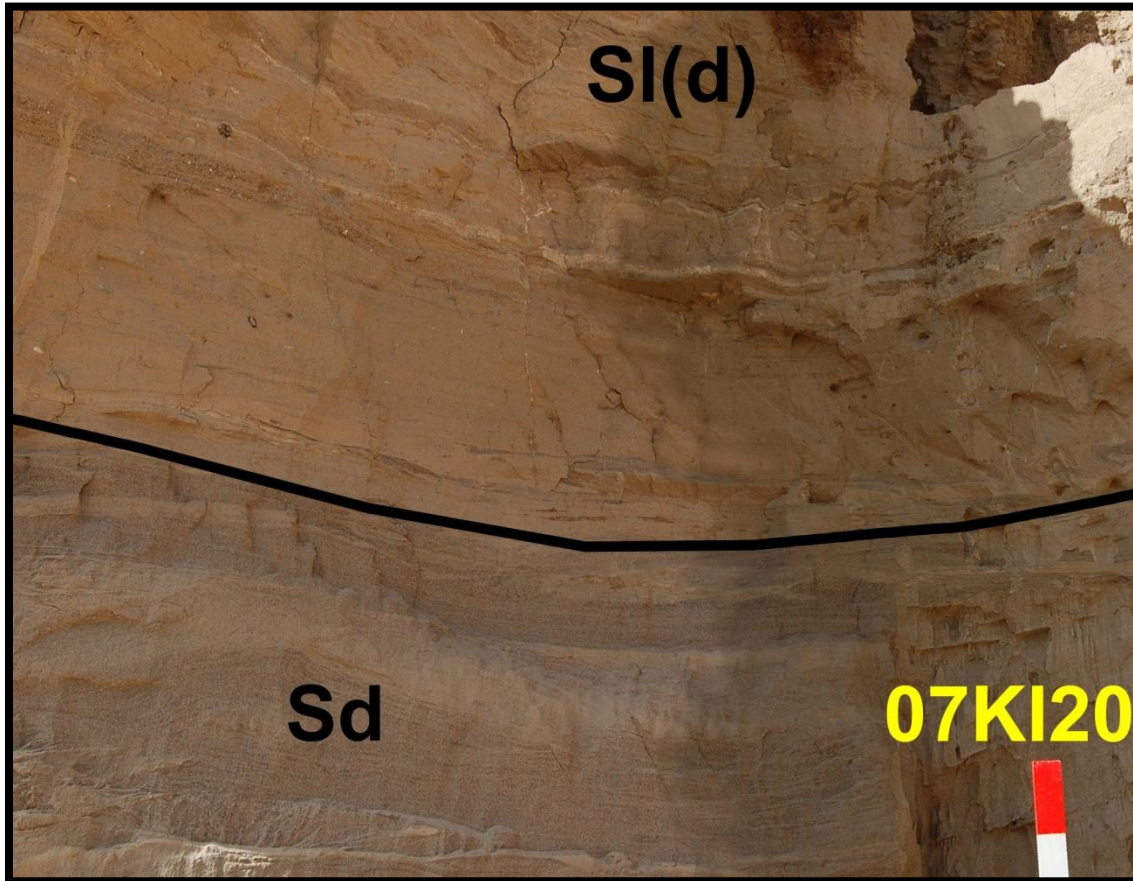


Figure 4-19: Isolated clasts, or possible dropstones, in laminated sandy material (top)

With the facies and their associations found at Kieswetter Holdings corresponding to the model proposed by [Russell & Arnott, 2003](#) along with the evidence documented meeting the criteria put forward by [Lønne, 1995](#), it is believed that the Waterloo Moraine area around the research site is contemporaneous or penecontemporaneous systems tract with an ice margin proximal heterogeneous and deformed domain grading into the more distal sandy assemblages formed by a subaqueous fan. This west to northwestern trend of decreasing heterogeneity and deformation ([Figure 4-20](#)) supports an ice lobe coming from the east-southeast, and the surficial presence of Maryhill and Port Stanley Till in the area gives support to the Erie-

Ontario lobe present here ([Karrow, 1993](#)). If the diamictons at the top of the sections are of glacial origin, a more significant glacier advance would be indicated. After the advance, the ice permanently retreated but a water column remained over the area producing the laminated and massive muds that cover the deformed sands in the eastern part of the pit. [Eyles & Eyles \(1992\)](#) characterizes ice proximal subaqueous deposition by evidence showing rapid deposition and resedimentation of meltwater deposits on subaqueous fans, complex facies associations and the domination of glacial processes, all noticeably seen in the eastern region.



Figure 4-20: Direction of decreasing heterogeneity and deformation for the research area

The Waterloo Moraine is a complex deposit. The evidence documented at Kieswetter Holdings supports an esker-subaqueous fan environment. It is quite possible for the Waterloo Moraine to be a summation of several geological processes, such as multiple jet effluxes, coalescing fan deposits and multiple glacial re-advances. The evidence recorded at Kieswetter Holdings was only within the first 15 metres of the surface, but the Waterloo Moraine unit is approximately 50 meters thick at the research site (Figures [2-3](#) & [2-4](#)).

Stratigraphical models of the Waterloo Moraine show there are till units within the Moraine system, but these incorporated tills were not found in any section at Kieswetter Holdings. Continuing study of the entire Waterloo Moraine will lead to a more comprehensive understanding of the origin of this deposit.

4.6 Testing the Borehole Database



Figure 4-21: Location of the tested boreholes around the study area (left) and location of the example borehole log (right); green dots represent excellent borehole logs while yellow symbolizes good borehole records and red characterizes poor data

The collection of borehole data, along with interpreted boundary data for the Waterloo Moraine and other significant stratigraphical units, were obtained from the report of [Bajc & Shirota, 2007](#). The numerous logs were restricted to a defined area outlined by the UTM coordinates of northings 4804000-4805500 and eastings 538000-540000. This 3km² area contained 50 boreholes to test against the observed data recorded in Kieswetter Holdings ([Figure 4-21](#)). In constructing this test, the upper and lower boundaries of the Waterloo Moraine were marked out using the available interpreted data from the ARCInfo grids in

[Bajc & Shirota, 2007](#). The test was then restricted to 17 boreholes that completely penetrated the moraine unit ([Table 7](#)), thus eliminating 33 boreholes that were either too shallow or were based on geophysical interpretations.

To test the accuracy of these boreholes, a comparison of facies proportions was conducted between the observed near-surface data with that recorded in the logs. The length of each unit for every borehole was measured and summed up with all equivalent units to be divided against the thickness of the Waterloo Moraine at that location to give a facies proportion. This measure was tested against virtually constructed models with proportions based on computer calculated volumes that reflect a division of the section as a whole. The borehole records were generally simplified in their sedimentology characterization and as such, all the documented information was simplified into the three basic sediment classes: muds, sands and gravels. Diamicton and silt units were lumped into the mud category as they are composed of fine material and this simplification was also done during the recording of all observed data.

Table 7: Calculated Facies Proportions from Boreholes Accessing the Entire Waterloo Moraine

Well	Moraine Thickness (m)	Sediment Facies	Total Facies Thickness (m)	Facies Proportion
1068237	47.24	Mud	18.29	38.71%
		Sand	28.96	61.29%
1068231	69.80	Gravel	8.84	12.66%
		Mud	48.77	69.87%
		Sand	12.19	17.47%
1070372	72.90	Gravel	72.90	100.00%
1070854	49.13	Gravel	1.52	3.10%
		Mud	46.39	94.42%
		Sand	1.22	2.48%
1071967	56.08	Mud	8.8392	15.76%
		Sand	47.24	84.24%
1072029	56.08	Mud	0.61	1.09%
		Sand	55.47	98.91%
1072220	47.24	Gravel	4.88	10.32%
		Mud	37.80	80.01%
		Sand	4.57	9.68%
1078821	44.20	Sand	44.20	100.00%
1115247	58.83	Mud	47.85	81.34%
		Sand	10.98	18.66%
1115250	41.15	Gravel	5.49	13.34%
		Mud	34.44	83.69%
		Sand	1.22	2.96%
1115251	39.01	Gravel	18.90	48.45%
		Mud	14.02	35.94%
		Sand	6.09	15.61%
1116094	49.99	Gravel	4.57	9.14%
		Mud	9.75	19.50%
		Sand	35.67	71.35%
1116099	64.62	Gravel	1.22	1.89%
		Sand	63.40	98.11%
1119750	37.18	Mud	22.24	59.82%
		Sand	14.94	40.18%
1122146	32.00	Gravel	14.94	46.69%
		Mud	1.52	4.75%
		Sand	15.54	48.56%
1122491	41.45	Gravel	19.20	46.32%
		Mud	13.41	32.35%
		Sand	8.84	21.33%
1122998	60.66	Gravel	6.40	10.55%
		Mud	0.91	1.50%
		Sand	53.35	87.95%
Average	51.03	Gravel	9.08	17.79%
		Mud	18.57	36.40%
		Sand	23.38	45.81%

Table 8: The Proportion of facies, based on well and type in alphabetical order, of the Near-Surface Boreholes

Well	Sediment Facies	Total Facies Thickness (m)	Facies Proportion
1068226	Mud	15.00	100.00%
1068231	Gravel	8.84	58.93%
	Sand	6.16	41.07%
1068237	Mud	13.44	89.60%
	Sand	1.56	10.40%
1069919	Mud	15.00	100.00%
1070372	Gravel	15.00	100.00%
1070854	Gravel	1.53	10.20%
	Mud	13.47	89.80%
1071967	Mud	0.67	4.47%
	Sand	14.33	95.53%
1072029	Mud	0.60	4.00%
	Sand	14.40	96.00%
1072220	Gravel	4.88	32.51%
	Mud	10.12	67.49%
1072281	Gravel	15.00	100.00%
1073952	Sand	15.00	100.00%
1115247	Mud	4.02	26.80%
	Sand	10.98	73.20%
1115250	Gravel	3.96	26.40%
	Mud	9.82	65.47%
	Sand	1.22	8.13%
1115251	Gravel	4.89	32.60%
	Mud	10.11	67.40%
1116094	Sand	15.00	100.00%
1116099	Gravel	1.22	8.13%
	Sand	13.78	91.87%
1118434	Gravel	10.73	71.53%
	Mud	1.22	8.13%
	Sand	3.05	20.33%
1119750	Mud	6.77	45.13%
	Sand	8.23	54.87%
1120962	Gravel	11.03	73.53%
	Sand	3.97	26.47%
1122146	Gravel	5.86	39.07%
	Mud	1.52	10.13%
	Sand	7.62	50.80%
1122491	Mud	6.16	41.07%
	Sand	8.84	58.93%
1122998	Gravel	6.40	42.67%
	Sand	8.60	57.33%
Average	Gravel	4.06	27.07%
	Mud	4.91	32.70%
	Sand	6.03	40.22%

The sections studied in the gravel pit reflect only a portion of the Waterloo Moraine unit. With this deposit being complex, it is quite possible that the near-surface element reflects a different composition than the whole unit. Altogether the sections excavated fifteen meters into the Waterloo Moraine below the surface and this depth would be classified as near-surface. Five boreholes, from the initially rejected 33 boreholes, were added as they fully penetrated this depth of the moraine but not the entire unit. The findings for the near-surface area of study can be found in [Table 8](#). It should be noted that the sediment facies are listed in alphabetic order for [Tables 7](#) and [8](#) and not in any particular stratigraphic sequence. These boreholes covered just the first 15 meters in depth from the surface of the Waterloo Moraine, and the facies proportions of muds, sands and gravels for this area are 32.7%, 40.2% and 27.1% respectively. Compared to [Table 2](#), which reflects the facies proportions from each section, the data is noticeably different as there is a proportion of 18.5% mud, 59.7% sand and 21.8% gravel. For the 17 boreholes that fully penetrated the complete Waterloo Moraine deposit, the proportions are 36.4% mud, 45.8% sand and 17.8% gravel, as seen in [Table 7](#), and all of these percentages are evaluated against each other in [Table 9](#).

Table 9: Comparison between all proportion methods

<i>Proportion Type</i>	Mud	Sand	Gravel
Section Data	18.5%	59.7%	21.8%
Near-Surface Boreholes	32.7%	40.2%	27.1%
Entire Waterloo Moraine unit	36.4%	45.8%	17.8%

The facies proportional data based on the direct observations from studied sections at Kieswetter Holdings provide a glimpse into the structure of the Waterloo Moraine and as such, this is verified, reliable data. Upon comparing the section data, it was found that the amount of gravel is comparable to the borehole records; however, the mud and sand estimates differ greatly. There is approximately 20% more sand in the pit sections than in the borehole intervals. The results from the borehole database suggest that the near-surface

proportions and the entire Waterloo Moraine are composed in the same manner. It is tempting to conclude that the borehole records underestimate the sand while overestimating mud. Possible causes could be linked to the drilling methods. For example, mud rotary cuttings are poor at representing in situ material, as samples contain the mud slurry used in drilling, leading to higher mud content. Alternately, it is possible that the section analysis underestimates the amount of mud because of the bulldozing of mud material away from aggregate rich areas. Yet, it is unlikely that this would have led to a 20% bias because if the mud layers on top of the sand were thick, they would still be evident on the sides of the pit. The muddy unit on top of the sand appeared to be relatively thin, although some outer walls were obscured by slumped material. More important, the mud layers in the borehole database are not concentrated at the top. As previously mentioned, there is no obvious fining-upward sequence in the database. Therefore, it can be reasonably concluded that the borehole database overestimates the amount of mud in the study area.

5 - Discussion

5.1 The Multi-Scale Approach

In this research, an approach was developed to collect georeferenced sedimentologic information from surficial excavations, and to store this information in a 3D system for use in sedimentologic and hydrostratigraphic analyses of complex aquifer systems such as the Waterloo Moraine. The method uses a reflectorless total station, RTK GPS, and sophisticated geomodelling software to link observed sedimentological information from the particle scale up to the kilometer scale. The first goal was to describe and analyze in three dimensions the lithofacies along a series of sections in an excavation in part of the Waterloo Moraine. The second step was to interpret facies assemblages and spatial transitions in terms of depositional environment. The third step was to classify the facies into hydrofacies based on grain size data, and to determine how these hydrofacies are organized into the various architectural elements that define the hydrostratigraphy at the Kieswetter Holdings study site. This documentation forms the basis of a 3D geodatabase that can be used to improve understanding of the Waterloo Moraine aquifer system. The following sub-sections discuss some aspects of the proposed methodology.

5.1.1 Application of Equipment and Tools

The use of all equipment in this study required extensive training and overcoming steep learning curves. However, it is believed that a trained professional could complete data acquisition of one pit from only a few days up to two weeks, depending on the size and complexity of the excavation, and accessibility issues. When computer work and interpretation are added, it is estimated that it would require approximately one year for two dedicated persons to produce a geodatabase of 10-15 pits across a watershed. This approach is thus considered to be realistic and feasible as the duration of watershed and regional hydrogeology studies is typically three years or more. In addition, it is likely that

improvements to the method and emerging technologies (see below) will help streamline and speed up the process while improving resolution and accuracy.

5.1.2 Field Data Acquisition

Attaining the georeferenced points proved to be an effective method that was fast and produced reliable data. With the process perfected, a sixty-metre section with over a hundred measured points could easily be completed within a day, including the gathering of samples and planar measurements of beds. However, this process involved going directly to the outcrop face to mark measured locations and to take samples. Safety was always a priority when conducting field work, but further measures should be implemented in future studies. An example of ensuring the protection of workers would be to identify and photograph in-situ markers instead of going up to the cliff face. To notate these markers, digital images of the outcrop would be taken and uploaded into a field computer where image-editing software would be employed to notate these locations, such as using a laptop with a tablet feature. This on-site computer work would prevent the risk of collapse of debris onto a person while providing a simple solution to collecting the necessary information. As well, the gathering of field measurements and samples should be conducted from areas where there is no threat of injury, such as the collapse of sediment from an outcrop wall. In the collection of field samples and measurements, a predetermined amount of samples should be gathered to ensure a satisfactory statistical analysis of all data collected and would be done prior to going out to the field.

Ground penetrating radar was employed in this approach to see if it could provide any additional information in defining architectural elements below the surface, as it is the preferred geophysical method in sand-rich deposits. The results were satisfactory as the sand and gravel units provided clear reflections, but the signals were easily weakened by the existence of silts and clays, most notably from wind-blown silt on the surface. To effectively use GPR to delineate architectural units, more profiles would have to be conducted to get a true 3D representation of these units (i.e. [Heinz & Aigner, 2003](#)), as long as there are no

muds to decrease the reflected signal. Given the complex formation of the Waterloo Moraine, seismic methods should be attempted as this technique can overcome the limitations of GPR profiling, and has proven to be effective in similar geological settings such as the Oak Ridges Moraine (i.e. [Pugin et al., 1999](#)).

5.1.3 Hydraulic Parameter Calculations

The estimation of hydraulic conductivity and porosity by empirical means in this project was produced essentially for the purpose of demonstrating the overall approach. For this purpose, these empirical calculations were the most appropriate and effective way to study the hydrofacies. The calculations are not a substitute for direct in-situ field measurements, and other techniques could be employed to supplement the hydraulic conductivity data. Some of the lithofacies appeared to be dense and possibly overconsolidated, which would decrease porosity and hydraulic conductivity values. This factor is not taken into account in the equations.

5.1.4 Summary of the Approach

The method developed and tested for this thesis proved to be an effective way to document the sedimentary and related hydrogeological features of surficial outcrops. Using the combination of a total station, GPS, traditional field techniques and a few software packages, the production of 3D representations of direct local observations can be done economically and in a reasonable amount of time. This data can be used to check the quality of other data sources such as the interpretation of borehole logs and groundwater modeling estimations. A test was attempted on the borehole records in the vicinity of the studied region which showed that they may underestimate the amount of sand relative to silt and clay in the study area. However, this testing of boreholes is based upon a study of 22 near surface and 17 fully penetrating boreholes of the Waterloo Moraine. A more complete and thorough test of the boreholes can be obtained by documenting more excavations.

5.2 Other Techniques

New technologies are emerging to improve data collection methods for remotely making 3D-measurements at inaccessible locations, and include such examples as handheld laser rangefinders (e.g. [Alfarhan, 2008](#)), terrestrial laser scanning tools (TLS) such as LiDAR (e.g. [Bellian et al., 2005](#); [Bonnaffe et al., 2007](#)) and close range photogrammetry (e.g. [Haneberg, 2008](#); [Stohr et al., 2009](#)). Laser rangefinders are similar to reflectorless total stations but have a longer range, generally up to 1 km, and are able to view the data being recorded in real time ([Alfarhan, 2008](#)). TLS and photogrammetry are different approaches to collect outcrop data than what was used in this thesis. TLS is best known for its use in digital elevation model (DEM) constructions of mine pits, as well as large inaccessible rock outcrops, while photogrammetry uses stereo pairs of photographs to make measurements.

5.2.1 Terrestrial Laser Scanning

The TLS is proving to be a powerful method of acquiring a high-resolution set of points that captures the detailed geometry of the surface of an outcrop in a short period of time. These points can then be used to create a triangulated surface used for the draping of high-resolution digital photographs to create virtual outcrops ([Bonnaffe et al., 2007](#)). This tool would be beneficial in the 3D modeling process as it would cut down the time of producing virtual surfaces. Also, if the TLS unit has a built-in camera, radial distortion would be minimized in the draping process producing more accurate results. TLS can easily be integrated into 3D geomodelling software for sound interpretations and visualizations ([Bellian et al., 2005](#)). The results of TLS provide a better 3D point cloud of data than that generated by using the total station, which could highlight key features missed by the total station (i.e. fault planes) and would produce a ‘true’ virtual image of all outcrops seen. If this equipment was used at Kieswetter Holdings, it is believed that the entire pit could have been mapped, georeferenced and imaged in one field season. However, the TLS method is quite new and still very expensive, and not yet as user-friendly as other more well-known surveying techniques. In addition, the TLS is capable of producing sub-centimetre resolution of an outcrop. A 3000m by 100m section at centimeter resolution requires 42GB of storage,

which can be handled by the most recent PC computers. However, a centimeter scale reconstruction of an outcrop may not always be necessary. TLS could be a very useful tool in acquiring georeferenced data points of inaccessible locations quickly as well as saving time in processing but it is still in development, and equipment and training costs are substantial. In time, this method will likely become the preferred way of surveying inaccessible locations once equipment costs become within reach of most organizations.

5.2.2 Photogrammetry

Close range photogrammetry (CLR) using uncalibrated high-resolution digital cameras is a relatively low-cost method for acquiring imagery to extract a georeferenced stereomodel of an outcrop. This technique is referred to as close-range because the object photographed is nearer than aircraft altitudes ([Stohr et al., 2009](#)). In the past, this method was a primitive way of calculating measurements, but modern technology has allowed for the combination of high-resolution photos with advanced software packages such as Sirovision and Sirojoint (<http://www.sirovision.com>) and created a renewed interest in this technique. The approach in stereophotogrammetry of geologic outcrops involves collecting at least two photographs of an exposure, surveying the camera location, determining and measuring the control points of the outcrop and the post-processing of all the data using geomodelling software.

This method was evaluated as an alternate approach during research for this thesis in collaboration with the Illinois State Geological Survey (ISGS) and is summarized in [Stohr et al., 2009](#). The results from this study found that the software package Sirovision provides great orthorectification of the photos, correcting for radial displacement in the images when it is able to. For optimal orthorectification, accuracy is dependent upon surveying and camera orientation, which must be aligned precisely so that the axes are parallel. Error was found to be an issue in [Stohr et al., 2009](#) as error of absolute measurements in the stereomodels was unusually high and likely stemmed from unbalanced setup spacing between the instrument station and backsight, a consequence of site limitations at the research site. The recent

version of Sirovision attempts to correct error by adding in more control points, but has yet to prove it can adequately reduce the inaccuracies ([Stohr, personal communication](#)).

Sirovision also has the ability to produce a 3D point cloud of data from at least two stereophotos and a few control points, giving the potential of creating a more accurate 3D representation of an outcrop than from using a total station alone. [Figure 5-1](#) illustrates this feature from data collected using the CLR approach at the Thornton Quarry in Illinois ([Stohr et al., 2009](#)). Using the approach developed for this thesis, radial displacement error reached up to the meter scale at some sections. As a comparison, Sirovision decreased this inaccuracy up to a factor of 50%, reducing the displacement into an acceptable range of a few decimeters. This software is a significant benefit in producing accurate, reliable, virtual representations of any outcrop. However, it should be realized that this software is demanding of camera orientation to produce accurate results; but if achieved, the results are worth the trouble. Being relatively low-cost software, Sirovision or an equivalent would make a great addition to the multi-scale approach tested here and should be considered in any future low-cost outcrop mapping projects.

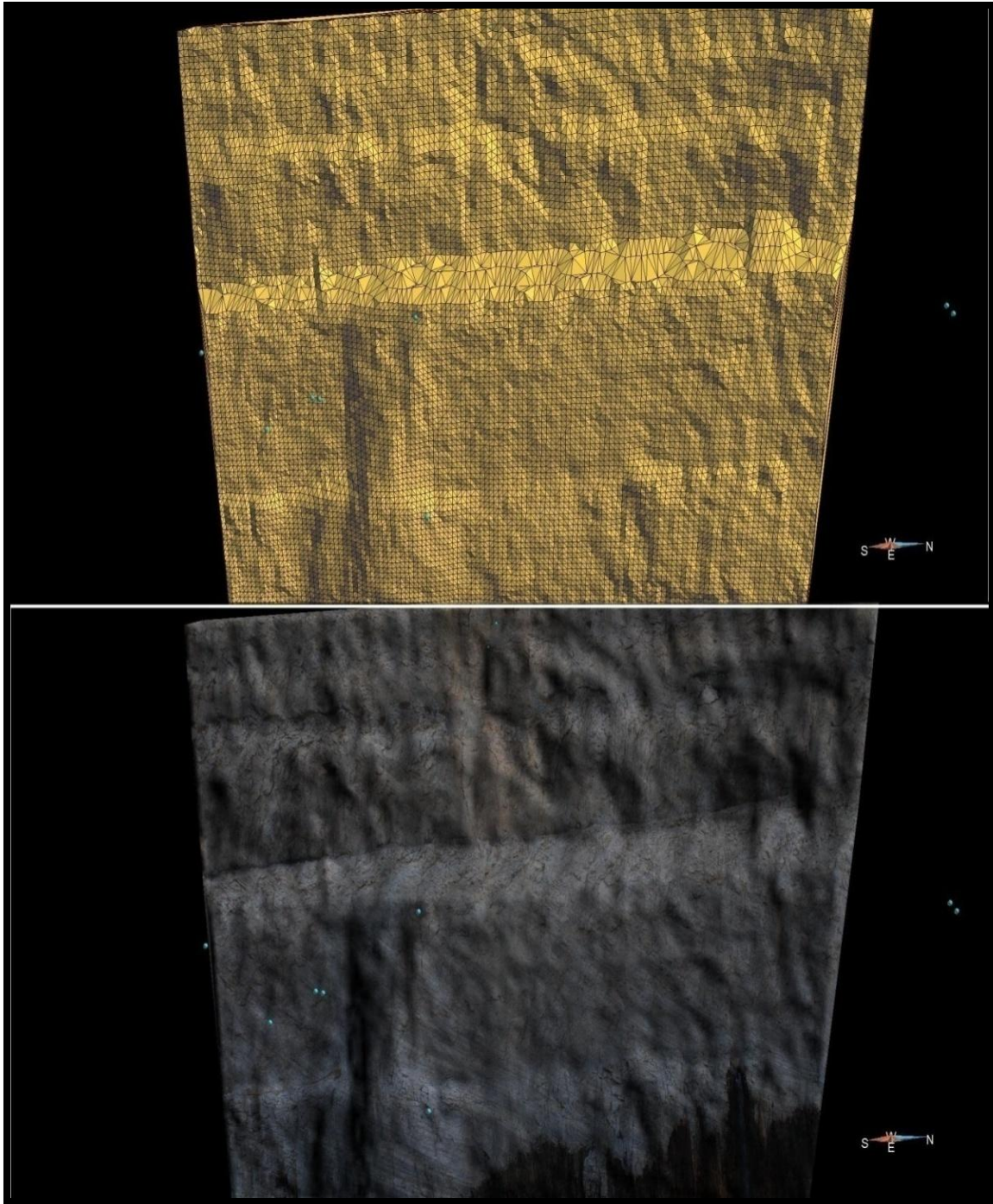


Figure 5-1: Creation of a virtual surface using data from Sirovision and measured control points

Top: Generated surface from 3D point cloud generated from Sirovision
Bottom: Orthorectified photos draped onto the generated surface

5.3 Initiation of a Waterloo Moraine Database

The creation of a geodatabase to stockpile and organize geological observations and data about the Waterloo Moraine is an ambitious project. The goal of this database is to help improve the three-dimensional geological understanding of the Waterloo Moraine system. Mapping the internal facies assemblages in 3D is an essential step to determine suitable depositional models. These models are needed to better represent spatial patterns of subsurface facies across the moraine and to build the next generation of hydrostratigraphic models of the Waterloo Moraine. The collected data from this thesis can be found in [Appendix G](#). It was the ambition of this project to inspire the instigation of a new database to digitally store georeferenced geological information of the Waterloo Moraine.

The storage of high-resolution and georeferenced images of sedimentological sections also helps preserve important geological information that would otherwise be lost due to the inherent activities taking place in aggregate pits, as well as during environmental rehabilitation of the site. The accumulation of this information will permit the continual improvement of Waterloo Moraine interpretations as researchers will have access to an increasing amount of high-resolution and georeferenced images instead of the traditional column-based files of standard databases. The latter do not allow reassessment of previous descriptions and interpretation. With increasing storage capacity of computer systems, a similar approach could be used with stratigraphic boreholes. High-resolution images of cores along with their description, instead of the description alone, could be a major improvement to regional borehole databases, even though continuously cored boreholes represent only a fraction of a regional well (and borehole) database.

In addition, some pits excavate down to the water table. During periods when the water table is lower, direct study of the aquifers could be conducted and this would produce real, observed results that can be applied in various hydrogeological applications. This database

would also provide a check on other less reliable data, as demonstrated in this thesis with the borehole records.

5.4 Groundwater Modelling Applications

In order to address problems related to water management, public water supply and ecological impacts of human activities, numerical models are often applied to simulate groundwater flow and contaminant transport. Some groundwater modeling codes used for these purposes are: FeFlow ([Diersch, 2006](#)), Modflow ([Harbaugh et al., 2000](#)), InHM ([VanderKwaak, 1999](#)) and HydroGeoSphere (HGS) ([Therrien et al., 2005](#)). Current groundwater modeling being conducted on the Alder Creek watershed ([Sousa, personal communication](#)) tests three different models, Modflow, FeFlow and HGS to compare groundwater flow simulations ([Figure 3-1](#)).

Modflow creates a grid of rectangular cells to represent a given area for modelling while FeFlow and HGS both use triangular elements. The average length of cell/element sides in Modflow is 270 metres, while in FeFlow/HGS it is 190 meters. Determining the amount of points in the subsurface beneath an element is based on numerical considerations to achieve convergence. The vertical distance between nodes in the Alder Creek study was found to be 10 cm apart for the first meter, 33cm apart for the next 5 meters and then 1 meter apart for the next 20 meters. When applying values to the modelling process, the hydraulic parameters determined from [Martin & Frind \(1998\)](#) are used to complete the process ([Sousa, personal communication](#)).

To create a successful hydrogeological model, a sound understanding of the geology must be known; however, the full integration from geological models to groundwater flow models is still lacking ([Rivera, 2007](#)). The development of three-dimensional stratigraphic grids in this study can be used to check the quality of existing groundwater models and will help build better models. Ideally, the technique developed and tested in this research should be extended and applied to all the excavations within a watershed. With hydraulic conductivities

calculated based on facies, the values stored in the Sgrids could be transferred to the centroids of the elements of a groundwater flow model. [Figure 5-2](#) shows this concept as Section L is located near a vertical succession of points which represent the centroid of elements. Where the points fall into areas of planar cross-bedded sands, a K value of 2.6×10^{-4} m/s could be assigned and where there are climbing ripples hydraulic conductivity of 2.1×10^{-5} m/s could be transferred. This detailed hydrofacies documentation is a simple example but the possible existence of more sophisticated techniques could be used to deal with scaling issues. Also, other numerical considerations could be taken into account. It is still not a straightforward process to exchange data between 3D geologic and groundwater flow models, and it is not insignificant to find the right balance between geologic accuracy and numerical modeling requirements; however, it is assumed that future developments will help improve interoperability of geological models and groundwater flow models.

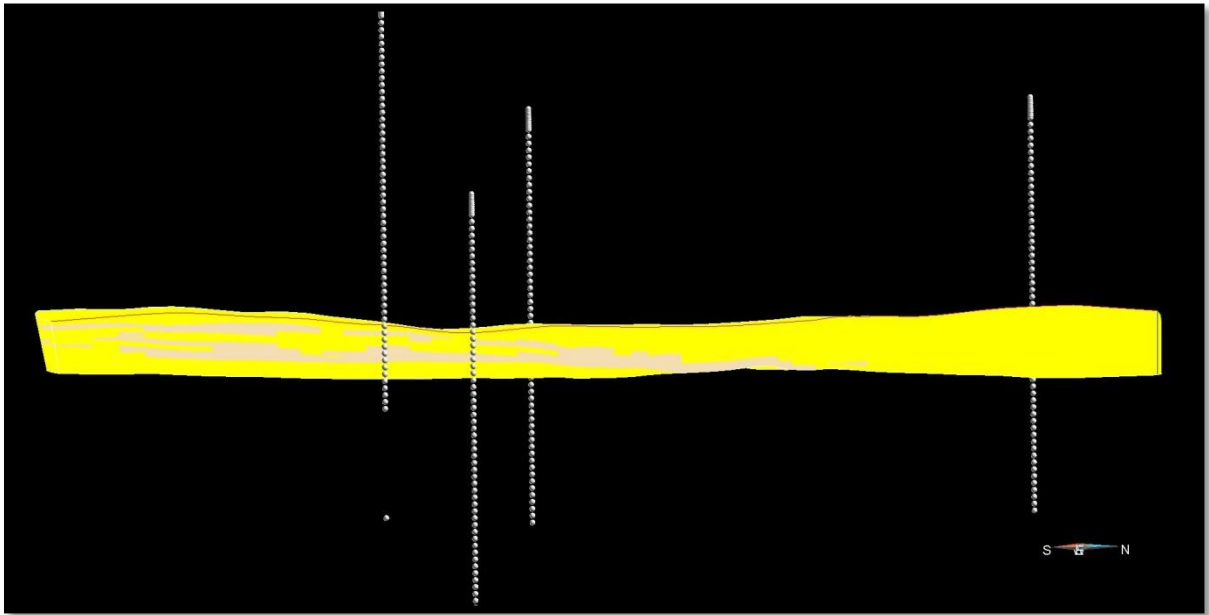


Figure 5-2: Location of groundwater modeling locations and points (white dots) compared against Section L

The consequences of the findings from testing the borehole database pose issues with current groundwater modeling. Recent studies use simplified stratigraphic models that essentially

rely on the borehole database. Mud units would act as obstructions that impede groundwater flow. The results from the borehole testing suggest that there is more mud and less sand than what there actually is. This difference would affect the nature of flow patterns that groundwater models predict based on boreholes. Borehole data have traditionally been considered inaccurate by geologists, and the results of this study also suggest they should be used with caution. The results also show that the Waterloo Moraine is indeed a very complex deposition and to truly model the complex stratigraphy of this feature will be an enormous challenge.

6 - Conclusion

The collection of three-dimensional data is becoming increasingly common in geological studies. This information allows for visualization and interpretation of data in a computer-based 3D environment which in turn facilitates the transfer of geological model outputs to hydrogeological models. With increasing awareness and the need to understand and protect source water areas, research conducted for water studies needs to be done quickly, efficiently and in an easily transferrable fashion for general use. The Waterloo Moraine is a very complex sedimentological setting that provides a source of fresh groundwater for the Regional Municipality of Waterloo, but has received only general sedimentologic study in previous years. With the need to better understand source water protection areas, a section of the Waterloo Moraine was thoroughly studied in order to provide detailed and georeferenced geological data. Specifically, the goal was to develop and test an approach to collect georeferenced sedimentologic information from surficial excavations, and to store this information in a 3D system for use in sedimentologic and hydrostratigraphic analyses. This research was motivated by the idea that if we can understand more about the sedimentology of an aquifer, we learn more about the geologic controls on heterogeneity and the processes that may have created it. This approach leads to a predictive model that can be used to constrain interpolation techniques, and to produce better hydrostratigraphic representations.

A combination of various tools such as surveying instruments, geophysical instruments, and computer workstations were utilized to carefully map and characterize fourteen different lithofacies within a small area of the moraine's unsaturated zone. These facies were then grouped into classes and then virtually modelled to assist in calculating their proportions in the near surface environment along with testing the quality of the borehole database. Grain size analyses were conducted to estimate the representative hydraulic conductivity of each facies. Results were used to further group the classes into hydrofacies that are more meaningful for hydrogeologic studies. The depositional setting at Kieswetter Holdings is interpreted to be that of a subaqueous fan, and is based on evidence generally attributed to

ice-contact and ice-proximal glaciofluvial processes, along with a facies transition into extensive and undeformed sandy bedforms representing the more distal portion of the fan. The near-surface observations reported herein suggest that the degree of heterogeneity and the intensity of deformation decreases locally toward the west and northwest.

The creation of a well-defined three-dimensional depositional model of a complicated accretion of sediment is challenging. A simplified approach to documenting all available information is required and the method tested here is adequate to produce precisely georeferenced data that can also be used to verify the quality of less reliable data, such as well records or borehole data for which the original cores, samples, or photos are unavailable. In the study area, the borehole records were found to be simplified documentations of the subsurface that potentially overestimate mud and under-represent sand content, based on the near-surface observations. This misrepresentation could potentially affect groundwater flow models by producing false representations in calculated flow patterns.

All the recorded information in this thesis forms the basis of a new Waterloo Moraine geodatabase. The proposed approach promises to deliver accurate results at a low cost for society making it possible to add large amounts of new observations and data from other excavations. This simplified method will in turn increase the feasibility of building a robust and fairly detailed 3D geologic model of the Waterloo Moraine to feed the next generation of groundwater flow models. The continuing development of the geodatabase thus has the potential to contribute significantly to our understanding of the Waterloo Moraine which is critical for designing sound groundwater policies that will lead to sustainable regional development.

Bibliography

- Alfarhan, M., L. White, D. Tuck, and C. Aiken. (2008). Laser rangefinders and ArcGIS combined with three-dimensional photorealistic modeling for mapping outcrops in the slick hills, Oklahoma. *Geosphere*, **4**(3): 576-87.
- Allen, J.R.L. (1984). *Sedimentary Structures: Their Character and Physical Basis: Developments in Sedimentology 30*. 2 vols., 611 pp. and 679 pp. Elsevier, Amsterdam.
- Alsop, G.I., Holdworth, R.E. and McCaffrey (2007). Scale invariant sheath folds in salt, sediments and shear zones. *Journal of Structural Geology*, **29**: 1585-1604.
- Asprion, U. (1998). *Ground-Penetrating Radar (GPR) Analysis in Aquifer Sedimentology: Case Studies with an Emphasis on Glacial Systems of SW-Germany*. Dissertation, Sedimentology Unit, Geological Institute, University of Tübingen.
- Bajc, A.F. "RE: Waterloo Moraine 3D Model." Message to Matthew Schumacher. 21 May 2009. Email.
- Bajc, A.F. and Karrow, P.F. (2004). 3-dimensional mapping of Quaternary deposits in the Regional Municipality of Waterloo, southwestern Ontario. Geological Association of Canada and Mineralogical Association of Canada, Joint Annual Meeting, 2004, Fieldtrip FT-&, St. Catharines, Ontario, pp. 72.
- Bajc, A.F. and Shirota, J. (2007). Three-dimensional mapping of surficial deposits in the Regional Municipality of Waterloo, southwestern Ontario; Ontario Geological Survey, Groundwater Resources Study 3, 41p.
- Bajc, A.F., Endres, A.L., Hunter, J.A., Pullan, S.E and Shirota, J. (2004). Three-dimensional mapping of Quaternary deposits in the Waterloo Region, southwestern Ontario. In: R.C. Berg, H.A.J. Russell and L.H. Thorleifson (Editors), *Three-Dimensional Geological Mapping for Groundwater Applications Workshops*. Illinois State Geological Survey, Open File Series 2004-8, St. Catharines, Ontario, Canada. Associated with the 2004 Geological Association of Canada Annual Meeting, pp. 12-15.
- Banerjee, I. and McDonald, B.C. (1973). Nature of esker sedimentation. In: A.V. Jopling and B.C. McDonald (Editors), *Glaciofluvial and Glaciolacustrine Sedimentation*. Society of Economic Paleontologists and Mineralogists Special Publication, **23**: pp. 132-154.

- Barnett, P.J., Cowan, W.R., and Henry, A.P. (1991). Quaternary geology of Ontario, southern sheet. Ontario Geological Survey, Map 2556, scale 1:1,000,000.
- Barnett, P.J., Sharpe, D.R., Russell, H.A.J., Brennand, T.A., Kenny, F.M. and Pugin, A. 1998. On the origins of the Oak Ridges Moraine. *Canadian Journal of Earth Sciences*, **35**: 1152– 1167.
- Bellian, J.A., Kerans, C and Jennette, D.C. (2005). Digital outcrop models: Applications of terrestrial scanning LIDAR technology in stratigraphic modeling. *Journal of Sedimentary Research*, **75**(2): 166-176.
- Benn, D.I. and Evans, D.J.A. (1998). *Glaciers and Glaciation*. Arnold, London.
- Bersezio, R., Bini, A. And Giudici, M. (1999). Effects of sedimentary heterogeneity on groundwater flow in a Quaternary pro-glacial delta environment: joining facies analysis and numerical modelling. *Sedimentary Geology*, **129**: 327-344.
- Binley, A. Winship, P. Middleton, R. Pokar, M. and West, J. (2001). High-resolution characterization of vadose zone dynamics using cross-borehole radar. *Water Resources Research* **37**: 2639–2652.
- Brennand, T.A. and Shaw, J. (1996). The Harricana glaciofluvial complex, Abitibi region, Quebec: its genesis and implications for meltwater regime and ice-sheet dynamics. *Sedimentary Geology*, **102**: 221-262.
- Browne, G.H. (2002). A large-scale flood event in 1994 from the mid-Canterbury Plains, New Zealand and implications for ancient fluvial deposits. In: I.P. Martini, V.R. Baker and G. Garzon (Editors) *Flood and Megaflood Processes and Deposits: Recent and ancient examples*. International Association of Sedimentologists Special Publication, **32**: pp. 99-109.
- Bonnaffe, F., Jennette, D. and Andrews, J. (2007). A method for acquiring and processing ground-based lidar data in difficult-to-access outcrops for use in three-dimensional, virtual-reality models. *Geosphere*, **3**(6): 501-510.
- Bouwer, H., and Rice, R.C. (1976). A slug test for determining hydraulic conductivities of unconfined aquifers with completely or partially penetrating wells. *Water Resources Research*, **12**: 423- 428.
- Boyce, J.I. and Eyles, N. (2000). Architectural element analysis applied to glacial deposits: Internal geometry of a late Pleistocene till sheet, Ontario, Canada. *GSA Bulletin* **112**(1): 98-118.

- Carman, P.C. (1956). *Flow of Gases through Porous Media*. Butterworths Scientific Publications, London, pp. 182.
- Chapman, L.J. and Putnam, D.F. (1943). The moraines of southern Ontario. *Transactions of the Royal Society of Canada*, **37**: 33-41.
- Chapman, L.J., and Putnam, D.F. (1984). *Physiography of Southern Ontario*. Ontario Geological Survey, Map 2715, scale 1:600,000.
- Cheel, R.J., Bridge, J.S., and Best, J.L. (1990). Flow, sediment transport and bedform dynamics over the transition from dunes to upper-stage plane beds: implications for the formation of planar laminae: discussion and reply: *Sedimentology*, **37**: 549–553.
- Cobbold, P.R., and Quinquis, H. (1980). Development of sheath folds in shear regimes. *Journal of Structural Geology*, **2**: 119-126.
- Croot, D.G. (1987). Glaciotectonic structures: a mesoscale model of thin-skinned thrust sheets? *Journal of Structural Geology*, **9**:797-809.
- Davis, J.L. and Annan, A. P. (1989). Ground-penetrating radar for high-resolution mapping of soil and rock stratigraphy. *Geophysical Prospecting*, **37**: 531-551.
- Diersch, H-J. G. (2006). FEFLOW Finite Element Subsurface Flow and Transport Simulation System - Reference manual, User's Manual, White Papers - Release 5.3. WASY Institute for Water Resources Planning and Systems Research. Berlin.
- Elfenbein, C., Ringrose, P. and Christie, M. (2005). Small-scale reservoir modeling tool optimizes recovery offshore Norway. *World Oil*, **Oct 2005**: 45-50.
- Eyles, N and Eyles, C.H. (1992). Glacial depositional systems. In: R.G. Walker and N.P. James (Editors) *Facies models: response to sea level change*. Geological Association of Canada, pp. 73-100.
- Frind, E.O., Molson, J.W. and Rudolph, D.L. (2006). Well vulnerability; a quantitative approach for source water protection. *Groundwater*, **44** (5): 732-742.
- Google Incorporated. *Google Earth* [computer software]. Version 5.0.1. Google Incorporated, Mountain View, CA, 2009.
- Hambrey, M. J. and Huddart, D. (1995). Englacial and proglacial glaciotectonic processes at the snout of a thermally complex glacier in Svalbard. *Journal of Quaternary Science*, **10**: 313-326.

- Haneberg, W.C. (2008). Using close range terrestrial digital photogrammetry for 3-D rock slope modeling and discontinuity mapping in the United States. *Bulletin of Engineering Geology and Environment*. Springer-Verlag.
- Harbaugh, A.W., Banta, E.R., Hill, M.C. and McDonald, M.G. (2000). The U.S. Geological Survey modular ground-water model - User guide to modularization concepts and the Ground-Water Flow Process: U.S. Geological Survey Open-File Report.
- Hazen, A. (1892). Some Physical Properties of Sands and Gravels, with Special Reference to their Use in Filtration. 24th Annual Report, Massachusetts State Board of Health, Publication Document **34**: 539-556.
- Hiscott, R.N. (1994). Loss of capacity, not competence, as the fundamental process governing deposition from turbidity currents. *Journal of Sedimentary Research*, **64**(2): 209– 214.
- Heinz, J. and Aigner, T. (2003). Hierarchical dynamic stratigraphy of various Quaternary gravel deposits, Rhine glacier area (SW-Germany): implications for hydrostratigraphy. *International Journal of Earth Science*, **92**: 923–938.
- Hodgetts, D., Drinkwater, N.J., Hodgson, J., Kavanagh, J., Flint, S.S., Keogh, K.J. and Howell, J.A. (2004) Geological Prior Information: Informing Science and Engineering. Geological Society of London, London, Special Publications, **239**: 57-75.
- Hvorslev, M.J. (1951). Time lag and soil permeability in ground water observations. US Army Corps of Engineers Waterways Experimentation Station, Bulletin 36. Vicksburg, MS, pp. 50.
- Huggenberger P., & Aigner T. (1999). Introduction to the special issue on aquifer-sedimentology: problems, perspectives and modern approaches. *Sedimentary Geology*, **129**: 179–186.
- Jones, J.P., Sudicky, E.A., and McLaren, R.G. (2008). Application of a fully-integrated surface-subsurface flow model at the watershed-scale: A case study, *Water Resources Research* **44**, W03407, doi:10.1029/2006WR005603.
- Karrow, P.F. (1987). Quaternary geology of the Hamilton-Cambridge area, Ontario Geological Survey, Report 255, 94pp.
- Karrow, P.F. (1993). Quaternary geology Stratford-Conestogo area. Ontario Geological Survey, Report 283, 104 pp.

- Karrow, P.F. and Paloschi, G.V.R. (1996). The Waterloo kame moraine revisited: new light on the origin of some Great Lake region interlobate moraines. *Zeitschrift Für Geomorphologie*, **40**: 305-315.
- Kessler, H., Mathers, S. and Sobisch, H-G. (2009). The capture and dissemination of integrated 3D geospatial knowledge at the British Geological Survey using GSI3D software and methodology. *Computers & Geosciences*, **35**: 1311–1321.
- Kleinhaus, M.G. (2005). Grain-size sorting in grain flows at the lee-side of deltas. *Sedimentology*, **52**: 291-311.
- Klingbeil, R., Kleinedam, S., Asprion, U., Aigner, T., and Teutsch, G.,(1999). Relating lithofacies to hydrofacies: outcrop-based hydrogeological characterisation of quaternary gravel deposits. *Sedimentary Geology*, **129**: 299-310.
- Kostic, B., Becht, A. & Aigner, T. (2005). 3-D sedimentary architecture of a Quaternary gravel delta (SW-Germany): Implications for hydrostratigraphy. *Sedimentary Geology*, **181**: pp.143-171.
- Kostic, S. and Parker, G. (2007). Conditions under which a supercritical turbidity current traverses an abrupt transition to vanishing bed slope without a hydraulic jump. *Journal of Fluid Mechanics*, **586**: 119–145.
- Lønne, I. (1995) Sedimentary facies and depositional architecture of ice-contact glaciomarine systems. *Sedimentary Geology*, **98**: 13–43.
- Mallet, J.L. (1989). Discrete Smooth Interpolation in Geometric Modeling. *ACM-Transactions on Graphics*, **8**(2): 121-144.
- Martin, P.J. and Frind, E.O. (1998). Modeling a complex multi-aquifer system: The Waterloo Moraine. *Groundwater*, **34** (6): 679-690.
- Miall, A.D. (1977). A review of the braided-river depositional environment. *Earth Science Reviews*, **13**: 1-62.
- Miall, A.D. (1985). Architectural-element analysis: a new method of facies analysis applied to fluvial deposits. *Earth Science Reviews*, **22**: 261-308.
- Miall, A.D. (1996). *The geology of fluvial deposits – Sedimentary facies basin analysis and petroleum geology*. Springer, Berlin, pp. 582.
- Miall, A.D. (2000). *Principles of sedimentary basin analysis*, 3rd edition: Springer, Berlin, New York, 616pp.

- Moore, A.L., Nishimura, Y., Gelfenbuam, G., Takanobu, K., and Triyono, R. (2006). Sedimentary deposits of the 26 December 2004 tsunami on the northwest coast of Aceh, Indonesia. *Earth Planets Space*, **58**: 253–258.
- Mulugeta, G. and Koyi, H. (1987). Three dimensional geometry and kinematics experimental piggyback thrusting. *Geology*, **15**: 1052-1056.
- Natural Resources Canada. “Southern Ontario Hydrogeology-Waterloo Moraine Study”. Geological Survey of Canada. Accessed Jan 16, 2008.
http://gsc.nrcan.gc.ca/hydrogeo/sontario/waterloo_e.php
- Neal, A. (2004). Ground-penetrating radar and its use in sedimentology: principles, problems and progress. *Earth-Science Reviews*, **66**: 261-330.
- Odong, J. (2008). Evaluation of empirical formulae for determination of hydraulic conductivity based on grain-size analysis. *The Journal of American Science*, **4**(1): 1-6.
- Ovenshine, A.T. (1970). Observations on iceberg rafting in Glacier Bay, Alaska, and the identification of ice-rafted deposits. *Geological Society of America Bulletin*, **81**: 891-894.
- Paton, D., Carr, M., Trudgill, B., Ortner, H. and Medwedeff, D.A. (2007). Alpine-scale 3D geospatial modeling: Applying new techniques to old problems. *Geosphere*, **3**(6): 527-549.
- Pinchin Environmental Limited. (2008). Groundwater monitoring and sampling program, 1873 Bleams Road, Kitchener, Ontario, Kieswetter Holdings Limited. Mississauga, Ontario. Pinchin Environmental Limited.
- Poeter, E. & Gaylord, D.R. (1990). Influence of aquifer heterogeneity on contaminant transport at Hanford Site. *Ground Water* **28**: 900–909
- Poulsen, T.G., Iversen, B.V., Yamaguchi, T., Moldrup, P. and Schjønning, P. (2001). Spatial and temporal dynamics of air permeability in a constructed field. *Soil Science* **166**(3): 153–162.
- Pugin, A., Pullan, S.E., and Sharpe, D.R. (1999). Seismic facies and regional architecture of the Oak Ridges Moraine area, southern Ontario. *Canadian Journal of Earth Sciences* **36**: 409-432.
- Rajaratnam, N. and Subramanyan, S. (1986). Plane turbulent denser wall jets and jumps. *Journal of Hydraulic Research*, **24**: 281–296



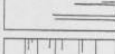
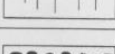
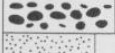
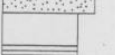


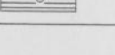
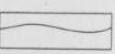
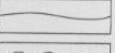
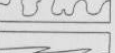
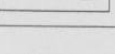
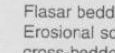
- Reading, H. G. (1996). *Sedimentary Environments and Facies*. Blackwell Scientific Publications, pp. 688.
- Rehfeldt, K. R., Boggs, J.M. and Gelhar, L.W. (1992). Field Study of Dispersion in a Heterogeneous Aquifer 3. Geostatistical Analysis of Hydraulic Conductivity, *Water Resources Research*, **28**(12): 3309–3324.
- Regional Municipality of Waterloo (RMOW). Planning, Housing and Community Services. Protecting Significant Moraines in Waterloo Region: A Supplementary Report in Support of Waterloo Region’s Growth Management Strategy. Waterloo, Ontario: Regional Municipality of Waterloo, February 23, 2007.
- Regional Municipality of Waterloo (RMOW). Planning, Housing and Community Services. Interim Population Forecasts. Report: P-06-016. Waterloo, Ontario: Regional Municipality of Waterloo, February 7, 2006.
- Regional Municipality of Waterloo (RMOW). “Water quality and treatment facilities.” Region of Waterloo. Accessed Oct. 7, 2009.
<http://www.region.waterloo.on.ca/web/region.nsf/8ef02c0fded0c82a85256e590071a3ce/62acf1865fede1ef8525734600517e64!OpenDocument>
- Rivera, A. Groundwater Modelling: From geology to hydrogeology [abstract]. In: Three-Dimensional Geologic Mapping for Groundwater Applications Workshop Extended Abstracts; 2007 Oct. 27, Annual Meeting, Geological Society of America, Denver, Colorado.
- Rivera, A., Crowe, A., Kohut, A., Rudolph, D., Baker, A., Pupek, D., Shaheen, N., Lewis, M. and Parks, K. (2003). Canadian Framework for collaboration on groundwater. Geological Survey of Canada, M40-62/2003E-PDF.
- Robertson, W.D., Ptacek, C.J. and Brown, S.J. (2007). Geochemical and hydrogeological impacts of a wood particle barrier treating nitrate and perchlorate in ground water. *Ground Water Monitoring & Remediation*, **27** (2): 85-95.
- Ross, M., Parent, M., and Lefebvre, R. (2005). 3D geologic framework models for regional hydrogeology and land-use management: a case study from a Quaternary basin of southwestern Quebec, Canada. *Hydrogeology Journal*, **13**: 690-707
- Ross, M., Schumacher, M., Conant, B., and Piggott, S. (2008) The generation of virtual sediment sections from the Kieswetter sandpit, Waterloo, Ontario. Unpublished report to the Geological Survey of Canada, University of Waterloo, 19 pages.

- Russell, H.A.J. and Arnott, R.W.C. (2003). Hydraulic-Jump and Hyperconcentrated-Flow Deposits of a Glacigenic Subaqueous Fan: Oak Ridges Moraine, Southern Ontario, Canada. *Journal of Sedimentary Research*, **73**(6): 887–905
- Russell, H.A.J., Cummings, D.I. and Shreve, D.R. (2009). Sedimentology of the Paris and Galt Moraines and hydrogeological implications. 2009 Joint Assembly fieldtrip guidebook. Geological Association of Canada, 40pp.
- Russell, H.A.J., Sharpe, D.R., and Bajc, A.F. (2007). Sedimentary signatures of the Waterloo Moraine, Ontario, Canada; *in* Hambrey, M.J., Christoffersen, P., Glasser, N.F., and Hubbard, B.(eds), *Glacial Sedimentary Processes and Products*, Special Publication Number 39 of the International Association of Sedimentologists, p. 85-108.
- Searle M.P. and Alsop G.I. (2007). Eye-to-eye with a mega-sheath fold: A case study from Wadi Mayh, northern Oman Mountains. *Geology* **35**(11): 1043.
- Sharpe, D.R., Hinton, M.J., Russell, H.A.L. and Desbarats, A.J. (2002). The need for Basin Analysis in Regional Hydrogeological Studies: Oak Ridges Moraine, Southern Ontario. *Geoscience Canada*, **29** (1): 3-20.
- Shaw, J. and Gorrell, G. (1991). Subglacially formed dunes with bimodal and graded gravel in the Trenton drumlin field, Ontario. *Geographie Physique Quaternaire*, **45**: 21-34.
- Stohr, Christopher. "Re: Greetings, eh!" Message to Matthew Schumacher. 30 Jul 2009. Email.
- Stohr, C.J., Petras, J. and Mikulic, D.G. (2009). Experimental stereophotographic measurement of rock properties at Thornton Quarry, Illinois. In press.
- Sousa, Marcelo. "Alder Creek Model Grids." Message to Matthew Schumacher. 27 Feb 2009. Email.
- Taylor, F.B. (1913). The moraine systems of southwestern Ontario. *Royal Canadian Institute Transactions*, **10**: 57-79.
- Technical Experts Committee (TEC) (2004) Watershed-based Source Protection Planning: Science-based decision-making for protecting Ontario's drinking water resources: A Threats Assessment Framework. Technical Experts Committee, Report to the Minister of the Environment.
- Terraqua Investigations Ltd. (1995). Study of the hydrogeology of the Waterloo Moraine. Unpublished report to the Regional Municipality of Waterloo, Ontario, Canada.

- Terzaghi, K., and Peck, R.B. (1964). *Soil Mechanics in Engineering Practice*. Wiley, New York, pp. 729.
- "The Waterloo Moraine and the Grand River Watershed" [map]. GRCA GIS Data [computer files]. Cambridge, Ont.: Grand River Conservation Authority, 2008. Using: ArcMap [GIS software]. Version 9.3. Redlands, CA: Environmental Systems Research Institute, 1992-2009.
- Therrien, R., McLaren, R., Sudicky, E.A., and Panday, S. (2006). *HydroGeoSphere, A Three-Dimensional Numerical Model Describing Fully Integrated Subsurface and Surface Flow and Solute Transport*, Groundwater Simulation Group, Waterloo, Ont., Canada.
- Thurmond, J.B. (2004). From collection to utilization; outcrop analog data in a 3-D world. *Annual Meeting Expanded Abstracts – American Association of Petroleum Geologists* **13**: 138.
- VanderKwaak, J. E. (1999). *Numerical simulation of flow and chemical transport in integrated surface-subsurface hydrologic systems*, Ph.D. thesis, 217 pp., University of Waterloo, Waterloo, Ontario, Canada.
- van der Wateren, D.F.M. (1985). A model of glacial tectonics, applied to the ice-pushed ridges in the central Netherlands. *Bulletin of the Geological Society Denmark*, **34**: 55-74.
- Venteris, E.R. (2007). Three-dimensional modeling of glacial sediments using public water-well data records: An integration of interpretive and geostatistical approaches. *Geosphere*, **3**(6): 456-468.
- Vukovic, M., and Soro, A. (1992). *Determination of Hydraulic Conductivity of Porous Media from Grain-Size Composition*. Water Resources Publications, Littleton, Colorado .
- Walker, R.G. (1992). Facies, facies models and modern stratigraphic concepts. In: R.G. Walker and N.P. James (Editors) *Facies models: response to sea level change*. Geological Association of Canada, pp. 1-14.
- Wawrzyniec, T.F. Jones, R.R., McCaffrey, K., Holliman, N., and Holdsworth, R.E. 2007. Introduction: Unlocking 3D earth systems – Harnessing new digital technologies to revolutionize multi-scale geological models. *Geosphere*, **3**(6): 406-407.
- Whittaker, J. and Teutsch, G. (1999). The simulation of subsurface characterization methods applied to a natural aquifer analogue. *Advances in Water Resources* **22**(8): 819–829.

Appendices

Appendix A – Facies Classification

Code	Description	SYMBOLS	
Diamictions			
	Very poorly sorted admixture of wide grain size range		
Dmm	Matrix-supported, massive.	 Diamict	
Dcm	Clast-supported, massive.		
Dcs	Clast-supported, stratified.		 stratified
Dms	Matrix-supported, stratified.		
Dml	Matrix-supported, laminated.		 sheared
--- (c)	Evidence of current reworking.		
--- (r)	Evidence of resedimentation.		
--- (s)	Sheared.	 jointed	
--- (p)	Includes clast pavement(s).		
Boulders			
Bms	Particles > 256 mm (b-axis)	 Gravel	
Bmg	Matrix-supported, massive.		
Bcm	Matrix-supported, graded.		
Bcm	Clast-supported, massive.		
Bcg	Clast-supported, graded.		
Bfo	Deltaic foresets.		
BL	Boulder lag or pavement.		
Gravels			
Gms	Particles of 8–256 mm		 Sand
Gm	Matrix-supported, massive.		
Gm	Clast-supported, massive.		
Gsi	Matrix-supported, imbricated.		
Gmi	Clast-supported, massive (imbricated).		
Gfo	Deltaic foresets.		
Gh	Horizontally bedded.		
Gt	Trough cross-bedded.		
Gp	Planar cross-bedded.		
Gfu	Upward-fining (normal grading).		
Gcu	Upward-coarsening (inverse grading).		
Go	Openwork gravels.	 Fines	
Gd	Deformed bedding.		
Glg	Palimpsest (marine) or bedload lag.		
Granules			
GRcl	Particles of 2–8 mm		 Laminations with intraclasts
GRch	Massive with clay laminae.		
GRh	Massive and infilling channels.		
GRh	Horizontally bedded.		
GRm	Massive and homogeneous.		
GRmb	Massive and pseudo-bedded.		
GRmc	Massive with isolated outside clasts.		
GRmi	Massive with isolated, imbricated clasts.		
GRmp	Massive with pebble stringers.		
GRo	Open-work structure.		
GRruc	Repeating upward-coarsening cycles.	 Laminations with dropstones	
GRruf	Repeating upward-fining cycles.		
GRt	Trough cross-bedded.		
GRcu	Upward coarsening.		
GRtu	Upward fining.		
GRp	Cross-bedded.		
GRfo	Deltaic foresets.		
Sands			
St	Particles of 0.063–2 mm		 Loaded
St	Medium to very coarse and trough cross-bedded.		
Sp	Medium to very coarse and planar cross-bedded.		
Sr(A)	Ripple cross-laminated (type A).		
Sr(B)	Ripple cross-laminated (type B).		
Sr(S)	Ripple cross-laminated (type S).		
Scr	Climbing ripples.		
Ssr	Starved ripples.		
Sh	Very fine to very coarse and horizontally/plane bedded or low angle cross-laminated.		
Sl	Horizontal and draped lamination.	 Interbedded	
Sl	Deltaic foresets.		
Silts & Clays			
Sfl	Flasar bedded		 Erosional
Se	Erosional scours with intraclasts and crudely cross-bedded.		
Su	Fine to coarse with broad shallow scours and cross-stratification.		
Sm	Massive.		
Sc -	Steeply dipping planar cross-bedding (non-deltaic foresets).		
Sd	Deformed bedding.		
Suc	Upward-coarsening.		
Suf	Upward-fining.		
Srg	Graded cross-laminations.		
SB	Bouma sequence.		
Scps	Cyclopsams.	 Conformable	
--- (d)	With dropstones.		
--- (w)	With dewatering structures.		
Silts & Clays			
Fl	Particles of <0.063 mm		 Loaded
Fl	Fine lamination often with minor fine sand and very small ripples.		
Flv	Fine lamination with rhythmites or varves.		
Fm	Massive.		
Frg	Graded and climbing ripple cross-laminations.		
Fcpl	Cyclopeis.		
Fp	Intraclast or lens.		
--- (d)	With dropstones.		
--- (w)	With dewatering structures.		

The lithofacies classification used in this study.
From Benn & Evans, 1998; modified from Miall 1977, 1996.

Element	Symbol	Principal Lithofacies Assemblage	Geometry and Relationships
Channels	CH	Any combination	Finger; lens or sheet; concave-up erosional base; scale and shape highly variable; internal concave-up secondary erosion surfaces common
Gravel bars and bedforms	GB	Gm, Gp, Gt	Lens, blanket; usually tabular bodies; commonly interbedded with SB
Sandy bedforms	SB	St, Sp, Sh, Sl, Sr, Se, Ss	Lens, sheet, blanket, wedge; occurs as channel fills, crevasse splays, minor bars
Foreset macroforms	FM	St, Sp, Sh, Sl, Sr, Se, Ss	Lens resting on flat or channeled base, with convex-up second-order internal erosion surfaces and upper bounding surface
Lateral accretion deposits	LA	St, Sp, Sh, Sl, Sr, Se, Ss; less commonly Gm, Gt, Gp	Wedge, sheet, lobe; characterized by internal lateral accretion surfaces
Sediment gravity flows	SG	Gm, Gms	Lobe, sheet; typically interbedded with GB
Laminated sand sheets	LS	Sh, Sl; minor St, Sp, Sr	Sheet, blanket
Overbank fines	OF	Fm, Fl	Thin to thick blankets; commonly interbedded with SB; may fill abandoned channels

Architectural elements in fluvial deposits. Modified from [Miall, 1985](#).

Appendix B – Section Data and Information

		UTM Coordinates <i>UTM Zone 17 NTS Map: 40P/7</i>		Latitude & Longitude		Elevation
Section	Station	Northing (m)	Easting (m)	Latitude (N) (decimal degrees)	Longitude (W)	(masl)
A	07KI01	4804792.40	538896.80	43.39500	80.51970	n/a
	07KI02	4804798.86	538897.48	43.39506	80.51969	n/a
	07KI03	4804804.44	538895.77	43.39510	80.51971	n/a
	07KI04	4804809.47	538898.34	43.39515	80.51968	n/a
	07KI05	4804809.69	538900.83	43.39515	80.51965	n/a
B	07KI06	4804759.20	538913.20	43.39470	80.51950	n/a
	07KI07	4804758.62	538908.44	43.39470	80.51955	n/a
	07KI08	4804765.56	538899.22	43.39478	80.51967	n/a
	07KI09	4804771.41	538895.28	43.39481	80.51972	n/a
	07KI10	4804778.87	538897.28	43.39488	80.51969	n/a
	07KI11	no station		no station		n/a
C	07KI12	4804739.71	538976.12	43.39452	80.51872	360.43
	07KI13	4804727.79	538968.04	43.39442	80.51882	361.99
	07KI14	4804722.03	538961.13	43.39436	80.51891	361.79
	07KI15	4804712.96	538955.19	43.39428	80.51898	361.73
	07KI16	4804708.41	538953.63	43.39425	80.51900	363.04
	07KI17	4804711.18	538944.57	43.39427	80.51911	361.12
D	07KI18	4804793.89	538816.08	43.39502	80.52070	364.05
	07KI19	4804796.61	538817.27	43.39504	80.52068	365.12
	07KI20	4804800.11	538821.97	43.39507	80.52062	365.67
	07KI21	4804799.66	538828.55	43.39507	80.52055	365.17
	07KI22	4804797.97	538835.26	43.39505	80.52046	364.58
	07KI23	4804794.47	538840.51	43.39502	80.52039	365.27
	07KI24	4804788.49	538845.04	43.39497	80.52034	364.12
E	E1	538977.64	4804770.20	43.39480	80.51870	363.68
	E2	538975.26	4804774.73	43.39484	80.51873	363.42
	E3	538976.34	4804773.44	43.39483	80.51872	363.91
F	08KI01	4804883.60	538555.42	43.39584	80.52391	366.87
	08KI02	4804883.75	538550.49	43.39584	80.52397	366.81
	08KI03	4804881.24	538545.68	43.39582	80.52403	366.31
	08KI04	4804878.86	538542.90	43.39580	80.52406	366.29
	08KI05	4804873.68	538540.33	43.39575	80.52410	366.23
	08KI06	4804871.52	538537.73	43.39573	80.52413	367.41
	08KI07	4804869.89	538535.39	43.39572	80.52416	368.07
	08KI08	4804865.68	538531.59	43.39568	80.52420	367.84

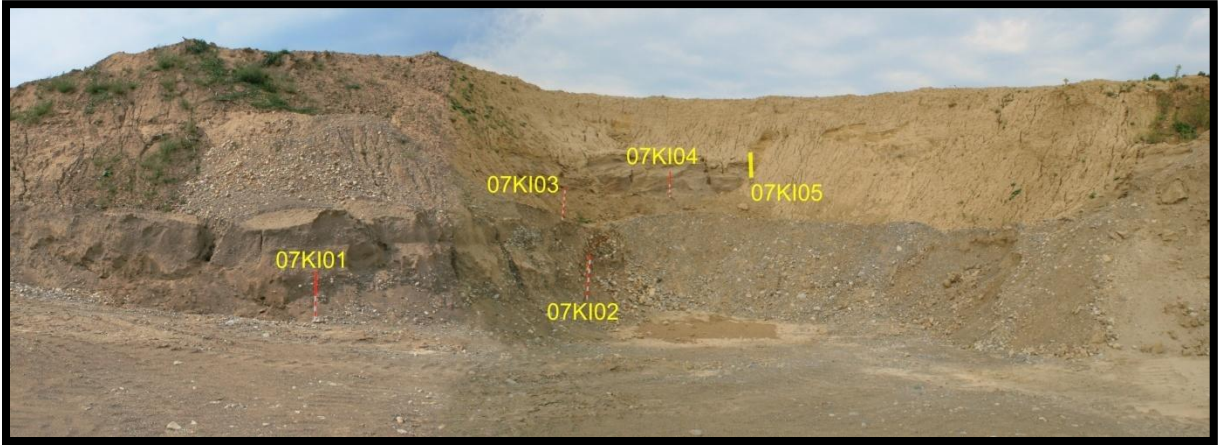
G	08KI09	4804859.77	538559.44	43.39562	80.52386	366.12
	08KI10	4804861.66	538562.12	43.39564	80.52383	366.70
	08KI11	4804863.71	538563.63	43.39566	80.52381	366.63
	08KI12	4804866.62	538565.55	43.39569	80.52378	366.84
	08KI13	4804868.99	538565.62	43.39571	80.52378	366.57
	08KI14	4804871.63	538565.49	43.39573	80.52379	366.78
	08KI15	4804875.83	538564.25	43.39577	80.52380	366.61
H	08KI16	4804861.19	538527.24	43.39564	80.52426	365.96
	08KI17	4804863.49	538522.99	43.39566	80.52431	365.36
	08KI18	4804863.88	538518.77	43.39566	80.52436	365.68
	08KI19	4804864.30	538515.12	43.39567	80.52441	365.88
	08KI20	4804864.42	538509.35	43.39567	80.52448	367.41
	08KI21	4804864.24	538504.42	43.39567	80.52454	368.34
	08KI22	4804859.34	538502.53	43.39562	80.52456	366.37
I	08KI23	4804757.00	538880.92	43.39468	80.51990	356.47
	08KI24	4804761.86	538877.86	43.39473	80.51994	356.90
	08KI25	4804763.23	538879.46	43.39474	80.51992	357.06
	08KI26	4804765.79	538877.74	43.39476	80.51994	358.08
	08KI27	4804768.81	538878.32	43.39479	80.51993	357.57
	08KI28	4804771.75	538877.90	43.39481	80.51993	358.43
	08KI29	4804774.41	538877.60	43.39484	80.51994	359.78
	08KI30	4804777.59	538880.84	43.39487	80.51990	358.80
	08KI31	4804780.21	538882.12	43.39489	80.51988	359.79
	08KI32	4804781.32	538884.28	43.39490	80.51986	359.52
	08KI33	4804785.28	538887.41	43.39494	80.51982	359.61
	08KI34	4804786.17	538890.60	43.39494	80.51978	358.71
	08KI35	4804786.01	538893.42	43.39494	80.51974	356.99
J	08KI36	4804719.48	538977.45	43.39434	80.51871	358.31
	08KI37	4804716.64	538980.17	43.39431	80.51868	358.88
	08KI38	4804712.40	538980.96	43.39428	80.51867	358.69
	08KI39	4804709.30	538980.09	43.39425	80.51868	359.60
	08KI40	4804706.78	538976.93	43.39422	80.51872	359.10
	08KI41	4804708.47	538972.90	43.39424	80.51877	358.23
	08KI42	4804707.97	538969.24	43.39424	80.51881	358.31
	08KI43	4804707.63	538965.69	43.39423	80.51886	357.80
K	08KI44	4804671.36	538426.80	43.39393	80.52551	368.96
	08KI45	4804666.65	538427.37	43.39389	80.52550	369.50
	08KI46	4804665.06	538424.69	43.39388	80.52554	369.41
	08KI47	4804661.56	538419.37	43.39385	80.52560	369.09
	08KI48	4804658.38	538412.75	43.39382	80.52569	368.65
	08KI49	4804656.94	538406.93	43.39381	80.52576	368.90
	08KI50	4804652.37	538403.50	43.39376	80.52580	370.49
	08KI51	4804652.44	538401.33	43.39377	80.52583	370.22

	08KI52	4804649.10	538398.27	43.39374	80.52587	370.39
	08KI53	4804645.96	538394.88	43.39371	80.52591	369.76
	08KI54	4804643.90	538389.50	43.39369	80.52597	368.78
	08KI55	4804643.72	538385.78	43.39369	80.52602	369.01
	08KI56	4804645.61	538382.67	43.39370	80.52606	368.38
L	08KI57	4804649.23	538378.68	43.39374	80.52611	368.99
	08KI58	4804658.00	538376.38	43.39382	80.52614	368.81
	08KI59	4804666.16	538377.17	43.39389	80.52612	368.28
	08KI60	4804674.95	538376.94	43.39397	80.52613	368.11
	08KI61	4804678.45	538372.74	43.39400	80.52618	368.51
	08KI62	4804684.22	538368.13	43.39405	80.52624	368.78
	08KI63	4804689.59	538361.50	43.39410	80.52632	368.31
	08KI64	4804696.35	538359.10	43.39416	80.52635	368.10
	08KI65	4804699.85	538358.18	43.39419	80.52636	368.16
M	08KI66	4804690.85	538934.31	43.39408	80.51924	359.27
	08KI67	4804687.01	538939.00	43.39405	80.51919	359.98
	08KI68	4804684.67	538943.11	43.39403	80.51914	361.07
	08KI69	4804684.55	538947.40	43.39403	80.51908	360.77
	08KI70	4804686.50	538952.69	43.39404	80.51902	360.78
	08KI71	4804689.34	538957.24	43.39407	80.51896	360.43
	08KI72	4804696.67	538961.97	43.39413	80.51890	358.96
	08KI73	4804700.10	538964.84	43.39417	80.51887	359.27
	08KI74	4804703.36	538965.41	43.39419	80.51886	359.26
	08KI75	4804707.21	538962.93	43.39423	80.51889	358.73
N	08KI76	4804788.26	538596.83	43.39498	80.52340	368.03
	08KI77	4804780.61	538596.67	43.39491	80.52341	367.72
	08KI78	4804774.83	538602.49	43.39486	80.52333	367.36
	08KI79	4804767.78	538604.10	43.39479	80.52332	367.28
	08KI80	4804759.06	538607.14	43.39471	80.52328	368.78

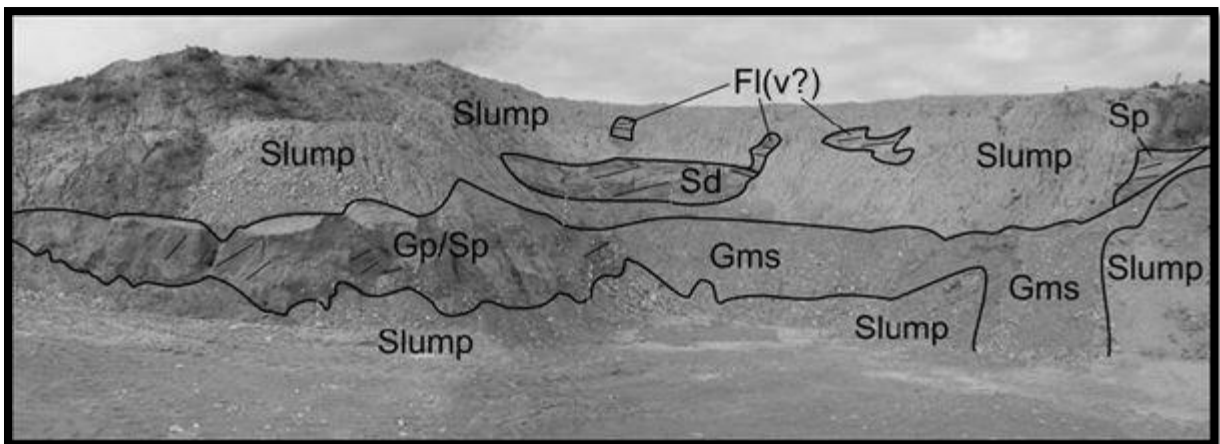
Section	Length (metres)	Height (metres)	Number of Points Surveyed	Number of Stations
A	20.8	5.4	5	5
B	31.4	2.8	5	5
C	52.4	3.6	28	6
D	40.5	3.9	17	7
E	5.4	1.2	8	3
F	31.7	5.1	70	8
G	18.3	2.6	32	7
H	27.3	9.1	36	7
I	40.9	5.1	96	13
J	32.3	3.6	71	8
K	60.9	2.9	101	13
L	63.7	3.5	71	9
M	48.1	8.1	103	10
N	32.2	4.9	10	5

Appendix C – Images for the Sections

Section A

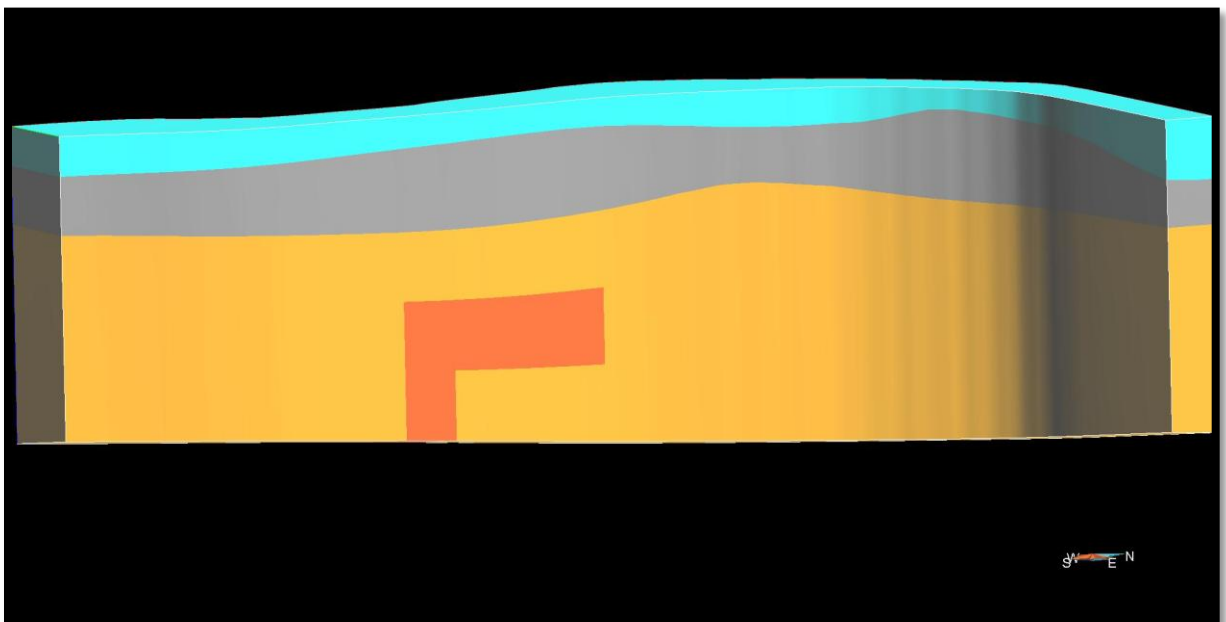


The stations of Section A with the scale sticks representing 1 meter in height (top) and the interpretation of the facies for this area (bottom).





Georeferenced photos used in the geomodelling for Section A

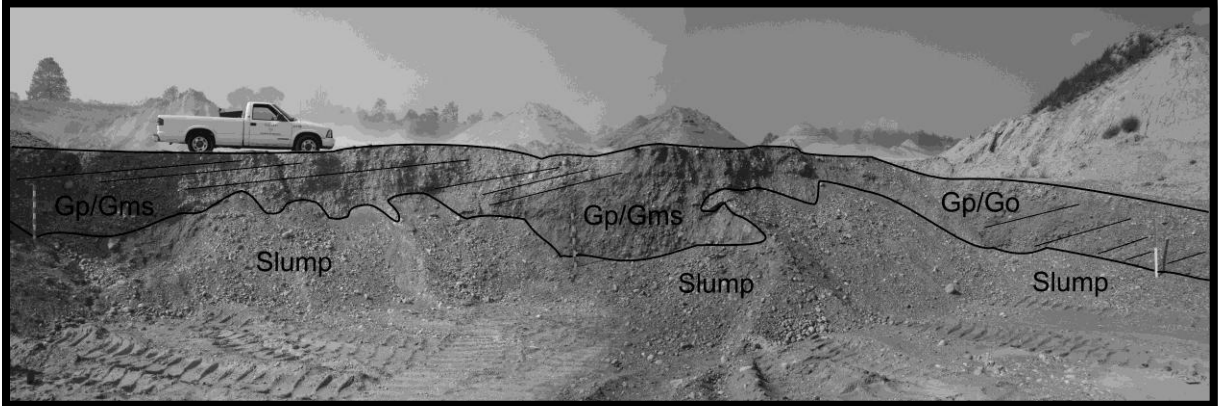


The three-dimensional (3D) stratigraphical grid constructed for Section A. Facies illustrated are laminated muds (light blue), deformed sands (Sd), massive gravel (light orange) and planar gravel (dark orange).

Section B



Section B with stations (top) and interpreted facies (bottom).

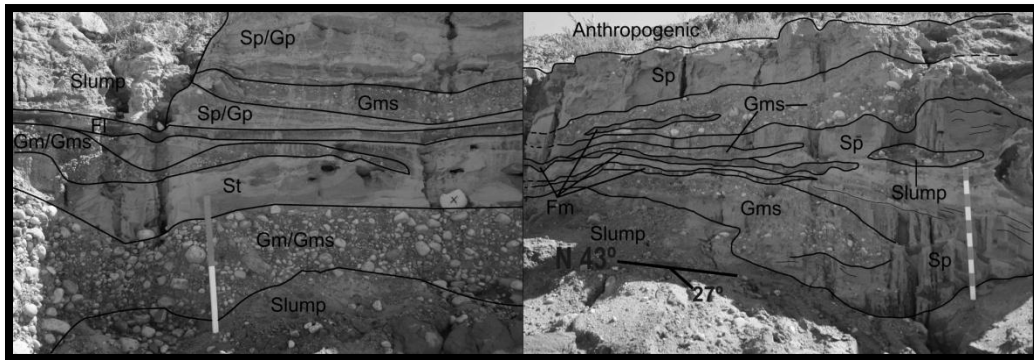




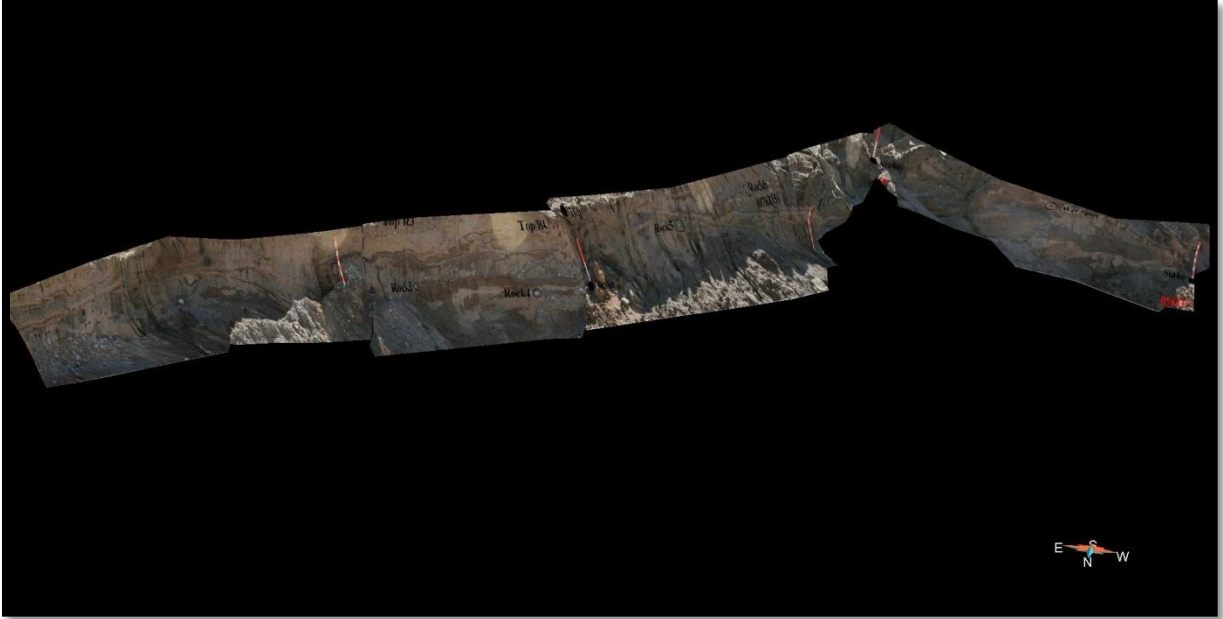
Georeferenced 2D voxets (top) used in the 3D construction of a stratigraphic grid (bottom) displaying the facies massive muds (dark blue), planar sands (yellow), massive gravel (light orange), planar gravel (dark orange) and openwork gravel (red).



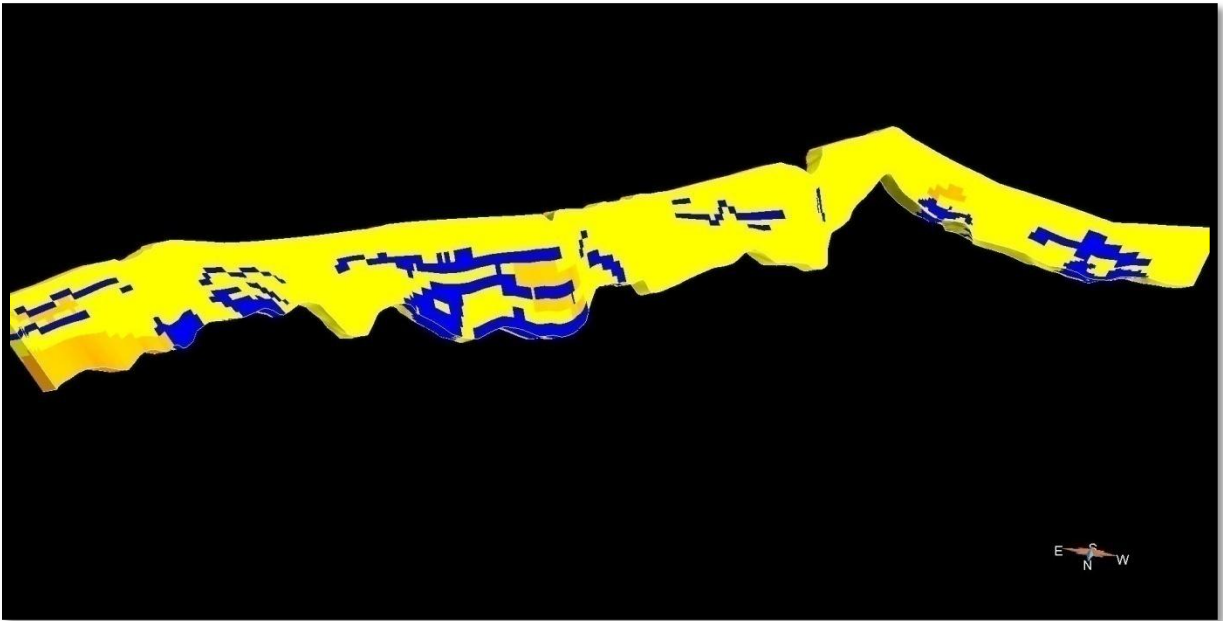
Section C



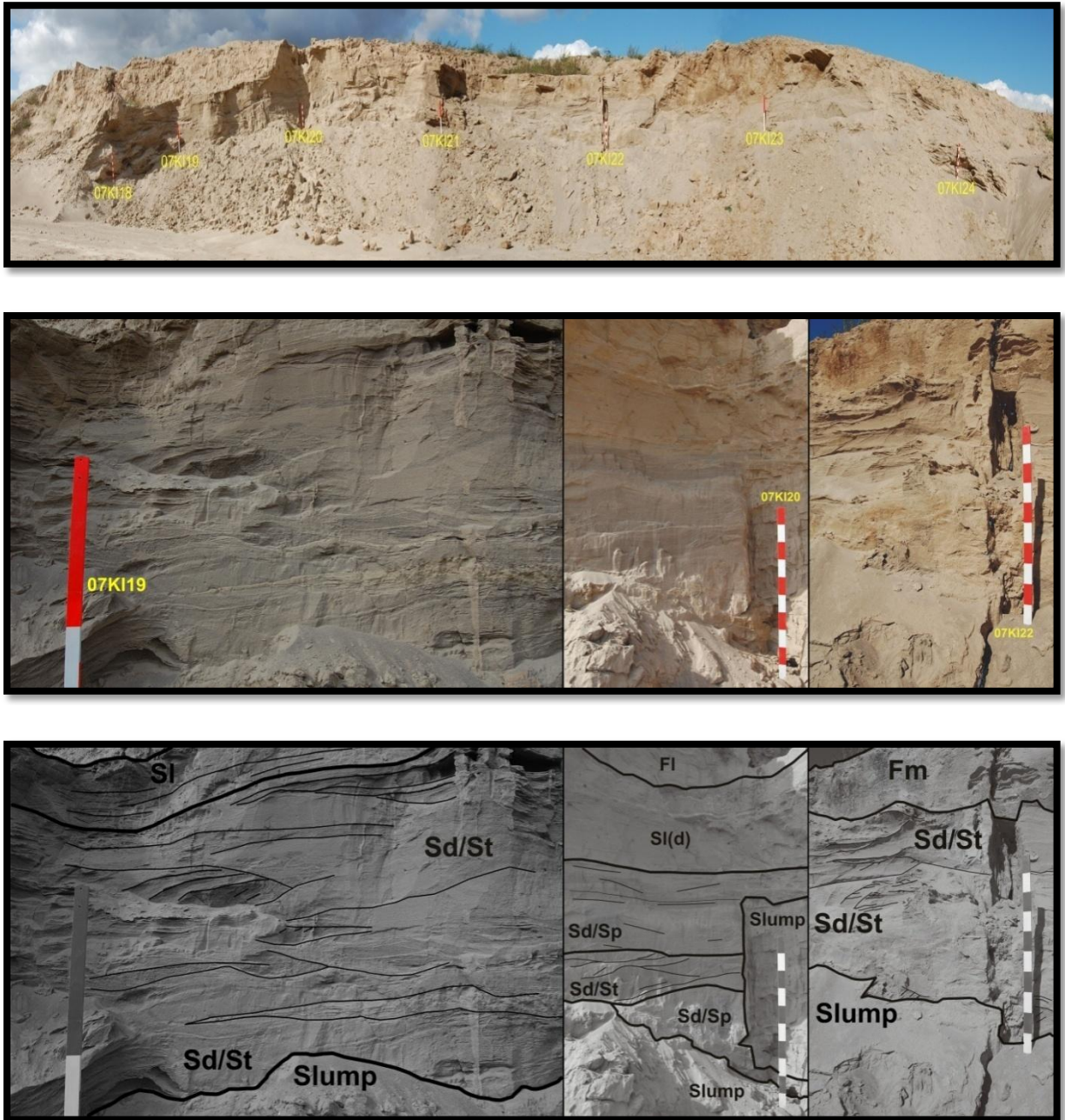
Combined images producing a 2D image of Section C with stations (top), with a close-up of two segments (middle) and their facies interpretation (bottom).



Georeferenced 2D voxets draped over the virtually generated surface (top) and used in the 3D construction of a stratigraphic grid (bottom) displaying the facies massive muds (dark blue), planar sands (yellow) and massive gravel (light orange).



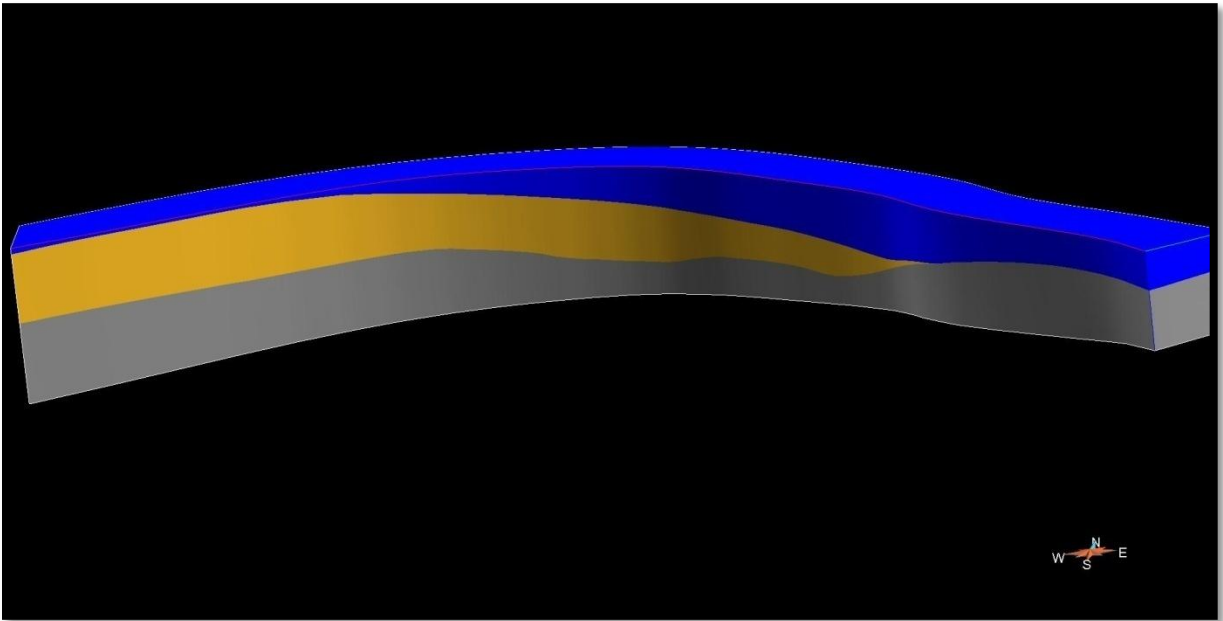
Section D



Photomosaic of Section D showing the locations of the stations (top) with a closeup of three selected areas (middle) and their interpreted facies (bottom).



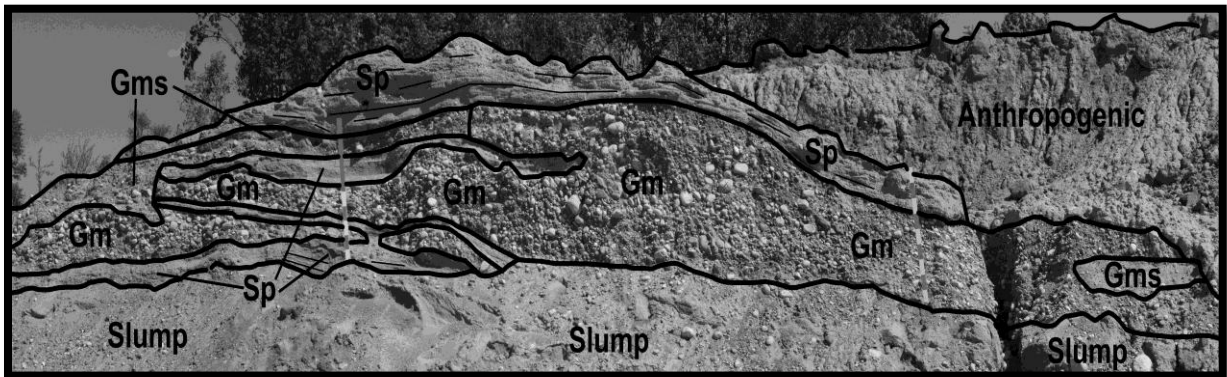
Georeferenced 2D voxets draped over the virtually generated surface (top) and used in the 3D construction of a stratigraphic grid (bottom) displaying the facies massive muds (dark blue), laminated sands (gold) and deformed sands (grey).

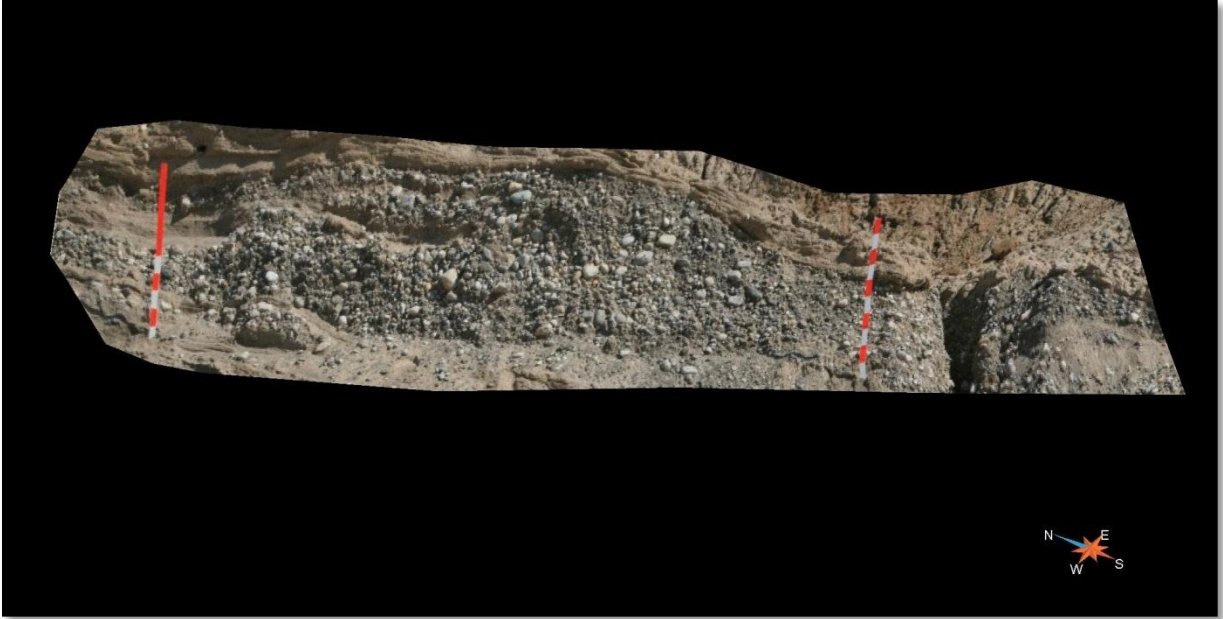


Section E

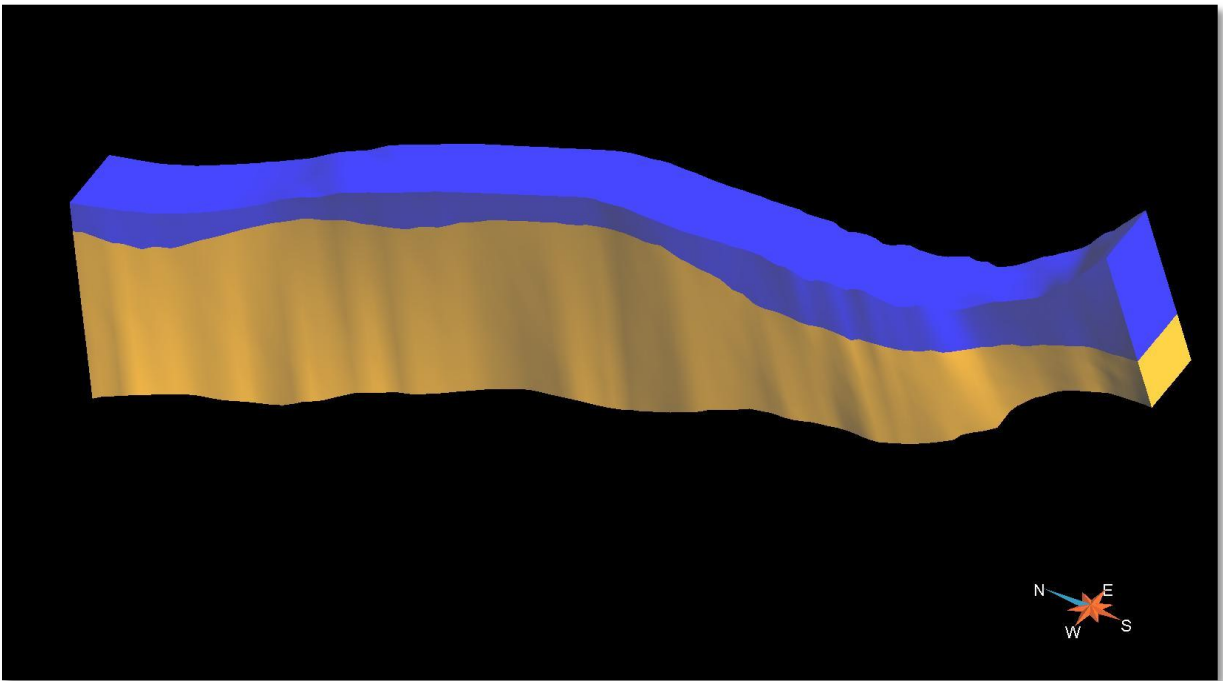


The stations of Section E (top), the smallest of the sections and the facies seen at that location (bottom).

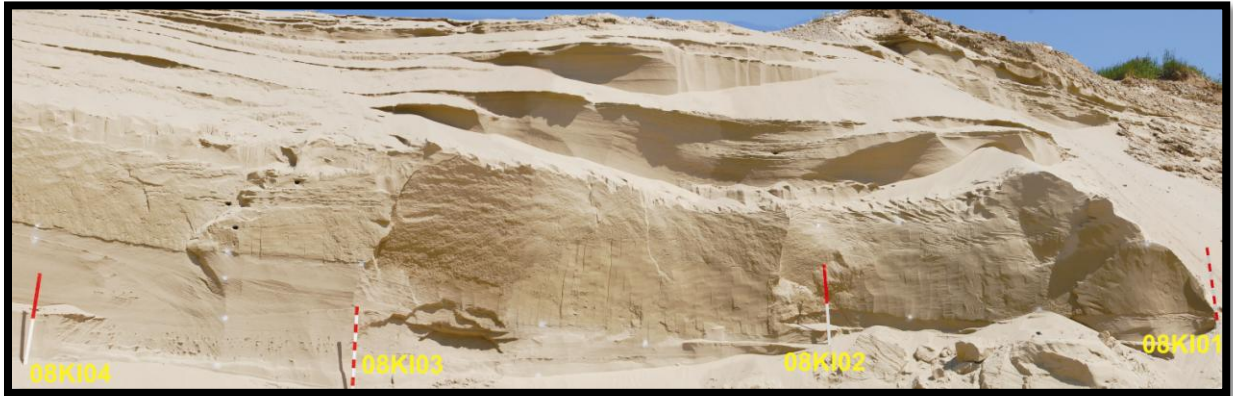




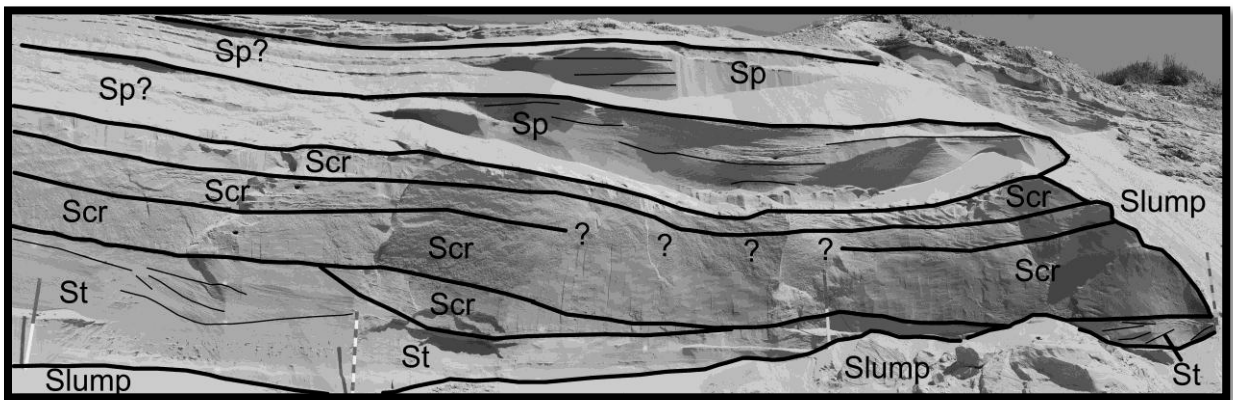
Georeferenced 2D voxets draped over the virtually generated surface (top) and used in the 3D construction of a stratigraphic grid (bottom) displaying the facies massive muds (dark blue), planar sands (yellow) and massive gravel (light orange).



Section F

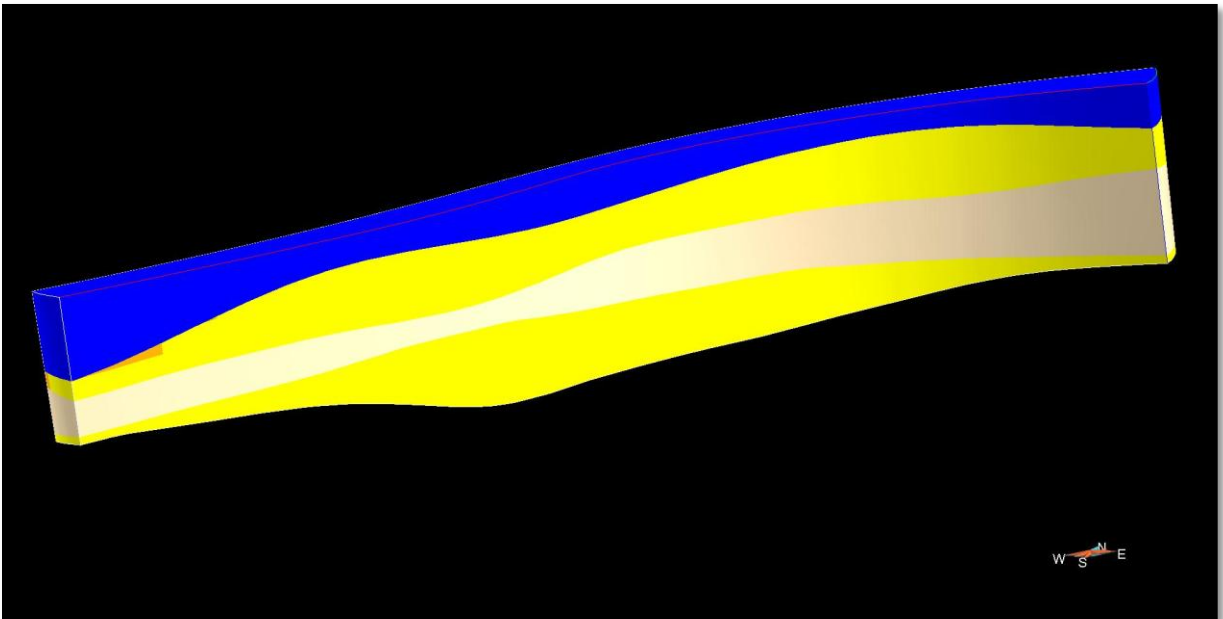


Part of Section F (top) and the interpreted facies for that region (bottom).

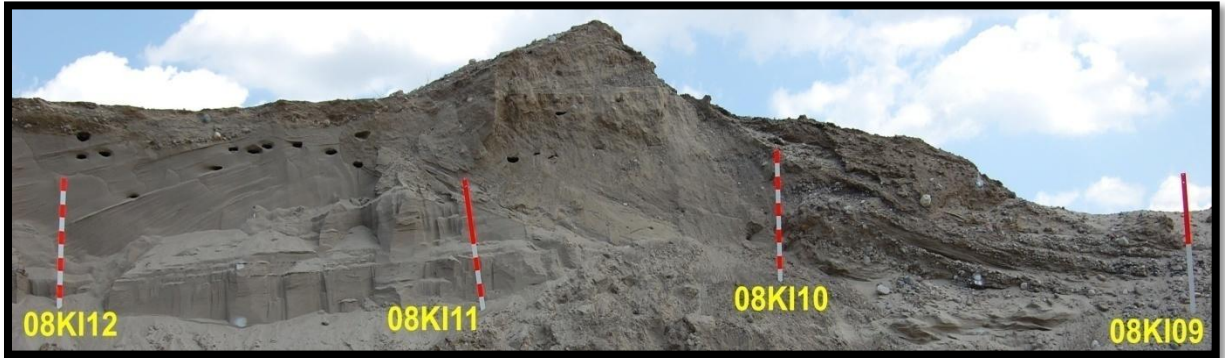




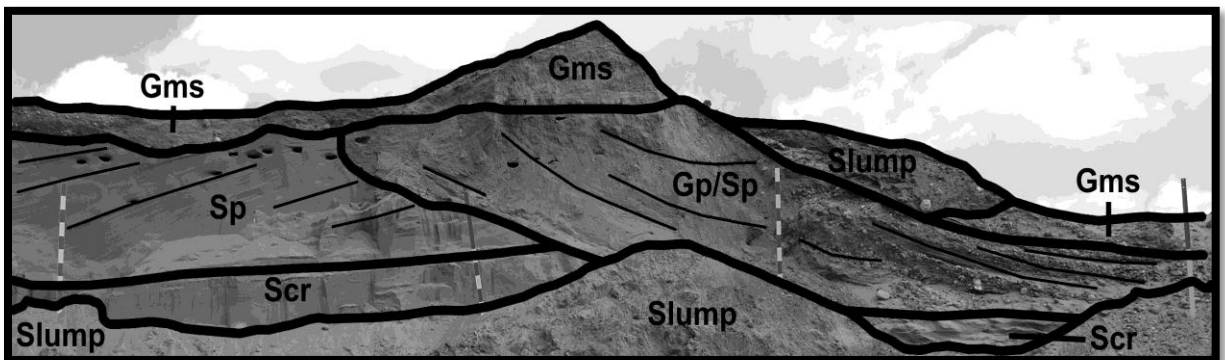
Georeferenced 2D voxets draped over the virtually generated surface (top) and used in the 3D construction of a stratigraphic grid (bottom) displaying the facies massive muds (dark blue), planar sands (yellow) and climbing ripples (biece).



Section G

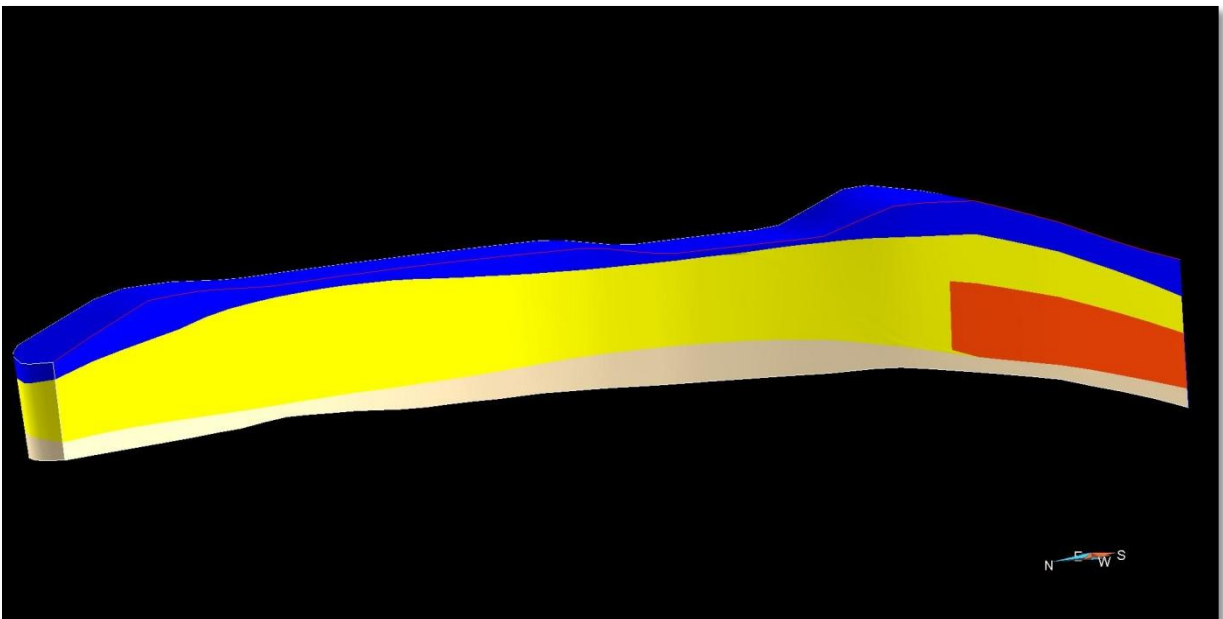


A portion of Section G with stations (top) and the facies observed for that part of the section (bottom).





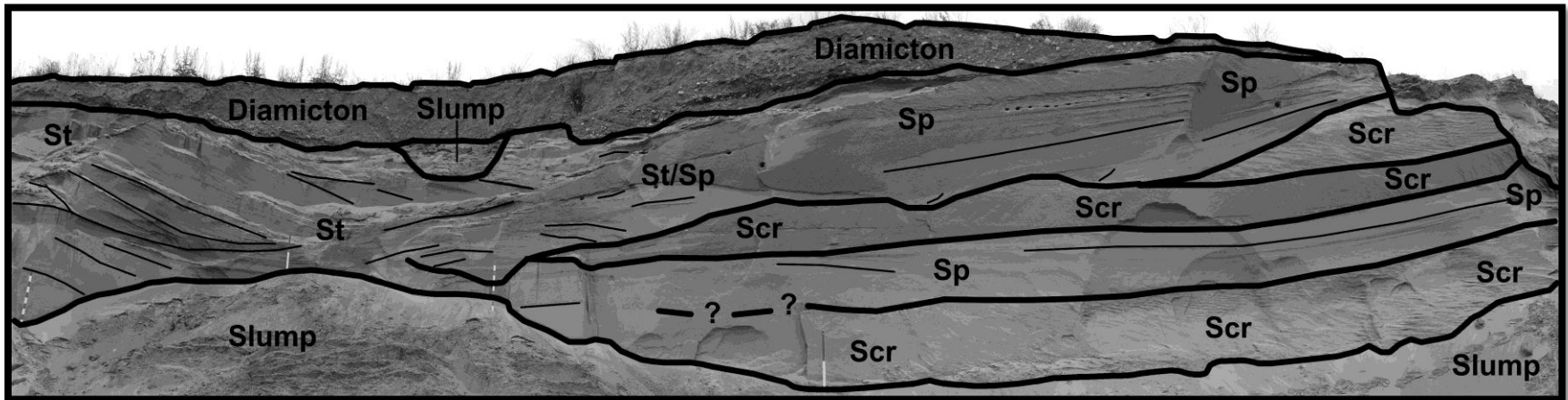
Georeferenced 2D voxets draped over the virtually generated surface (top) and used in the 3D construction of a stratigraphic grid (bottom) displaying the facies massive muds (dark blue), planar sands (yellow), planar gravel beds (dark orange) and climbing ripples (biede).

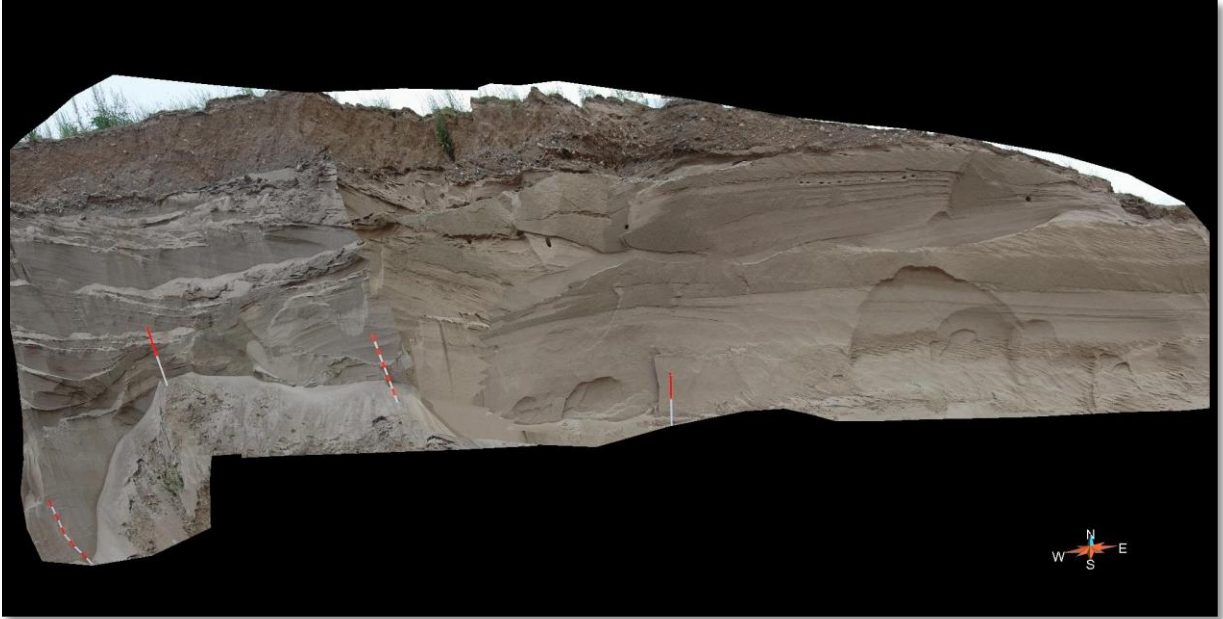


Section H

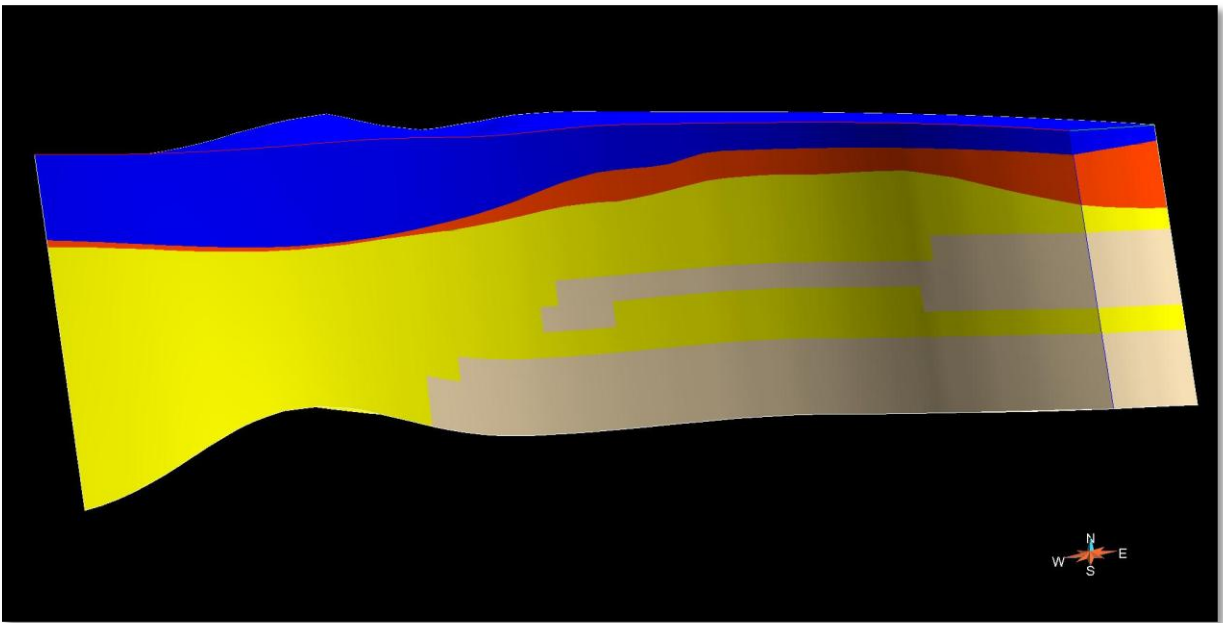


Section H and its stations (top) and the interpreted facies assemblage occurring there (bottom).

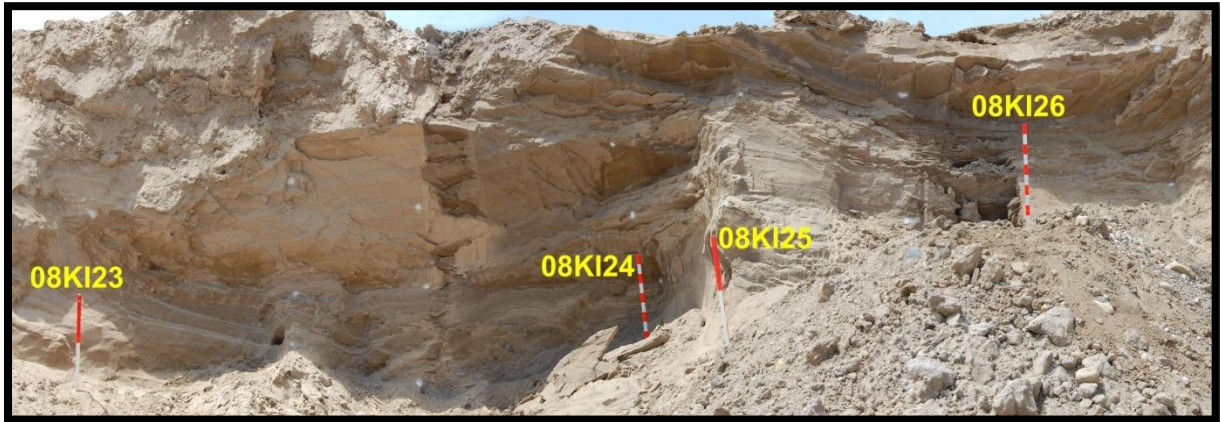




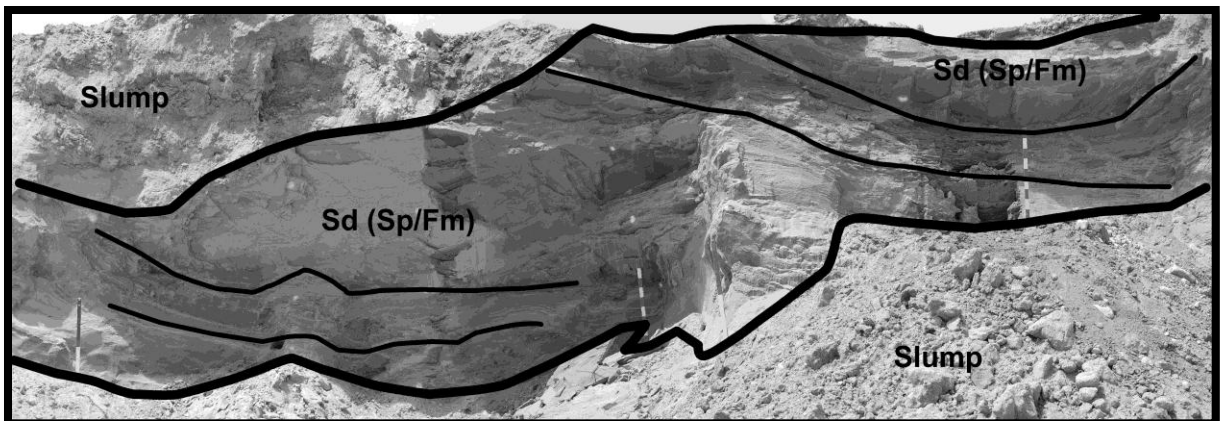
Georeferenced 2D voxets draped over the virtually generated surface (top) and used in the 3D construction of a stratigraphic grid (bottom) displaying the facies massive muds (dark blue), planar sands (yellow), deformed sands (grey) planar gravel beds (dark orange) and climbing ripples (beige).

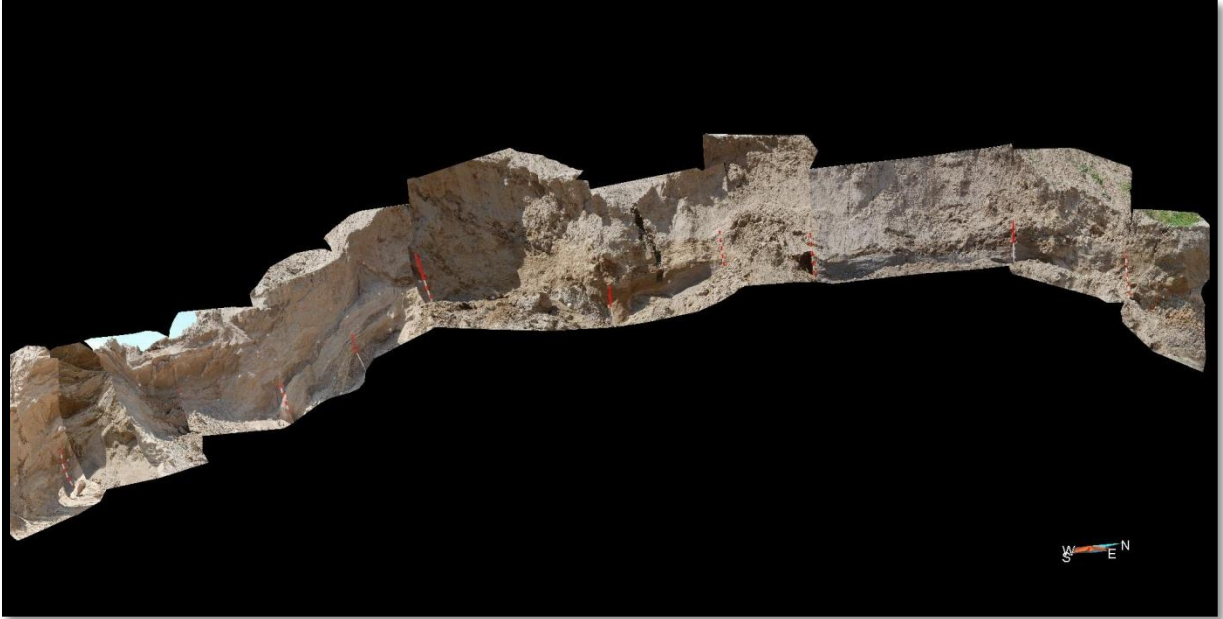


Section I

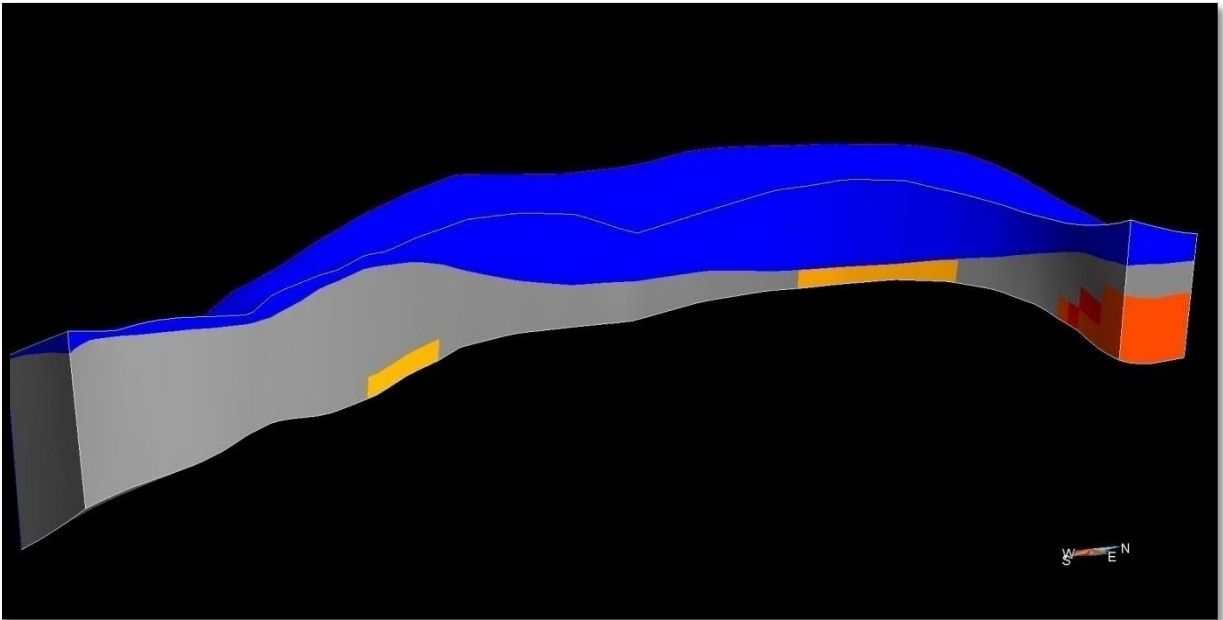


Highly deformed area of Section I with stations (top) and the result facies classification (bottom).

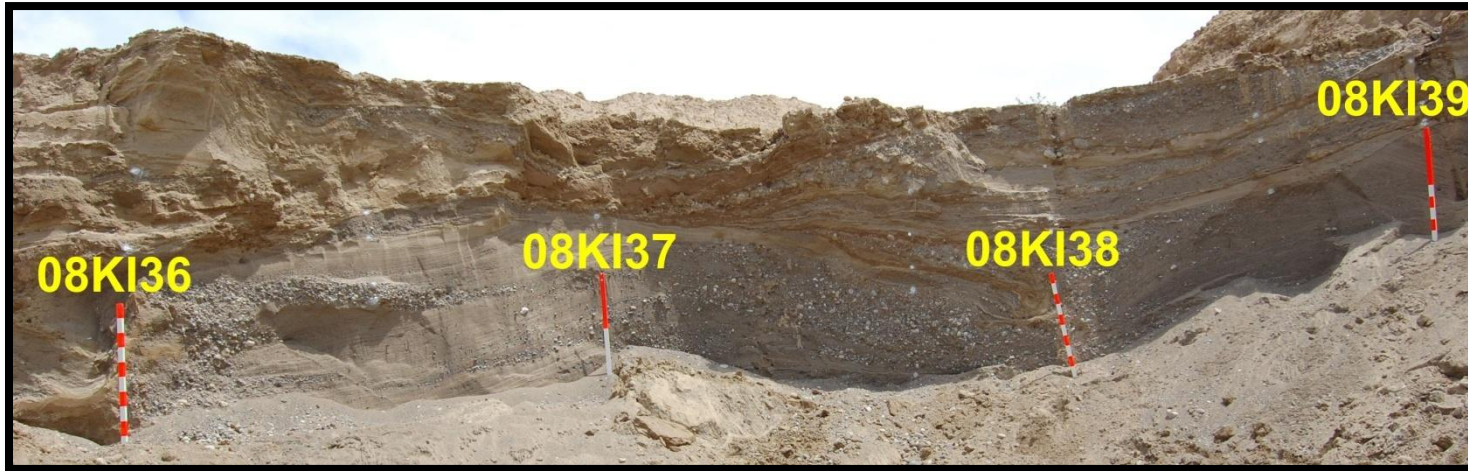




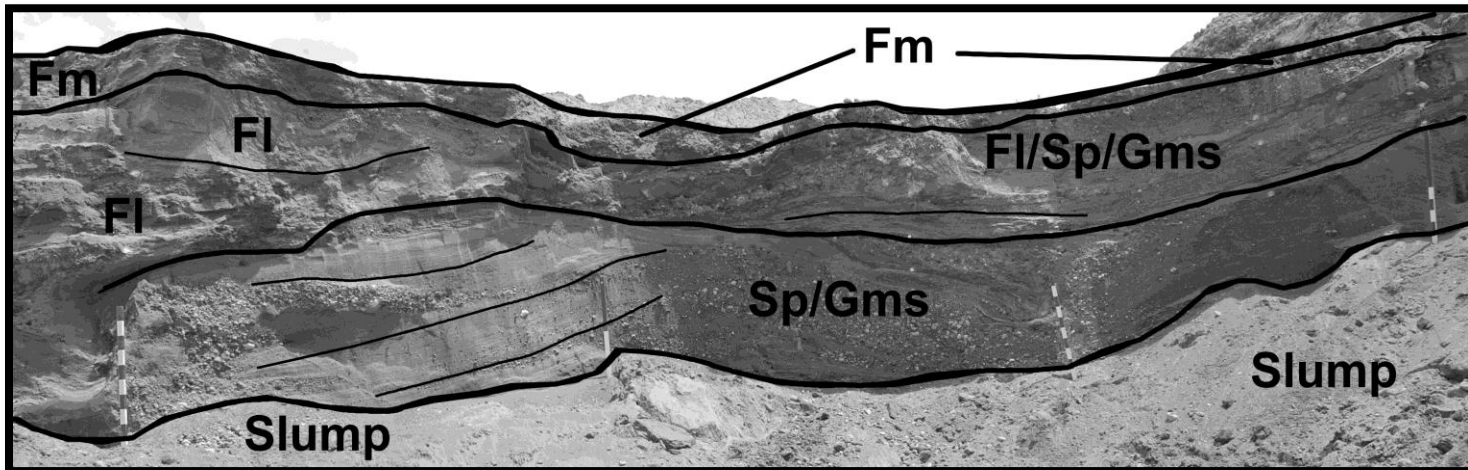
Georeferenced 2D voxets draped over the virtually generated surface (top) and used in the 3D construction of a stratigraphic grid (bottom) displaying the facies massive muds (dark blue), deformed sands (grey), massive gravel (light orange), planar gravel (dark orange) and openwork gravel (red).



Section J

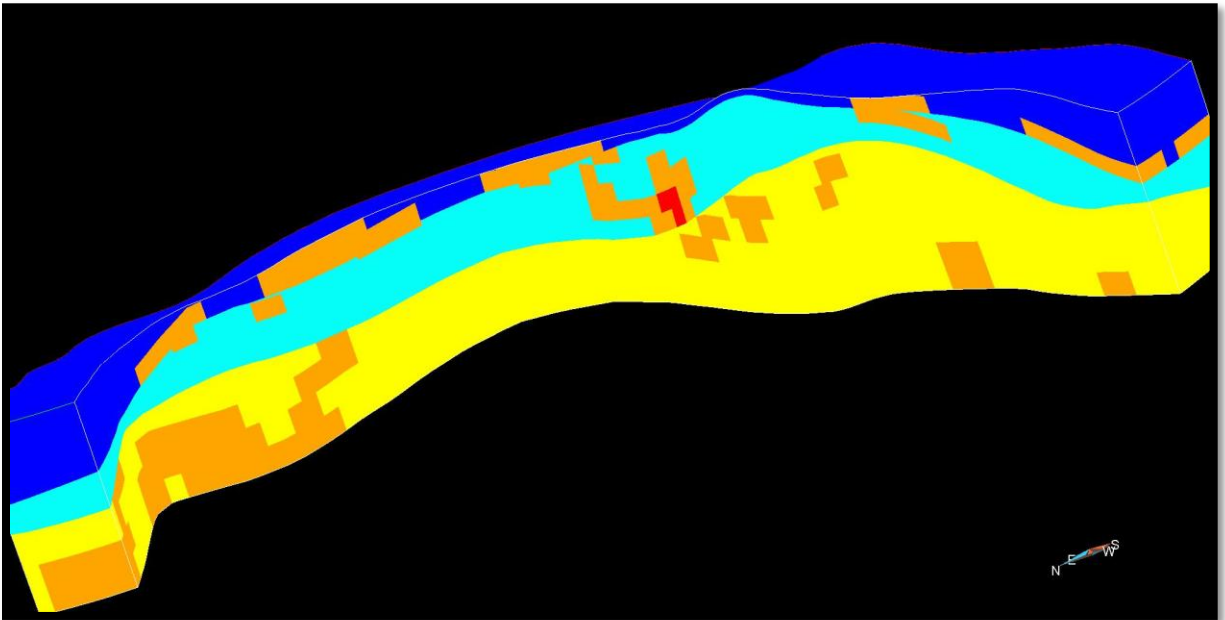


A portion of Section J displaying the stations located there (top) with the complex facies association (bottom).

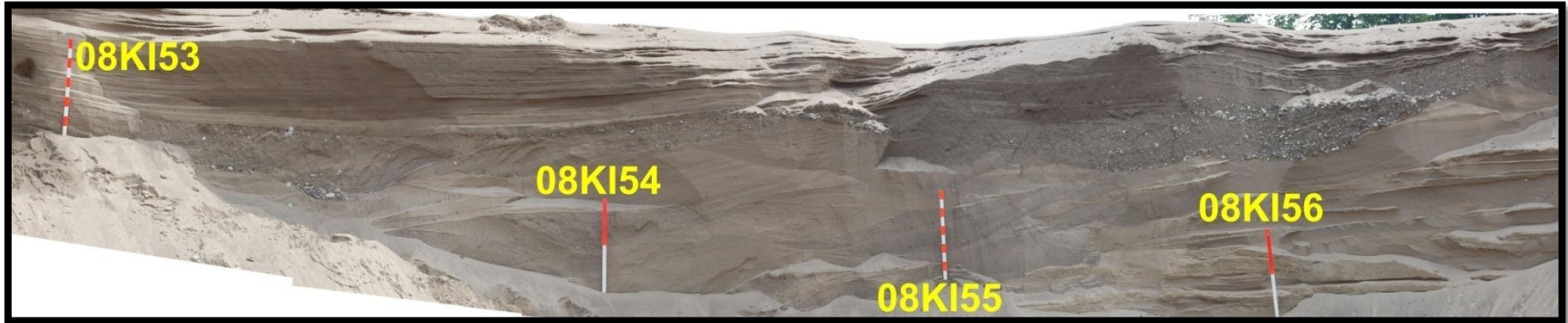




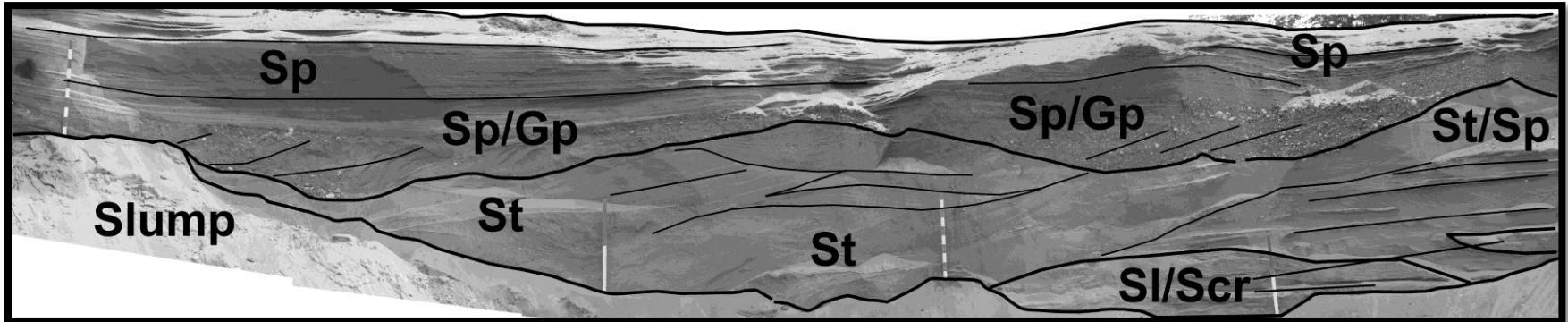
Georeferenced 2D voxets draped over the virtually generated surface (top) and used in the 3D construction of a stratigraphic grid (bottom) displaying the facies massive muds (dark blue), laminated muds (light blue), planar sands (yellow), massive gravel (light orange), and openwork gravel (red).

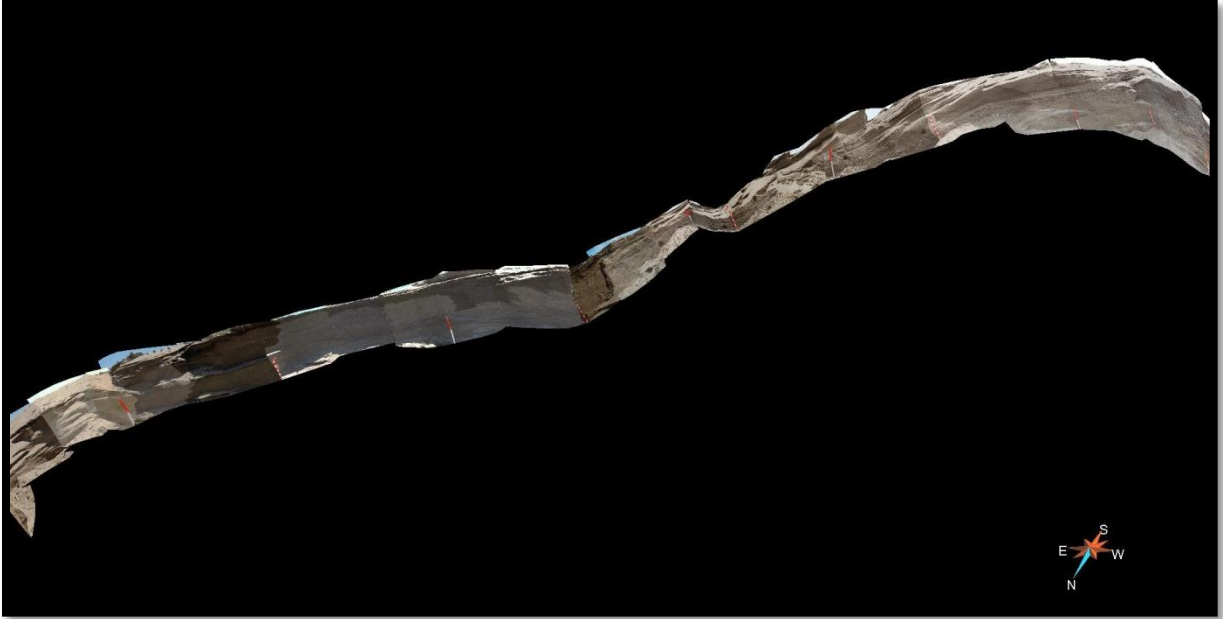


Section K

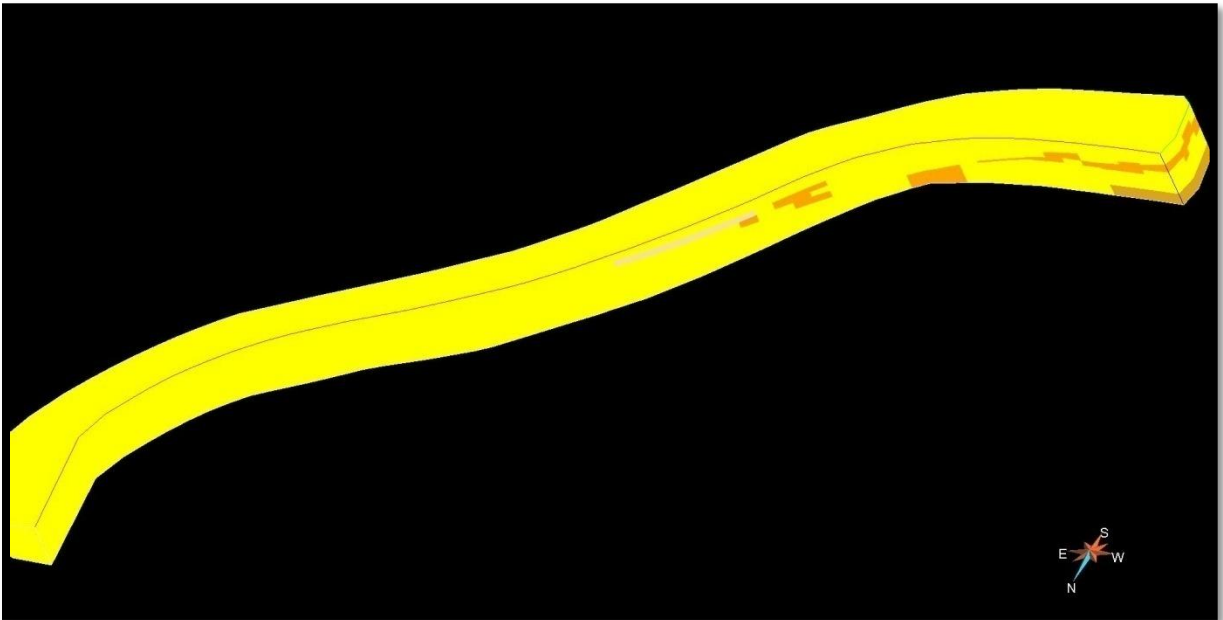


A segment of Section K with associated stations (top) and the interpreted facies (bottom).





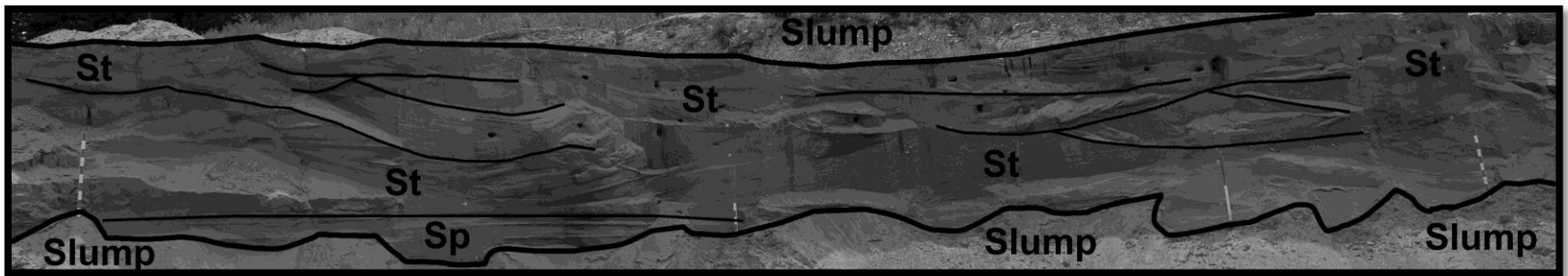
Georeferenced 2D voxets draped over the virtually generated surface (top) and used in the 3D construction of a stratigraphic grid (bottom) displaying the prominent planar sands (yellow), massive gravel (light orange), climbing ripples (biece) and laminated fine sands (brown).



Section L

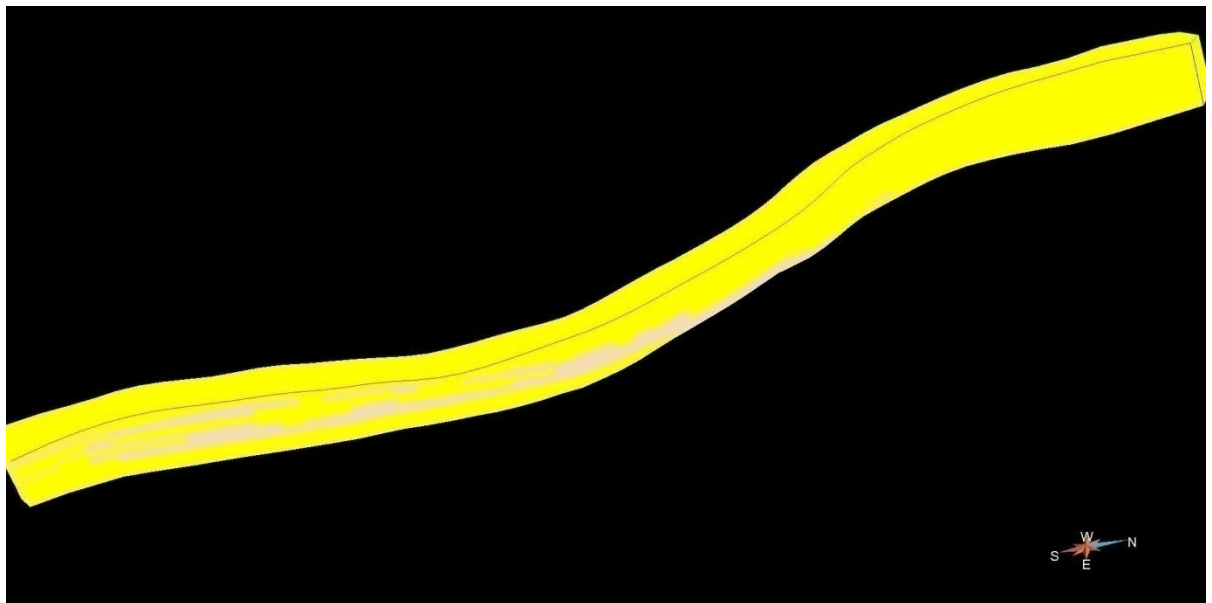


Part of Section L with noted stations (top) and interpreted facies (bottom).

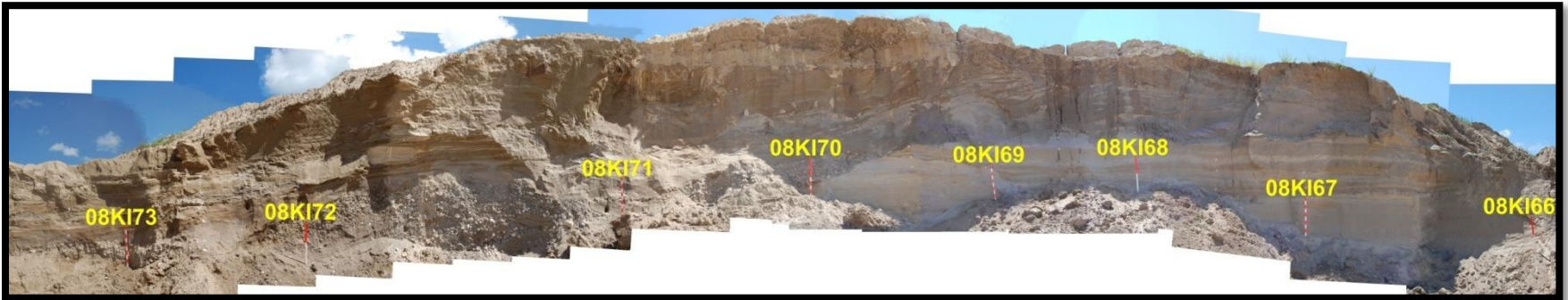




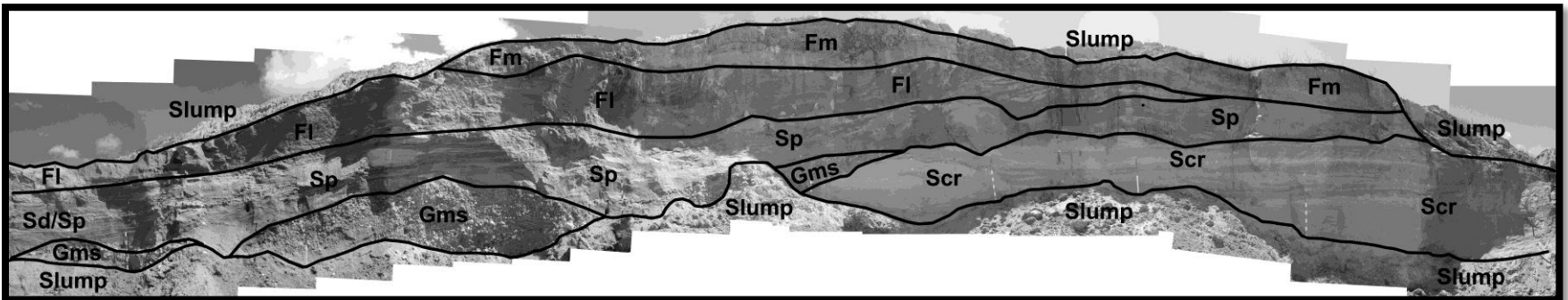
Georeferenced 2D voxets draped over the virtually generated surface (top) and used in the 3D construction of a stratigraphic grid (bottom) displaying the prominent planar sands (yellow) and climbing ripples (biece).



Section M

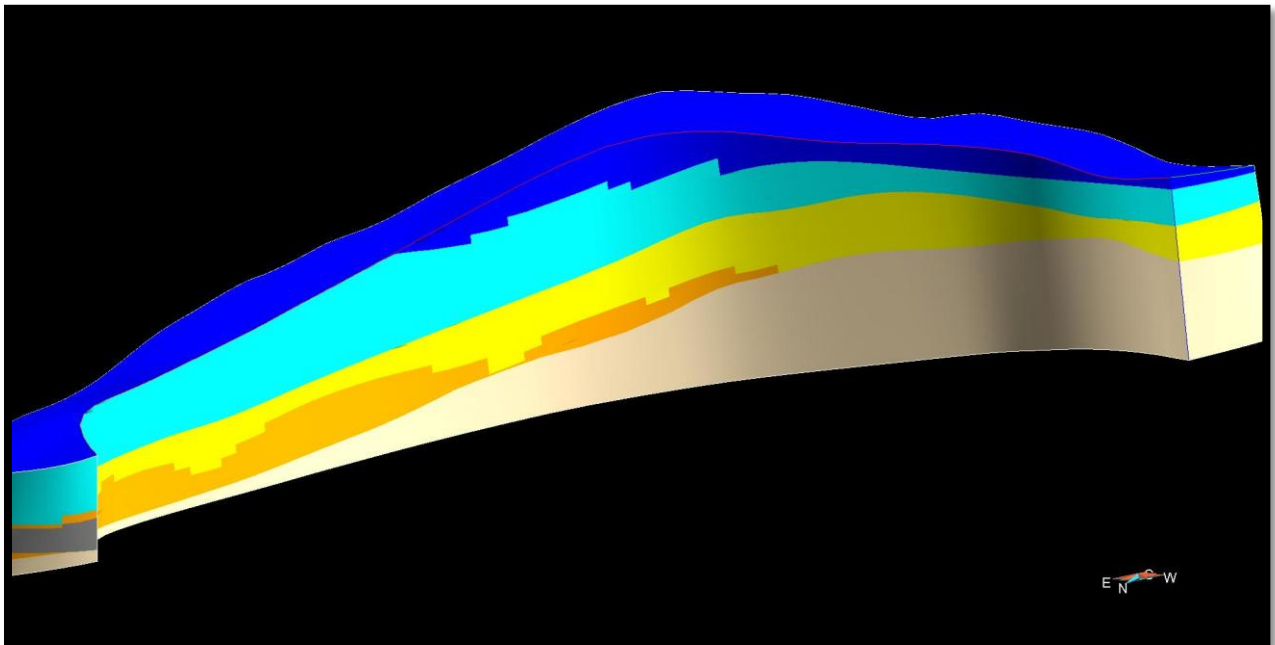


Labeled stations for Section M (top) and the facies assemblage for the Section (bottom).

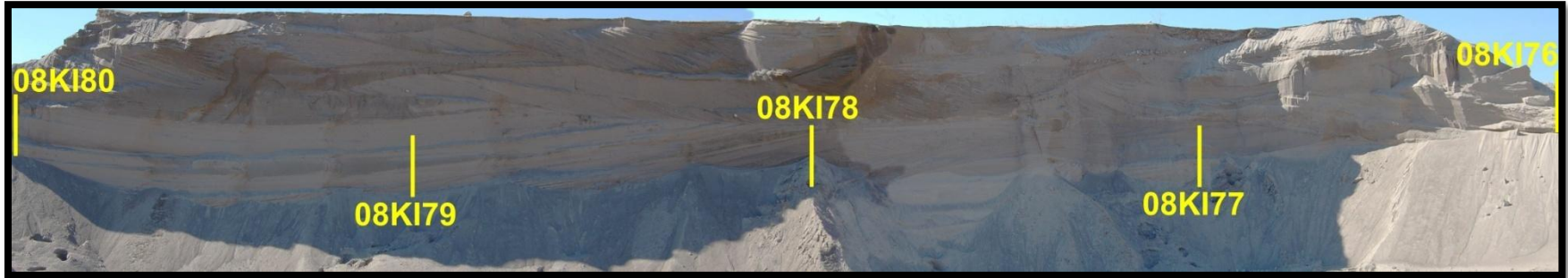




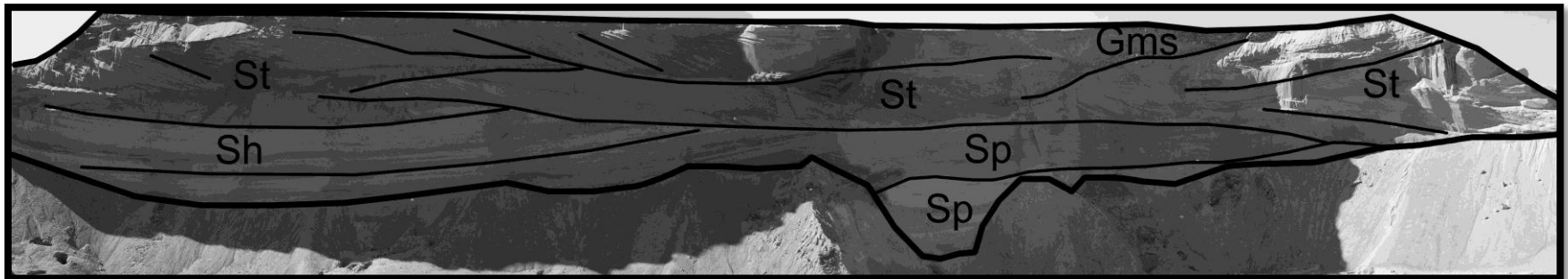
Georeferenced 2D voxets draped over the virtually generated surface (top) and used in the 3D construction of a stratigraphic grid (bottom) displaying the massive muds (dark blue), laminated muds (light blue), planar sands (yellow), climbing ripples (beige), deformed sands (grey) and massive gravel (light orange).

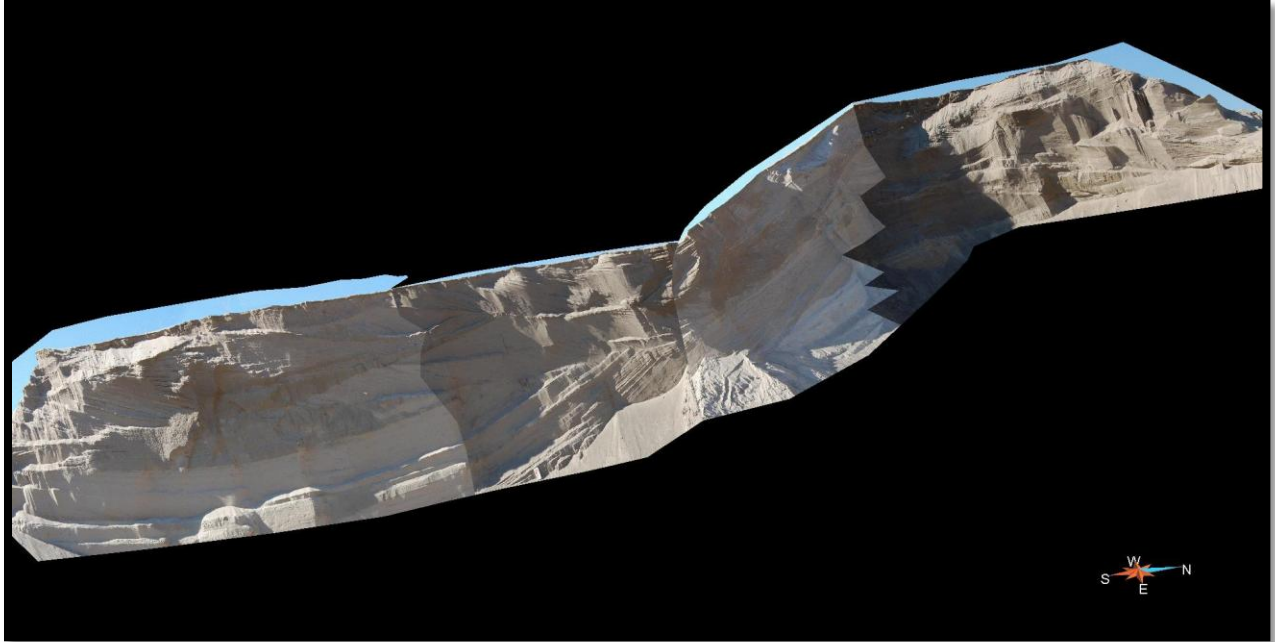


Section N

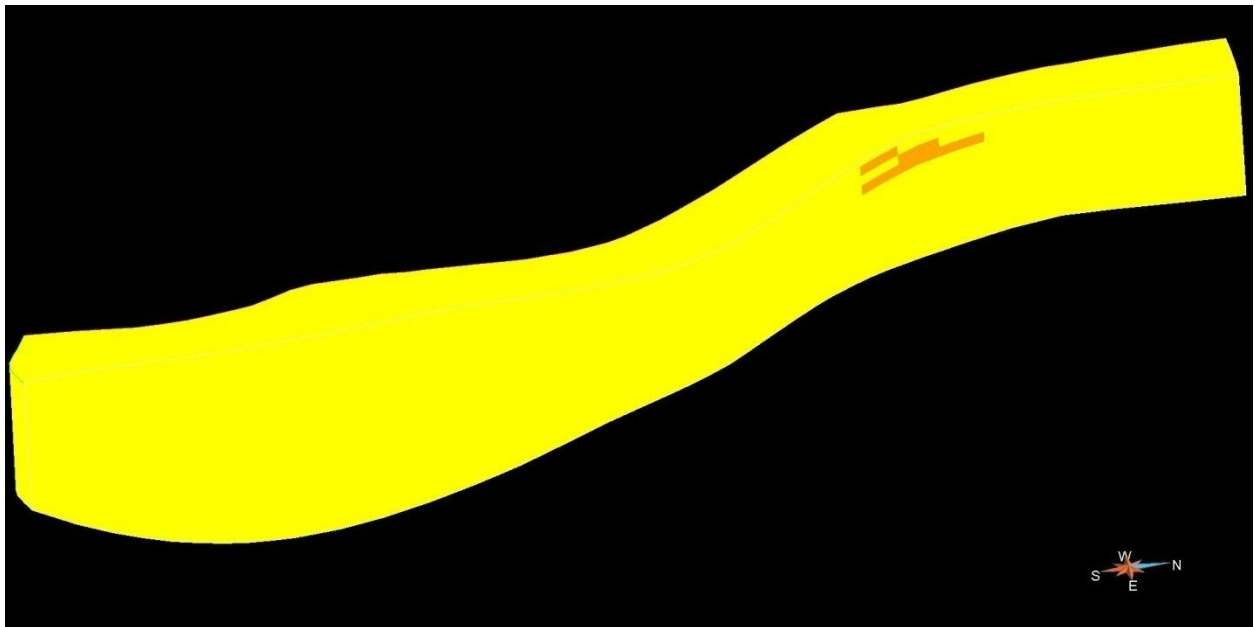


The stations at Section N denoting meter scale (top) and the interpreted sand trough cross-stratification facies (bottom).





Georeferenced 2D voxets draped over the virtually generated surface (top) and used in the 3D construction of a stratigraphic grid (bottom) displaying the dominant planar sands (yellow) and massive gravel (light orange).



Appendix D – Hydraulic Conductivity Calculations

Sample Number	Textural Classification	d ₁₀ (mm)	d ₆₀ (mm)	U	n	C	Hazen	K-C	Breyer	Terzaghi
07KI03-01	Muddy Sandy Gravel	2.7E-01	2.0E+00	7.52	0.32	1.59	5.19E-04	3.14E-04	6.00E-04	5.46E-02
07KI03-02	Muddy Sandy Gravel	3.5E-02	3.0E+01	859.71	0.26	3.89	5.37E-06	2.34E-06	-1.33E-06	8.92E-04
07KI03-03	Muddy Sandy Gravel	1.1E-02	8.0E+00	699.95	0.26	14.77	5.77E-07	2.51E-07	-8.87E-08	3.63E-04
07KI04-01	Slightly Gravelly Sand	9.7E-02	3.0E-01	3.10	0.40	2.29	1.04E-04	1.05E-04	9.63E-05	2.57E-02
07KI04-02	Gravelly Muddy Sand	1.4E-02	1.9E-01	13.18	0.28	6.91	1.13E-06	5.42E-07	1.52E-06	3.90E-04
07KI05-01	Slightly Gravelly Sandy Mud	1.5E-03	2.1E-02	13.88	0.27	13.47	1.21E-08	5.75E-09	1.65E-08	8.02E-06
07KI05-02	Slightly Gravelly Sandy Mud	4.8E-03	6.7E-02	13.99	0.27	6.93	1.21E-07	5.74E-08	1.66E-07	4.11E-05
07KI07-01	Slightly Gravelly Sand	2.5E-01	7.0E-01	2.79	0.41	2.42	7.21E-04	7.72E-04	6.59E-04	1.97E-01
07KI07-02	Gravel	1.2E+00	5.1E+01	42.80	0.26	0.66	6.27E-03	2.73E-03	7.04E-03	1.77E-01
07KI09-01	Gravel	3.0E+00	8.0E+01	26.67	0.26	0.70	4.05E-02	1.77E-02	5.32E-02	1.22E+00
07KI09-02	Muddy Sandy Gravel	7.9E-01	3.5E+01	44.43	0.26	0.67	2.74E-03	1.19E-03	3.03E-03	7.78E-02
07KI12-01	Sandy Gravel	2.6E-01	2.4E+01	91.51	0.26	1.95	3.04E-04	1.32E-04	2.36E-04	2.52E-02
07KI12-02	Gravelly Mud	2.2E-03	4.2E-03	1.90	0.43	19.71	6.19E-08	7.97E-08	5.47E-08	1.61E-04
07KI12-03	Gravelly Muddy Sand	4.4E-02	1.8E-01	4.11	0.37	7.03	1.90E-05	1.63E-05	1.85E-05	1.25E-02
07KI13-01	Slightly Gravelly Muddy Sand	5.0E-03	1.4E-01	27.96	0.26	9.02	1.12E-07	4.91E-08	1.46E-07	4.36E-05
07KI15-01	Slightly Gravelly Sandy Mud	1.0E-03	1.4E-02	13.86	0.27	30.62	5.41E-09	2.57E-09	7.38E-09	8.14E-06
07KI15-02	Slightly Gravelly Sand	2.3E-01	5.7E-01	2.49	0.42	1.99	6.19E-04	7.02E-04	5.58E-04	1.46E-01
07KI16-01	Slightly Gravelly Mud	7.0E-04	3.1E-03	4.43	0.37	3.53	4.71E-09	3.87E-09	4.67E-09	1.49E-06
07KI16-02	Sandy Gravel	2.9E-01	2.0E+01	68.58	0.26	1.64	3.75E-04	1.63E-04	3.41E-04	2.62E-02
07KI17-01	Muddy Sandy Gravel	2.5E-02	1.3E+00	52.77	0.26	8.59	2.68E-06	1.17E-06	2.75E-06	9.81E-04
07KI17-02	Slightly Gravelly Muddy Sand	1.9E-02	2.0E-01	10.59	0.29	6.07	2.16E-06	1.11E-06	2.77E-06	7.21E-04
07KI17-03	Slightly Gravelly Mud	1.1E-03	6.0E-02	56.10	0.26	5.92	5.05E-09	2.20E-09	5.05E-09	1.27E-06
07KI18-01	Gravelly Muddy Sand	2.6E-02	1.6E-01	6.10	0.34	5.36	5.66E-06	3.85E-06	6.13E-06	2.27E-03
07KI18-02	Gravelly Sand	1.2E-01	3.5E-01	2.89	0.40	2.46	1.66E-04	1.74E-04	1.52E-04	4.55E-02
07KI19-01	Slightly Gravelly Muddy Sand	3.6E-02	2.8E-01	7.74	0.32	5.11	9.43E-06	5.62E-06	1.10E-05	3.13E-03
07KI20-01	Gravelly Muddy Sand	2.0E-02	1.0E-01	5.07	0.35	3.80	3.52E-06	2.67E-06	3.61E-06	1.11E-03
07KI20-02	Slightly Gravelly Sand	9.2E-02	3.0E-01	3.26	0.39	2.22	9.19E-05	9.03E-05	8.58E-05	2.15E-02
07KI20-03	Gravelly Muddy Sand	2.1E-02	2.2E-01	10.63	0.29	5.25	2.59E-06	1.33E-06	3.32E-06	7.47E-04
07KI23-01	Slightly Gravelly Mud	1.6E-03	9.0E-03	5.67	0.34	4.80	2.15E-08	1.53E-08	2.28E-08	8.06E-06
08KI04-01	Sand	8.5E-02	1.9E-01	2.24	0.42	1.852	8.77E-05	1.05E-04	7.84E-05	2.02E-02
08KI04-02	Sand	1.1E-01	3.1E-01	2.78	0.41	2.001	1.43E-04	1.54E-04	1.31E-04	3.24E-02
08KI04-03	Slightly Gravelly Muddy Sand	2.9E-02	8.0E-02	2.81	0.41	2.151	9.30E-06	9.93E-06	8.50E-06	2.26E-03
08KI12-01	Gravelly Muddy Sand	4.0E-02	1.8E-01	4.50	0.37	3.982	1.53E-05	1.24E-05	1.52E-05	5.40E-03

08K112-02	Sand	1.3E-01	2.4E-01	1.88	0.43	1.674	2.09E-04	2.71E-04	1.84E-04	4.64E-02
08K144-01	Slightly Gravelly Sand	1.7E-01	3.0E-01	1.81	0.44	2.351	3.54E-04	4.65E-04	3.12E-04	1.12E-01
08K144-02	Sand	1.1E-01	2.5E-01	2.25	0.42	1.837	1.51E-04	1.81E-04	1.35E-04	3.45E-02
08K144-03	Slightly Gravelly Sand	1.6E-01	3.0E-01	1.88	0.43	1.628	3.27E-04	4.23E-04	2.89E-04	7.06E-02
08K145-01	Slightly Gravelly Sand	1.5E-01	3.0E-01	2.00	0.43	1.621	2.83E-04	3.56E-04	2.51E-04	5.94E-02
08K146-01	Slightly Gravelly Sand	2.0E-01	4.0E-01	2.00	0.43	1.731	5.03E-04	6.33E-04	4.46E-04	1.13E-01
08K146-02	Sand	1.6E-01	3.1E-01	1.94	0.43	1.703	3.24E-04	4.14E-04	2.87E-04	7.24E-02
08K146-03	Sand	1.5E-01	3.0E-01	2.06	0.43	1.673	2.65E-04	3.29E-04	2.35E-04	5.68E-02
08K146-04	Slightly Gravelly Sand	2.0E-01	4.1E-01	2.00	0.43	1.887	5.28E-04	6.65E-04	4.68E-04	1.29E-01
08K148-01	Slightly Gravelly Sand	1.3E-01	2.8E-01	2.23	0.42	1.763	1.93E-04	2.32E-04	1.73E-04	4.24E-02
08K148-02	Slightly Gravelly Sand	2.2E-01	5.5E-01	2.53	0.41	2.028	5.58E-04	6.29E-04	5.04E-04	1.34E-01
08K148-03	Slightly Gravelly Sand	2.0E-01	4.0E-01	1.96	0.43	1.818	5.27E-04	6.70E-04	4.66E-04	1.25E-01
08K150-01	Slightly Gravelly Sand	2.3E-01	5.0E-01	2.17	0.43	1.989	6.51E-04	7.89E-04	5.80E-04	1.63E-01
08K150-02	Slightly Gravelly Sand	6.5E-02	2.5E-01	3.84	0.38	2.684	4.32E-05	3.87E-05	4.16E-05	1.12E-02
08K158-01	Sand	1.6E-01	3.0E-01	1.89	0.43	1.636	3.19E-04	4.12E-04	2.82E-04	6.90E-02
08K158-02	Slightly Gravelly Sand	1.5E-01	3.1E-01	2.07	0.43	2.079	2.80E-04	3.47E-04	2.49E-04	7.45E-02
08K158-03	Muddy Sand	3.2E-02	8.5E-02	2.62	0.41	2.141	1.23E-05	1.36E-05	1.12E-05	3.06E-03
08K160-01	Slightly Gravelly Sand	1.8E-01	3.1E-01	1.72	0.44	1.599	4.24E-04	5.70E-04	3.73E-04	9.27E-02
08K160-02	Muddy Sand	3.4E-02	8.5E-02	2.51	0.41	2.030	1.36E-05	1.54E-05	1.23E-05	3.28E-03
08K160-03	Slightly Gravelly Sand	1.3E-01	3.0E-01	2.28	0.42	1.725	2.10E-04	2.49E-04	1.88E-04	4.47E-02
08K163-01	Slightly Gravelly Sand	1.7E-01	3.4E-01	1.98	0.43	1.691	3.71E-04	4.69E-04	3.29E-04	8.16E-02
08K163-02	Slightly Gravelly Muddy Sand	3.0E-02	8.0E-02	2.65	0.41	2.107	1.06E-05	1.17E-05	9.62E-06	2.58E-03
08K163-03	Gravelly Sand	1.3E-01	3.1E-01	2.32	0.42	1.954	2.15E-04	2.53E-04	1.93E-04	5.15E-02
08K164-01	Sand	1.2E-01	2.7E-01	2.27	0.42	1.732	1.72E-04	2.05E-04	1.54E-04	3.68E-02
08K164-02	Slightly Gravelly Sand	1.5E-01	3.5E-01	2.28	0.42	1.970	2.88E-04	3.41E-04	2.57E-04	6.99E-02
08K164-03	Slightly Gravelly Sand	1.6E-01	5.0E-01	3.10	0.40	2.388	2.88E-04	2.91E-04	2.67E-04	7.40E-02
08K166-01	Slightly Gravelly Muddy Sand	3.1E-02	7.0E-02	2.24	0.42	1.919	1.19E-05	1.42E-05	1.06E-05	2.83E-03
08K167-01	Slightly Gravelly Sandy Mud	2.1E-02	5.5E-02	2.66	0.41	2.147	4.95E-06	5.43E-06	4.50E-06	1.23E-03
08K167-02	Slightly Gravelly Sand	8.7E-02	2.3E-01	2.65	0.41	1.989	8.78E-05	9.67E-05	7.97E-05	2.02E-02
08K167-03	Slightly Gravelly Sandy Mud	2.0E-02	5.6E-02	2.77	0.41	2.178	4.68E-06	5.03E-06	4.27E-06	1.16E-03
08K167-04	Slightly Gravelly Muddy Sand	3.5E-02	7.0E-02	1.97	0.43	1.776	1.59E-05	2.01E-05	1.41E-05	3.67E-03
08K169-01	Slightly Gravelly Muddy Sand	4.9E-02	1.0E-01	2.05	0.43	1.834	2.96E-05	3.68E-05	2.63E-05	6.96E-03
08K169-02	Slightly Gravelly Sandy Mud	1.9E-02	4.8E-02	2.59	0.41	2.083	4.04E-06	4.50E-06	3.66E-06	9.84E-04

08KI70-01	Slightly Gravelly Sandy Mud	2.1E-02	5.2E-02	2.49	0.42	1.987	5.17E-06	5.86E-06	4.66E-06	1.22E-03
08KI70-02	Gravel	9.3E-01	1.5E+01	16.05	0.27	0.668	4.37E-03	2.01E-03	6.06E-03	1.37E-01
08KI70-03	Slightly Gravelly Muddy Sand	3.6E-02	2.0E-01	5.55	0.35	4.472	1.12E-05	8.06E-06	1.18E-05	3.96E-03
08KI71-01	Gravel	1.2E+00	1.0E+03	837.54	0.26	0.667	6.29E-03	2.74E-03	-1.48E-03	1.79E-01
08KI71-02	Gravel	8.0E-01	3.0E+01	37.50	0.26	0.667	2.83E-03	1.23E-03	3.34E-03	8.07E-02
08KII1-01	Sandy Gravel	5.5E-01	2.0E+00	3.64	0.38	1.340	3.15E-03	2.92E-03	3.00E-03	4.21E-01
08KII1-02	Muddy Gravel	3.5E-03	1.2E-01	34.29	0.26	55.18	5.43E-08	2.37E-08	6.62E-08	1.28E-04
08KIM1-01	Slightly Gravelly Sandy Mud	2.1E-03	3.0E-02	14.49	0.27	17.89	2.23E-08	1.05E-08	3.06E-08	1.93E-05
08KIM1-02	Slightly Gravelly Sandy Mud	2.1E-03	3.0E-02	14.26	0.27	17.95	2.32E-08	1.09E-08	3.18E-08	2.03E-05
08KIM1-03	Gravel	8.0E-01	3.0E+02	375.00	0.26	0.689	2.82E-03	1.23E-03	3.71E-04	8.30E-02
08KIM1-04	Gravel	7.1E-01	5.1E+01	71.83	0.26	0.690	2.22E-03	9.68E-04	1.97E-03	6.55E-02
08KIM1-05	Slightly Gravelly Sandy Mud	1.9E-03	2.5E-02	12.98	0.28	15.25	2.03E-08	9.79E-09	2.73E-08	1.56E-05

Note: <0.063mm fraction was lost in the 08KI46-01 sample

Hazen Method: $K = g/v \cdot 6 \times 10^{-4} \cdot [1 + 10(n - 0.26)] \cdot d_{10}^2$

Kozeny-Carmen Method: $K = g/v \cdot 8.3 \times 10^{-3} \cdot [n^3 / (1 - n)^2] \cdot d_{10}^2$

Breyer Method: $K = g/v \cdot 6 \times 10^{-4} \cdot \log(500/U) \cdot d_{10}^2$

Terzaghi Method: $K = g/v \cdot C \cdot [(n - 0.13)^2 / (1 - n)^{1.5}] \cdot d_{10}^2$

g = gravitational constant = 9.81 m/s²

n = Porosity = 0.255 (1 + 0.83U)

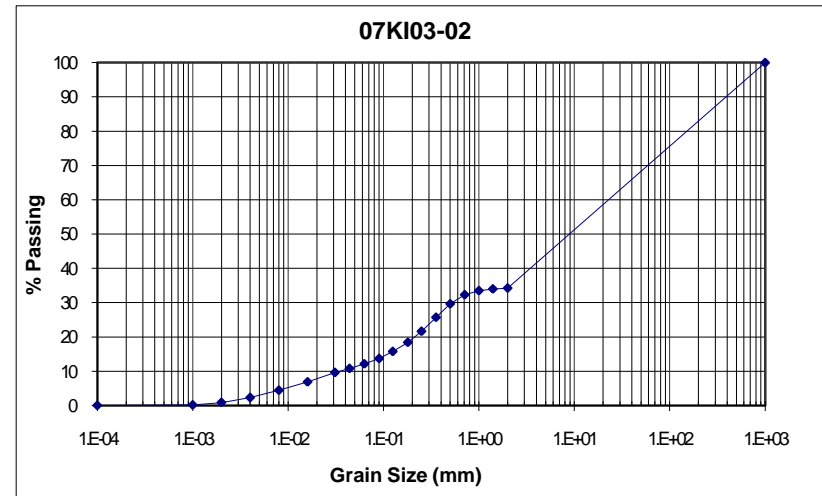
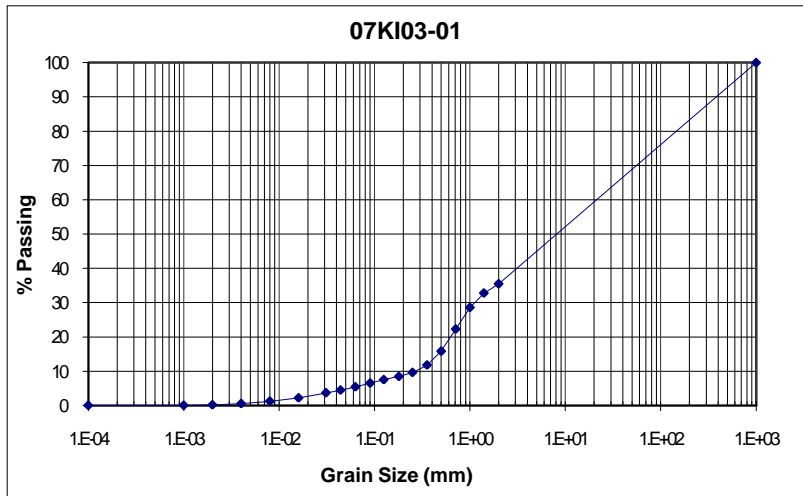
v = kinematic viscosity = μ/ρ = 1.267x10⁻⁶ m²/s @ 10°C

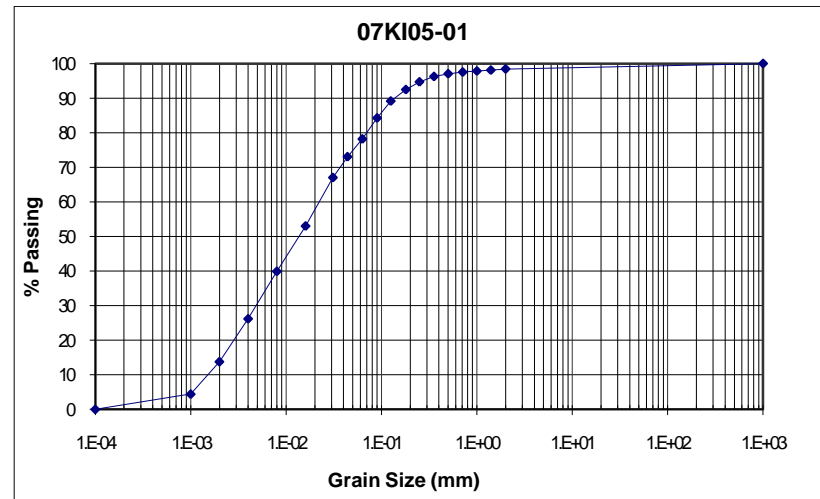
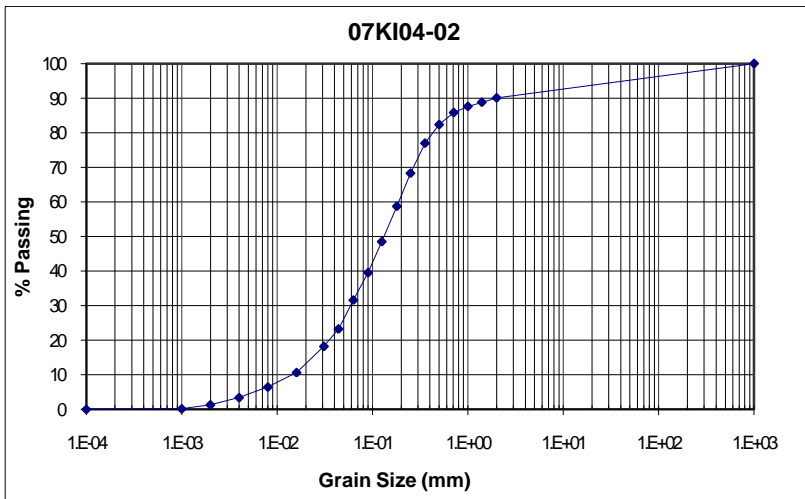
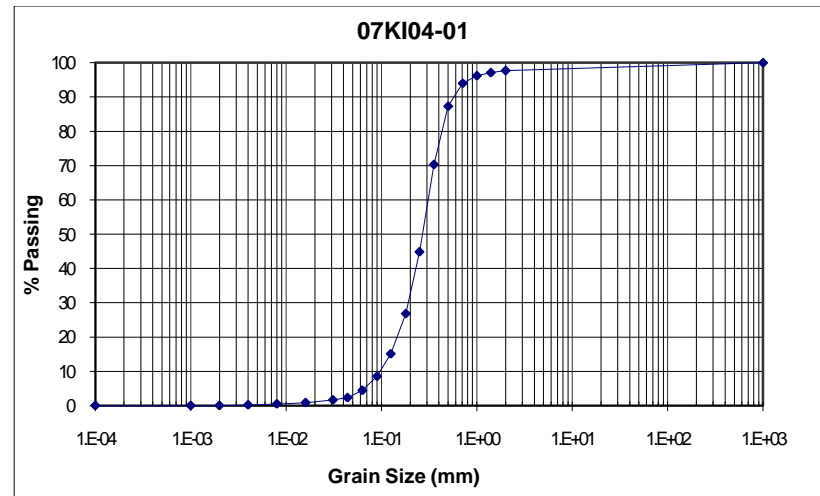
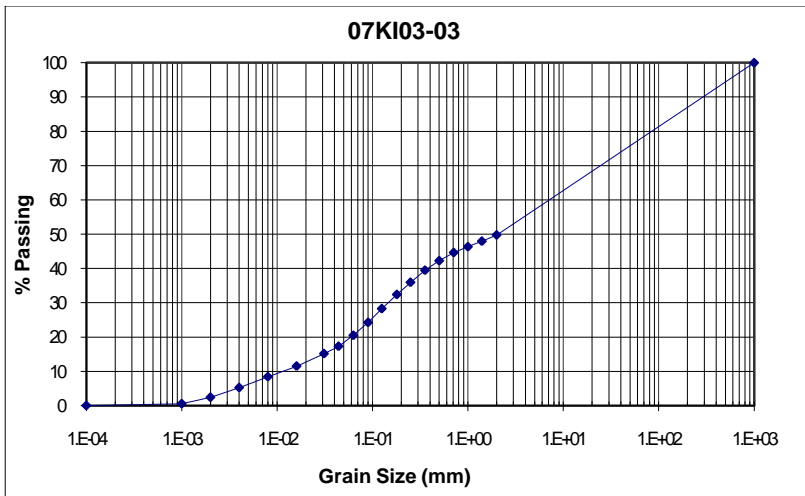
d_{10} = Effective grain size = finest 10% grain size

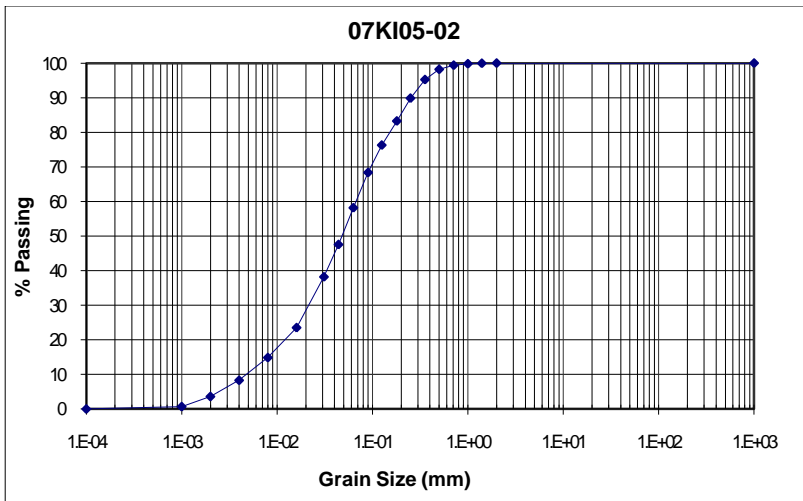
U = Uniformity Coefficient = d_{60}/d_{10}

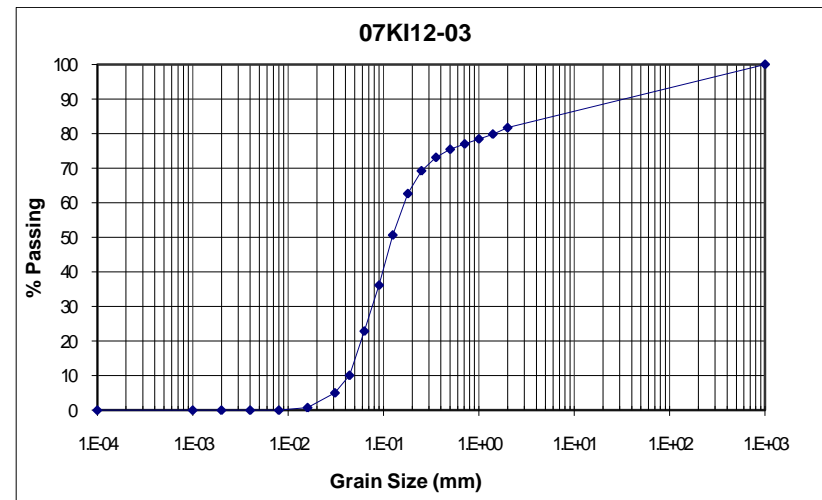
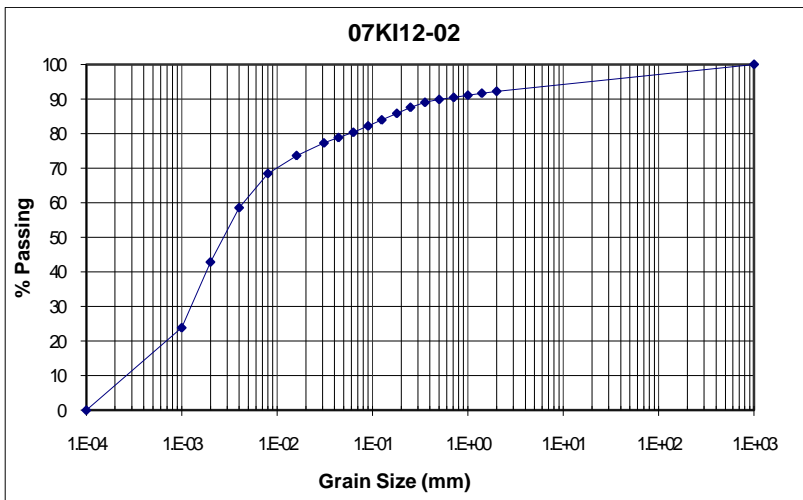
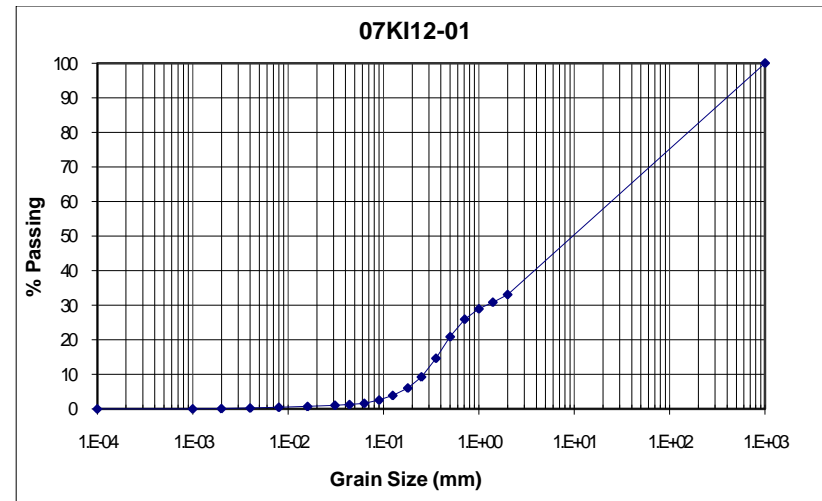
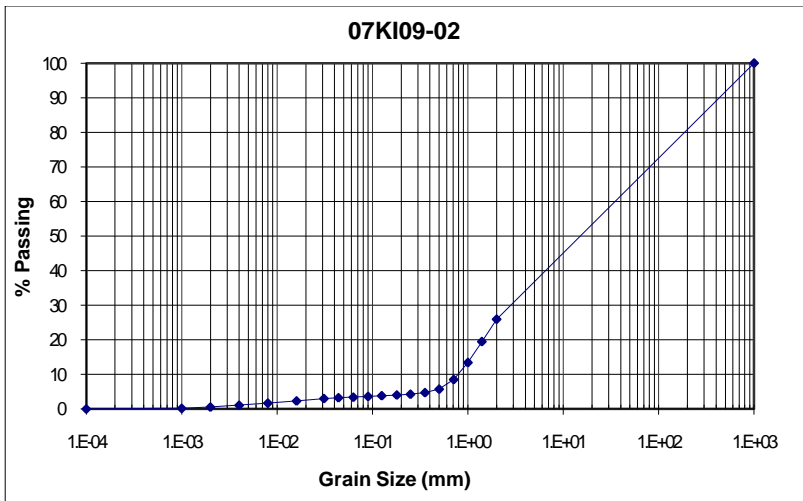
Appendix E – Grain Size Distribution Curves

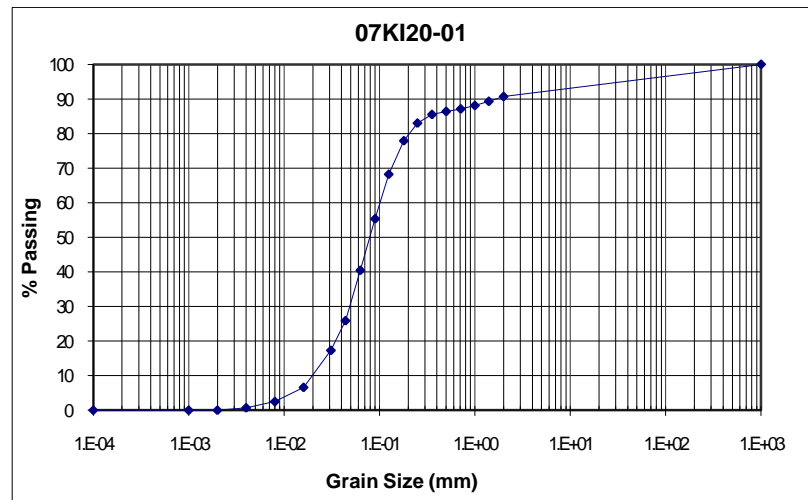
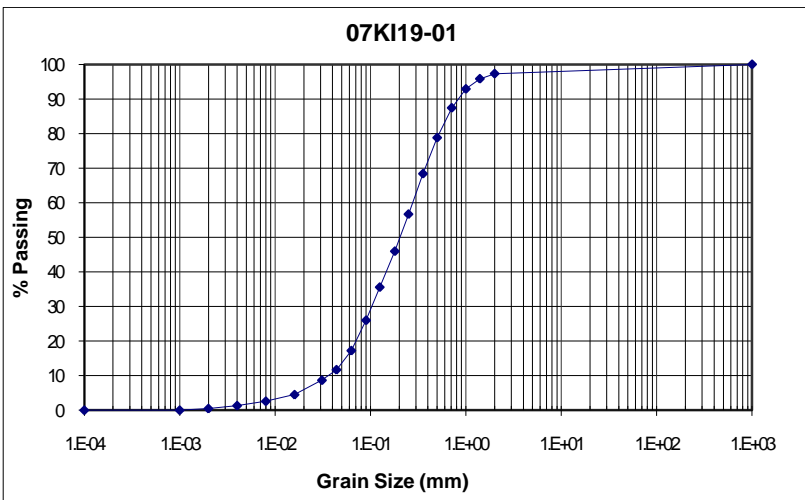
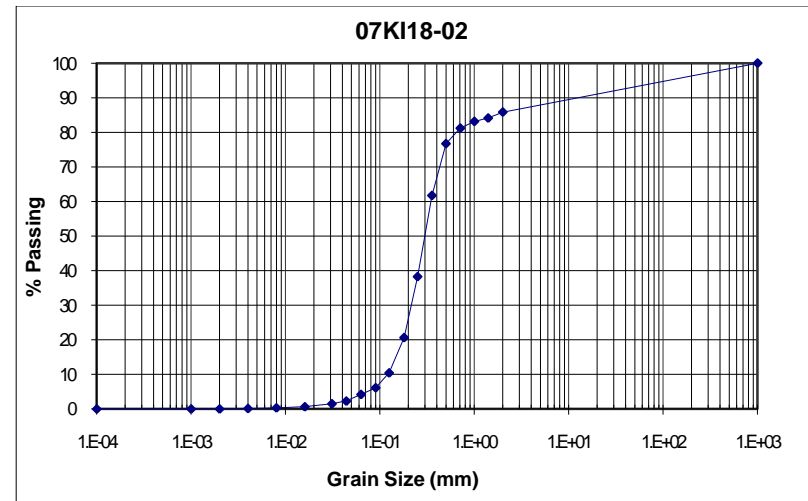
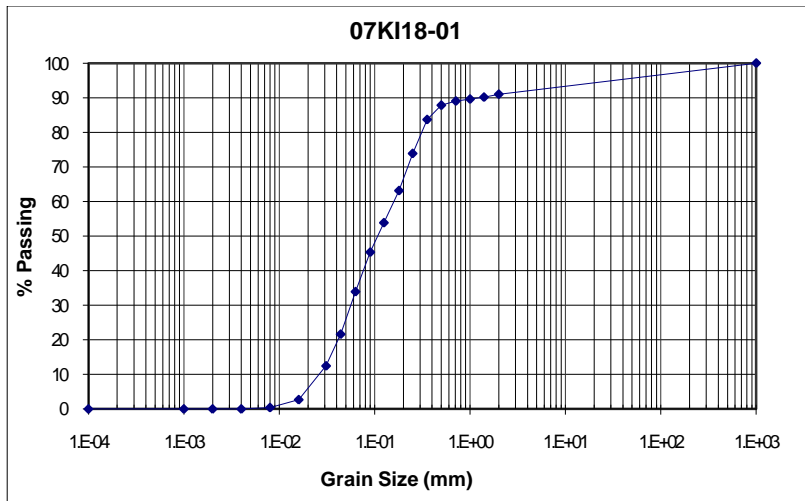
2007 Grain Size Analyses



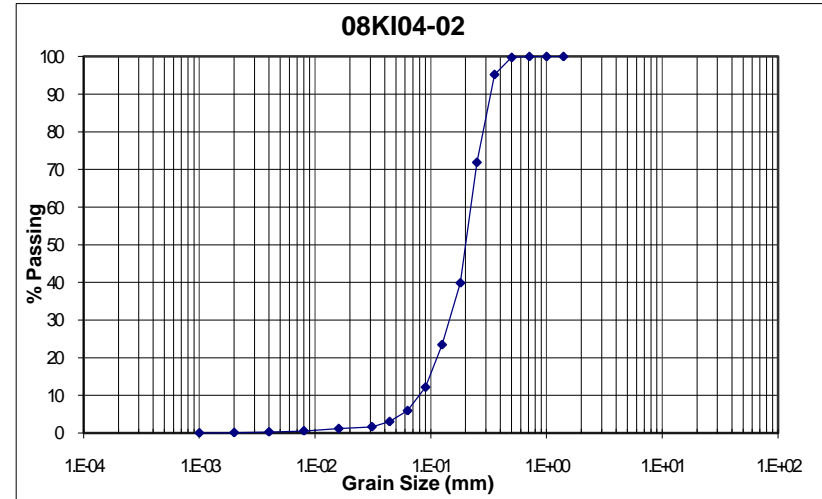
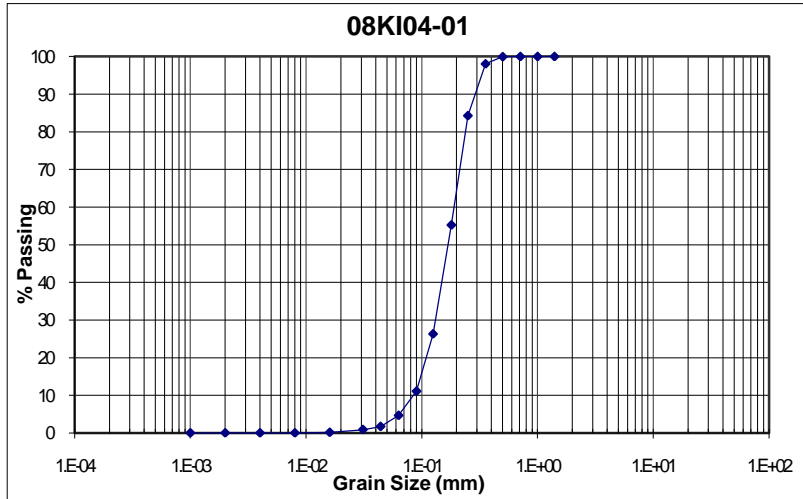


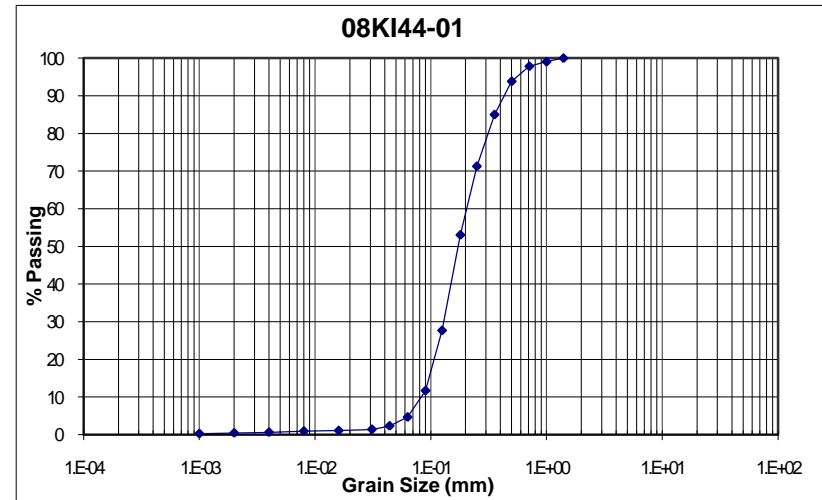
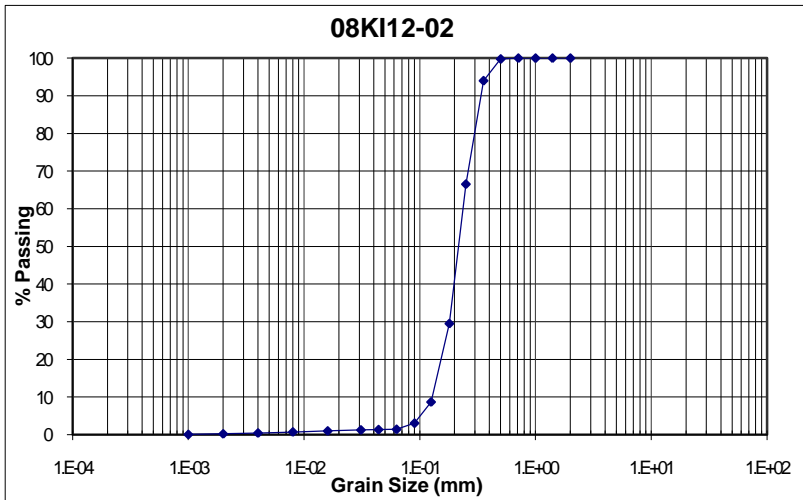
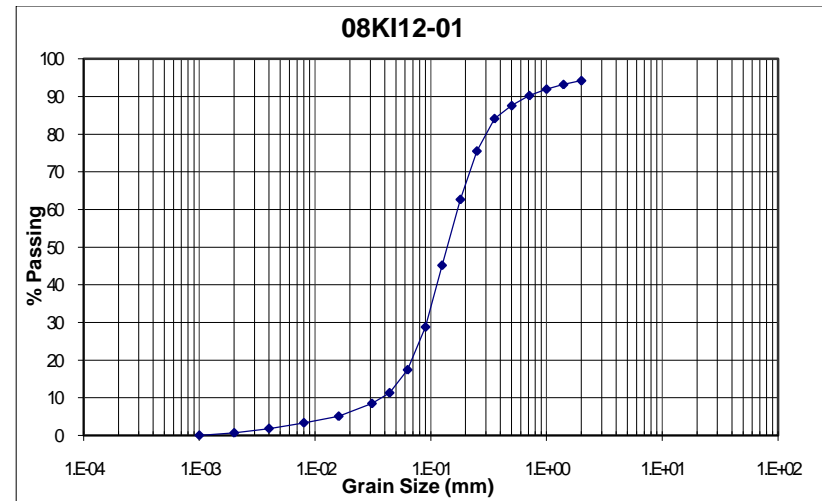
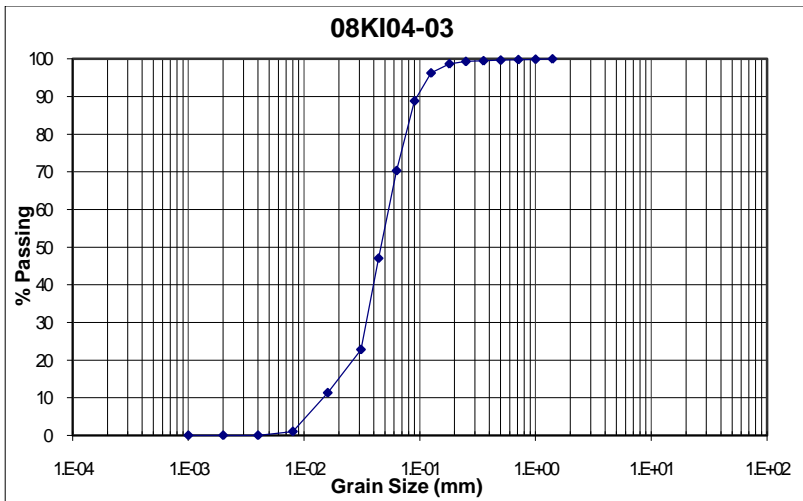


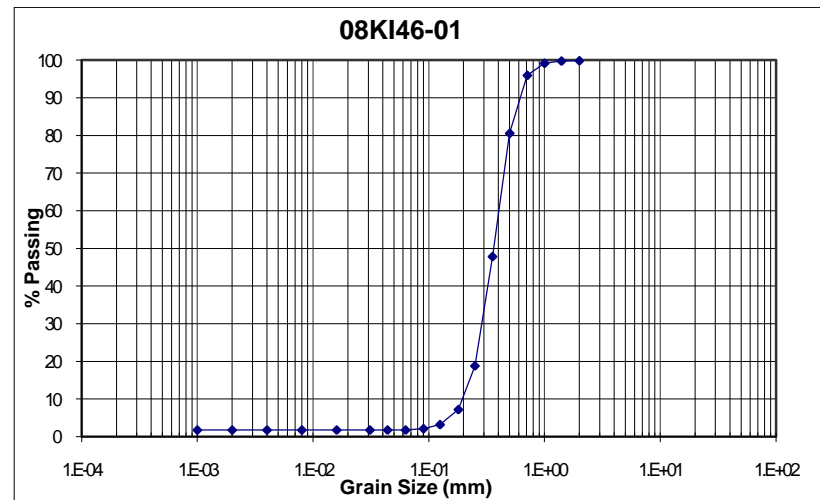
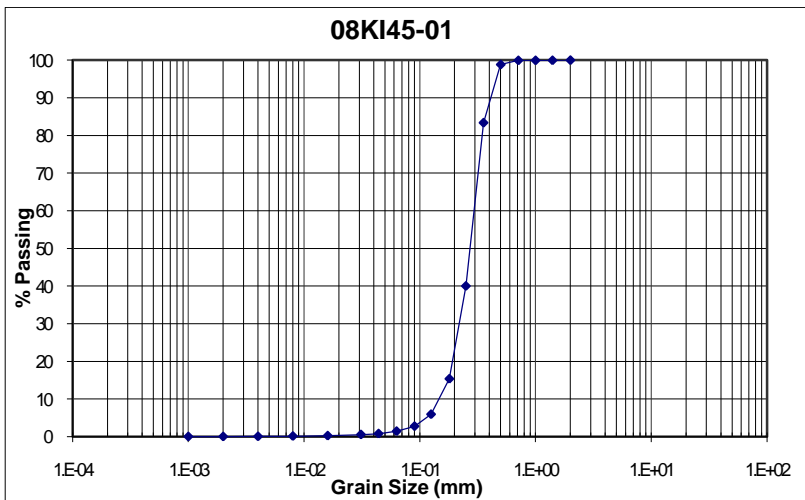
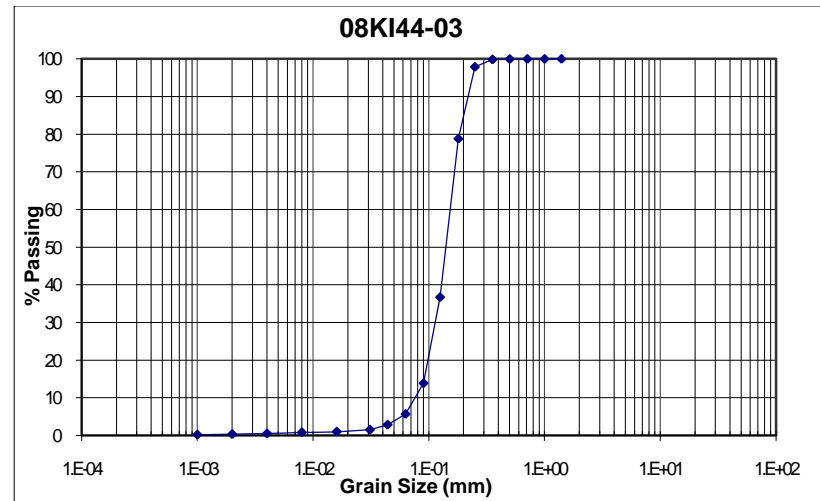
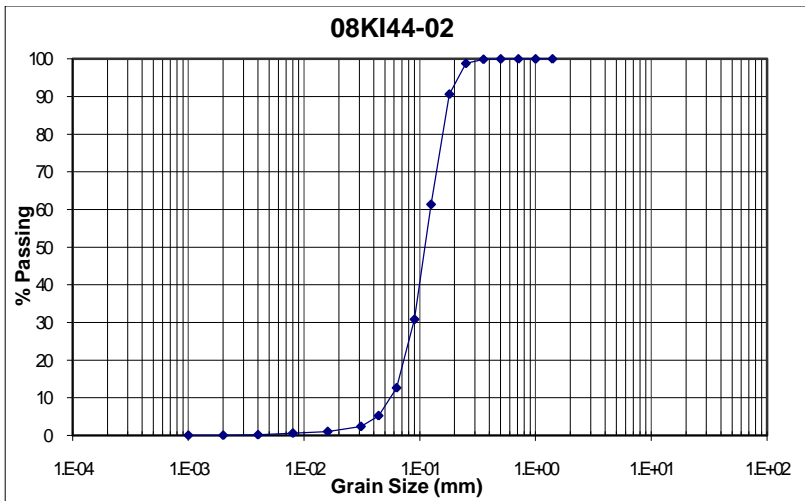


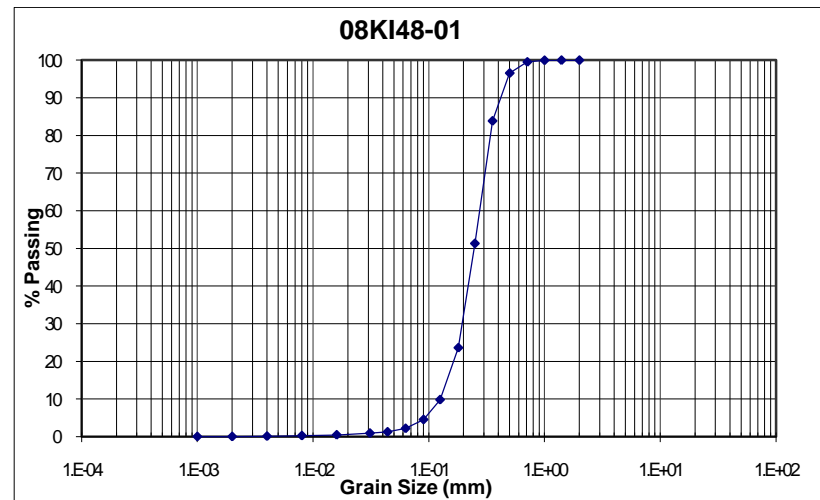
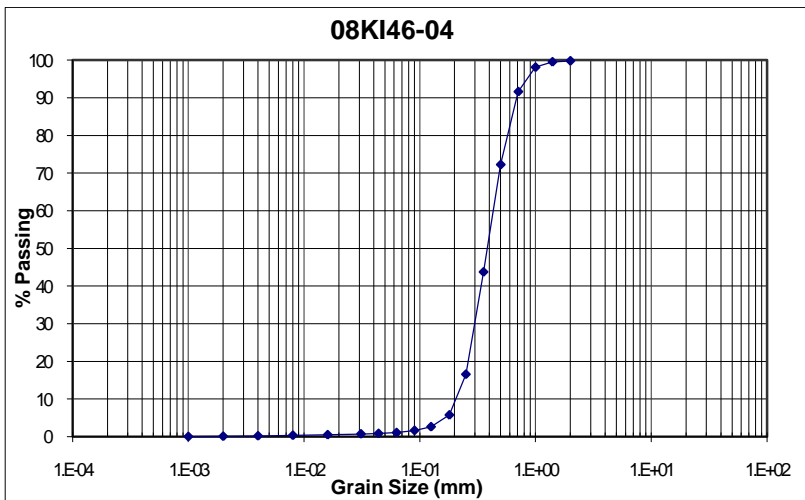
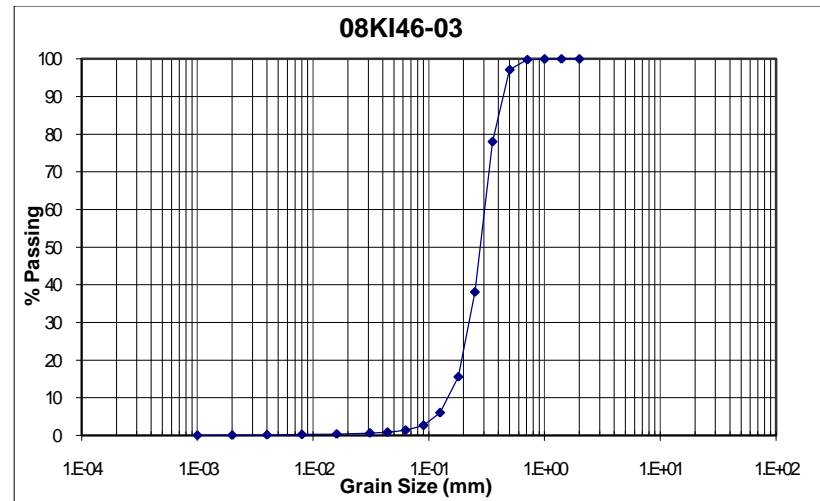
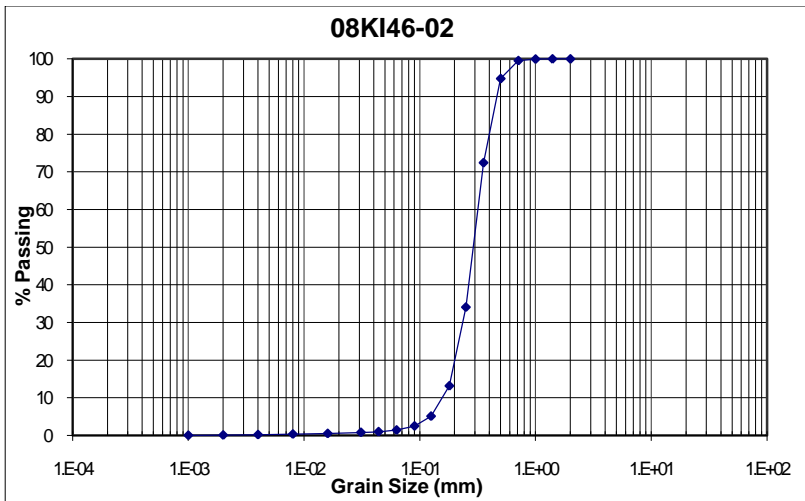


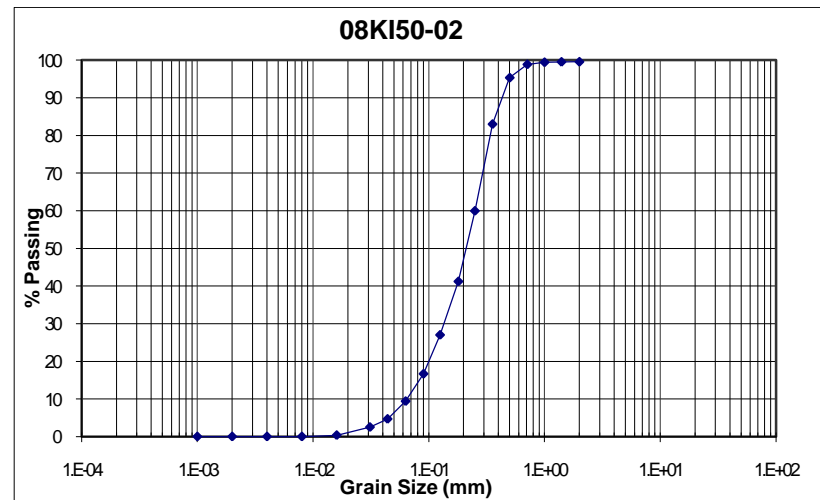
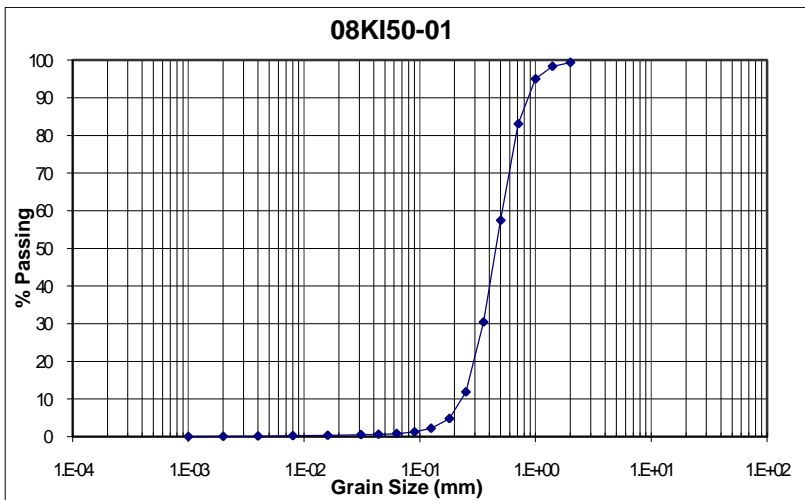
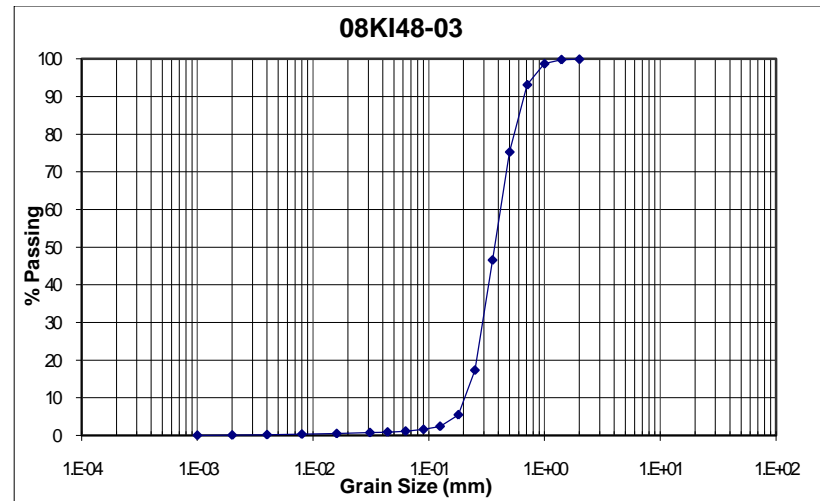
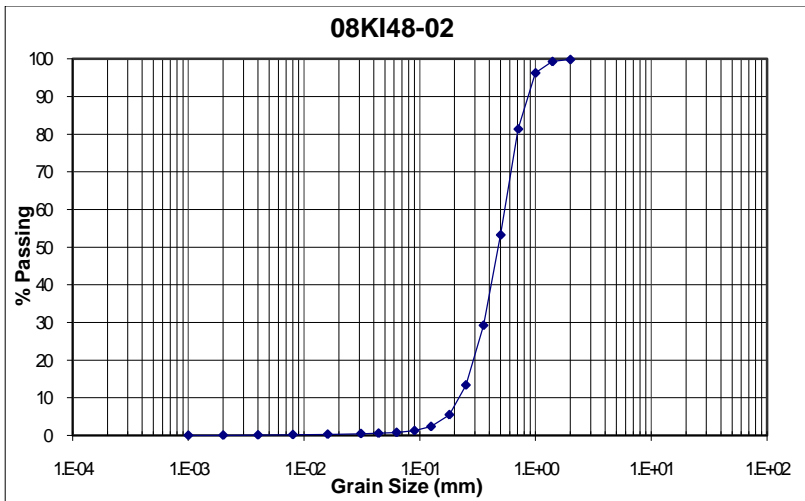
2008 Grain Size Analyses

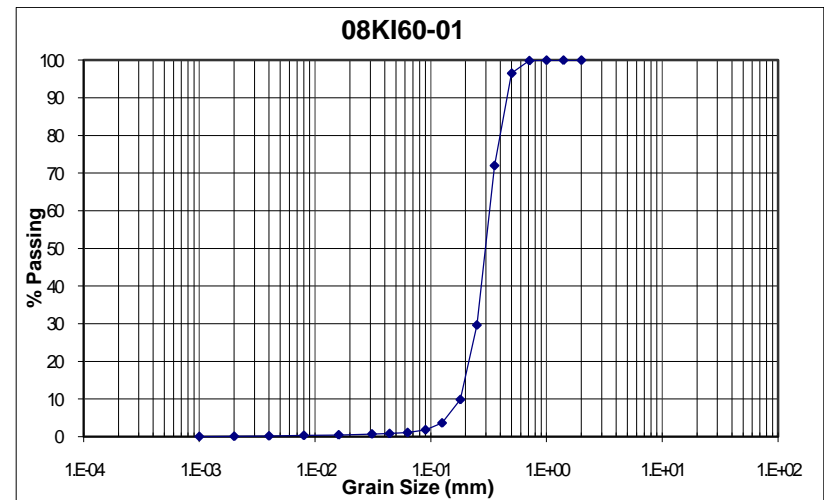
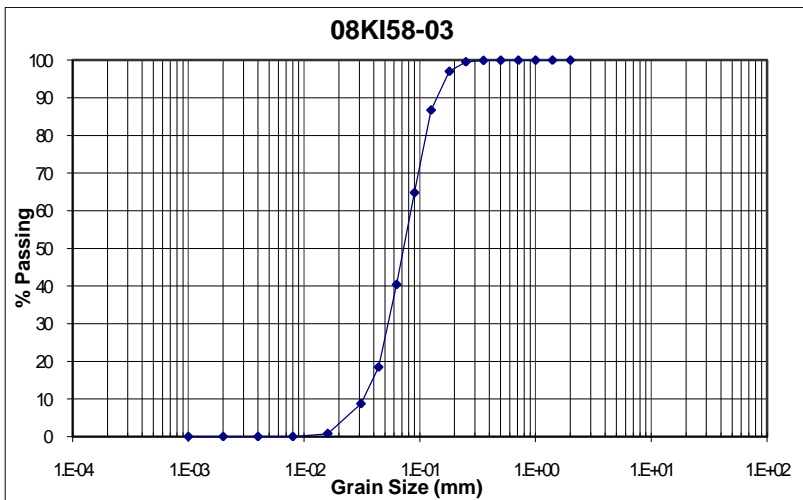
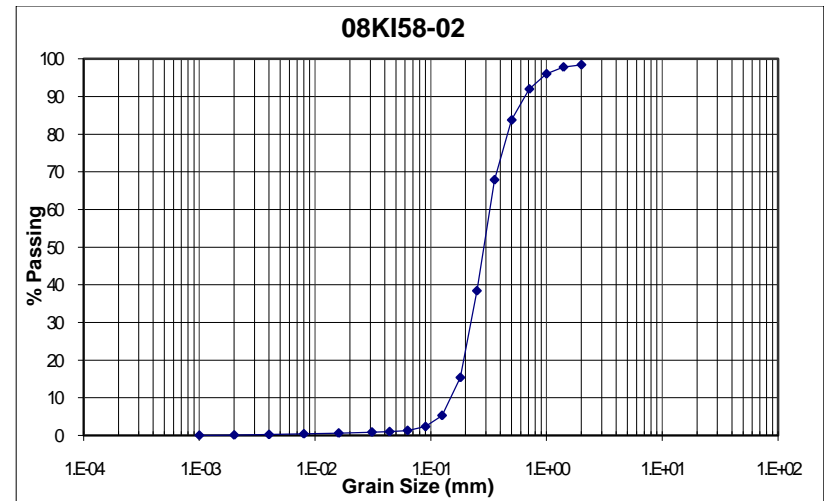
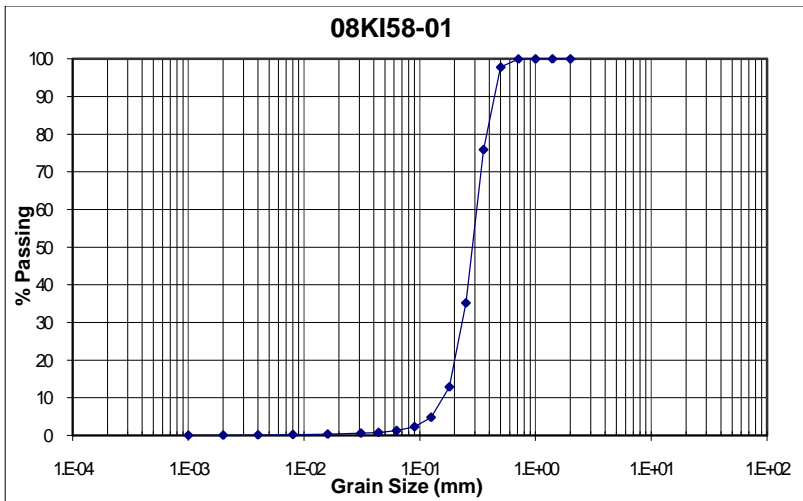


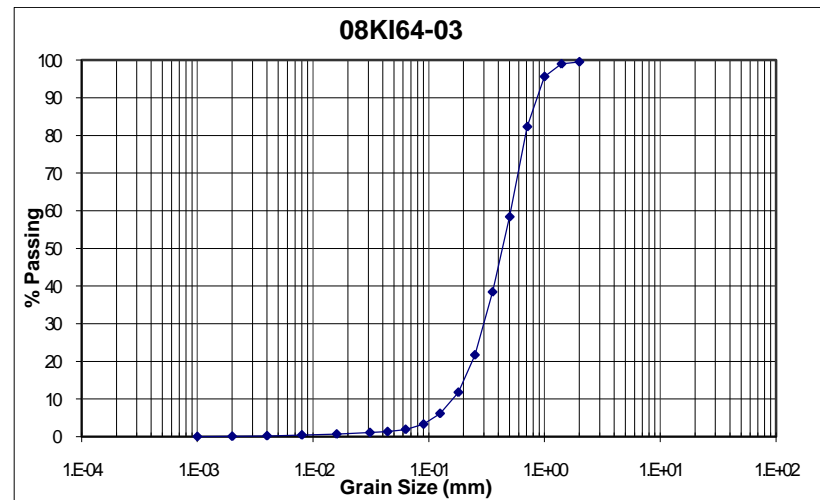
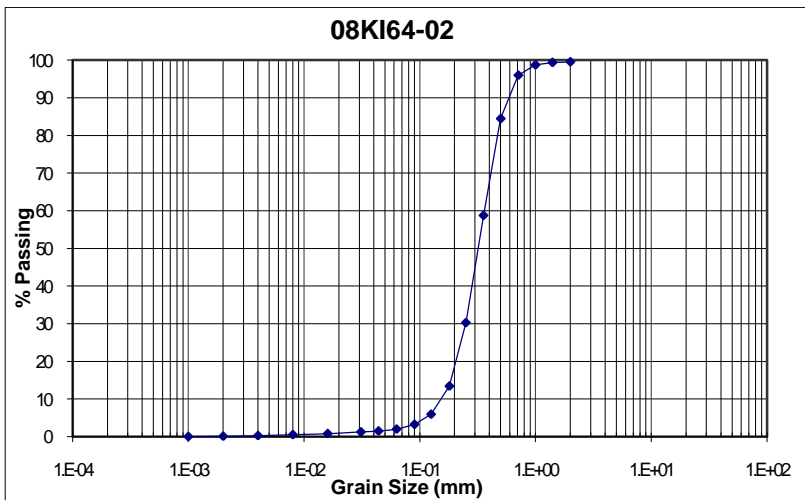
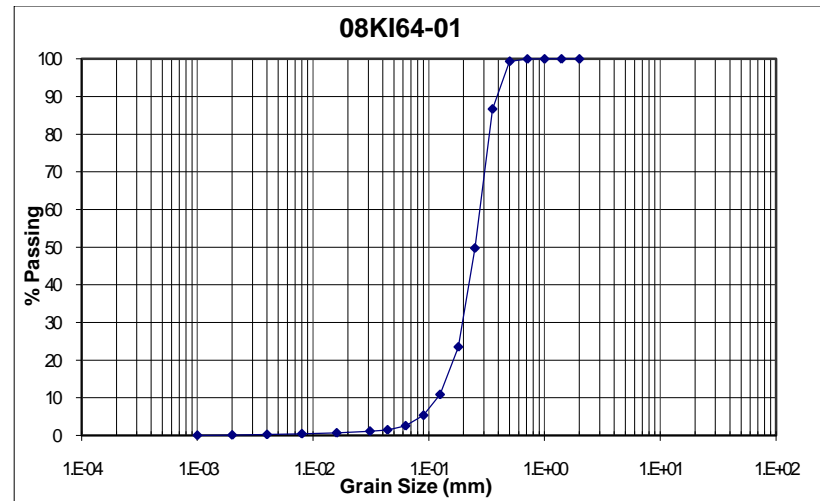
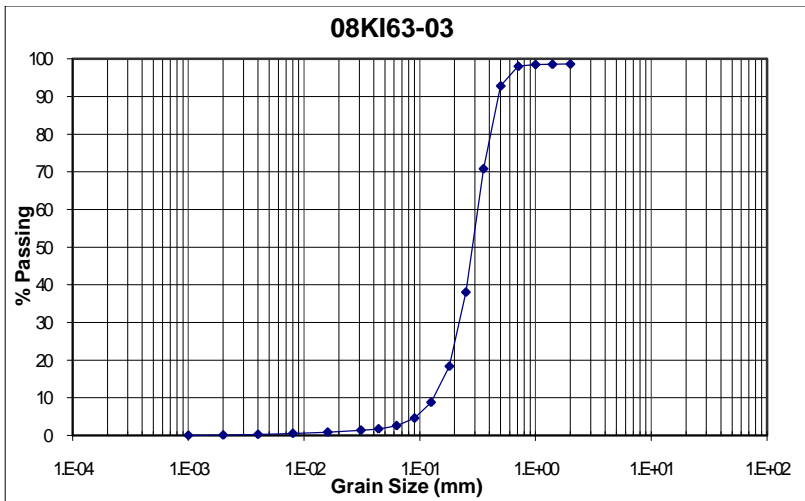


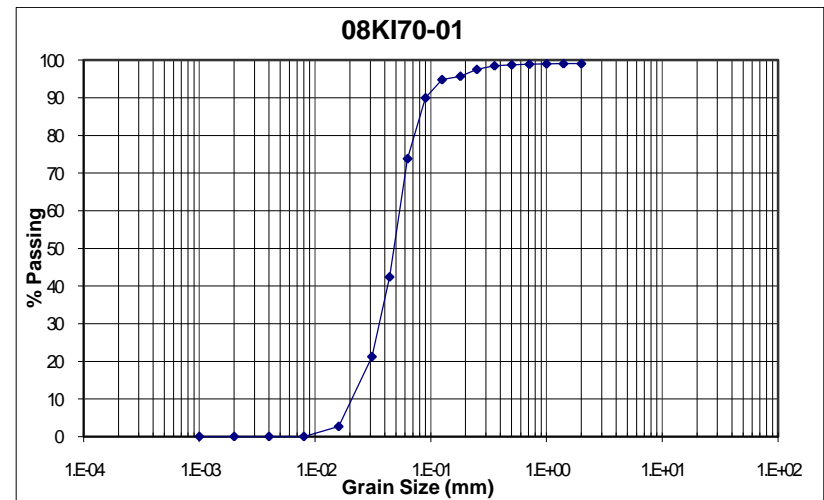
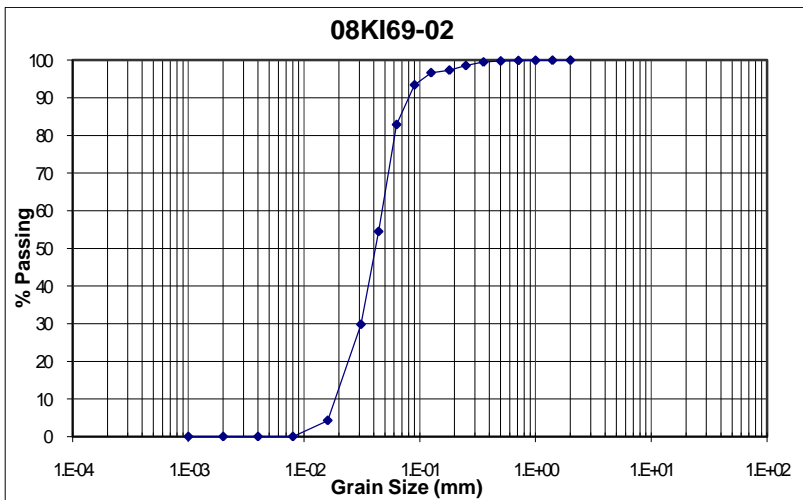
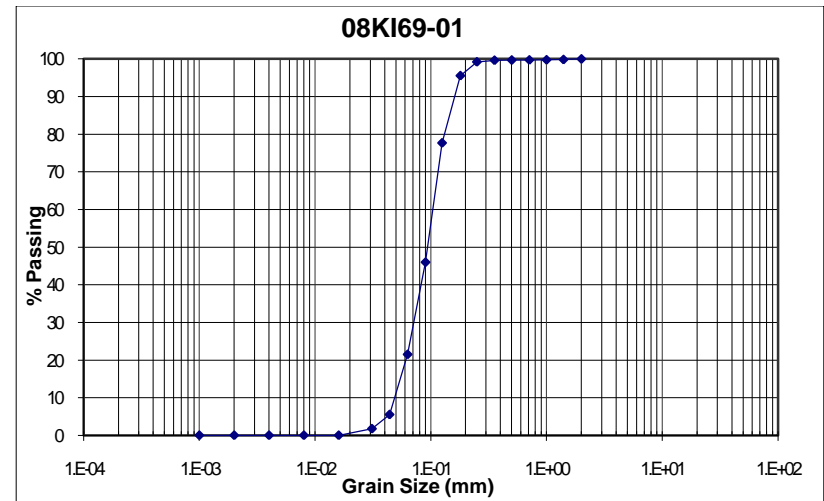
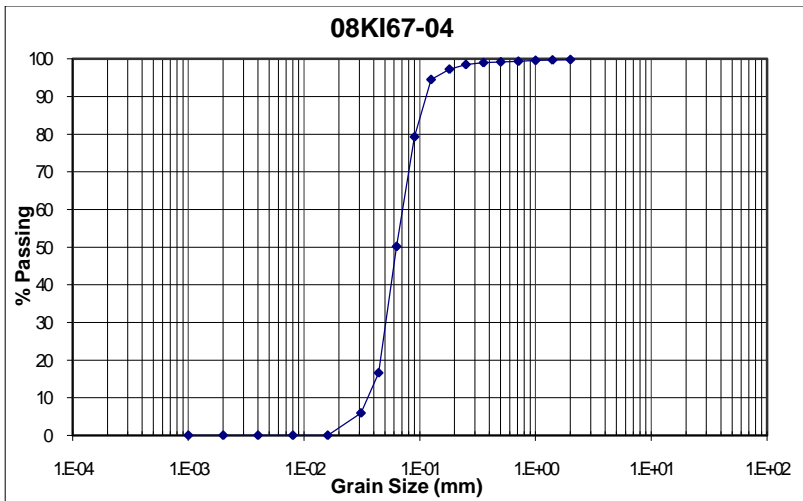


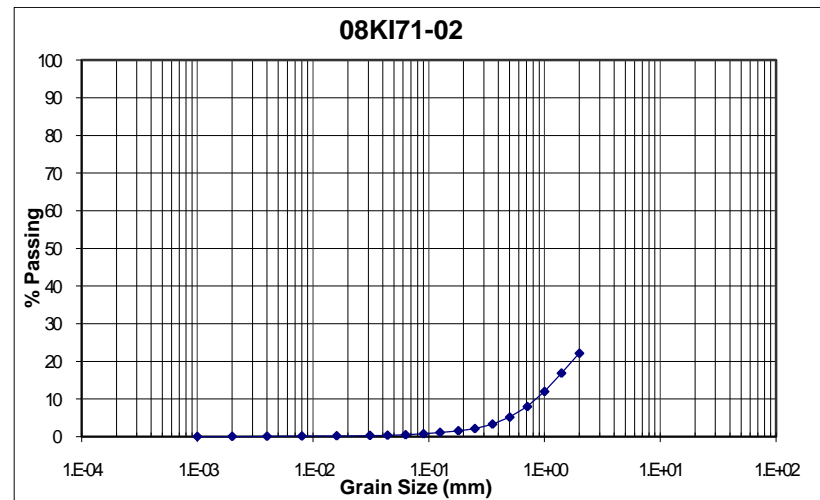
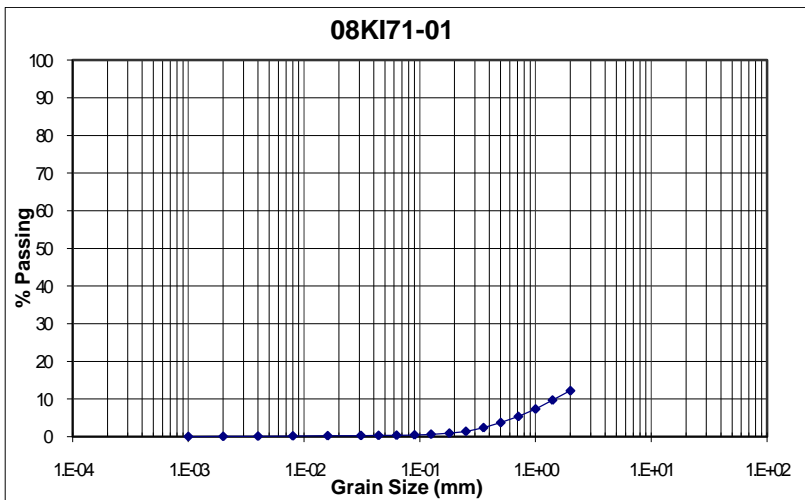
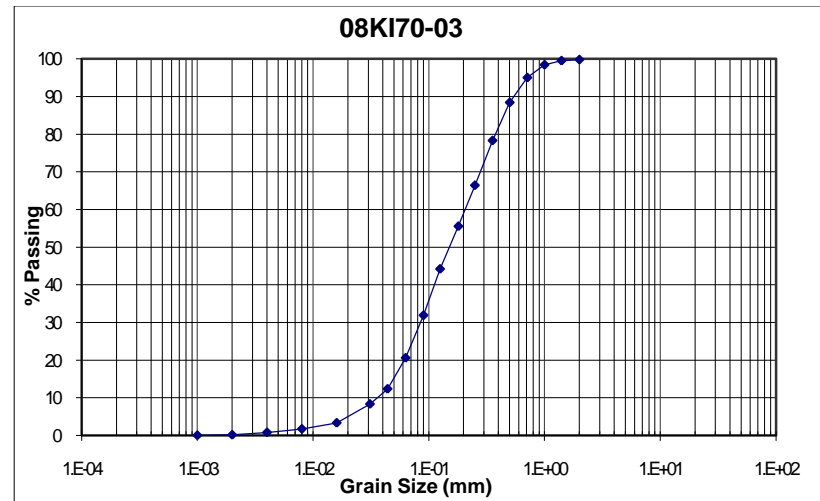
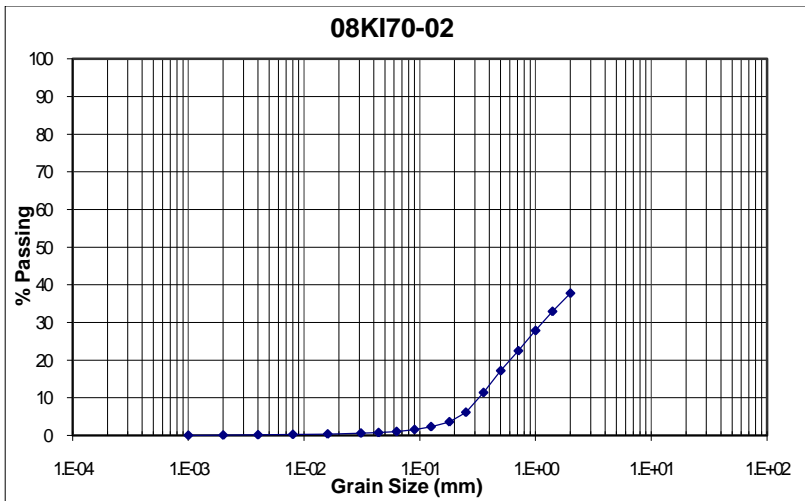


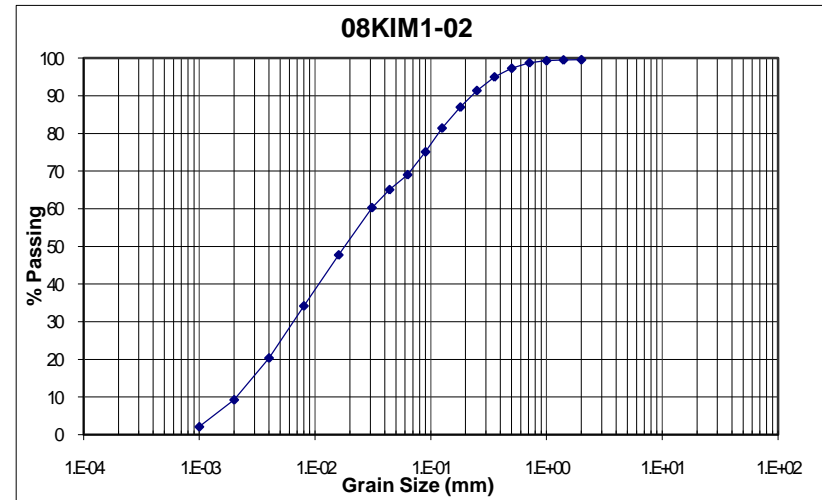
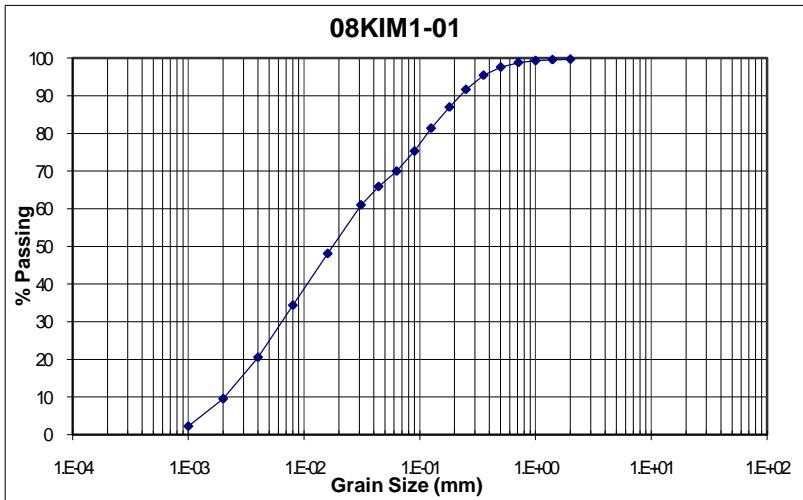
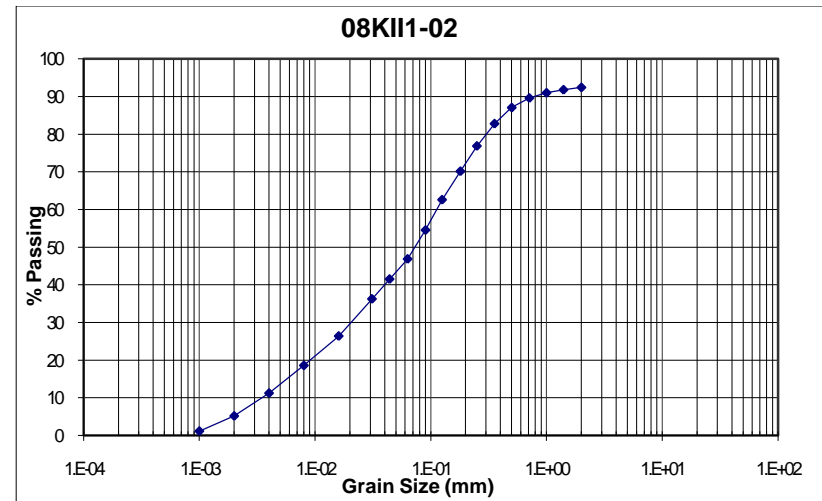
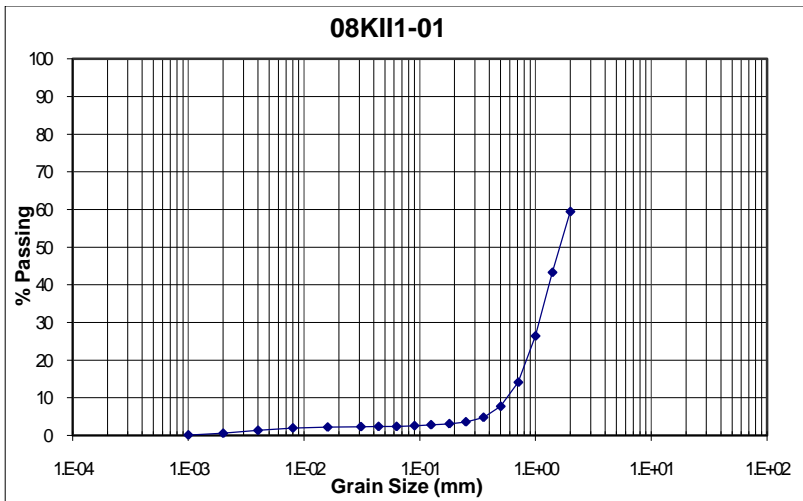


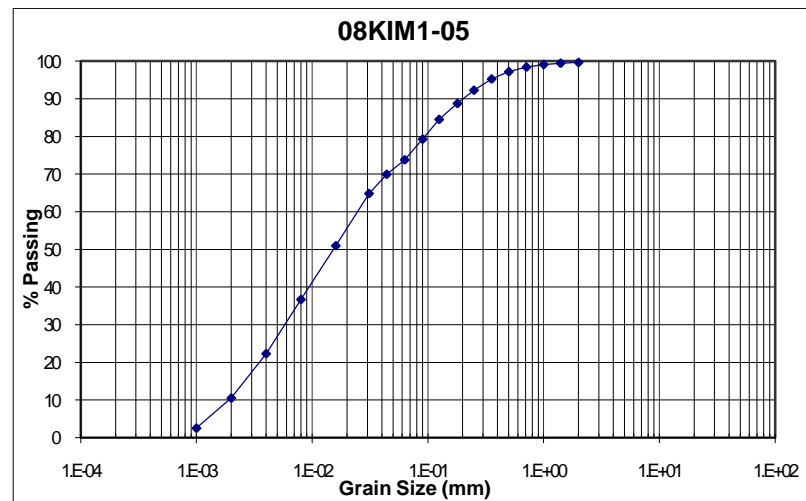
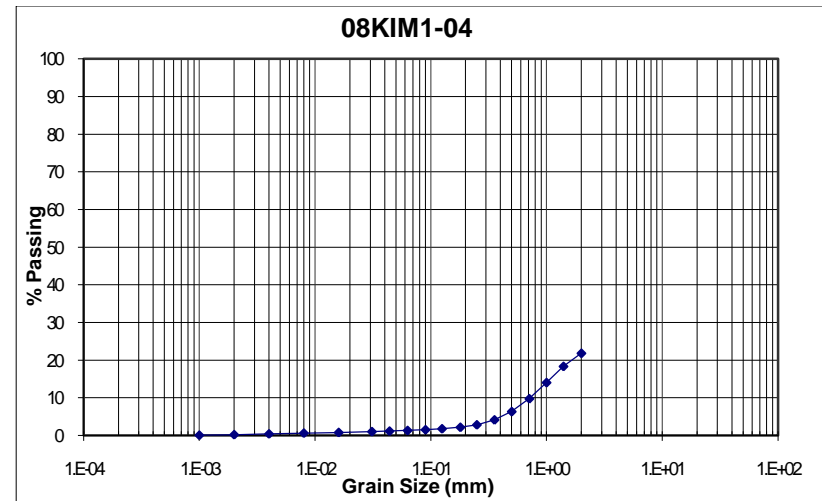
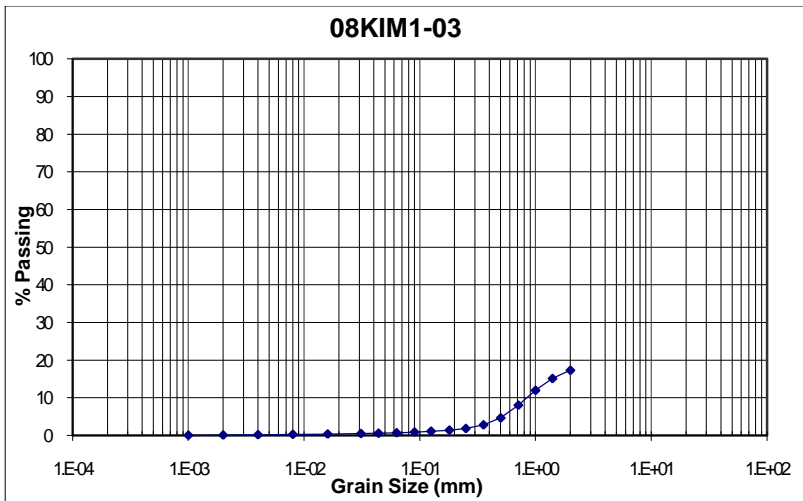










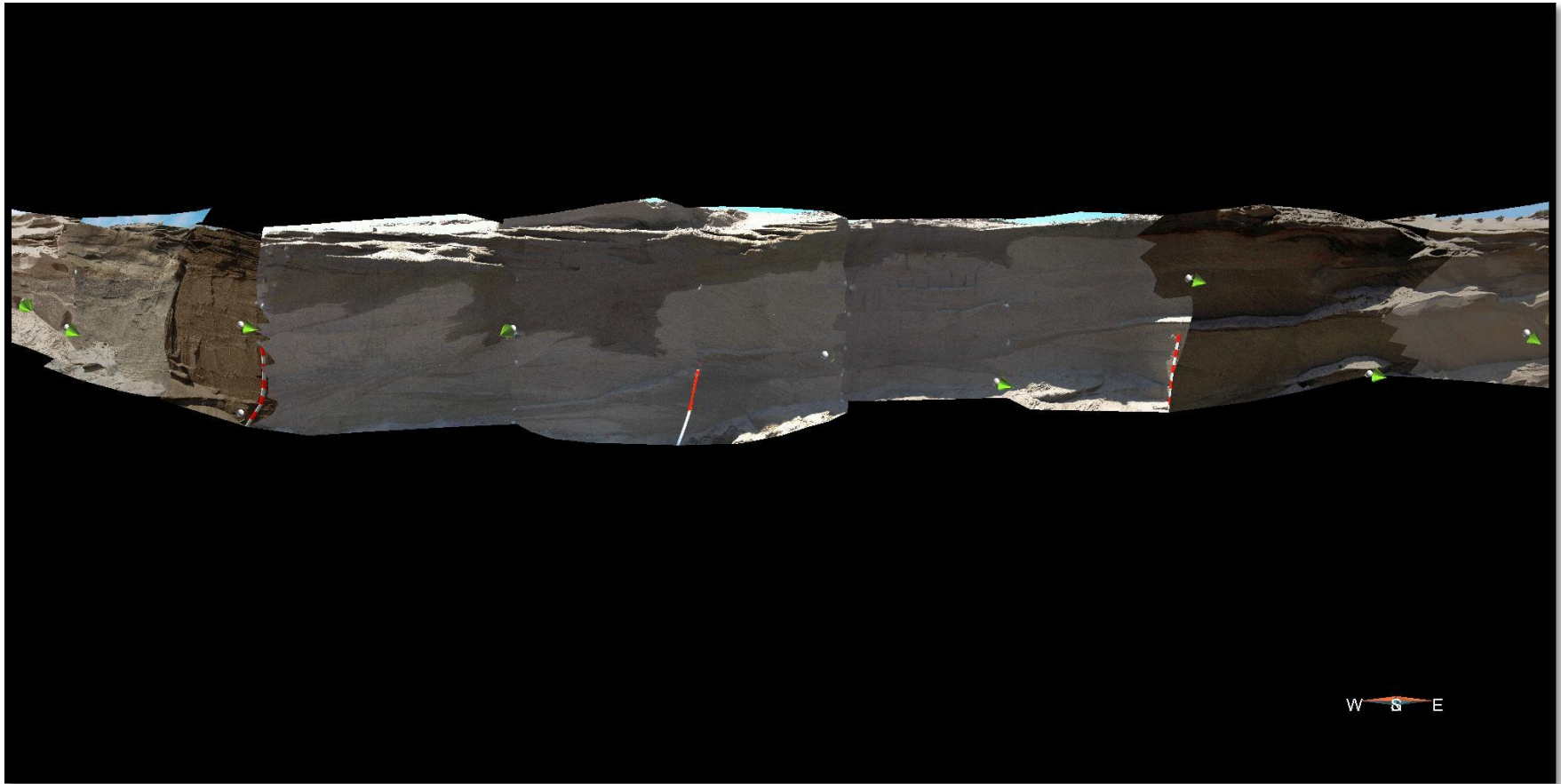


Appendix F – Paleoflow Measurements

Location	Measurements				Radians				Cartesian Coordinates					
									<i>Planar (adjusted)</i>			<i>Linear</i>		
	Trend	Strike	Dip	adjusted	Trend	Strike	Dip	adjusted	X	Y	Z	X	Y	Z
07KI01		192	41	49	0.0000	3.3510	0.7156	0.8552	-	0.1569	-			
07KI07		113	4	86	0.0000	1.9722	0.0698	1.5010	-	-	-			
07KI09		107	17	73	0.0000	1.8675	0.2967	1.2741	-	-	-			
07KI21		320	30	60	0.0000	5.5851	0.5236	1.0472	0.6634	0.5567	-			
08KI01		235	44	46	0.0000	4.1015	0.7679	0.8029	-	0.5892	-			
08KI03		245	36	54	0.0000	4.2761	0.6283	0.9425	-	0.7332	-			
08KI04		238	9	81	0.0000	4.1539	0.1571	1.4137	-	0.8376	-			
08KI09		74	31	59	0.0000	1.2915	0.5411	1.0297	0.2363	-	-			
08KI11		68	37	53	0.0000	1.1868	0.6458	0.9250	0.2992	-	-			
08KI12		281	22	68	0.0000	4.9044	0.3840	1.1868	0.1769	0.9101	-			
08KI13		321	25	65	0.0000	5.6025	0.4363	1.1345	0.7043	0.5704	-			
08KI13		278	23	67	0.0000	4.8520	0.4014	1.1694	0.1281	0.9115	-			
G	60		12	78	1.0472	0.0000	0.2094	1.3614				0.8471	0.4891	0.2079
08KI23		192	42	48	0.0000	3.3510	0.7330	0.8378	-	0.1545	-			
I		226	57	33	0.0000	3.9444	0.9948	0.5760	-	0.3918	-			
I		175	46	44	0.0000	3.0543	0.8029	0.7679	-	-	-			
<i>I fault</i>		356	54	36	0.0000	6.2134	0.9425	0.6283	0.5864	0.0410	-			
08KI28		126	68	22	0.0000	2.1991	1.1868	0.3840	-	-	-			
08KI35		268	30	60	0.0000	4.6775	0.5236	1.0472	-	0.8655	-			
08KI36		293	31	59	0.0000	5.1138	0.5411	1.0297	0.3349	0.7890	-			
08KI37		226	6	84	0.0000	3.9444	0.1047	1.4661	-	0.7154	-			
08KI37		252	29	61	0.0000	4.3982	0.5061	1.0647	-	0.8318	-			
08KI38		242	34	56	0.0000	4.2237	0.5934	0.9774	-	0.7320	-			
08KI40		274	31	59	0.0000	4.7822	0.5411	1.0297	0.0598	0.8551	-			
08KI42		257	15	75	0.0000	4.4855	0.2618	1.3090	-	0.9412	-			
F Scr	25		30	60	0.4363	0.0000	0.5236	1.0472				0.3660	0.7849	0.5000
G Sp 12		315	15	75	0.0000	5.4978	0.2618	1.3090	0.6830	0.6830	-			

I		242	34	56	0.0000	4.2237	0.5934	0.9774	-	0.7320	-			
I		257	28	62	0.0000	4.4855	0.4887	1.0821	-	0.8603	-			
I		255	42	48	0.0000	4.4506	0.7330	0.8378	-	0.7178	-			
08K144		301	23	67	0.0000	5.2534	0.4014	1.1694	0.4741	0.7890	-			
08K144		203	17	73	0.0000	3.5430	0.2967	1.2741	-	0.3737	-			
08K144		151	24	66	0.0000	2.6354	0.4189	1.1519	-	-	-			
08K146		3	37	53	0.0000	0.0524	0.6458	0.9250	0.7975	-	-			
08K146		15	12	78	0.0000	0.2618	0.2094	1.3614	0.9448	-	-			
08K147		357	16	74	0.0000	6.2308	0.2793	1.2915	0.9599	0.0503	-			
08K147		21	16	74	0.0000	0.3665	0.2793	1.2915	0.8974	-	-			
08K147		310	21	69	0.0000	5.4105	0.3665	1.2043	0.6001	0.7152	-			
08K148		135	22	68	0.0000	2.3562	0.3840	1.1868	-	-	-			
08K149		250	26	64	0.0000	4.3633	0.4538	1.1170	-	0.8446	-			
08K149		195	17	73	0.0000	3.4034	0.2967	1.2741	-	0.2475	-			
08K167		37	27	63	0.0000	0.6458	0.4712	1.0996	0.7116	-	-			
08K168		48	26	64	0.0000	0.8378	0.4538	1.1170	0.6014	-	-			
08K170		256	24	66	0.0000	4.4680	0.4189	1.1519	-	0.8864	-			
08K171		346	19	71	0.0000	6.0388	0.3316	1.2392	0.9174	0.2287	-			
08K171		351	31	59	0.0000	6.1261	0.5411	1.0297	0.8466	0.1341	-			
08K171		315	12	78	0.0000	5.4978	0.2094	1.3614	0.6917	0.6917	-			
08K171		285	12	78	0.0000	4.9742	0.2094	1.3614	0.2532	0.9448	-			
08K171	115				2.0071	0.0000	0.0000	0.0000				0.9063	-	0.0000
08K175	231				4.0317	0.0000	0.0000	0.0000				-	-	0.0000
08K144		211	44	46	0.0000	3.6826	0.7679	0.8029	-	0.3705	-			
08K122		195	32	58	0.0000	3.4034	0.5585	1.0123	-	0.2195	-			
08K149		60	25	65	0.0000	1.0472	0.4363	1.1345	0.4532	-	-			
08K150		30	26	64	0.0000	0.5236	0.4538	1.1170	0.7784	-	-			
F Scr	345				6.0214	0.0000	0.0000	0.0000				-	0.9659	0.0000

The paleoflow measurements and vector calculations for measurements taken at Kieswetter Holdings.



An example of how the paleoflow points were georeferenced into the geomodelling process and show the direction of the sandy bedform foresets at Section K.

Appendix G – Data Disc

All collected data used in this thesis can be found on the accompanying data disc. This disc was created to initiate a Waterloo Moraine database in order to lead to an improved and thorough geological understanding of this glacial deposit. It is anticipated that enhanced decisions regarding water resource management and planning will be made from this geological insight as the Region of Waterloo depends upon the Waterloo Moraine for its water supply. There are nine folders on the disc, contained all the data and are titled by the data they contain. The folders are labeled geomodelling, GIS, GPR, grain size analyses, images, paleocurrents, papers and surveyed points.

The data from [Bajc & Shiota, 2007](#) was used extensively in this thesis and is available to the public at Geology Ontario (<http://www.geologyontario.mndm.gov.on.ca>). It is suggested to read the readme files before examining the information. Data, other than that from [Bajc & Shiota, 2007](#) and GPR, is presented in text files for geomodelling purposes and other raw data, such as grain size, paleocurrent and surveying data, is presented in Microsoft Excel 2003 & 2007 formats. To download a free excel viewer, visit <http://www.microsoft.com/downloads>. Google Earth was the primary GIS tool used as it is available as freeware, it is user friendly and was the software chosen by the Ontario Geologic Survey to be used in presenting their findings. These reasons are why the GIS data for the Kieswetter site is available for Google Earth and can be downloaded for free at <http://earth.google.com>. The raw data from the GPR profile can be opened with EKKOView Deluxe. It is recommended to contact Sensors and Software (<http://www.sensoft.ca>) for any queries. All images are saved as jpeg files and any picture viewer will be adequate. Any reports or referenced papers are saved as a PDF file. Adobe Reader is required to view these files and is available for free at <http://www.adobe.com/products/reader>.

Table of Contents for the Folders on the Data Disc

Geomodelling											
<i>Point sets</i>				<i>Sgrid</i>		<i>Surfaces</i>		<i>Voxets</i>		<i>Boreholes</i>	
Bajc's Model	Paleoflows	Sections	Other	Bajc's Model	Sections	Sections	Other	GPR	Sections	Data	Boreholes

GIS
<i>Kieswetter KMZ file</i>

GPR		
<i>GPR Data</i>	<i>Survey Data</i>	<i>Images</i>
	Excel & Text files	JPGs

Grain Size Data
<i>2007 & 2008 Excel Files</i>

Images	
<i>2007</i>	<i>2008</i>
Folders based on section	Folders based on section

Paleocurrents
<i>Excel Files</i>

Papers
<i>PDF Files</i>

Surveyed Points	
<i>Excel 2003</i>	<i>Excel 2007</i>
Excel Files	Excel Files